Staphylococcus aureus DNA gyrase: mechanism and drug targeting

Terence Tsz-Hong Chung

John Innes Centre

September 2012

This thesis is submitted in partial fulfilment of the requirements of the
degree of Doctor of Philosophy at the University of East Anglia

Statement

This work is entirely my own, except where due reference has been made to other authors, and has not been submitted to this or any other university as part of any degree.

Abstract

Increases in *Staphylococcus aureus* resistance against existing treatment options and the shortage of new antibiotics signals an urgent need for new treatments for the ongoing battle against the development of antibiotic resistance.

DNA gyrase is an essential bacterial type II DNA topoisomerase that manipulates DNA topology by performing transient double-strand breaks and DNA strand passage. As gyrase is vital for bacterial survival, it is an effective antibacterial target. By understanding the mechanistic differences between *S. aureus* gyrase and the better studied *Escherichia coli* counterpart, we aim to better utilise *S. aureus* gyrase as an antibacterial target and improve the design of future antibacterial drug.

This study has investigated features unique to *S. aureus* DNA gyrase: the potassium glutamate (KGlu) salt-dependent and salt-specific supercoiling. This KGlu dependency in *S. aureus,* but not *E. coli* gyrase, was partially attributed to the differences in the C-terminal domain of the gyrase A-subunit (GyrA). The discovery of the two novel monovalent alkali metal cation (M^+) binding sites located in N-terminal domain of GyrB by protein crystallography has suggested a novel role of these M^+ ions in the supercoiling functions of DNA gyrase, providing theoretical links to the unique KGlu dependency in *S. aureus* gyrase and the dependency of monovalent ions in *E. coli* and *B. subtilis* gyrase.

Diospyrin, a phyto-naphthoquinone, was found to be active against *S. aureus in vivo*. It inhibits *S. aureus* gyrase and topo IV *in vitro*, with gyrase as the preferred target. Further studies suggested the binding site of Diospyrin to be located in the N-terminal domain of GyrB. Diospyrin also partially inhibits the ATPase activity of GyrB in an allosteric manner. Diospyrin is hypothesized to bind to a novel binding site between the ATPase domain and the transducer domain. Diospyrin also inhibits both the relaxation and the DNA cleavage ability of gyrase, suggesting it inhibits gyrase with a novel mechanism.

Table of content

Abbreviations

3D – 3-dimensinal

ADMET – absorption, distribution, metabolism, excretion and toxicity

ADP – adenosine-5′-diphosphate

ADPNP – 5′-adenylyl β,γ-imidodiphosphate

ATP – adenosine-5′-triphosphate

Aw – water activity

bp – base pair

CTD - C-terminal domain

DNA – deoxyribose nucleic acid

Ec – Escherichia coli

GrlA/ParC – topo IV A- subunit

GrlB/ParE – topo IV B-subunit

GyrA – DNA gyrase A-subunit

GyrB – DNA gyrase B-subunit

GHKL – Gyrase, Hsp90, Histidine Kinase, MutL

K_d – dissociation constant

KAsp – potassium aspartate

KCl – potassium chloride

KGlu – potassium glutamate

Lk – linking number

Lk_0 – ground state linking number

M^+ – monovalent metal cation

MIC – minimum inhibitory concentration

MPC – mutation prevention concentration

MRSA – Methicillin-resistant *Staphylococcus aureus*

MS – mass spectrometry

NaAsp – sodium aspartate

NaCl – sodium chloride

NaGlu – sodium glutamate

NTD – N-terminal domain

P_i – inorganic phosphate

QRDR – Quinolone resistance-determining regions

Sa – Staphylococcus aureus

SM-FRET - Single-Molecule Fluorescence Resonance Energy Transfer

T_m – melting temperature

T_w – twist

WHD – winged-helix-domain

W_r – writhe

Acknowledgements

First and foremost I would like to thank my supervisor Prof. Tony Maxwell for giving me the opportunity to work on this amazing project. Without his continuous support throughout the last four years the completion of this project would not be possible. Secondly, I would like to thank my supervisory committees, Dr Dave Lawson, Dr Nick Burton and Dr Stephen Bornemann for their generous advice and technical support. In particular, Dave for his input and help especially on the protein crystallography work; Nick, for his help and input on some of the technical aspects of this project (in particular on ATPase assay); and Stephen for his expert opinions on the enzymological aspect of the project.

I thank Dr Shantanu Karkare for the initiation of the diospyrin work. I would like to thank Dr Clare Stevenson on the generous help on protein crystallography, which has been pivotal to my work. I have to especially thank my collaborators Prof. Vishnu Tandon (University of Lucknow, India) and Prof. David Kingston (Virginia Tech, USA) for generously providing the rare naphthoquinone analogs assayed. I would like to thank Lesley Mitchenall, who has provided a lot of the technical help and emotional support throughout the project. I would like to thank Dr Stephen Hearnshaw for the massive technical help and assurance during my wander into the world of protein-crystallography. Special thanks to Dr Sandra Greive for her incredible support in the early stage of my project.

I would also like to thank other unmentioned colleagues within the Maxwell lab and the *Biological Chemistry* department for making it such an enjoyable environment to work in.

I would like to thank my grandparents, in particular my grandfather, who have provided most of the scientific influence in my earlier life and indirectly guided me into the wonderful world of science. Most importantly, my parents, who I would like to give my greatest thanks, for supporting me my entire life and provided the freedom for me to explore science.

Last but not least, thank you Kelly for your support and encouragement, and being a perfect company during the course of this project.

This work is dedicated to my parents, everyone around me and to the unfortunate people who suffer from MRSA infections.

Chapter 1 Introduction

1.1 Antibiotic resistance

1.1.1 History and latest development

Development of antibiotic resistance has been the result of the constant competition between humans and bacterial evolution ever since the discovery of the first antibiotic, penicillin. Penicillin was first famously discovered in 1928 by Sir Alexander Fleming by a fortuitous accident when a mould (*Penicillin rubens*) contaminated a petri dish of *Staphylococcus aureus* [1]. Since then, penicillin has been industrially mass produced and became a prescription antibacterial for the treatment of a wide spectrum of bacterial infections, saving numerous lives over the past decades. However, as early as the 1940s it was discovered that resistance can be observed in bacterial cultures incubated in the presence of penicillin [2-3].

It was then understood that bacteria have the ability to gradually acquire resistance upon exposure to antibiotics and there are needs for more novel antibiotics to compensate for the development of bacterial resistance against older antibiotics. Examples of antibacterial resistance developed by bacteria are listed in figure 1.1. Despite the gradual development of antibiotic resistance, the boom of antibiotic discovery and availability of a wide range of antibiotics has led to complacency and developed a general misconception that bacterial infections are no longer life-threatening diseases. Compounded by the generally short-dosage schedule of antibiotics, low profitability and the rising cost of developing antibacterials in comparison to other human targeting drugs [4], traditional antibacterials discovery is deemed unprofitable and was slowly phased out over the last 2 decades [4].
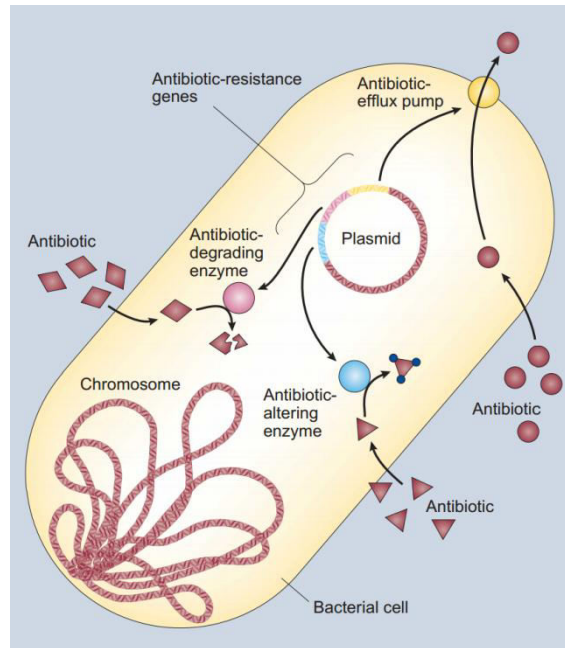
Figure 1.1. A schematic diagram showing of some of the mechanisms contributing to multi-drug resistance in bacteria via horizontal gene transfer. *The resistant genes transferred via a plasmid are typically capable of producing resistance phenotypes via: i) enzymatic degradation or modification of the specific antibiotic or ii) removal of antibiotics out of the intracellular space by efflux pumps* [5].

While discoveries of antibiotics have slowed, antibacterial resistance continues to rise, accelerated by years of their overuse in clinics [6]. This rise in demand for novel antibiotics is met with the decline in newly approved antibacterials. With this ongoing trend, bacterial infections are predicted to again become the deadliest disease in the clinic [6]. The World Health Organisation has voiced concerns of late and regards antimicrobial resistance as one of the biggest threat to global health [7].

1.1.2 Methicillin-resistant-*Staphylococcus aureus*

Methicillin-resistant-*Staphylococcus aureus* (MRSA) was first isolated in 1961, shortly following the introduction of Methicillin in 1959 in the clinic. MRSA developed Methicillin resistance by acquisition of a copy of *mecA*, which encodes penicillin-binding protein PBP 2A[8]. PBP 2A, unlike its wide type counterpart, does not bind to Methicillin and subsequently confers methicillin resistance. In recent years, MRSA has become a highly prominent opportunistic hospital-acquired pathogen in western

countries. This has created a huge economic burden on health-care systems worldwide [9-10]. As statistical studies suggested, the increasing number of MRSA cases are closely related to the increase in the misuse of antibiotics compounded with the decrease of susceptibility in *S. aureus* to major antibiotics in recent years [11]. Due to its multi-drug resistance ability, MRSA is extremely resilient to antibiotic treatment and is difficult to eradicate once contracted. Its ability to survive on human skin (a high salt environment) [12], nose [13-14] and common antiseptic, [15] has enabled MRSA to spread swiftly between patient and medical staff through human contact, causing major outbreaks and deaths in hospitals. Subsequent series of campaigns and media coverage raising concern over the rise of MRSA infection has led to establishment of stricter hygiene procedure in the UK ("cleanyourhands" campaign [16]) to tackle the spread of the bacteria in hospitals. As an effect, the number of MRSA-related deaths in the UK has seen a sharp drop in the past 2-3 years (fig.1.2).

Sources: Office for National Statistics, UK
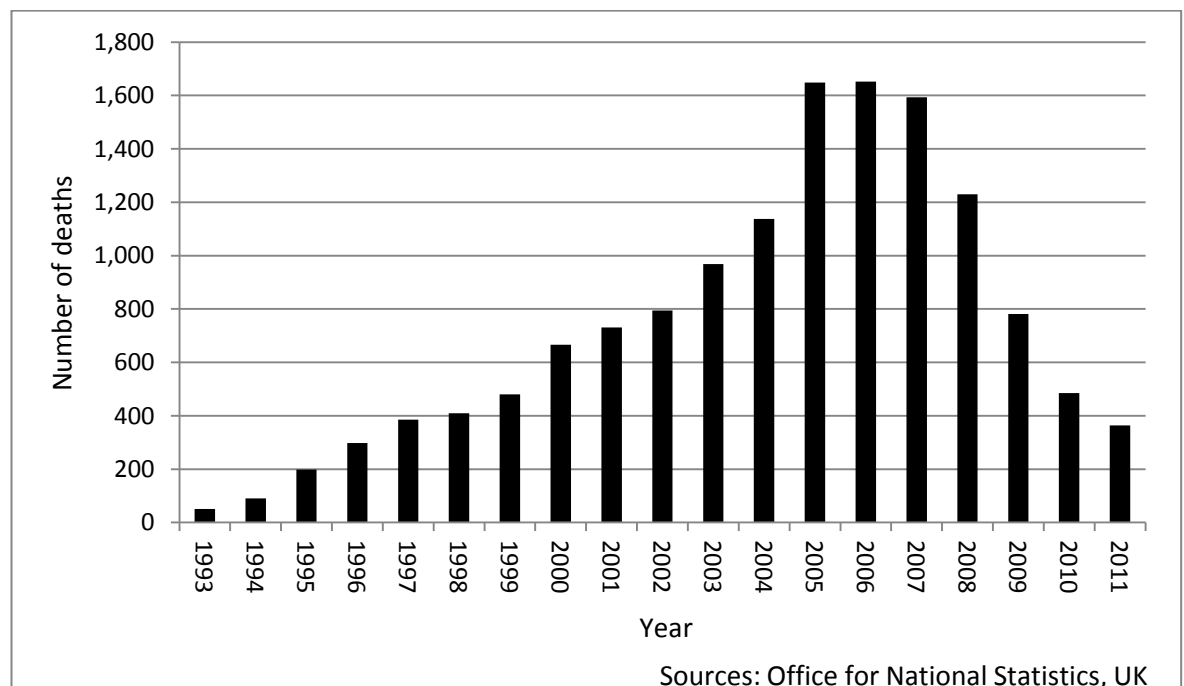
Figure 1.2 Age-standardised mortality rates for deaths mentioning Staphylococcus aureus: by methicillin resistance in England and Wales, 1993 to 2011 [17].

Despite the recent successes in tackling hospital-acquired MRSA in the UK and US [18], community-acquired MRSA cases in the USA has doubled in the past five years [19]. The lower number of infection cases, however, does not reflect the continual development

of resistance against antibiotics while they are being administrated in the clinic. Moreover, increasing cases of multidrug resistance development has been observed over a wide range of other bacterial pathogens such as *Escherichia coli* [20-21], *Mycobacterium tuberculosis* [22], *Pseudomonas aeruginosa* [23] and *Clostridium difficile* [24], etc. This has become a major concern and there are fears about imminent outbreak of infections cause by these pathogenic bacteria in the hospital settings and community.

1.1.3 Modern antibiotics discovery – strategies revised

During the 50s-60s, the golden era of antibiotics, discoveries of new antibiotics primarily relied on relatively empirical, trial and error methodologies [4]. These included cultivation of a wide range of soil bacteria (of the genus *Streptomyces*) from world-wide sources[25], and *in vitro* co-culture inhibition tests with the pathogenic bacteria. These traditional antibacterials from natural sources have predominantly been found to target a narrow subset of protein targets key to limited cellular processes such as cell wall synthesis, protein biosynthesis, DNA and RNA replication etc. [26].

The discovery of DNA, DNA sequencing and protein crystallography, and the advances in biology has allowed a much improved understanding of target-based medicine. The so-called "post-genomic era" of bioscience has profoundly changed the face of drug discovery. There is a general belief that utilisation of advance genomic technology could lead to discovery of a wider range of crucial housekeeping genes in bacteria vital to survival. By creating new drugs that target these novel housekeeping genes *via* chemical library screening and medicinal chemistry, it was believed we would be able to rapidly expand the repertoire of antibiotics at our disposal. However, this approach has serious disadvantages, with the limited structural diversity offered in existing chemical libraries and many novel targets discovered *via* genomic approaches proven to be ineffective[4].

It is argued by David et al [4] that the shift in the drug discovery strategy in the post-genomic era has led to the inefficiency in antibiotics discovery. To meet with the rising cost of drug research, exploring novel inhibitors targeting "old" established

antibacterial targets is currently deemed a more economical option for pharmaceutical companies and has gained momentum in recent years.

To ensure we are prepared for the battles with pathogenic bacteria in the coming decades, increased effort on discovery and development of novel antibiotics, narrow or wide spectrum, is urgently needed.

1.2. DNA topological problems

1.2.1 Twist, Writhe and Linking number

The existence of DNA topoisomerases in all known cellular organisms stems from the inherent topological problems created by the use of DNA as a genetic information carrier. DNA is a linear macromolecule consisting of two polymeric molecules intertwined with each other to form a double-helical spiral. The frequencies with which the two strands are wound together are described quantitatively by Twist (Tw) and Writhe (Wr) (fig. 1.3). The variation of Tw and Wr therefore determines the overall topological properties of the double helix.
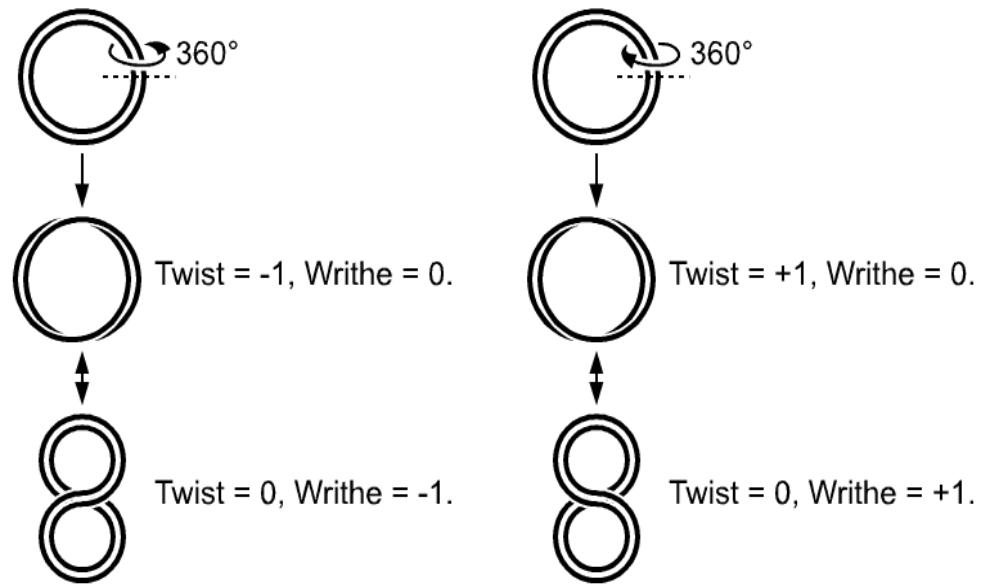
Figure 1.3 Introduction of twist and writhe in circular DNA. *The top-left and top-right of the figure depicts close DNA circle with zero linking number. Following double stranded breakage on the circular DNA (top-left), a 360° unwinding rotation on one end of the breakage and subsequent resealing. The circular DNA subsequently acquires -1 in Linking number and a negatively supercoiled state. The figure also illustrates two of the many possible topological states that the resultant -1 Lk circular DNA can adopt, -1 twist and 0 writhe (middle-left) and 0 twist and -1 writhe (bottom-left), both interchangeable to one another. The right-side of the figure depicts an opposite scenario, with positive supercoiling being introduced to the circular DNA by a +1 change in Lk number. **Figure is reproduced from Wheeler 2007 [27].***

Tw describes the frequency with which one strand of the double-helix wraps around the other with respect to the helical axis, while Wr describes the number of times the double-helix crossovers itself. In circular DNA or DNA with two ends immobilised, the topological system is closed. In this situation Tw and Wr are interchangeable, as depicted in figure 1.3. The sum of Tw and Wr give rise to an integral number called the linking number (Lk), which describes the number of times one strand of DNA wraps around the other:

Lk = Tw + Wr

A fully relaxed segment of DNA has a topological state of the lowest energy (Lk_0) and the linking number is approximately equal to the number of base pairs (N) divided by the periodicity of DNA helix (~ 10.5 bp/turn):

$$Lk_0 \approx N / 10.5$$

In a circular DNA molecule, a linking number below Lk_0 mean a decrease in the sum of Tw and Wr, resulting in negatively supercoiled DNA with right-handed crossovers. The number of bp per turn may increase thus the DNA base stacking is weaker at Lk_0. Linking numbers above Lk_0 results in an increase in the sum of Tw and Wr. Increases in linking numbers equate to increases in left handed positive supercoils on the DNA and DNA base stacking. The majority of chromosomal DNA displays characteristics of a closed or semi-closed topological system due to the compact nature of the chromosome and the hindrance of DNA-binding proteins. In these closed topological systems, protein binding and DNA unwinding during cellular processes such as DNA replication and transcription can produce a "ripple" of negative and positive supercoils. The imbalance of the supercoiling distribution can have a major effect on the cell's survival.

1.2.2 Biological importance of DNA topology

In order for the genetic information to be accessed and replicated, unwinding of the DNA double helix is necessary to allow the recognition of the internal nucleotide sequences by protein complexes. In the course of DNA replication and transcription, protein complexes process DNA and travel downstream at a high speed [28]. As the transcription or the replication fork advances, the rapid DNA unwinding generates an enormous twist on both the downstream and upstream of the DNA strands. The build up of twist generates an opposite writhe and create various forms of torodial and plectonemic DNA superstructure (fig. 1.3). Downstream of the DNA fork, positive supercoiling can build up [29], while precatenates and negative supercoiling accumulate upstream of the DNA fork during replication and transcription respectively (fig. 1.3).
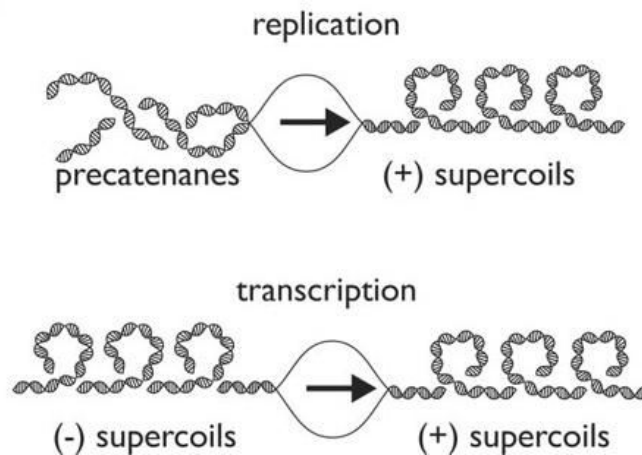
Figure 1.4.Schematic diagram showing the build-up of secondary DNA structure caused by topological stress in DNA processing events. *Precatenates and negative supercoiled DNA accumulate upstream of the DNA fork in DNA replication and transcription, respectively. Positive supercoils are found on the downstream of the fork in both events [30].*

Accumulation of these local strains and high energy DNA structures can prevent the progression of transcription [29] and/or the replication fork [31] thus inhibiting cell growth and replication. DNA topological problems could arise towards the end of the circular chromosomal DNA replication in prokaryotes as two closed, interlinked circular daughter DNA molecules will unavoidably be produced [32]. Unlinking of this catenated DNA is need for successful chromosome segregation during cell division. Similarly in DNA recombination events, knotted and catenated DNA could be generated and unlinking of these DNA structures are required prior to the partition of cells [33]. These topological problems often arise from DNA processing events is detrimental to cell survival. Nature has therefore evolved a wide range of topoisomerases to perform DNA linking and unlinking reactions to solve these problems [34].

1.3. DNA topoisomerases

1.3.1 Major types of topoisomerases

DNA topoisomerases can be divided into two major classes, type I and type II, distinguished by the changes in linking number (Lk) introduced in the DNA substrates per reaction: type I introduces +1/-1 Lk, while type II produces +2/-2 Lk in each reaction [35]. They are further divided into five subtypes according to their overall structural distinction: IA, IB, IC, IIA and IIB (fig.1.4).

As a result of convergent and divergent evolution, organisms have evolved and inherited a unique set of topoisomerases[36]. In general, cellular organisms possess at least one type I and one type II topoisomerase. While some organisms can possess up to four different topoisomerases with overlapping functions, the entire set of DNA topoisomerases are usually required to compensate each other for the survival of the organism (fig. 1.4). In *E. coli*, DNA gyrase is mainly responsible for negative supercoiling of DNA, while topo IV is mainly responsible for DNA decatenation and has a minor role in DNA relaxation. While *E. coli* DNA gyrase has decatenation activity, it is too weak to compensate for the function of topo IV *in vivo* [37].
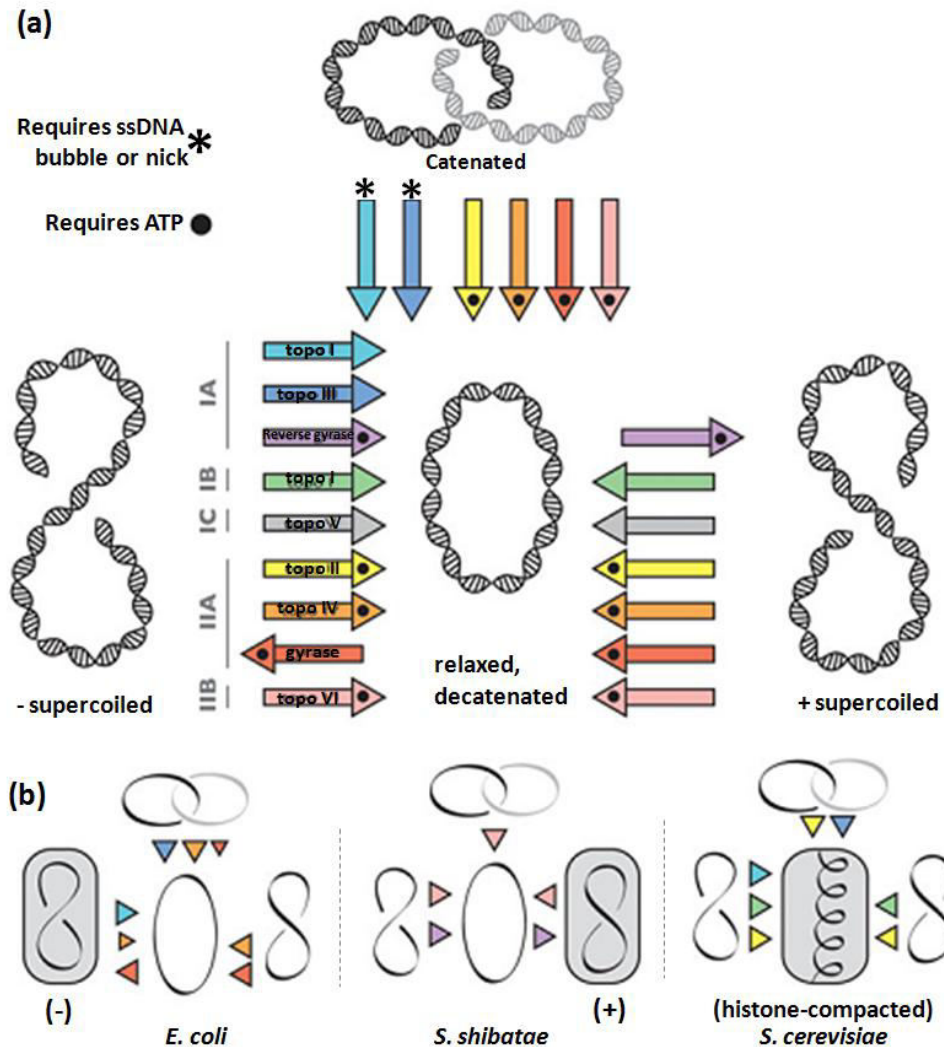
Figure 1.5 Various classes of topoisomerases performs overlapping functions in the maintenance of cellular DNA topology. Reproduced from Schoeffler & Berger 2008 [38].

 (a) DNA modifying activities of various families of DNA topoisomerase are displayed in colour coded arrows. Different DNA topoisomerases are capable of carrying out DNA negative supercoil relaxation (left to centre), positive supercoil relaxation (right to centre), decatenation (top to centre), positive and negative supercoiling (centre to right and centre to left). ATP co-factor and ssDNA requirements for particular activities are indicated.

(b) Examples of topoisomerase activity complements in E. coli, S. shibatae and S. cerevisiae. The colours of the triangles correspond to the colour keys displayed in (a), demonstrating the type of topoisomerases presence in each organism [30]. The overall topological state of the chromosome in each organism is highlighted with a grey box. E. coli and S. shibatae chromosomes are topologically biased as a result of the presence of the DNA negative and positive supercoiling enzymes, DNA gyrase and reverse gyrase respectively. S. cerevisiae does not possess DNA supercoiling enzymes; its overall supercoiled state of the chromosome is achieved by wrapping of DNA around histones in a positive sense.

10

1.3.2 Type I topoisomerases

Type I topoisomerases carry out transient backbone breakage on one strand of the substrate DNA through a transesterification reaction and enable changes in the linking number of the substrate DNA by +/-1 on each round of reaction. Type I topoisomerases can be further divided into IA, IB, IC. Type IA topoisomerases include topo I, topo III and reverse gyrase. They all possess a toprim fold, a protein domain conserved in primase and type IIA topoisomerase (topo IIA), critical for the catalytic function of the enzyme. They carry out DNA unlinking reactions by enabling the passage of a single strand of intact DNA through the transiently broken strand. As topo I and topo III reactions do not require ATP hydrolysis, they are only able to modify DNA towards topology with ground state energy. The ability to carry out single strand DNA passage enables both topo I and topo III to remove catenated DNA. Unlike topo I & III, the archeae enzyme reverse gyrase utilises ATP and is the only topoisomerase known to produce positive supercoils [39].

Conversely, type IB and type IC topoisomerases induce DNA topology changes through transient breakage of a single strand DNA backbone, followed by the rotation of the broken strand around the intact strand and the subsequent resealing of the broken strand [40]. Similar to type IA topoisomerase, this mechanism is energy free and the DNA substrate will result in a more relaxed state post-reaction. Hence, the cellular role of most type I topoisomerases is to relax DNA.

1.3.3 Type II topoisomerases

Type II topoisomerases utilises a "two-gate" DNA strand passage mechanism to unlink DNA [41]. This involves transient transesterification breakage on both strands of a DNA segment (G or Gate segment) to create a four base staggered breakage, followed by the passage of an intra/intermolecular DNA segment (T or transported segment) through the two broken ends of DNA and the subsequent resealing of the cleaved DNA [42]. Most type II topoisomerase reactions require ATP hydrolysis to induce the necessary conformational change for the passage of the T-segment DNA.

Type IIA topoisomerases are conserved in bacteria and eukaryotes but absent in archea. This suggests that these enzymes evolved after the divergence of eubacteria. Type IIA topoisomerases (topo IIA) of eukaryotes consist of one dimer, whereas prokaryotes topo IIA consist of two pairs of dimers. Despite the differences, both eukaryotic and prokaryotic topo IIA enzymes have a highly conserved domain organisation (fig. 1.5). The availability of crystal structures of *E. coli* gyrase [43-46] and topo IV [47-48], and *S. cerevisiae* topo II fragments [49-51] showed type IIA topoisomerases to share highly conserved protein folds despite the difference in protein sequences.
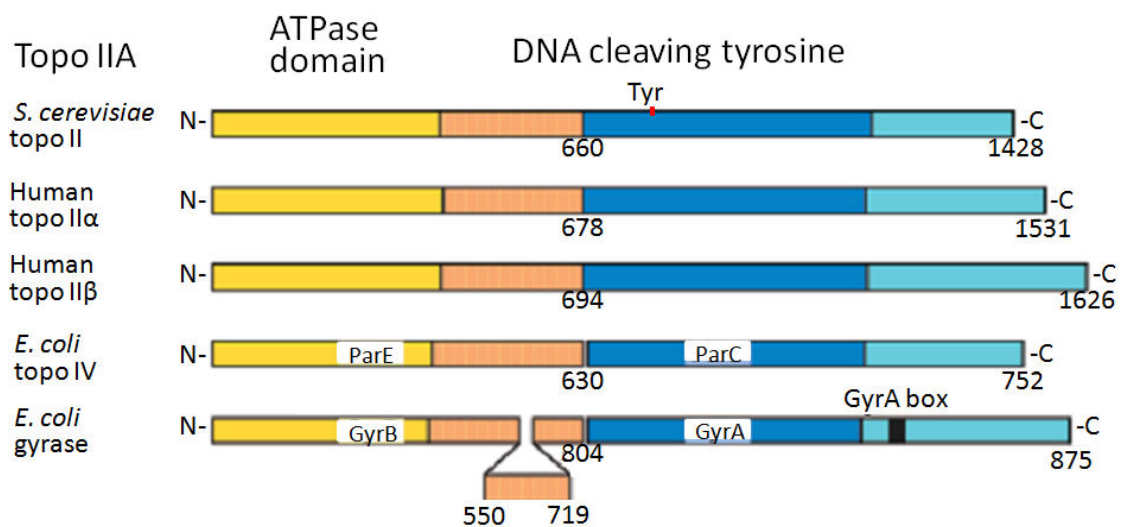
Figure 1.6 Domain structure and alignments of type IIA topoisomerases. *The yellow and orange colours represent the ATPase and C-terminal domains of GyrB. Blue and cyan represents the NTD and the CTD of GyrA. E. coli GyrB has an additional ~170 amino acid of unknown function as an insert in the CTD. Note: domain structure display above is the monomers of each of the Topo IIs, a functional Topo II require two sets of monomers. Taken from Bates and Maxwell, 2007* [52].

Topo VI is the only enzyme from the type IIB category and its existence is confined to plants, archea and plasmodia [38].

1.4. DNA gyrase

DNA gyrase is a widely conserved bacterial DNA topoisomerase. It belongs to the family of type IIA topoisomerases and is the only topoisomerase capable of generating negative DNA supercoils in an ATP-dependent manner [53]. Although its major function is to carry out DNA negative supercoiling and relaxation of positive supercoils, DNA gyrase is highly versatile and can demonstrate weak relaxation and decatenation activity [54]. Intriguingly, for reasons not yet known, gyrase is the only type II topoisomerase able to relax negatively supercoiled DNA in the absence of ATP [55].

A functional DNA gyrase enzyme consists of two subunits, GyrA and GyrB, which, in the presence of the DNA substrate, form an A_2B_2 tetramer-DNA complex. The binding of the gate-segment (G-segment) DNA to the A_2B_2 tetramer is followed by the T-segment DNA wrapping around the exterior of the cylindrical GyrA C-terminal domain (CTD) beta-propeller fold[56] (fig. 1.6). The wrapping motion presents a T-segment DNA towards the N-gate, which is then captured by the N-terminal domain (NTD) of GyrB during a range of conformational changes coordinated by the binding and hydrolysis of ATP. The capture of T-segment DNA triggers a series of events resulting in the transient cleavage of the backbone of both strands of DNA. This creates a four base stagger, allowing the DNA-gate to open and the passage of the captured T-segment DNA through the cleavage. The subsequent closure of the DNA-gate and the exit of the T-segment DNA *via* the C-gate completes the reaction cycle and produces a change of -2 to the linking number of the DNA substrate.

Top-down view

ATPase

T-segment

G-segment

T-segment

CTD

A

B

PDI

1

2 ATP

2

- 2 (ADP + Pi)

T-segment

3

C-gate

N-gate

DNA-gate

4

5
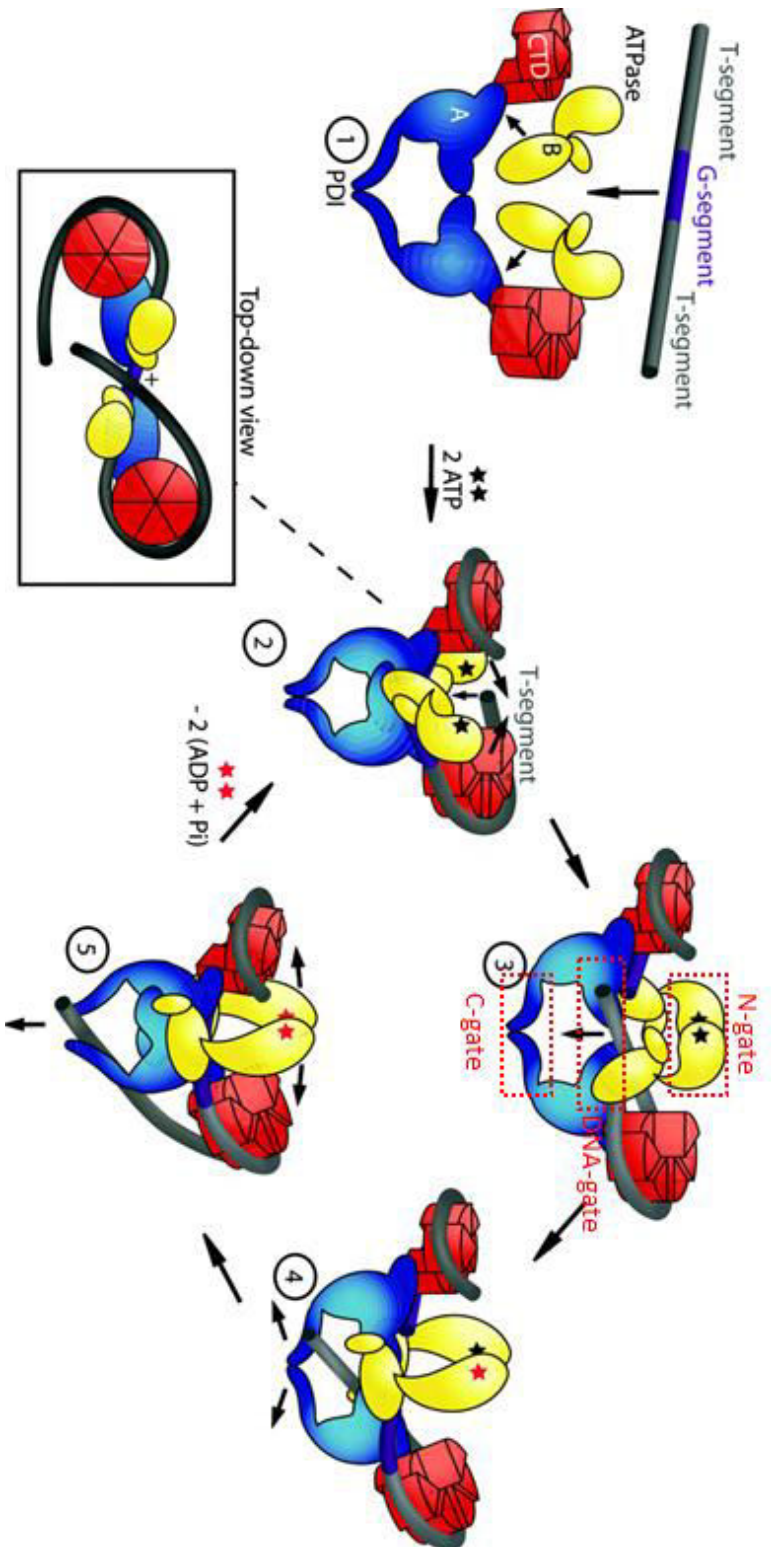
Figure 1.7 Illustration of the DNA gyrase supercoiling reaction cycle. 1. *The capture of the G segment and the assembly of A_2B_2 tetramer.* **2.** *The captured DNA wraps around the CTD of GyrA and positions the T segment DNA between the two assembled GyrB dimers. Binding of one ATP per B subunit allows the release of the N-terminal straps.* **3.** *Binding of both straps to the opposing B subunit causes closure of the N-gate and may exert strain to activate the G segment cleavage and force the opening of the DNA gate. The T segment is forced through the cleaved G segment DNA.* **4.** *Passage of the T segment through the DNA gate is followed by the closure of the DNA gate and reunion of the G segment.* **5.** *The opening of the exit-gate allows the escape of the T segment. The hydrolysis of the second ATP and the release of 2 ADP and Pi reset GyrB and reopens the N-gate. Gyrase either disassembles or carries out another cycle of the supercoiling reaction. The figure is reproduced from Ruthenburg et al 2005 [46].*

14

1.4.1 Structural aspects of DNA gyrase

Each B subunit of DNA gyrase consists of the N-terminal GHKL (Gyrase, Hsp90, Histidine Kinase, MutL) ATPase domain (fig. 1.7) [58], the transducer domain, the Toprim domain and the C-terminal tail domain [59]. The ATPase activity of the GHKL domain requires Mg^{2+} as a co-factor [60] while monovalent ions such as sodium or potassium are implicated as a possible co-factor [61]. The conformational changes induced by ATP hydrolysis of this domain are transmitted towards the C-terminal portion of GyrB, which is essential to the strand passage and the supercoiling activity of gyrase [46,62]. At the C-terminus of the transducer domain is the Toprim domain. It is a protein fold conserved in type IA and type II topoisomerases [63], and primases [64], which plays a major role in the catalytic activity of these enzymes. The characteristic DXDXD motif within the Toprim domain (D498-D502 in *E. coli*) can hold one Mg^{2+}, while two Mg^{2+} ions are bound to this region in the presence of the G-segment DNA [65]. This transition is suggested to be crucial to facilitating the DNA cleavage reunion reaction [66-67]. The tail domain of GyrB makes extensive contacts with GyrA.
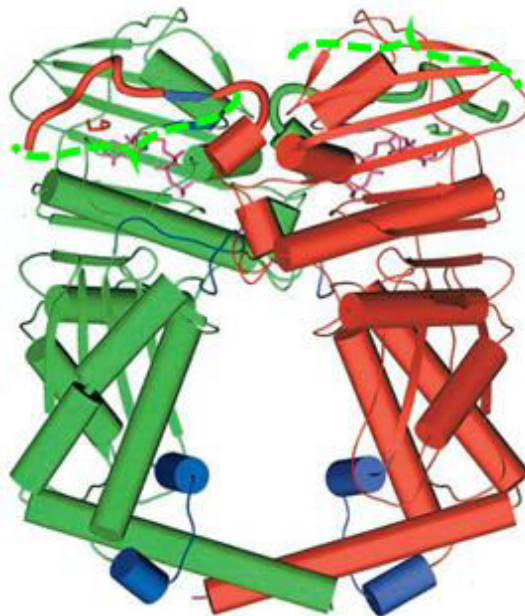
Figure 1.8. Ribbon representation of the crystal structure of a dimerised E. coli GyrB N-terminal fragment in the presence of ATP. *The N-terminal "straps" (the extended structures indicated by the two bright green dotted braces) from each monomer (red and green) were extended to bind to the other monomer to form a dimerised structure in the presence of ATP (magenta) [46]. [68]*

In addition, it was observed in a crystallographic study of gyrase-DNA complex that Ile 833[69], which is surface-exposed and located in a domain equivalent to the tower

motif of GyrA-NTD, intercalates between +4 and +5 bases on both arms of the G-segment DNA [51]. The intercalation appeared to induce a strong DNA distortion by causing a rotation of 70° of DNA on each arm of the G-segment DNA [70]. This bending was later confirmed in eukaryotic topo II by a FRET study [71], although the exact role of the bending in the function of the enzyme is yet to be established; substitution of the isoleucine with alanine completely abolishes relaxation activity of the enzyme. This intercalation appears to "staple" the G-segment DNA to the GyrA subunit, thus enabling stabilisation of the catalytic complex and remotely assists the DNA-enzyme transesterification reaction.

The A subunit of gyrase consists of two main separately folded domains: the NTD which forms part of the GyrA-GyrB interface [72] (fig. 1.8a blue) and the CTD which has a characteristic beta-propeller fold [57], essential for DNA wrapping (fig. 1.8a red) [73-74]. Under physiological conditions, the GyrA subunit exists as a stable homodimer [75] and helix-3 of the winged-helix-domain (WHD) motif of the N-terminal domain forms a crucial dimer interface and "the DNA gate" [44]. The closure of this dimer interface allows the formation of the DNA "saddle" [44]. This "saddle" together with the Toprim domain of GyrB forms the DNA channel that accommodates the G-segment DNA. The catalytic Tyr122 of GyrA is critical for the transesterification reaction [76] and is located in the WHD domain of GyrA. This tyrosine is positioned adjacent to the DXDXD motif of the GyrB toprim domain when the A_2B_2 tetramer is assembled [51].
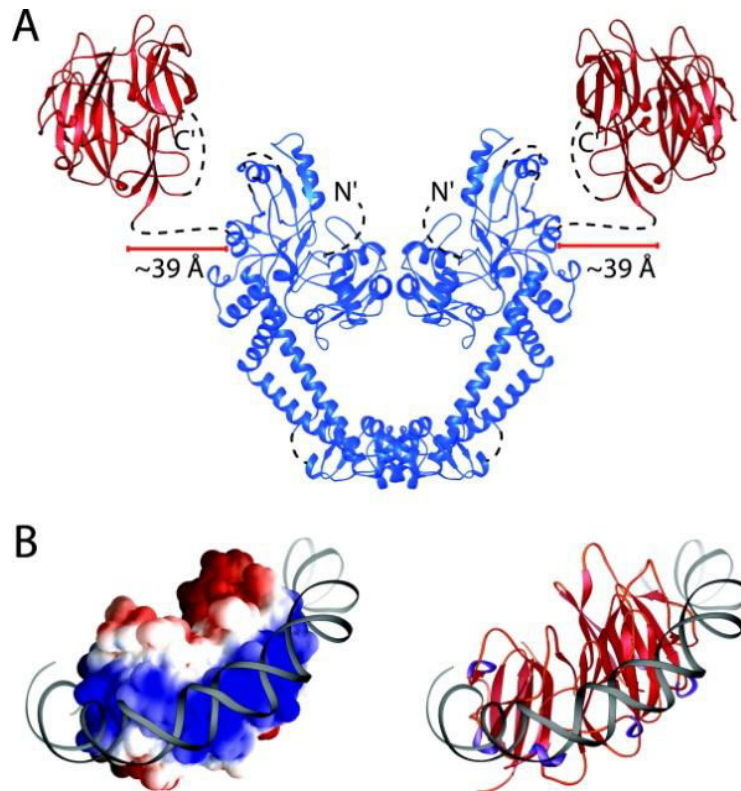
Figure 1.9. Domain structure organisation of DNA gyrase
A. *The crystal structure of GyrA NTD and CTD are shown in blue and red, respectively.*
B. *Illustrative diagram of DNA wrapped onto the electro-positive circumference of GyrA-CTD, in electrostatic colour-coded molecular surface (bottom left) and ribbon (bottom right) representations. Reproduced from Ruthenburg et al 2005 [57]*

Towards the C-terminus of the N-terminal domain (NTD) of GyrA, a coiled coil motif protrudes out of the major globular fold to form the second dimer interface or the "exit gate" [44] (fig. 1.8a). The CTD of GyrA is a separate a six-bladed beta-propeller structure[57] connected with the NTD through a 15 amino acid flexible linker region [77]. This special cylindrical fold allows the T-segment DNA to wrap around the electropositive surface in a positive sense (fig. 1.8b) [57], which is critical to the ability for gyrase to negatively supercoil DNA. While the CTD of all gyrases were found to have six blades and adopt a full beta-propeller fold, the CTD of topo IVs have a varying number of blades and often have an incomplete beta-propeller fold [48]. The missing blades in the CTD of topo IV has led to its inability to wrap DNA and thus carry out supercoiling.

1.4.2 Mechanistic aspects of DNA gyrase

1.4.2.1 Two-gate strand passage mechanism

It was first proposed by Roca et al [78] that in order for type II DNA topoisomerases to function without inducing DNA damage, a "two-gate" mechanism is required for the double-stranded DNA passage to ensure the religation of the transiently cleaved DNA. While the gate that controls the cleavage of the DNA is open to allow the passage of the second DNA segment, the second gate has to be closed to ensure the integrity of the enzyme-DNA cleavage complex and prevent dsDNA breakage from occurring [79-80].

In fact, DNA gyrase possesses three "gates" in the symmetric axis of the tetramer: the Amino-terminal-gate (N-gate) of the NTD of the GyrB dimer, the DNA-gate that guards the separation of the transiently cleaved G-segment DNA, and the C-gate of protruded segment of the GyrA dimer (fig. 1.6). These three gates operate sequentially during a strand passage reaction to allow passage of a T-segment DNA through the centre of the A_2B_2-DNA complex without disintegration of the enzyme.

DNA gyrase can perform dsDNA strand passage (including DNA cleavage and religation) in the absence of the N-gate, as reconstituted mutants with the NTD of GyrB truncated still demonstrate weak relaxation activity [81]. This shows strand passage in gyrase to operate as a two-gate enzyme, albeit inefficiently. DNA gate is crucial to the function of the DNA gyrase as it controls the double-stranded cleavage of DNA and the separation of the two transiently-cleaved DNA ends during a supercoiling reaction. C-gate forms a crucial second interface between the GyrA dimer independent of the DNA-gate. It is therefore proposed to be vital to the integrity of the the Gyrase-DNA complex during the opening of DNA-gate. This strand-passage mechanism is the core function of gyrase and is conserved in topo IIA enzyme (including topo IV and eukaryotic topo II) across all species.

1.4.2.2 ATP-dependent capture of the T-segment DNA in a DNA-wrapped gyrase complex

Following the capture of the G-segment DNA and the assembly of the A_2B_2 tetramer, the wrapping of the end of the G-segment DNA on the CTD [82] allows the T-segment to

be positioned into the cleft between the two GyrB subunits in their nucleotide-unbound state.   At this stage, the ATPase domain of GyrB is in equilibrium between the ATP-bound and -unbound states. In the ATP-bound state, the ~20 amino acid N-terminal "strap" of both B subunits bind to the binding site in the opposing B subunit to form the DNA clamp or the N-gate [83]. Once the T-segment DNA makes contacts with the B subunits, it triggers the ATP hydrolysis reaction by activating the ATPase activity of the GHKL domains [84-85]. Although the role of ATP hydrolysis is unclear, its structural homolog, topo VI, has a dramatically different conformation in the interface between the ATPase domain and the transducer region in the ATP- and ADP-bound states.   The linker helix that connects both domains is found to swing outwards by 11° during ATP hydrolysis (fig. 1.9) [86]. It is therefore possible that in gyrase, this movement induced by ATP hydrolysis could transmit strain towards the DNA gate activating the cleavage reaction, the opening of the DNA gate and the passage of the T-segment.
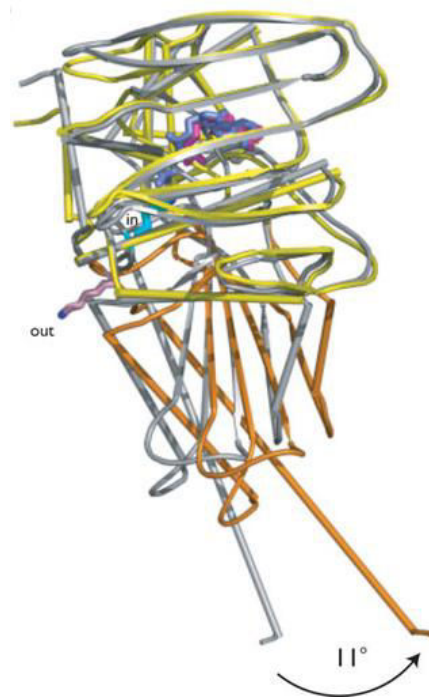
Figure 1.10. Ribbon representation of topo VI GHKL domain, homologous to type IIA topoisomerase, demonstrating the 11° movement in the transducer domain from the ATP (grey) to the ADP (orange) bound state. [30,86]

19

1.4.2.3 Phospho-tyrosyl transesterification reaction

Prior to the passage of the T-segment, the transesterification reaction between the two catalytic tyrosines, one from each GyrA monomers, and the 5′phosphate group on both DNA backbones four bases apart from each other is needed to introduce the double-strand break. Prior to the reaction, the DXDXD motif of GyrB, the reactive tyrosine residue of GyrA and the phosphate group of the scissile DNA backbone have to be in close proximity to form the pre-reaction complex [51] (fig. 1.10). The reaction is then initiated by a nucleophilic attack from the activated tyrosine hydroxyl group onto the phosphate group. Once the tyrosine-phosphate bond is formed, a 3′OH group of the backbone sugar is found after bond breakage [76]. The overall result of this reaction will leave a 5′ backbone phosphate on each strand of the G-segment DNA covalently linked with the hydroxyl tyrosine group (Tyr122 in *E. coli* gyrase) of each GyrA subunit and result in a staggered 4 base double-stranded DNA cleavage.
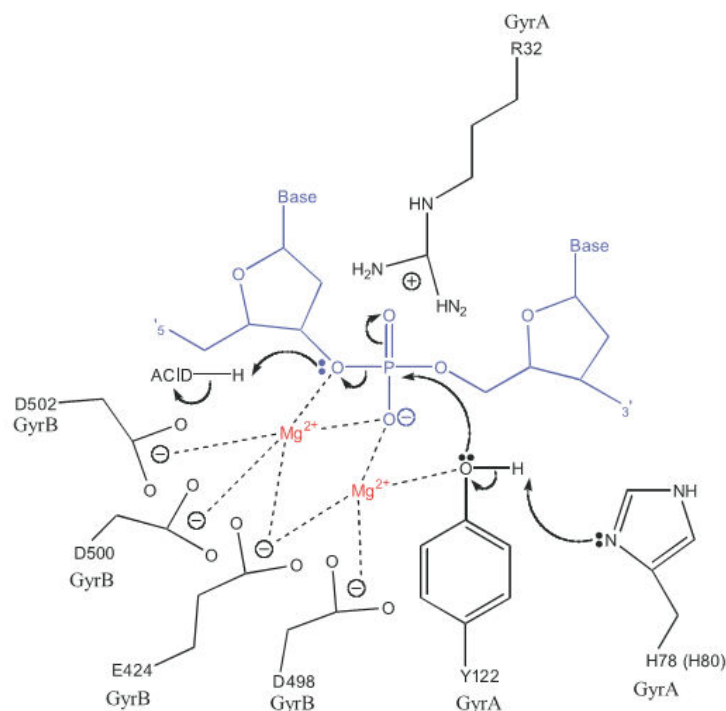
Figure 1.11. An illustrative model of the DNA cleaving catalytic complex formed between residues from the DXDXD motif of GyrB (E424, D498, D500, D502), *GyrA (R32, H78, Y122) and the scissile phosphate group from the DNA stabilised by two Mg^{2+} ions.* [66]

The DXDXD motif of GyrB is responsible for holding Mg^{2+} ion(s) involved in the stabilisation of the reaction complex [66] (fig. 1.10). The exact molecular context of the Mg^{2+} ion(s) within the reaction complex is unclear, although it can bind to oxygen atoms from either the backbone phosphate, the tyrosine residue or a reactive water molecule, as suggested in various hypothetical models [67]. The physical properties (*e.g.,* radius, charge density, hardness) of this divalent Mg^{2+} ion is critical to the equilibrium of the reaction as replacement with other divalent metal ions alters the nature of the reaction, *e.g.,* calcium induce DNA cleavage as it is poor at promoting the DNA religation reaction [67,87]. There has been a debate over whether one or two Mg^{2+} ion(s) is/are involved in the religation reaction. One hypothesis states that although two Mg^{2+} are involved with the reaction, only one Mg^{2+} is stably incorporated with the enzyme, while the second Mg^{2+} is more dynamic and could escape depending on the state of the reaction [65,67].

1.4.2.4 Passage of the T-segment DNA, closure of the DNA gate and conformation reset

Following the cleavage of the G-segment DNA and the opening of the DNA gate, the T-segment DNA is passed through the two cleaved staggered ends of the G-segment DNA. After the T-segment passes the DNA gate, it remains in the cavity between the DNA gate and the exit-gate until the DNA gate is fully shut. It is unclear how the opening of the exit gate is operated, although it is proposed that it is opened after the closure of the DNA gate [30]. The exit gate opening allows the T-segment to escape. The subsequent release of 2 ADP and 2 inorganic phosphate (P_i) ions resets the GyrB back to its unbound state and reopens the N-gate. The enzyme then either continues another cycle of strand passage on the same DNA segment or becomes disassembled, depending on the supercoiled state of the DNA [88]. Processivity between reaction cycles is dependent on the availability of ATP [88].

One round of completed intra-strand passage reaction results in a more negatively supercoiled DNA substrate with a change of -2Lk.

1.4.3 Cellular role of DNA gyrase

As mentioned previously, during DNA processing events such as replication and transcription, rapid DNA unwinding is required to allow access to the internal nucleotides. As a result, torsional stress can accumulate up and downstream of the progressing DNA fork. In this situation, DNA gyrase is employed to actively remove the downstream positive supercoils by introducing negative supercoils. In the absence of gyrase, a torsional stress can build up on the DNA and this can become critical to the progression of replication and transcription [89].

Another important function of DNA gyrase is to maintain the underwound state of the bacterial chromosome, especially during log phase growth [90]. Relaxed DNA requires high energy for the formation of a localised "DNA bubble", which contains DNA strands that can be readily melted and separated for the initiation of transcription and replication [91]. Maintaining DNA in its negatively supercoiled state allows easier formation of these "DNA bubbles" and permits greater access of protein complexes to chromosomal DNA during transcription and replication, thus favouring cell growth.

The maintenance of this superhelical state is suggested to be controlled by the cellular ATP/ADP ratio, and this is be affected by the difference in growth conditions *i.e.,* temperature[92], pH and the availability of nutrients. As gyrase activity is closely linked to the cellular ATP/ADP ratio [93-94], these external conditions could mediate changes to the hyperhelicity of the chromosome through altering gyrase activity. Often as a result of changes in superhelicity, gene expression patterns are affected and therefore gyrase can act as a gene expression regulator and controls gene expression in response to changes in external conditions. For example, the aerobic and anaerobic growth of *Salmonella typhimurium* is controlled by DNA gyrase and topo I activity, respectively, where mutants with defective gyrases will only grow in anaerobic conditions [95]. In addition, the reduced gyrase activity in anaerobic growth of bacteria is reflected by the fact that anaerobically grown bacteria are less susceptible to quinolones[96].

1.5. Topoisomerase IV

Topo IV is another conserved bacterial type IIA topoisomerase that usually coexists with gyrase. Different from DNA gyrase, it does not supercoil DNA. Instead topo IV is extremely efficient at relaxing and decatenating DNA. Topo IV is crucial to cell division due to its decatenation ability which assists segregation of the chromosome. It has a domain structure analogous to gyrase and consists of two subunits, ParC and ParE subunits (alternatively known as GrlA and GrlB), and forms a tetrameric A_2B_2 enzyme.

1.5.1 Structural differences between topo IV and DNA gyrase

While GyrA-CTD consist of a conserved six bladed beta-propeller domain structure across species, the number of blades found in the CTD of ParC is more variable [48]. The CTD of ParC in a number of organisms has 4 or 5 blades. In certain cases it is completely truncated, similar to a eukaryotic topo IIA. Evidence from a structural study suggested ParC CTD appears as a broken beta-propeller and forms a partial cylindrical structure. The inability to form a completed beta-propeller is suggested to led to topo IV's inability to bend DNA and carry out supercoiling similar to DNA gyrase [97].
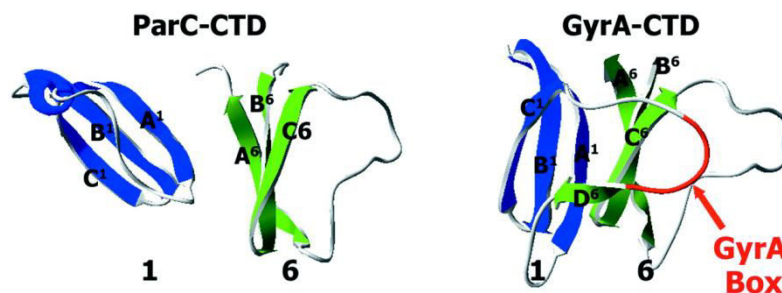
Figure 1.12 Diagram showing the difference in the interfaces between blade 1 and 6 in B. stearothermophilus ParC-CTD and B. stearothermophilus GyrA-CTD represented in ribbon structure. *The GyrA box is labelled in red. Figure is reproduced from Hsieh et al 2004 [97].*

Despite *E. coli* topo IV having a six bladed ParC-CTD, sequence comparison and mutant studies found ParC-CTD to lack the "GyrA box" (fig. 1.11) [98], a stretch of 7 amino acids located in blade 1. This is consistent with the fact that the removal of the GyrA box in gyrase has a deleterious effect on its supercoiling activity [98]. Further evidence from a structural study suggests the GyrA box to form a crucial interface between blade 1 and blade 6 [97] and as a result topo IV ParC-CTD is unable to form a fully cylindrical beta-propeller fold (fig. 1.11) thus can not perform DNA wrapping required for intra-molecular strand passage.

1.5.2 Mechanistic aspects

Similar to DNA gyrase and all topo IIA enzymes, topo IV carries out transient double-strand breakage and dsDNA passage by utilising the "two gate" mechanism. Although its overall protein folding and mechanistic action is somewhat similar DNA gyrase, it does not generate DNA supercoils but instead performs DNA relaxation and decatenation.
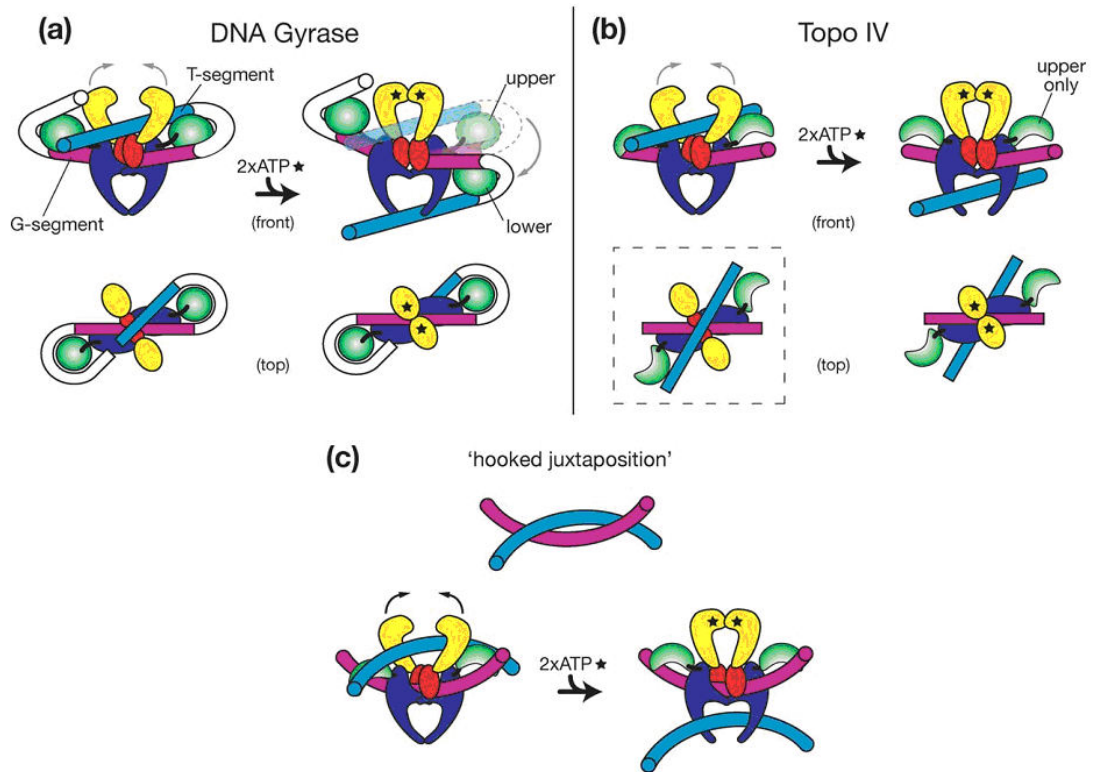
Figure 1.13 The differences between gyrase and topo IV in DNA substrate recognition*. The DNA clamp of the NTD of the B subunit is coloured yellow. Red represents the CTD of the B subunit. Blue and green is the NTD and the CTD of the A subunit respectively. (a) Wrapping of DNA around the CTD of GyrA in DNA gyrase and the intra-strand DNA passage. (b) Recognition of DNA hooked juxtaposition by topo IV ParC CTD and inter-strand DNA passage. (c) Recognition of DNA hooked juxtaposition by topo IV [99].*

This difference of enzymatic function in topo IV stems from the lack of "GyrA box" in the CTD of ParC as mentioned previously, which affects the preference of substrate DNA. Instead of wrapping DNA around its CTD and negatively supercoiling DNA by intra-strand passage, the CTD of topo IV is proposed to bind to the T-segment DNA carrying out inter-strand DNA passage to relax and decatenate DNA efficiently in a ATP-dependent manner (fig. 1.12). One hypothesis stated that topo IV ParC-CTD promotes preferential binding to DNA with the hooked juxtaposition[100], a DNA geometry predicted to be ubiquitous in tightly wound, knotted or catenated DNA. This could explain the enzyme's catalytic preference.

1.5.3 Cellular role

Topo IV is an essential enzyme for successful chromosome segregation and cell division in most prokaryotes. The replication of a circular chromosome and recombination events produce catenated and knotted DNA and topo IV is required to resolve these problems by performing DNA unlinking reactions [101]. In addition, topo IV is an efficient DNA relaxing enzyme and has a secondary role of supporting the elongation of the DNA fork during replication and transcription by removing negative supercoils and precatenates in the upstream region of the DNA fork [102].

M. tuberculosis is one of the rare exceptions that lack a topo IV [103] although its DNA gyrase appears to function similar to a hybrid between a normal gyrase and topo IV[104] and covers functions of both enzymes depending on its reaction conditions.

1.6 Gyrase-targeting antibacterial agents

The function of gyrase involves the dangerous act of cleaving and religating dsDNA. The completion of this process is crucial to the survival of the cell as failure to religate cleaved DNA can lead to permanent DNA breakage and chromosome fragmentation. This mechanism can be utilised to our advantage, by developing agents that inhibit the DNA reunion step of these enzymes and turning them into potent antibacterial agents. Quinolones are a classic example of bacterial topo II "poisons", which mediate bactericidal action by inhibition of the DNA reunion reaction and turning gyrase and topo IV into "poisons", inducing cellular DNA breakage. Due to the ubiquitous presence of gyrase and topo IV in prokaryotes, most of the known bacterial topo II inhibitors tend to be effective against a wide spectrum of bacteria.

Despite the huge variety of quinolone analogs reaching the clinic since the first introduction of nalidixic acid in 1962, there has been little success in the discovery of other classes of gyrase/topo IV-targeting drugs. Given the example of the clinical and commercial success from quinolones and the fact that bacterial topo II has been a relatively under-exploited target compared to other anti-bacterial strategies, bacterial topo II targeting agents still have enormous developmental potential.

1.6.1 Quinolones

Quinolones are the most successful gyrase/topo IV inhibitors ever introduced into the clinic. As a class of antibacterials, quinolones are worth almost a quarter of the entire antibacterial drug market, with the best selling drug Cipro (ciprofloxacin) currently worth over $1bn in gross annual sales. The success of quinolones has been contributed by their effectiveness for treatment against a wide spectrum of bacterial pathogens as well as the excellent safety profile and good ADMET (absorption, distribution, metabolism, excretion and toxicity) properties. In 1962 , the first quinolone, nalidixic acid [105], a derivative of quinoline, was discovered and found to be an excellent antibacterial agent. Since then, hundreds of analogues with improved potency against both gram-negative and gram-positive pathogens have been produced (fig.1.13) and they can generally be classified into generations I, II, III and IV. The first generation of quinolone was initially used for urinary tract infections and was mainly restricted to anti-gram-negative treatments due to its poor efficacy against gram-positive pathogens [106]. The second generation quinolones had improved serum distribution over the first generation plus improved potency against gram-negative organisms thus are suitable for a wider range of indication [106]. In spite of that they are only mildly effective against most gram-positive pathogens. The third generation quinolones have an improved gram-positive coverage and potency against atypical pathogens [106]. The fourth generation quinolones have similar properties to the third generation with additional coverage against anaerobes [106].
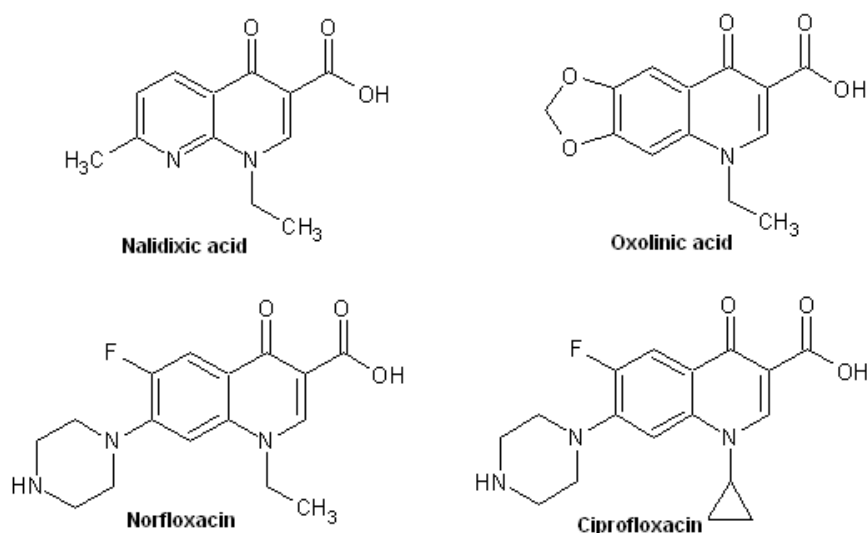
Figure 1.14 Chemical structures of various quinolone drugs

1.6.1.1 Quinolone-induced ternary complex, polymerase collision and oxidative damage

Whilst quinolones inhibit the catalytic activity of gyrase and topo IV, their potency is mainly attributed to the DNA damage they induce [107]. By inhibiting the DNA religation process of gyrase/topo IV, quinolones trap gyrase/topo IV on DNA to form a stable quinolone-DNA-enzyme ternary complex [108]. As the 5′ phosphate group of the cleaved DNA is covalently attached to the enzyme in the ternary complex, its collision with the advancing replication or transcription complex can generate DNA double-strand breaks[109]. While collisions with polymerase can occur, most of the advancing DNA fork is proposed to stall by the excessive torsional strain on DNA as a result of gyrase inhibition, before the collision happens [110]. It is suggested that the DNA repair mechanism recognises the stalled DNA forks and in an attempt to restore these DNA structures, DNA damage may be generated. On the cellular scale, the DNA damage can lead to chromosome fragmentation and cell death.

In addition, DNA damage induced by quinolones was found to generate high energy free radicals at each end of the broken bond [111]. They then trigger an oxidative chain

reaction that inflicts further damage to DNA, protein and induces the SOS responses [111].

1.6.1.2 Preference of quinolone drugs in targeting gyrase/topo IV

While gyrase is the primary target of quinolones in *E. coli* [112] and other gram-negative organisms, [113-115] for the majority of quinolones developed (80-90%) the target preference is reversed in gram-positive bacteria such as *S. aureus* [116], *E. faecalis* and *S. pneumoniae* [117], with topo IV being the primary target. Despite the availability of Quinolone binding pocket crystal structure, the reason behind such changes in target preference is currently unknown. This shift in quinolone target preference has been suggested to have contributed to the ineffectiveness of quinolones in gram-positive pathogens.

While the primary target of quinolones contributes to the most cellular damage, targeting of the secondary target generates significant damage and provides a synergistic effect to the drug's potency [118]. Therefore, a dual-targeting quinolone that targets both gyrase and topo IV with similar minimum inhibitory concentrations (MICs) is often more potent than quinolones that targets gyrase predominately. This dual-targeting strategy can decrease the mutant prevention concentration (MPC) of the drug, as it is less likely for the bacteria to develop resistant mutations on gyrase and topo IV simultaneously in the same generation [119].

1.6.1.3 Structure-activity-relationships and the evolution of quinolone

The precise mechanism of quinolone binding remains a long-standing question despite its medicinal advancement over generations. Much quinolone development has been dependent purely on medicinal chemistry and structural-activity relationship studies *in vitro* and *in vivo*. Among all the changes across generations of quinolones, the quinolone bicyclic ring and the C3 and C4 groups has remained the most conserved feature of the quinolone pharmacophore (fig. 1.14). The function of the quinolone bicyclic ring is unclear, although several lines of evidence showed it to be involved with DNA stacking [120]. Numerous physico-chemical studies of quinolones have suggested the C3 and C4 groups form a bidentate complex with a

metal ion in solution in a 1:1 or 2:1 ratio [121-122], and Mg^{2+} is considered to be the most biologically relevant candidate for such a complex. Alternatively, the C3/C4 group is conceived to contribute some form of electrostatic or H-bond interaction with the enzyme or the DNA substrate.
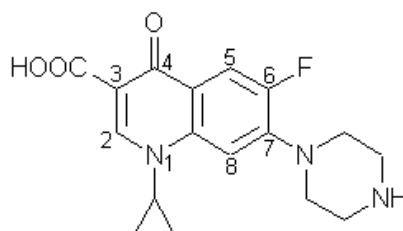
Figure 1.15. Chemical structure of Ciprofloxacin with group numbers assigned.

The C1/N1 (as shown in fig. 1.15, position 1) substituted group has been relatively unchanged throughout generations and its small molecular weight and its generally hydrophobic nature is regarded to be important for maintaining the potency of the drug [123]. However introduction of a larger group (difluorobenzene) at the C1 position was seen in a recent class of quinolones (*i.e.,* trovafloxacin) with improved anti-gram-positive activity [124]. The C5 position has remained un-substituted throughout chemical evolution. The introduction of a fluorine atom on the C6 position has dramatically increased the potency of the drug and this feature was kept unchanged since the emergence of the second generation of quinolone drugs and the start of the fluoroquinolone era [125].   Although little is known about the function of the substituted fluorine, it was found to improve drug binding. Although methoxyl substitution on the C8 position is found to favour the drug's potency, the size of the substituted group at this position is relatively restricted. The C7 group is the most flexible and the most extensively modified group in quinolone class drugs as most medicinal improvement of the latest generations of quinolones were achieved by manipulating the C7 group. Quinolones with bulky C7 groups tend to have stronger resistance against efflux mechanisms [126] and prefer targeting gram-positive gyrases over topo IVs [126]. The addition of methyl groups to the piperazine ring of C7 groups enhances the activity of quinolones against mammalian topo II[127-128], which suggested

that the C7 group might have direct interactions with the enzyme. Ofloxacin is one of the few quinolones with a chiral methyl group extended from the N1 position. Interestingly, the potency and binding of ofloxacin displays strong chirality and its L-enantiomer (levofloxacin) was found to bind 12-fold stronger than its D-enantiomer [129].

Moreover, quinolone drugs were suggested to bind to eukaryotic topoII in a similar fashion to other human topo II inhibitors [130]. Quinolones display a protective effect to mammalian cells against these cytotoxic agents [131]. As the success of novel bacterial topo II inhibitors is highly dependent on their cytotoxicity in eukaryotic cells, it is favourable to have the least interaction with human topo II. Therefore, it is important to further understand the human-bacterial topo II preference of these agents as well as how topo II poisons induce the cleavage complex at the molecular level. This knowledge can be applied to the development of antineoplastic topo II drug against drug-resistant cancer cells with improved potent.

1.6.1.4 Quinolone resistance

The trend of increasing overuse and misuse of antibiotics has led to the emergence of fluoroquinolone resistance in most clinically relevant bacteria and therefore the decreasing effectiveness of the entire class of quinolone antibiotics [132]. Numerous different quinolone resistance mechanisms have been discovered since the introduction of the drug in clinics. These include intrinsically up-regulated efflux mechanisms (*e.g.,* NorA in *S. aureus)* [133-134] and qnr-containing plasmid-acquired resistance [135], expression of DNA mimicking proteins and plasmid-encoded pentapeptide-repeat-proteins that can inhibit gyrase activity and prevent the binding of quinolone [136-137]. However, the majority of the resistant strains arise from mutations that occur in the quinolone resistance-determining regions (QRDR) located on helix 4 of gyrase/topo IV A subunits [138]. In particular, the Ser83 and Asp87 of *E. coli* gyrase [139] and the equivalent residues in gyrase and topo IV of gram-positive bacterial species [113-115,140] are the most frequently found sites of first-step mutations. These mutations as studied *in vitro*, were found to greatly reduce quinolone binding without greatly affecting the activity of the enzyme [141]. In the light of the recent

availability of crystal structures from quinolone-DNA gyrase complex [142], it appears that C3 and C4 group of quinolone chelate with a Mg^{2+} ion in a bidentate manner, while Ser83 and Asp87 of the GyrA subunits make contact with the quinolone chelated Mg^{2+} *via* two of its octahedrally coordinated waters.

While mutations in GyrB [143-144] and in GyrA [145] away from the QRDR region were found to confer quinolone resistance, it remains difficult to establish the exact role of these mutations in reducing quinolone potency without understanding quinolone binding at the molecular level.

1.6.1.5 Molecular details of quinolone binding

There have been numerous studies on quinolone binding to DNA or enzyme alone, where quinolone was found to bind weakly to DNA alone or enzyme alone [146]. Quinolone was shown to bind to negatively supercoiled DNA and ssDNA [147], and that guanine is favoured [148-149].   Intriguingly, quinolone binding to the DNA-enzyme complex does not require DNA cleavage [150] and this exclude the possibility of quinolone binding to the staggered ssDNA bases when the G-segment is cleaved. The fact that quinolones have little affinity for the enzyme or DNA alone suggests that quinolones might bind to both gyrase and DNA in a cooperative manner [151]. One possibility is that the localised DNA bubble created within the 4 staggered bases when the G-segment DNA is bound to gyrase could create the environment suitable for quinolone binding [149,151]. Numerous other quinolone models have been proposed [151] based on experimental data although they all lack solid support from other studies. Quinolone binding might also involve Mg^{2+} [152] as both crystallographic tests and NMR show the quinolone drug to form complex with Mg^{2+} ion in a 1:1 or 2:1 ratio in physiological conditions [153-154]. The dynamic nature of the breakage-reunion region [155] and the complex multi-component interaction required for quinolone binding has made it extremely difficult to determine the molecular detail of quinolone binding without crystallographic data.

1.6.1.6 Recent quinolone structures

Recently, two x-ray crystal structures of *S. pneumoniae* topo IV including the ParC-NTD and a fragmented ParE-CTD have been solved in complex with a 19 bp of dsDNA and two quinolone drugs, clinafloxacin and moxifloxacin (PDB code: 3FOF and 3FOE) [69]. Structure of the moxifloxacin bound topo IV-DNA complex is shown in fig. 1.15 (Left and Right)[69]. The two crystal structures solved at 4.00Å show an electron density between the +1 and -1 nucleotide bases respective to the cleavage position.
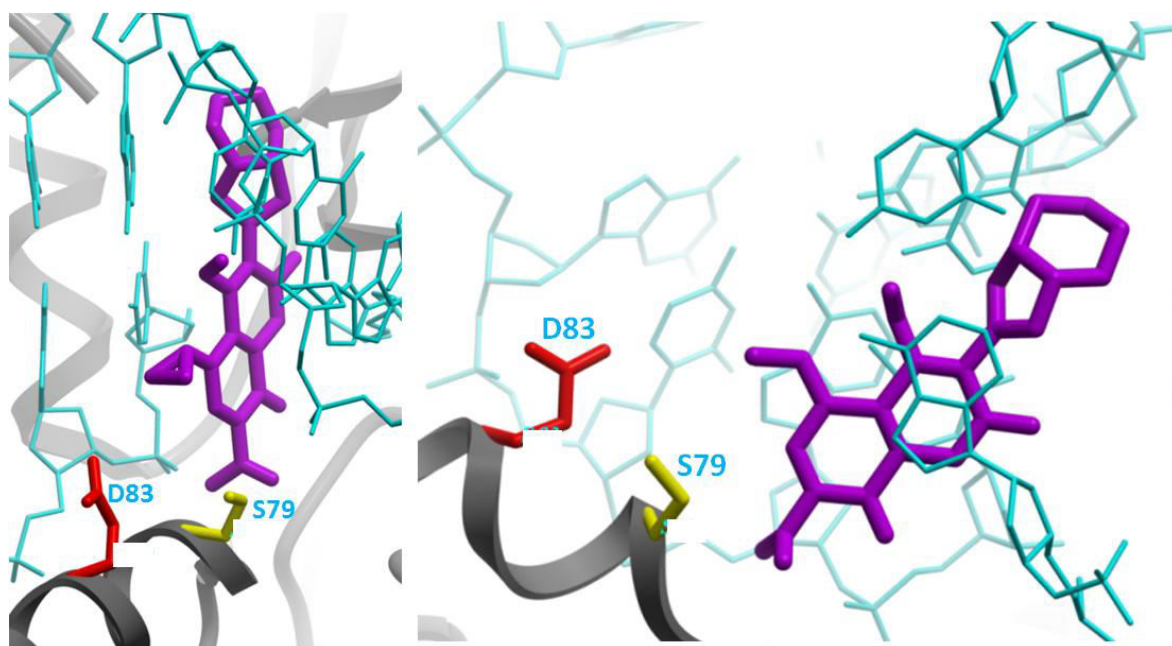
Figure 1.16. (Left & Right) Pictures of a 3D model built based on 4.0 Å crystal structure of moxifloxacin-DNA-S. pneumoniae Topo IV complex at different angles (PDB:3FOF) . *Position of the G-segment DNA (cyan) and moxifloxacin (purple), QRDR resistant residues (D83 (red) & S79 (yellow) of ParC) are represented as sticks [69]. Figure on the left: the C-3 group of moxifloxacin is positioned near S79. Figure on the right: the fluorine attached ring of moxifloxacin stacked between the +1 and -1 nucleotides.*

The additional electron density was speculated to be contributed by the quinolone drug. In the drug coordinates modelled into the electron density by the authors, the fluorine attached ring of both moxifloxacin (figure 1.15) and clinafloxacin stacks between the +1 and -1 nucleotides while the C-7 group protrudes out into the minor groove, possibly making contact with the B-subunits. Interestingly, this model coincides with the previous suggestion made about the drug binding position on the DNA [66] and partly agrees with the quinolone-DNA-protein co-operative binding mechanism. The C-3 oxygen of the modelled drug is in proximity to form a hydrogen bond to Ser79 (equivalent to Ser83 in *E. coli* gyrase) which is in agreement with the increased resistance associated with the quinolone resistance conferred by the mutation in this residue.

The poor resolution of the structure of the protein and the drug render it difficult to identify the exact conformation of the drug and the exact nature of the protein-drug contacts, which weakens the reliability of the model [69]. The model fails to explain the chiral nature of the inhibition displayed in ofloxacin enantiomers, the importance of the C-4 oxygen to the drug potency and the role of the mutation of Asp87 of *E. coli* gyrase in quinolone resistance. In summary, the structure gives a rough hint of the positioning of quinolone binding, however it is does not have enough details to provide the conclusive answer about the binding mechanism of quinolone.

1.6.2 Aminocoumarins

2-Aminocoumarins are secondary metabolites produced by *Streptomyces* species, which inhibit gyrase and topo IV (fig.1.16). 2-aminocoumarins share a core coumarin moiety and inhibit gyrase and topo IV by targeting the ATPase domain of the B subunits of gyrase/topo IV. Structural studies have shown that 2-aminocoumarins binds to the entrance to the ATP-binding site, thereby abolishing the catalytic ability of the enzyme. Novobiocin was the only 2-aminocoumarin used in the clinic as an antibacterial. Despite proving its clinical efficacy [156], strong albumin binding [157] and serious side effects such as hepatic impairment and skin eruption [157] has led to its withdrawal from the market.   Although novobiocin has failed to enter the clinic, it has offered hope that ATPase-targeting bacterial topo II inhibitors with improved ADMET properties could have the potential to become successful drug candidates.

Following the identification of biosynthetic gene clusters for novobiocin [158], Flatman et al. had attempted to produce novobiocin analogs with varying side groups by manipulating these metabolic gene clusters [159]. Disappointingly, the analogous inhibitors generated through this approach displayed no improved potencies against bacterial topo II compared to the original compound [159]. The study had nevertheless provided additional insight on the structural-activity-relationship of aminocoumarins.
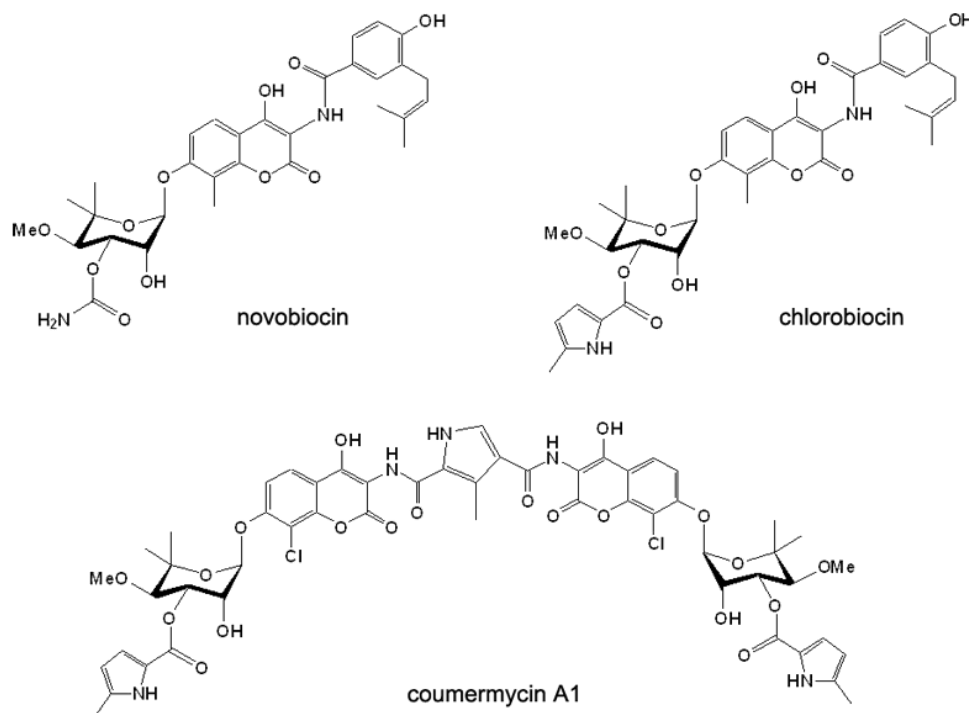
Figure 1.17. Chemical structures of various 2-aminocoumarin gyrase inhibitors.

1.6.3 Other Agents

1.6.3.1 Proteinaceous inhibitors

Numerous proteinaceous inhibitors of DNA gyrase such as CcdB [160] and microcin B17 [161], penta-peptide repeat proteins [162] and monoclonal antibodies [163] have been discovered over the years. However, developments of protein-based therapeutics tend to be difficult due to various reasons such as poor bioavailability, poor bacterial penetration, and instability and they are in general difficult to formulate. Although the potential for converting these proteinaceous inhibitors into clinical drugs is low, their mode of interaction with gyrase could provide insight into the development of novel small molecule gyrase inhibitors. It is observed in the structural studies of CcdB [164] and penta-repeat peptide gyrase complex [162], these protein-protein interaction interfaces are likely to be flat and involve large surface contact. Unfortunately, these relatively flat regions of the protein are generally inappropriate for binding small molecule inhibitors. Microcin B17, a plasmid maintenance toxin is

considered to be one of the most promising candidates as it can promote gyrase-induced DNA cleavage [165] similar to quinolones by inhibiting the breakage-reunion reaction. Understanding the interaction between microcin B17 and gyrase could yield important insights for novel inhibitor development.

1.6.3.2 Simocyclinones

In recent years, a novel coumarin gyrase inhibitor, simocyclinone, produced in *Streptomyces antibioticus* Tü 6040 has been identified (fig. 1.17 Top) [166]. Although simocyclinone shares a coumarin structure with aminocoumarins, instead of targeting the GyrB subunit of gyrase it was found to be an inhibitor of the GyrA subunit [167].   Further investigation suggested 2 simocyclinone molecules to bind to a GyrA dimer at low drug concentration while at high concentration, simocyclinone was suggested to induce the formation of a GyrA tetramer binding 4 simocyclinone molecules [168].

simocyclinone D8   R = Cl
simocyclinone D4   R = H
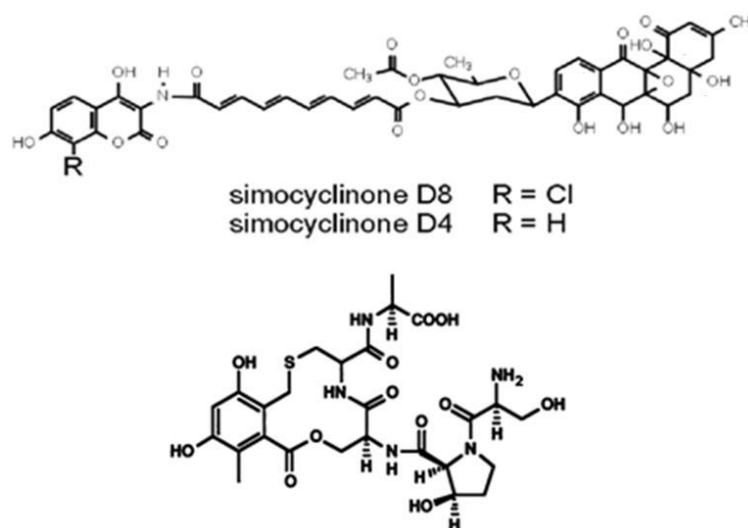
Figure 1.18. Chemical structure of Simocyclinone D8/D4 (top) and Cyclothialidine (bottom).

1.6.3.3 Cyclothialidine

Cyclothialidine is a natural gyrase ATPase inhibitor produced in *Streptomyces filipinesis* (fig. 1.17 bottom) [169].   It was found to display a two-fold higher gyrase binding affinity than novobiocin and has little activity against eukaryotic topoisomerases [169]. Unfortunately it has a weak antibacterial property due to poor

penetration [159].   To improve the antibacterial activity of cyclothialidine, several analogs were made with increased enzyme inhibition and *in vitro* antibacterial potency [170], although they failed to display sufficient potency in *in vivo* animal models.

1.6.3.4 Plant natural products – Flavonoids and Naphthoquinones

Plants are capable of producing thousands of different secondary metabolites as signalling molecules and provide defence mechanisms towards herbivores and competing micro-organisms such as fungi and bacteria. Flavonoids and naphthoquinones are a series of natural products with similar chemical scaffolds. Both are present in plants and plant-derived food products (*e.g.,* honey). Many flavonoids have been proven to be good gyrase/topo IV inhibitors and were found to be potent against pathogenic organisms [171-181]. Several studies found these compounds to target the ATPase domain of DNA gyrase and topo IV [181] by inhibiting ATP hydrolysis [182-183]. Surprisingly some flavonoids were able to induce gyrase/topo IV-mediated DNA cleavage [181] , a feature absent in other gyrase/topo IV ATPase inhibitors such as novobiocin. Naphthoquinones, another class of secondary metabolites with a chemical scaffold similar to flavonoids were found to be a defence compound against bacterial infection. They were found to interact with topo II and induce DNA cleavage [184] by a mechanism possibly involving DNA binding. Despite the potency of these compounds against bacteria, they also interact with various kinases [185-186] in eukaryotic cells. This leads to cytotoxicity and other undesirable side-effects, which prevented their development into potential antibacterials. The availability of other GHKL (Gyrase, Hsp90, Histidine Kinase, MutL family) ATPase structures has provided hope that allosteric binding site could be exploited to develop enzyme-specific inhibitors [58].

1.7. *Staphylococcus aureus*

Staphylococcus aureus is a gram positive, facultative anaerobe. It produces arrays of endotoxins and is able to induce fatal conditions such as toxin shock syndrome. As a result of stress, *S. aureus* can form chemoresistant endospores, which enable it to evade chemical attacks and transmit itself through the air current. Its ability to

produce Beta-lactamase and the presence of NorA efflux pump [187] as well as its effectiveness in obtaining resistant genes through horizontal gene transfer [188] has offered intrinsic resistance mechanisms to Beta-lactam antibiotics and many other classes of antibacterials such as macrolides, aminoglycosides, lincosamides, sulfonamides, tetracyclines, aminocoumarins and quinolones.   Its prevalence in the human body in the nasal passage [189], hair [190] and human skin [191] means it could inhabit a healthy individual and cause opportunistic infection, or it can be easily transmitted to other hosts through skin-to-skin contact.

1.7.1 Halotolerance and *S. aureus* induced food poisoning

Staphylococci are notoriously halotolerant organisms and some strains have even been found to grow in salt concentrations as high as 3 - 4.5 M NaCl [192-193]. *S. aureus* is one of the most halotolerant pathogens and therefore high salt conditions (1.28 M NaCl) is commonly used for its isolation [194-195]. This halotolerant ability of *S. aureus* is considered as a pathogenic factor by allowing it to colonise in high salt environments, such as the human skin [196], thereby increasing the chances of opportunistic subcutaneous infection and transmission through direct skin contact. Some clinically isolated strains of MRSA displayed strong halotolerance, although no correlation was found between antibiotic resistance and halotolerance [197].

S. aureus-induced food poisoning has been an important issue in the food industry. Usually food products are prepared at a low water activity or high osmolarity to prevent the growth of microorganisms. Distinct from other food poisoning bacteria, *S. aureus* is able to grow in extremely salty conditions (table 1.1) and is therefore often the source of processed food spoilage.

Organism	Minimum A_w for growth
Caulobacter	1.00
Spirillum	1.00
Pseudomonas	.91
Salmonella/E. coli	.91
Lactobacillus	.90
Bacillus	.90
Staphylococcus	.85
Halococcus	.75

Table 1.1 Limiting water activities (A_w) for growth of prokaryotes.

Organisms with lower Minimum A_w can withstand saltier environments [198].

1.7.2 *In vitro* properties of *S. aureus* gyrase and topo IV

Intriguingly, the supercoiling activity of *S. aureus* gyrase is highly tolerant to salt *in vitro*. While *E. coli* gyrase negatively-supercoils DNA optimally in the presence of 100-200 mM potassium glutamate (KGlu) and is inhibited at high salt condition, *S. aureus* gyrase can achieve optimal supercoiling activity similar to *E. coli* DNA gyrase in the presence of >800 mM of KGlu [199]. A similar study from Blanche et al. had reported similar results that describe a 500-fold increase in supercoiling activity of *S. aureus* gyrase with the increase of KGlu concentration from 0 to 750 mM [200]. At KGlu concentrations of 0-200 mM, *S. aureus* gyrase could not supercoil DNA but instead decatenates catenated DNA in the presence of ATP and relaxes negatively supercoiled plasmid DNA in the absence of ATP [199]. In contrast, *S. aureus* topo IV is less salt sensitive and requires 100-200 mM KGlu for optimal DNA relaxation and decatenation activity.

A follow up experiment found that high salt is required for *S. aureus* gyrase DNA wrapping, which could explain the salt requirement for its supercoiling activity [199]. The authors suggested this particular feature to be due to the relatively high acidity

of *S. aureus* GyrA C-terminal domain (*Sa*GyrA-CTD) in comparison to *E. coli* gyrase. Using homology modelling, the CTD of *Sa*GyrA was found to have a much lower basicity on the circumference of the beta-propeller fold in comparison with *E. coli*. Similarly, gyrase from *Streptococcus pneumoniae* (*Sp*) was reported to require a moderate level of salt for its supercoiling activity [201] and has reduced basicity in the DNA binding region of the beta-propeller fold.

Despite the strong similarity in surface electrostatic potential in homology models of the *Sa* and *Sp* gyrase CTD, *Sa* gyrase CTD is ~2 to 3-fold more salt-sensitive than *Sp* gyrase CTD *in vitro*. Further sequence alignment analysis has found a >40 amino acid addition at the C-terminal end of GyrA-CTD of *Sa* gyrase. Surprisingly, this addition is extremely acidic (~38% Asp/Glu) and *in silico* protein foldability prediction (foldindex) suggests this region to be unfolded and highly disordered. In addition, BLAST analysis of this region has yielded the same unique homologous addition in gyrases of all staphylococci organisms sequenced to date. If the acidic addition is indeed contributing to the enzyme's salt-sensitivity, it might be possible that this addition could contribute to the unique halotolerance character of staphylococci bacteria.

In addition, the requirement of KGlu could be due to a difference in co-factor required for ATPase activity as monovalent ions such as potassium and sodium were suggested to bind to the ATPase region and catalyse ATP hydrolysis [61]. It would be interesting to investigate if ATPase activity was affected by the KGlu concentration and whether monovalent ions indeed facilitate ATPase reaction of *S. aureus* gyrase.

Conversely, *S. aureus* topo IV has a less distinct salt sensitivity than gyrase and requires moderate salt concentration (100-200 mM KGlu) for its decatenation and relaxation activity [199].

1.7.3 Quinolone target preference in *S. aureus*

Whilst most *in vitro* inhibitory studies of quinolones were carried out using *E. coli* gyrase and topo IV, relatively little work has been done on the gyrase and topo IV of

gram-positive bacteria. It is established that in *E. coli*, DNA gyrase is the preferred target of norfloxacin and topo IV is 18-fold less sensitive in inducing DNA cleavage *in vitro* [112].   Conversely, *S. aureus* topo IV is 2.5-fold more sensitive to norfloxacin than gyrase [112]. This trend of target preference in gram-positive and gram-negative bacteria is also observed *in vivo* [202-203]. The reason behind such preference is currently unknown. It could be dependent on multiple factors including the changes in the conformation of the quinolone-binding site on the enzyme as well as the difference in the *in vivo* activity of the enzyme and physiological state of the cell (ATP/ADP ratio, osmolarity, pH etc.)

Hiasa et al. carried out nascent chain elongation experiments to study the cleavage induced by collision between quinolone induced enzyme-DNA complexes and the replication fork [199]. The experiment showed that ciprofloxacin induced *S. aureus* gyrase-DNA ternary complex was unable to arrest replication fork progression in low salt conditions. In contrast, *E. coli* gyrase and topo IV, and *S. aureus* topo IV were all able to arrest replication. This indicates that DNA fork arrests require gyrase-DNA wrapping [109,204] and the inability of *S. aureus* gyrase to wrap to DNA in the absence of salt could be the reason behind *S. aureus* gyrase quinolone insensitivity. Moreover, while *Sa* gyrase is capable of DNA wrapping in high salt, quinolone-induced cleavage was found to be inhibited in similar salt conditions [199]. It is reasonable to assume quinolone binding to involve in electrostatic interaction, it could be greatly impaired in high concentrations of counter ions. It is yet to be proven whether quinolone binding is affected in high salt.

Considering the salt sensitivity of *S. aureus* gyrase, it is possible for the change in osmolarity of the bacterial habitat to affect the activity of gyrase as well as the potency of quinolones and other gyrase inhibitors. This hypothesis could be supported by the evidence that *S. aureus* DNA is more negatively supercoiled in the presence of 0.5 M NaCl [205], which reflects an increase in *in vivo* gyrase activity in high osmolarity. Therefore in low salt growth conditions, the *in vivo S. aureus* gyrase activity could be much lower than topo IV and could lead to the apparent *in vivo* quinolone target preference.

1.7.4 Possible connection between KGlu sensitivity of *S. aureus* gyrase and its halotolerance

Based on the data from a 1978 study measuring the amino acid content of *S. aureus* growing exponentially in a low salt medium, it was found that *S. aureus* has a high amount of intracellular dicarboxylic amino acids [206]. Previous investigations on *Sa* gyrase and topo IV were carried out under the assumption that high KGlu is required to mimic the intracellular conditions. Therefore KGlu has since remained an essential additive in the *in vitro* tests of these enzymes. The authors suggested that the salt sensitivity of *Sa* gyrase could be the result of the enzyme's adaption to the high intracellular KGlu content in *S. aureus* [199]. However, several recent studies provide contradicting observations that suggest a high concentration of betaine and proline as compatible solutes instead of glutamate in *S. aureus* cytoplasm at high osmolarity growth condition [207-208]. It was found that during osmotic shock, *S. aureus* decreases its cell volume [209] as a result of osmosis and this is gradually restored by increasing its internal betaine [210-212] and proline [213-214] concentration by up-regulation of the active transport system. As both betaine and proline are placed high in the kosmotropic end of the hoffmeister ion series, they could provide a strong osmoprotective effect to cellular proteins even at high molarity [215]. Similar to betaine and proline, the glutamate ion is a kosmotrope. It is therefore possible that KGlu rich conditions used consistently in these *in vitro* studies of *Sa* gyrase and topo IV could resemble a physiological condition similar to a betaine- and/or proline- rich environment.

While these studies reported the salt-dependency of *Sa* gyrase, the fact that *S. aureus* is extremely halotolerant was ignored. *S. aureus* gyrase, being highly salt-dependent, can function in 4-8 times more salt than *E. coli* gyrase, thus possibly giving the organism an advantage whilst growing in a high osmolarity environment. Alternatively *Sa* gyrase could act as an osmosensing gene regulator in *S. aureus* that promotes or represses gene expression by offsetting chromosome hyperhelicity in response to osmotic changes. In fact, Epicatechin gallate, a flavonoid with structure

that highly resembles flavonoids that inhibit gyrase [182-183,216] and topo IV [181], was found to reduce halotolerance of *S. aureus* [12]. This further supports the role that gyrase has in the halotolerance of *S. aureus* and it would be interesting to test out these hypotheses.

1.8. Conclusions and future prospects

The emergence of multi-drug resistant *S. aureus* and the shortage in the supply chain of novel antibacterial discoveries has led to a great urgency in the discoveries of new drugs. DNA gyrase and topo IV are targets of the clinically important quinolone drugs and are proven antibacterial targets for a wide spectrum of pathogenic bacteria. While the majority of antibacterial targets have more than one class of drug currently on the market, DNA gyrase and topo IV are considered to be under-exploited. Almost 30 years of *in vitro* functional, catalytic and structural knowledge of gyrase and topo IV is now providing a vital platform for the development of novel inhibitors. These include various GyrB ATPase binding inhibitors and DNA-GyrA binding agents that have been developed over the years. Despite numerous gyrase inhibitors discovered, the mode of action and binding site of most of these compounds are largely undetermined. The difficulties in obtaining crystals of these enzyme-drug complexes have limited the medicinal improvement of these potential antibacterials. With the tightened drug safety regulations in recent years and the exceptionally high attrition rate of antibacterials in comparison to drug in other therapeutic area, the discovery of novel antibacterial is harder than ever. The success of novel gyrase inhibitors will be heavily dependent on a collaborative effort between biologists, chemists and pharmacologists to identify successful leads in the early stage of the drug development process.

1.9 Aims of the project

1.9.1 Mechanistic exploration of *S. aureus* gyrase and elucidation of the origin of KGlu dependent supercoiling

While *E. coli* gyrase has been the main subject of interest for bacterial topo II investigations, relatively little work has been carried out on gyrases in gram-positive organisms. Evidence from various studies highlighted the unique KGlu-dependence and specific supercoiling stimulation displayed by *S. aureus* gyrase. Hiasa et al. [199] has extended the finding by suggesting the linkage between GyrA-CTD of *S. aureus* gyrase and its KGlu dependency. However, it is far from conclusive as it does not support the role of K^+/Glu^- in compensating the difference in supercoiling activities between *E. coli* and *S. aureus* gyrase. Moreover, it does not explain the specific requirement of the presence of K^+/Glu^- ions for supercoiling stimulation. By building on evidence from previous studies on KGlu dependency supercoiling of *S. aureus* gyrase, we attempt to locate the enzymatic origin of this phenomenon using mechanistic based biochemical assays and mutant studies.

1.9.2 Naphthoquinones as novel gyrase inhibitors

Evidence from Karkare et al. 2013 suggested a novel mode of inhibition on *M. tuberculosis* gyrase by diospyrin, a naphthoquinone of plant origin. This novel discovery has raised an interesting proposition of developing naphthoquinones as a new class of gyrase-targeting antibiotics. This also suggested the possibility of utilising naphthoquinones as anti-*staphylococcal* agents. In order to further confirm naphthoquinones' potential as tial antibacterial/anti-*staphylococcal* drug leads, we aim to further investigate the *in vivo* potency of a variety of natural naphthoquinones against *S. aureus*. We also aim to investigate the activity of these natural naphthoquinones against *S. aureus* gyrase and topo IV *in vitro*. In addition, we aim to identify the mode of inhibition, structure-activity-relationship and binding position for these compounds using a variety of techniques (*e.g.,* mechanistic enzyme assays and protein crystallography).

Chapter 2 Materials and methods

2.1 Buffers and Solutions

Assay Buffers	Content
S. aureus DNA gyrase supercoiling buffer /*E. coli* DNA gyrase supercoiling buffer /*S. aureus* DNA gyrase decatenation buffer /*S. aureus* DNA cleavage buffer	40 mM HEPES.KOH (pH 7.6) 10 mM magnesium acetate 10 mM Dithiothreitol 2 mM ATP *500 mM potassium glutamate 0.05 mg/mL Bovine serum albumin
S. aureus DNA gyrase relaxation buffer /*E. coli* DNA gyrase relaxation buffer /thermal shift assay buffer	40 mM HEPES.KOH (pH 7.6) 10 mM magnesium acetate 10 mM Dithiothreitol *500 mM potassium glutamate 0.05 mg/mL Bovine serum albumin
S. aureus topo IV relaxation buffer	50 mM Tris.HCl (7.5) 5 mM $MgCl_2$ 5 mM DTT 1.5 mM ATP 350 mM potassium glutamate 0.05 mg/mL Bovine serum albumin
S. aureus gyrase dilution buffer	50 mM Tris.HCl (pH 7.5) 1 mM DTT 1 mM EDTA 30 % (w/v) glycerol
ATPase buffer	40 mM HEPES.KOH (pH 7.6) 10 mM magnesium acetate 10 mM DTT 500 mM potassium glutamate 0.05 mg/mL Bovine serum albumin
Electrophoresis buffers	
STEB(x2)	100 mM Tris.HCl (pH 8.0) 100 mM EDTA 40 % (w/v) sucrose 0.5 mg/mL bromophenol blue
TAE	40 mM Tris.acetate (pH 8.0) 1 mM EDTA
SAB	125 mM Tris.HCl (pH 6.8) 4% (w/v) SDS 20 % (w/v) glycerol 10 % (w/v) β-methcaptoethanol 0.5 mg/mL bromophenol blue

Table 2.1 Buffers and solutions used in this study

2.2 Bacterial strains

Bacterial strains	Genotype
Escherichia coli Rosetta™ 2 pLysS	F⁻*ompT hsdS*$_B$(r$_B^-$ m$_B^-$) *gal dcm* pRARE2 *pLysS* (Cam^R)
Escherichia coli BL21 (DE3) pLysS	F⁻*ompT hsdS*$_B$(r$_B^-$ m$_B^-$) *gal dcm* (*DE3*) *pLysS* (Cam^R)
Escherichia coli TOP10 (invitrogen)	F– *mcr*A Δ(*mrr-hsd*RMS-*mcr*BC) Φ80*lac*ZΔM15 Δ*lac*X74 *rec*A1 *ara*D139 Δ(*ara leu*) 7697 *gal*U *gal*K *rps*L (StrR) *end*A1 *nup*G
Staphylococcus aureus ATCC 29213	No specific genotype.

Table 2.2 Strains of bacteria used in this study

2.3 Media

Luria-Bertani medium was used for the selection and cultivation of both *E. coli* and *S. aureus* in solution.

Luria –Bertani medium:

Tryptone	1% (w/v)
Yeast extract	0.5% (w/v)
Sodium Chloride	1% (w/v)

Terrific Broth is the preferred medium used for high density bacterial growth of up to OD$_{600}$ ~8. It was used for the large scale production of pBR322 plasmids, where high quantities of bacteria were required to provide maximum DNA production.

Terrific Broth:

Tryptone	1.2% (w/v)
Yeast extract	2.4% (w/v)
K_2HPO_4	9.4% (w/v)
KH_2PO_4	2.2% (w/v)
Glycerol	4% (v/v)

All of the media described above were sterilised before use by autoclaving. Unused liquid media were stored at RT and remained sterile until use.

Solid Luria-Berth agar media was used for colony isolation and cultivation of newly transformed competent *E. coli*.

Luria –Bertani agarose solid medium:

Tryptone	1% (w/v)
Yeast extract	0.5% (w/v)
Sodium Chloride	1% (w/v)
Agarose	1.5% (w/v)

The solid medium was produced by first autoclaving the mixed ingredients listed. The autoclaved mixture was then stored until later use. Once ready for use, the autoclaved mixture was reheated in the microwave until all solid agarose was thoroughly melted. The molten LB agar solution was then left to cool to ~40-50°C, at which point the desired antibiotics were added and mixed. The agar was then immediately poured into Sterilin® Petri dishes and left to cool in a sterile environment until it solidified. The LB agar plates can be stored at 4°C in a dark environment for later use.

2.4 Antibiotics

Antibiotics were frequently included in bacterial media for the isolation and cultivation of *E. coli* with the desired transformed plasmids. The type of antibiotics and the concentration used in this study are described in Table 2.3

Antibiotics	Stock concentration	Working concentration
Ampillicin	100 mg/mL	100 µg/mL
Chloramphenicol	30 mg/mL	30 µg/mL

Table 2.3 Types of antibiotics and their concentrations used for bacterial cultures in this study.

2.5 Bacterial Methods

2.5.1 Preparation of chemically competent cells (BL21(DE3), Rosetta II (pLysS))

Glycerol stocks containing the desired *E. coli* cells were streaked onto fresh LB agar plates and grown overnight at 37°C. A single colony was then isolated and inoculated into 5 mL of LB containing the respective antibiotic, and incubated overnight. 1 mL of the overnight culture was then used to further inoculate a fresh 100mL LB. The cell culture was grown at 37°C until OD_{600}= 0.4-0.6 was reached.

The culture was then cooled on ice for 10 mins before the cells were harvested *via* centrifugation at 3,500x g. Pelleted cells were carefully resuspended in 20 mL of cold 100 mM CaCl and incubated on ice for a further 20 mins. Cells were pelleted again by gentle centrifugation at 3,500 x g and subsequently resuspended in 2.4 mL of 100 mM CaCl, 20% (v/v) glycerol. Finally, the resuspended cells were aliquoted into 50 µL portions and flash frozen using liquid nitrogen. The cell aliquots were stored at -80°C until later use.

2.5.2 Plasmid DNA transformation of chemically competent cells

Aliquots of chemically competent cells were removed from -80°C and allowed to thaw in ice for ~15-20mins. Once thawed, ~0.5-2ul of plasmid DNA (2-25 µg/ml) was gently injected into the cell aliquots. The resulting cell aliquots were incubated in ice for a further 20 mins in order to allow for the diffusion and uptake of the injected plasmids by the competent cells. To initiate plasmid transformation, the cell/DNA mixtures were then heat shocked at 42°C for 30-45s using the heating blocks. The cells were immediately transferred back to ice for one minute before 200 µL of LB media medium was added. The cells were incubated at 37°C for a further 1 hr (in shaking incubators), then were plated onto LB agar containing the relevant antibiotic and were subsequently incubated overnight at 37°C for colony selection.

2.6 DNA methods

2.6.1. Agarose gel electrophoresis

Agarose gel electrophoresis is a technique used for the separation and identification of DNA by their molecular weight or their topology. Firstly, an agarose gel was prepared by melting and dissolving 1% (w/v) agarose into buffer TAE. The hot agarose was then poured into gel casks with well spacers positioned accordingly and then allowed to cool at RT for 20-30 mins until the agarose had fully set; once set, the 1% (w/v) agarose gel is ready for use. To initiate electrophoresis, the 1% (w/v) agarose gel is submerged into an electrophoresis gel tank filled buffer TAE. An adequate quantity of TAE is added to ensure that the gel is covered with ~1 cm depth of buffer in order to prevent dehydration. DNA samples containing loading buffer (STEB) were then injected and allowed to settle into preformed wells. The loaded gel was then subjected to an electric current of ~80 V to allow separation of the DNA molecules until the dye front had reached ~2/3 the way of the full length of the gel. The gel was then stained in TAE buffer containing 2 µg/mL ethidium bromide for 10-20 mins. The gel was visualised under an ultraviolet transilluminator and photographed using the Syngene Bio-imaging system.

2.6.2. DNA gel-extraction

The DNA products of desired molecular weight that were separated by agarose gel electrophoresis could be extracted using QIA quick gel extraction kit and by following the manufacturer's recommended protocol.

2.6.3. DNA precipitation

DNA precipitation was occasionally carried out for the purification, concentration and storage of DNA samples. Ethanol or isopropanol were used interchangeably; to the DNA sample were added 1/10 the volume of sodium acetate (3 M, pH 5.2) and either ethanol (2.5-3.0x vol) or isopropanol (1x vol). The resulting mixture was incubated on ice for 15 mins to >8 hours (depending on the quantity of the DNA in the sample) to allow precipitation. The sample was then centrifuged at 4°C at >14,000 x g for 30 mins to pellet the DNA. The supernatant was removed and the DNA pellet was washed with 70% (v/v) ethanol to remove any remaining sodium acetate. The sample was again centrifuged at >14,000 x g for a further 15 mins. The supernatant was then removed and the DNA pellet was redissolved into the desired solvent. Alternatively, the DNA pellet was dried in a vacuum dessicator and then stored at RT.

2.6.4. Small scale plasmid DNA production and purification

Plasmid DNA was transformed into chemically competent *E. coli* top10 (invitrogen) cells according to 2.5.2. It was then used for inoculating 5 mL of LB medium and was grown overnight to reach stationary growth. The bacteria were then harvested, lysed and the DNA was extracted using the appropriate Qiaprep spin miniprep kit (Qiagen) and by following the manufacturer's recommended protocol.

2.6.5. DNA sequencing

DNA sequencing was carried out using BigDye® v3.1 kit (Applied Biosciences). A typical sequencing reaction (10 µl) consisted of:

Reaction buffer	1.5 µl
BigBye v3.1 mix	1 µl
Sequencing primer (2 µM)	1 µl
Template DNA	100 ng
Total volume	10 µl

The following sequencing oligonuleotides were used for sequencing of *S. aureus* GyrA mutants:

Name	Primer sequences (5′ -3′)
SaA1	5′ -GGTATGGCAACGAATATTCC-3′
SaA2	5′ -GGTGTGAATATGATTGCAC-3′
SaA3	5′ -GGTATGAATACATTGGAAG-3′
SaA4	5′ -GGTTATGGTAAACGTACGCC-3′

Table 2.4 Sequences of the sequencing primers using for validation of mutants produced via site directed mutagenesis

The reaction was prepared according to the above recipe with the correct sequencing primer is then subjected to the thermocycler program describe in table 2.5 to carry out the sequencing reaction.

Step	Temperature (°C)	Time (min:sec)	Description
1	95	1:00	Denaturation of dsDNA
2	95	0:30	Denaturation of dsDNA
3	45	0:15	Primer annealing
4	60	4:00	DNA elongation
5	-	-	Loop to step 2 (29 times)
6	72	10	Ensure completion of DNA elongation
7	4	N/A	End of program

Table 2.5 Thermocycler program used for DNA sequencing reaction. Reactions were carried out using a PCT-200 thermal cycler.

The products of the sequencing reactions were submitted to the John Innes Genome Laboratory for analysis. Sequences were aligned with the expected sequences to confirm the fidelity of the DNA samples and to examine the occurrence of any unexpected mutation.

2.6.6 DNA concentration determination

DNA concentration was determined using a BioPhotometer (Eppendorf) by measuring A_{260} of a DNA sample diluted in milli-Q-water.

2.6.7 Mutagenesis

2.6.7.1 Oligonucleotides

Construct	Name	Direction	Primer sequences (5′-3′)
S. aureus GyrA NTD (Δ489-888)	SaA59QCfor	Forward	5′-ACCGAAATTCAGTAGGGTGGTTTTGAA-3′
	SaA59QCrev	Reverse	5′-TTCAAAACCACCCTACTGAATTTCGGT-3′
*Sa*GyrA ΔCterm-tail(Δ811-888)	SaAtrunQCfor	Forward	5′-GCCAAAGTTAAATAAGATGCCGAGGAC-3′
	SaAtrunQCrev	Reverse	5′-GTCCTCGGCATCTTATTTAACTTTGGC-3′
*Sa*ANTD(1-489)-*Ec*ACTD (523-875) chimeric GyrA	T7 forward	Forward	5′-ACCGAAATTCAGTAGGGTGGTTTTGAA-3′
	SaANTDrevDS	Reverse	5′-GTCTGCGCTGTTGGCTTGAATTTCTGTACG-3′
	EcACTDforDS	Forward	5′-CGTACAGAAATTCAAGCCAACAGCGCAGAC-3′
	EcACTDrev	Reverse	5′-ATATATATGGATCCTTATTCTTCTTCTGG-3′

Table 2.6 DNA primers used for the PCR based site directed mutagenesis.

2.6.7.2 QuikChange® plasmid Site-directed mutagenesis (*Sa*GyrA-NTD / *Sa*GyrA ΔCterm-tail plasmid construction)

QuikChange® site-directed mutagenesis developed by Qiagen was used to introduce point mutations (*e.g.,* premature termination codons) into plasmid DNA sequences for the production of mutant proteins (*Sa*GyrA-NTD/*Sa*A54, *Sa*GyrA ΔCterm-tail). The plasmid DNA template consisted of coding sequence of a full length wt *Sa*GyrA inserted between NdeI and BamHI of the multiple cloning site. Site-directed mutagenesis was performed *via* polymerase chain reaction (PCR), whereby the a stop codon was introduced after the desired termination amino acid using DNA primers with the designed stop codon (SaA59QCfor/SaA59QCrev and SaAtrunQCfor/ SaAtrunQCrev). A typical 50 μl PCR reaction contained:

Template DNA	100 ng
dNTPs	200 μM
Phusion DNA polymerase (NEB)	1 unit
DNA primers	0.5 μM
Phusion HF buffer	Added to 1x

The DNA primers used are listed in table 2.6. Table 2.7 Shows a typical thermocycler program used.

Step	Temperature (°C)	Time (min:sec)	Description
1	95	1:00	Denaturation of dsDNA
2	95	1:00	Denaturation of dsDNA
3	50-68	0:15	Primer annealing
4	72	1:00 – 8:00	DNA elongation (time = 30s/1kb)
5	-	-	Loop to step 2 (15 times)
6	72	10	Ensure completion of DNA elongation
7	4	N/A	End of program

Table 2.7 Thermocycler program used for the Quickchange® site-directed mutagenesis reaction. Reactions were carried out using a PCT-200 thermal cycler. Annealing temperature and time for DNA elongation step are determined by the Tm of primers used and the length of the template DNA.

Following the amplification of the mutant, 10-20 units of DpnI, a restriction enzyme, is added to the reaction. The mixture was incubated at 37°C for one hour. The mutated DNA product was then transformed into *E. coli* top10 cells (invitrogen) and grown in LB agar plates containing the required antibiotics. The plasmid DNA was then isolated from the colonies and the introduction of the mutation was confirmed by DNA sequencing (2.6.5).

2.6.7.3 Chimeric *Sa*NTD-*Ec*CTD GyrA construct production

Production of the expression construct for the chimeric *Sa*NTD-*Ec*CTD GyrA (*Sa*ANTD (1-489) - *Ec*ACTD (523-875)) mutant was achieved by carrying out two separate PCR reactions of the *Sa*NTD and *Ec*CTD sequence. The *Sa*NTD PCR reaction uses T7forward and *Sa*ANTDrevDS (table 2.6) as primers. The *Ec*CTD PCR reaction uses *Ec*ACTDforDS and *Ec*ACTDrev as primers (table 2.6) as primers. This produces two DNAs with 30 nt of sequence compatible overhangs for the 2nd step PCR. The 2nd step PCR used the two PCR products from the 1st step PCR as templates. The forward primer of the SaANTD PCR reaction (T7 forward) and reverse primer of *Ec*CTD PCR reaction (EcACTDrev) to produce a final PCR product with DNA sequence encoding the *Sa*NTD-*Ec*CTD GyrA protein. Sticky-ends were then introduced to the construct using restriction enzymes (NdeI and BamHI), following the recommended standard protocol. The DNA product was subsequently ligated into an empty pET22b plasmid

(with the compatible NdeI/BamHI ends) overnight using T4 DNA ligase (Invitrogen) in accordance to the manufacturer's instructions. The ligated plasmid was then transformed into *E. coli* top10 cells (invitrogen) and grown in LB agar plate containing the required antibiotics. The plasmid DNA was then isolated from the colonies and the introduction of the mutation was confirm by DNA sequencing (2.6.5).

2.7 Protein Methods

2.7.1 Basic protocol

2.7.1.1 Dialysis

The dialysis procedure was usually required for removal of salt and solute from the protein samples. The process involved the submergence of the dialysis apparatus containing the protein samples into desired buffers of 200x the volume of the sample. Various dialysis equipments were used depending on the volume of the sample:

10-500 μL   Slide-A-Lyzer MINI Dialysis Units, 10K MWCO (Thermo Scientific)

500 μL – 3 mL   Slide-A-Lyzer Dialysis Cassettes, 10K MWCO (Thermo Scientific)

>3 mL   SnakeSkin Dialysis Tubing, 10K MWCO (Thermo Scientific)

2.7.1.2 Protein concentration

Concentration of protein solution was typically carried out by ultrafiltration using Amicon® filter spin concentrators.

2.7.1.3 Protein concentration determination

The Bradford Method [217] was used throughout this study for the determination of protein concentration in protein samples. Bradford reagents were acquired from Sigma. 5 μL of protein solution were diluted into 100 μL of 50 mM Tris.HCl (pH 7.5). The diluted protein sample was then mixed with 900 μL of Bradford reagent. Samples were allowed to incubate at RT for 5 mins and their absorbance at 595 nm

was subsequently measured using a spectrophotometer. The recorded value corresponded to the background value subtracted by the value recorded from a blank sample consisting of 100 µL of 50 mM Tris.HCl (pH7.5) mixed in 900 µL of Bradford reagents. The protein concentration was then derived by a calibration curve obtained from measurements generated from identically treated BSA standards.

2.7.1.4 SDS PAGE

Analysis of protein samples were carried out by sodium dodecyl sulphate polyacrylamide gel electrophoresis (SDS-PAGE). Samples were heated in a boiling water bath for ~1 min in 1x SAB buffer (125 mM Tris.HCL, 4% (w/v) SDS, 20% (w/v) glycerol, 10% (v/v) β-mercaptoethanol, 0.002% (w/v) bromophenol blue). The boiled samples were next loaded onto and run on discontinuous polyacrylamide gels (12.5%, 4% stacking gel) mounted in a Bio Rad Miniprotein-III setup for ~1.5 hrs at 200 V until the dye front had reached end of the gel. Samples were run together with LMW marker (GE healthcare) protein standards used as molecular weight references. Gels were then stained with a Coomassie stain (15% (v/v) acetic acid, 10% (v/v) methanol and 0.1% (w/v) Coomassie stain). The gels were subsequently destained in Milli-Q water and photographed using a Syngene GeneGenius Bio-Imaging system.

2.7.2 Recombinant protein expression

Expression plasmids with corresponding constructs listed in table 2.8 were transformed into expressing *E. coli* strains according to 2.5.2. The *E. coli* strain carrying the desired expression plasmid was then inoculated into 5 ml of LB broth containing the appropriate antibiotic and then grown overnight (~12-16 hrs) with constant shaking at 37°C. 500 µL of the grown saturated *E. coli* were used to inoculate a 50 ml subculture with fresh LB broth containing antibiotic. This subculture was then grown overnight at 37°C under constant shaking for~12-16 hrs. 10 ml of the grown subculture were then used to inoculate 1 L LB expression culture containing the relevant antibiotic. The expression culture was grown at 37°C in

shaking incubator until the log phase growth level was reached (OD600 ~0.4-0.6). The expression culture was subsequently induced by addition of IPTG to a final concentration of 0.5 mM. The induced culture was then incubated in 25°C for a further (~12-16 hrs) to allow total expression of the protein. To harvest the generated cells, the culture was subjected to centrifugation at 9,900 x g for 10 mins at 4°C. The resulted supernatant was discarded and the cell pellet was resuspended using TGED buffer (50 mM Tris.HCl pH 7.5, 1 mM DTT, 1 mM EDTA, 10% (v/v) Glycerol). The resuspended cells were then flash frozen using liquid nitrogen and were stored at -80°C until further use.

Protein expressed	Expression plasmid	Expression *E. coli* strain	Antibiotics used	Protein affinity tag
S. aureus GyrA	pET11a	*Escherichia coli* Rosetta™ 2 pLysS	Ampicillin, chloramphenicol	N/A
S. aureus GyrB	pET11a	*Escherichia coli* Rosetta™ 2 pLysS	Ampicillin, chloramphenicol	N/A
S. aureus ParC	pET11a	*Escherichia coli* Rosetta™ 2 pLysS	Ampicillin, chloramphenicol	N/A
S. aureus ParE	pET11a	*Escherichia coli* Rosetta™ 2 pLysS	Ampicillin, chloramphenicol	N/A
S. aureus GyrA NTD	pET11a	*Escherichia coli* Rosetta™ 2 pLysS	Ampicillin, chloramphenicol	N/A
E. coli GyrBNTD	pAJ1	*Escherichia coli* BL21 (DE3) pLysS	Ampicillin, chloramphenicol	N/A
*Sa*GyrA ΔCterm-tail	pET11a	*Escherichia coli* Rosetta™ 2 pLysS	Ampicillin, chloramphenicol	N/A
*Sa*NTD-*Ec*CTD GyrA	pET22b	*Escherichia coli* Rosetta™ 2 pLysS	Ampicillin, chloramphenicol	C-terminal His-tag

Table 2.8 Expression systems used for the expression of recombinant proteins.

2.7.3 Cell lysis and protein extraction

The frozen cells referred to in 2.7.2 were thawed and incubated at RT for 30 mins to allow lysozyme-induced cell lysis. The cell lysate was then centrifuged at 48,000 x g for 1 hr at 4°C to remove the cell debris. The resulting supernatant containing the expressed protein was then subjected to SDS-PAGE analysis to assess the expression level of the protein.

2.7.4 Protein purification protocol

2.7.3.1 Purification of *S. aureus* GyrA and *Sa*GyrA mutants (*SaGyrA NTD and SaGyrA* ΔCterm-tail)

S. aureus GyrA and the *Sa*GyrA ΔCterm-tail mutant were both purified by applying three FPLC protein affinity column steps. Firstly, powdered ammonium sulphate was gradually added into the cell lysate containing the expressed protein, to a final concentration of 1.5 M. The lysate was loaded onto a Phenyl sepharose 20 ml column pre-equilibrated with 3 column volumes of 1.0 M ammonium sulphate TGED (50 mM Tris. HCl pH 7.5, 1 mM DTT, 1 mM EDTA, 10% (v/v) Glycerol) buffer. The column was then washed with one column volume of 1.5 M ammonium sulphate TGED buffer. Any bound proteins were eluted using a gentle gradient of 1 M - 0 M ammonium sulphate TGED buffer. Eluted fractions containing the desired protein were dialysed against TGED buffer overnight. The dialysed sample was passed through a 5 ml Q sepharose column pre-equilibrated with TGED buffer. The column was washed with excess TGED buffer and any bound proteins were eluted with 0-1 M NaCl TGED buffer salt gradient. The eluted protein fraction containing the desire protein was then dialysed against excess TGED buffer overnight. Finally, the dialysed protein fraction was loaded onto a 20 ml MonoQ column pre-equilibrated with TGED buffer. The column was washed with excess TGED buffer and the bound proteins were eluted with 0-1 M NaCl TGED salt buffer gradient. Eluted fractions containing the desired protein were dialysed against excess TGED (30% (v/v) Glycerol) buffer overnight. The dialysed protein was then aliquoted, flash-frozen with liquid nitrogen and finally stored at -80°C. The sample of the purified protein was then digested by trypsin by the proteomics service in John Innes Centre. The mw of digested fragement was

examined by MALDI-ToF mass spectrometry (in-house). The mass spectrum generated was then searched against the SPtrEMBL database using the MASCOT search tool to confirm the identity of the protein.

.

2.7.3.2 Purification of *S. aureus* GyrB

S. aureus GyrB was purified using protein affinity chromatography over two steps. Firstly, cell lysate with expressed *S. aureus* GyrB protein was passed through a 5 ml Heparin sepharose column pre-equilibrated with TGED buffer. The column was then washed with excess TGED buffer and any bound proteins were eluted with 0-1 M NaCl TGED salt buffer gradient. The eluted protein fraction containing desired protein was then dialysed against excess TGED buffer overnight. The dialysed protein fraction was then loaded onto a Q sepharose 5 ml column pre-equilibrated with TGED buffer. The column was washed with excess TGED buffer and bound proteins were eluted with 0-1 M NaCl TGED salt buffer gradient. Eluted fractions containing the desired protein were dialysed against excess TGED (30% (v/v) Glycerol) buffer overnight. Dialysed protein was then aliquoted, flash-frozen with liquid nitrogen and stored at -80°C. The identity of the purified protein was then examined by MALDI-ToF fingerprint.

2.7.3.3 Purification of *S. aureus* ParC

S. aureus ParC was purified using protein affinity chromatography over two affinity column steps. Firstly, cell lysate with the expressed *S. aureus* ParC protein was passed through a 2x5 ml Heparin sepharose column pre-equilibrated with TGED buffer. The column was then washed with excess TGED buffer and bound proteins were eluted with 0-1 M NaCl TGED salt buffer gradient. The eluted protein fraction with the desired protein was then gradually mixed with powdered ammonium sulphate until a final concentration of 1.5 M ammonium sulphate was reached. The protein fraction was loaded onto a 20 ml Phenyl sepharose column pre-equilibrated with 3 column volumes of 1.0 M ammonium sulphate TGED (50 mM Tris. HCl pH 7.5, 1 mM DTT, 1 mM EDTA, 10% (v/v) Glycerol) buffer. The column was next washed with one column volume of 1.5 M ammonium sulphate TGED buffer. Any bound proteins were eluted by application of a gentle gradient consisting 1 M - 0 M

ammonium sulphate TGED buffer. Eluted fractions containing the desired protein were dialysed against excess TGED (30% (v/v) Glycerol) buffer overnight. The dialysed protein was then aliquoted, flash-frozen with liquid nitrogen and stored at -80°C.

2.7.3.4 Purification of *S. aureus* ParE

S. aureus ParE was purified using protein affinity chromatography over two affinity column steps. Firstly, cell lysate with the expressed *S. aureus* ParE protein was passed through a 5 ml Heparin sepharose column pre-equilibrated with TGED buffer. The column was washed with excess TGED buffer and bound proteins were eluted with 0-1 M NaCl TGED salt buffer gradient. The eluted protein fraction containing the desired protein was then dialysed against an excess of TGED buffer overnight. The dialysed protein fraction was then loaded onto a 20 ml MonoQ column pre-equilibrated with TGED buffer. The column was washed with excess TGED buffer and bound proteins were eluted with 0-1 M NaCl TGED salt buffer gradient. Eluted fractions containing the desired protein were dialysed against excess TGED (30% (v/v) Glycerol) buffer overnight. The dialysed protein was then aliquoted, flash-frozen with liquid nitrogen and stored at -80°C. The identity of the purified protein was then examined by by MALDI-ToF fingerprint.

2.7.3.5 Purification of *E. coli* GyrBNTD

E. coli GyrBNTD was purified using protein affinity chromatography over two affinity column steps. Firstly, cell lysate with the expressed *E. coli* GyrBNTD protein was passed through a 2x5 ml Q sepharose column pre-equilibrated with TGED buffer. The column was washed with excess TGED buffer and bound proteins were eluted with 0-1 M NaCl TGED salt buffer gradient. The eluted protein fraction containing the desired protein was then gradually mixed with powdered ammonium sulphate until a final concentration of 1.5 M ammonium sulphate was reached. The protein fraction was then loaded onto a 1 ml Phenyl sepharose column pre-equilibrated with 3 column volumes of 1.0 M ammonium sulphate TGED (50 mM Tris. HCl pH 7.5, 1 mM DTT, 1 mM EDTA, 10% (v/v) Glycerol) buffer. The column was then washed with one column volume of 1.5 M ammonium sulphate TGED buffer. Any bound proteins were next eluted by applying a gentle gradient of 1 M - 0 M ammonium sulphate TGED

buffer. Eluted fractions containing the desired protein were dialysed against excess TGED (30% (v/v) Glycerol) buffer overnight. The dialysed protein was then aliquoted, flash-frozen with liquid nitrogen and stored at -80°C. The identity of the protein purified was then examined by by MALDI-ToF fingerprint. Part of the EcGyrBNTD protein used in this study was gifted by Lesley Mitchenall.

2.7.3.6 Purification of *Sa*NTD-*Ec*CTD GyrA chimeric mutant

Purification of *Sa*NTD-*Ec*CTD GyrA involved a one-step nickel affinity chromatography step. The Hi-trap column used was discharged by passing 3 column volumes of 50 mM EDTA buffer through it. It was then recharged by passing 1 ml of 100 mM NiCl$_2$ and washed with 3 column volumes of water. The cell lysate with the expressed protein was then passed through a 2x 5 ml pre-charged Hi-Trap column pre-equilibrated with buffer A (50 mM Tris.HCl, 0.5 M NaCl, 5 mM imidazole, pH 7.5). The column was washed with excess buffer A to remove non-specifically bound protein. The bound proteins were finally eluted using a 0-100% buffer B gradient (50 mM Tris.HCl, 0.5 M NaCl, 500 mM imidazole, pH 7.5). Eluted fractions containing the desired protein were dialysed against excess TGED (30% (v/v) glycerol) buffer overnight. The dialysed protein was then aliquoted, flash-frozen with liquid nitrogen and subsequently stored at -80°C. The Identity of the protein purified was then examined by by MALDI-ToF fingerprint.

2.8. Biochemical and bacterial Assays

2.8.1. DNA supercoiling/relaxation assays

DNA supercoiling and relaxation assays were used throughout the study to assess the enzymatic ability to supercoil and relax circular DNA. Using pBR322 closed circular plasmid DNA as a substrate, DNA supercoiling activity of the enzyme could be assessed semi-quantitatively by determining the quantity and the supercoiling state of the DNA substrate at the end of the reaction. Both of these assays were typically carried out in 30 μL.

2.8.1.1 DNA supercoiling assays

For the DNA supercoiling assay reactions, the supercoiling assay buffers described in table 2.1, as well as 0.5 μg of relaxed DNA plasmid and 1 U of DNA gyrase (~64 nM

concentration for *S. aureus* / 1-40 nM of *E. coli*) were utilised. 1 U of DNA gyrase is defined as the quantity of enzyme required to fully supercoil 0.5 μg of relaxed DNA plasmid at 37°C in 30 mins in a typical reaction. The reactions were carried out by incubating the samples at 37°C in a temperature controlled water bath for 30 mins. To terminate the reaction, equal volumes (30 μL) of 2x STEB buffer and chloroform were added into the reaction mixture and were subsequently thoroughly mixed by vortexing. The samples were then briefly centrifidged (15,700 x g, 1 min) to separate the aqueous and the organic phase. The aqueous (upper) phase of the mixture, containing the DNA substrate, was then analysed *via* agarose gel electrophoresis (80 V, three hours).

2.8.1.2 DNA relaxation assays

The DNA relaxation assays were carried out using an almost identical protocol to the DNA supercoiling assays; the only exception was that fully negatively supercoiled DNA was used instead of relaxed plasmid DNA. Additionally, DNA relaxation buffer, which lacks ATP, was used instead of the DNA supercoiling buffer (table 2.1) as DNA gyrase only relaxes DNA in the absence of ATP.

2.8.1.3. DNA decatenation assays

Decatenation assays were used for assessing enzymatic activity of the enzymes to unlink catenated circular DNA. The format of the assay is highly similar to that of the supercoiling and relaxation assays. The reaction contained decatenation assay buffer, which was identical to that of the DNA supercoiling assay. The DNA substrate used in this case was kinetoplast DNA (kDNA) extracted from *Crithidia fasciculata*. kDNA is a network of catenated circular DNA consisting of maxi DNA circles of 20 and 40kb and mini circles of 0.5 and 1kb. In the presence of enzyme exhibiting decatenation activity, DNA circles were released from their DNA networks (fig. 2.1) and were subsequently separated and visualised by gel electrophoresis. To prepare the decatenation reaction, 200 ng of kDNA, in conjunction with 1 unit of gyrase and decatenation buffer were added to a volume of 30 μL and mixed. The reaction

mixture was immediately incubated for 30 mins at 37°C. It was then terminated by addition of equal volumes of 2x STEB buffer and chloroform, followed by vigorous vortexing and finally by centrifugation at 15,700 x g for 1 min. DNA from the upper aqueous phase was then analysed by agarose gel electrophoresis.
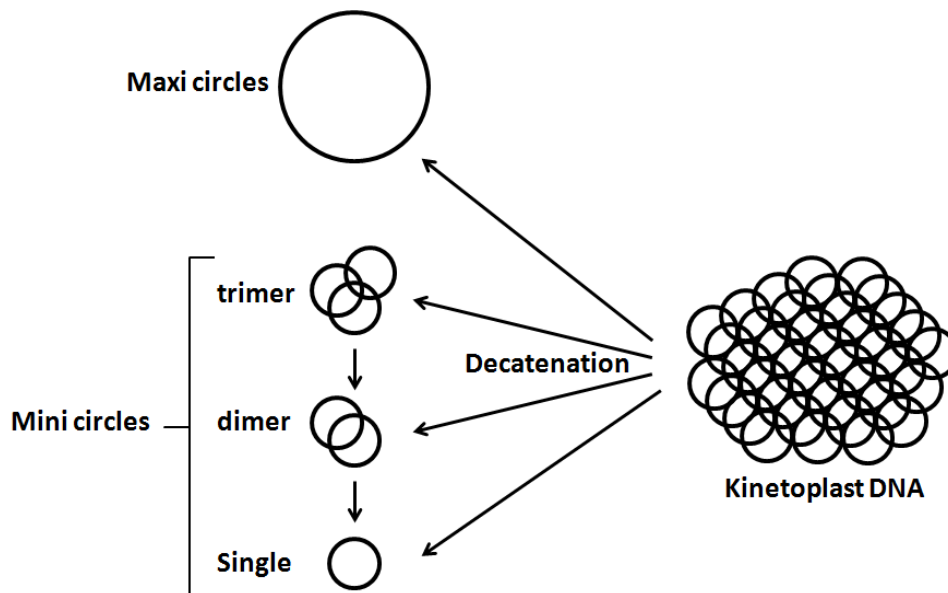
Figure 2.1. DNA products generated from decatenation of Kinetoplast DNA

2.8.1.4 DNA cleavage assays

DNA cleavage assays were used for the detection of the formation of cleavage complex formation caused by interruption of DNA gyrase strand passage. In the usual strand passage reactions of DNA gyrase, DNA cleavage only occurs transiently, and is subsequently rapidly resealed to ensure the integrity of the DNA substrate. In the event that the strand passage, between the cleavage and resealing steps, is interrupted by external factors, DNA gyrase could be stalled, resulting in a DNA-DNA gyrase covalent complex and a permanent double-stranded DNA cut. The DNA cleavage reaction is typically carried out by incubation of supercoiled pBR322 together with 1 U of DNA gyrase and DNA relaxation assay buffer in a 30 μL reaction in 37°C for 30 mins. To terminate the reaction, 0.2 % SDS and 0.1 mg/ml of proteinase K were added and incubated at 37°C for a further 1 hr to denature and digest the DNA gyrase. Equal volumes of 2xSTEB buffer and chloroform:isoamylalcohol (24:1) were then added to the samples, mixed thoroughly

using a vortex shaker, and centrifuged (15,700 x g, 1 min) briefly to separate the proteinaceous material from the DNA substrate. The DNA substrate (upper aqueous phase) was then directly loaded onto a 1% (w/v) agarose gel for electrophoresis analysis.

2.8.2. PK/LDH ATPase assay

The PK/LDH enzyme coupled ATPase assay was deployed for the analysis of the rate of ATP hydrolysis of GyrB over a time period of 30-60 mins. The assay was prepared by mixing ~0.6 μM of enzyme with ATPase buffer, 20 mM NADH, 80 mM PEP and . The ATPase reaction was initiated by the addition of 2 mM final concentration of ATP. The changes in OD_{340} were monitored using SPECTRAmax GEMINI microplate reader (25°C temperature control) and the data was collected at 1min time intervals, with at least 20 continuous time intervals (20 mins). As it was an enzyme coupled assay in the presence of excess of NADH and PEP, ADP was constantly converted to ATP during the reaction. At a theoretically fixed substrate concentration, linear kinetics is expected during the reaction.
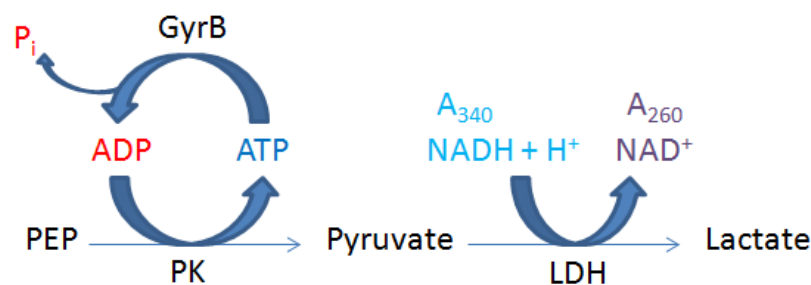
Figure 2.3 Schematic diagram showing components of PK/LDH coupled enzyme ATPase assay.

To ensure that the data collected is statistically significant, the coefficient of determination (R^2) of the sets of data points collected from each experiment were assessed to examined how well the data sets fitted the linear regression model. Sets

of data with their R^2 value below 0.98 are omitted to ensure accuracy of the rate recorded and the entire experiment was repeated until R^2 value of above 0.98 is achieved. As ATP is consumed, ADP is then regenerated by pyruvate kinase; through the enzyme coupled system, this would result in an equal molar conversion of NADH to NAD^+. As the maximum absorbance at 340 nm of NADH is not shared by NAD^+, the reduction in OD at 340 nm over time can be used to directly calculate the ATP consumed using Beer-Lambert law:

$$A = \varepsilon.l.c$$

A = absorbance
ε = extinction coefficient
c = concentration

With the extinction coefficient (ε) of NADH being 6.22 $mM^{-1}.cm^{-1}$ and the path length (l) being 0.67 cm , concentration (c) of NADH or ATP decrease over time can be calculated using absorbance data (A) of NADH at OD_{430} using the Beer-Lambert law.

2.8.3. *S. aureus* susceptibility drug test

A broth microdilution procedure was used to determine the MIC of reagents against *S. aureus ATCC 29213*. A 50 mL Mueller-Hinton broth inoculated with *S. aureus* was grown overnight at 35°C whilst shaking was maintained. 50 μL of the overnight culture was then used to inoculate 25 mL of fresh Mueller-Hinton broth and the resulting inoculum was incubated at 35°C with shaking until OD_{600} ~0.4 was reached. The culture was then diluted to OD_{600} ~0.13 with fresh Mueller-Hinton broth and then further diluted 150x. The *S. aureus* culture was then diluted 2x by mixing with final concentrations of 64, 32, 16, 8, 4, 2, 1, 0.5, 0.25 μM of the desired drug and 5% (v/v) DMSO with the total volume being 200 μL. The drug containing *S. aureus* cultures were then incubated at 35°C for 18 hrs. OD_{600} of the cultures were then recorded with the Gemini Spectramax microplate reader, with baseline absorbance subtracted against uninoculated cultures.

2.8.4. Thermal-shift assays

25 μL reactions containing 0.5 mg/mL of protein (SaGyrA/SaGyrB/EcGyrA/EcGyrB), 1x SYPRO orange dye, 1x thermal shift buffer (table 2.1) and KGlu at final concentrations of 0, 150, 300, 450, 600, 750 and 900 mM were heated from 20 to 95 °C in 0.2°C steps using MJ research Opticon2 qPCR system. Each temperature step was held for 12 s. Fluorescent intensity was measured over time at excitation/emission wavelengths of 490/575nm.

2.8.5. DNA densitometry

After the DNA sample(s) is ran and separated in size on 1% agarose gel, it is left to stain in in TAE buffer containing 2 μg/mL ethidium bromide for 10-20 mins. The gel was visualised under an ultraviolet transilluminator and photographed using the Syngene Bio-imaging system. Imagine taken was then analysed using GeneTools (Syngne) software package, were intensity of all DNA bands in each lane on the gel image were quantified.

2.9.1 Protein crystallography: protein crystallisation

2.9.1.1 Crystallisation trials of EcB-NTD (EcB 43) in the presence of diospyrin and 7-methyjuglone (7MJ) and *S. aureus* GyrB-NTD (SaGyrB49)

Crystallisation trials with a combination of *Ec*B43 +/-ADPNP +/- diospyin +/- 7-methyljuglone and *S. aureus* GyrB-NTD (*Sa*GyrB49) were tested with in-house commercial crystallisation screens (table 2.9): JSCG-plus (Molecular Dimension), The PEGs suite (Qiagen) and Structure Screen (Molecular Dimension). The vapour diffusion crystallisation screens were set up in a sitting drop format using 96-well MRD plates (Molecular Dimensions) with 50 µL of crystallisation well solutions. The sitting drops were prepared by mixing 0.6 µL of 10 mg/ml of *Ec*GyrBNTD with equal volumes of well solution. The crystallisation screens were then sealed and stored at 20°C in a dark environment.

Crystallisation trials	JSCG-plus	The PEGs suite	Structure Screen
*Ec*B43	Yes	Yes	N/A
*Ec*B43 + 1.6 mM diospyrin	Yes	Yes	N/A
*Ec*B43 + 0.5 mM 7MJ	Yes	Yes	N/A
*Ec*B43 + 40 µM ADPNP + 1.6 mM diospyrin	Yes	Yes	Yes
*Ec*B43 + 40 µM ADPNP + 0.5 mM 7MJ	Yes	Yes	Yes

Table 2.9 Crystallisation screening using commerical crystallisation screens with various different combinations of proteins and ligands.

2.9.1.2 Production of *E. coli* GyrBNTD-ADPNP crystals in the presence of K+/Na+/K+ and Na+

E. coli GyrBNTD-ADPNP crystals in various M+ were grown by mixing of the *Ec*GyrBNTD containing solution (~10 mg/ml in TGED buffer (50 mM Tris. HCl pH 7.5, 1 mM DTT, 1 mM EDTA, 10% (v/v) Glycerol)) with equal volumes of well solution (typically 0.6 µl : 0.6 µl) at a range of refined crystallisation conditions (described in table 2.10) adapted from conditions described in Jackson et al [218]. The drops were then prepared in a vapour diffusion, sitting format using 96-well MRD plates (Molecular Dimensions) with 50 µL of crystallisation well solution. All crystallisation trials were performed in a dark, constant temperature room at 20°C. Observable sizes of crystals typically appeared within 1 hr-1 day after the crystallisation trials were initiated. Crystals of >0.8 µm^3 in size were consistently produced. Crystals were successfully obtained in both sitting drop and hanging drop crystallisation settings.

M+ used	Crystallisation conditions	Cryprotectants
No salt	100 mM Tris.HCl pH 8.0, 15-25% (v/v) PEG3350, 2 mM MgCl$_2$	100 mM Tris.HCl pH 8.0, 15-25% (v/v) PEG3350, 10% (v/v) Glycerol
K+	100 mM Tris.HCl pH 8.0, 15-25% (v/v) PEG3350, 200 mM KCl, 2 mM MgCl$_2$	100 mM Tris.HCl pH 8.0, 15-25% (v/v) PEG3350, 200 mM KCl, 10% (v/v) Glycerol
Na+	100 mM Tris.HCl pH 8.0, 15-25% (v/v) PEG3350, 200 mM NaCl, 2 mM MgCl$_2$	100 mM Tris.HCl pH 8.0, 15-25% (v/v) PEG3350, 200 mM NaCl, 10% (v/v) Glycerol
K+/Na+	100 mM Tris.HCl pH 8.0, 15-25% (v/v) PEG3350, 100 mM KCl, 100 mM NaCl, 2 mM MgCl$_2$	100 mM Tris.HCl pH 8.0, 15-25% (v/v) PEG3350, 100 mM KCl, 100 mM NaCl, 10% (v/v) Glycerol

Table 2.10 Crystallisation conditions of EcGyrBNTD-ADPNP co-crystals

2.9.2 Protein Crystallography: Data collection and structure determination

2.9.2.1 X-ray data collection

Protein crystals were mounted using CryoLoops (Hampton Research) with cryprotection by soaking the crystals in cryoprotectants (described in table 2.10) for 5-10 s. X-ray data were collected at a synchrotron radiation facility (Diamond Light Source, Oxford). Cryoprotected protein crystals were flashed-cooled by submerging them into liquid nitrogen (<-196°C). The protein crystals were stored in liquid nitrogen in a vacuum flask for transport to the synchrotron facility. Remotely controlled robotic arms were then used to mount the crystals on the goniostat. The temperature of the crystal containing loop was maintained at 100 K with a nitrogen cryosteam. The wavelengths of the X-ray source used for diffraction for each of the crystals examined are listed in table 2.10). Grid diffraction scans were performed to identify highly diffracting regions of the crystals. Once a strongly diffracting portion of the crystal was located, diffraction images were taken at 0° and 90° to assess the estimate resolution of the diffraction. These images were also used for indexing purposes in order to identify the crystal symmetry and cell parameters using MOSFILM[219]. The optimal starting angle and the total number of degrees required for completion of the dataset collection were then calculated.

2.9.2.1 Processing of diffraction data

Diffraction data collected was processed by MOSFILM [219] and SCALA [220].   Molecular replacement was performed using PHASER[221]. Refmac5 software was used to perform auto-refinement of the model. The auto-refined model was then manually refined using *Coot* [222]. The Phenix software package was used for the modelling of the water molecules [223].

Chapter 3 Origin of *Staphylococcus aureus* DNA gyrase supercoiling activity dependency on potassium glutamate (KGlu)

3.1 Introduction

In a previous *in vitro* enzyme study [224], *S. aureus* DNA gyrase was found to behave differently from other gyrases studied. Initially, Blanche et al. established that the ability of *S. aureus* gyrase to negatively supercoil DNA substrate was strictly dependent on high concentrations of KGlu (700 mM), unlike the well-studied *E. coli* gyrase [224]. In addition, this stimulation is also shown to be salt specific as Blanche et al. were unable to activate *Sa* gyrase supercoiling by substituting KGlu with tris(hydroxymethyl aminomethane) or sodium glutamate. Furthermore, substitution of KGlu with various amino acids (*e.g.,* Ala, Arg, Gly, Lys, Pro, Ser) and metabolites of similar properties (4-aminobutyrate, glutarate, succinate, trans-glutaconate, γ-glutamyl-glutamate) were unable to activate supercoiling. Also, KCl of up to 800 mM was unable to support *Sa* gyrase. Surprisingly, despite the failure to activate *Sa* gyrase with various different supplements, the potassium salts of D-Glu, Asp, 2-methylglutamate (fig 3.1) were all able to stimulate *Sa* gyrase supercoiling.
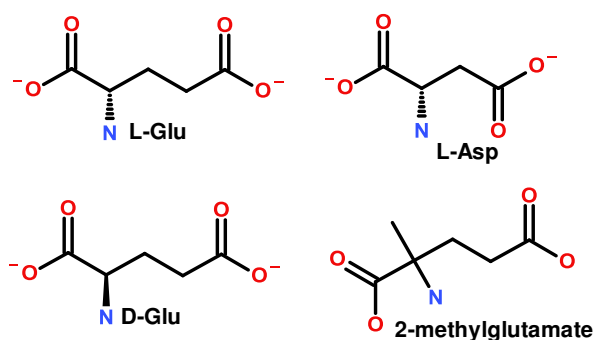
Figure 3.1 Glutamate-compatible anion: L-Glu, L-Asp, D-Glu, 2-methylglutamate.

Overall, the study suggested K^+ to be strictly essential for the supercoiling activation of *Sa* gyrase. The anion requirement for supercoiling stimulation was possibly less specific than the cation salt component, as anions with similar physiochemical

properties to glutamate were also able to stimulate *Sa* gyrase. This intriguing phenomenon subsequently led Hiasa et al [199] to attempt to elucidate the enzymatic origin of the KGlu dependency of *Sa* gyrase and also to examine the reason behind the differential behaviour between *S. aureus* and *E. coli* gyrase.

Again, Hiasa et al [199]discovered *Sa* DNA gyrase to only display DNA supercoiling activity in the presence of high concentrations of KGlu (400-800 mM), while the *E. coli* counterpart showed optimal supercoiling activity at a much lower KGlu concentration (100-200 mM) and was mildly inhibited at high KGlu concentration (800 mM). Interestingly, both the DNA relaxation and decatenation activities of *S. aureus* gyrase were found to require little KGlu, which suggested that this KGlu dependency originates from a mechanistic aspect of the enzyme related to DNA supercoiling. Further evidence suggested the salt-dependent supercoiling activity is the result of the salt-dependent GyrA-CTD-DNA wrapping in *S. aureus* gyrase [199].

Current evidence suggests that the high KGlu requirement for *Sa* gyrase supercoiling activity is distinct from any gyrases studied so far. However, apart from one experiment suggesting the CTD of *Sa* GyrA to be responsible for the KGlu-dependency, evidence for its origin is limited. In particular, we currently have no understanding of the salt-specificity requirements observed in *Sa* gyrase supercoiling stimulation.

The biological implications of this enzymatic effect *in vivo* are currently unknown. It is interesting to note that *Staphylococcus* is halotolerant and well known for its ability to grow at a wide range of salt [225]. This implies that *Staphylococcus* organisms could adjust their cytoplasm to a wide range of ionic strengths to counteract their surrounding environment to relieve tension on the cell envelope generated by the osmotic pressure. *In vivo*, gyrase will be expected to subject to fluctuations in salt concentration intracellularly, affecting its activity and thereby influencing the supercoiling state of the bacterial chromosome. Gyrase could potentially act as an osmotic sensor that regulates the topology of the bacterial chromosome and could trigger gene expression and repression as a response to osmotic changes. As the potency of DNA gyrase inhibitors such as fluoroquinolones are influenced by the *in vivo* activity of gyrase, the osmotic pressure of the habitat of *S. aureus* (*e.g.,* nose

versus skin) can potentially affect the frequencies of mutant emergence against these antibiotics.

In relation to the potential biological and therapeutic significance, it is therefore important to gain further understanding the origin of salt effect on *Sa* gyrase. In this study, it was decided to deploy a series of in-depth experiments to probe the origin of the salt dependency and specificity demonstrated in *Sa* gyrase, hopefully discovering the mechanistic difference between the two enzymes.

3.2 *Sa* gyrase supercoiling is dependent on high concentration of KGlu

To confirm and extend the findings of Hiasa et al [199], we conducted a range of electrophoresis assays to assess *Sa* gyrase supercoiling activity in a broader range of KGlu concentration with finer intervals. We chose to perform the experiments in 7 different concentrations of KGlu in the range of 0-900 mM at 150 mM concentration intervals. As a direct comparison, we have also tested *E. coli* gyrase in the same sets of reaction conditions.

As shown in figure 3.2, a typical supercoiling gel assay involves the incubation of 1 U of gyrase (A and B subunits) with 0.5 μg of relaxed pBR322 plasmid as DNA substrate at 37°C, as describe in chapter 2.8.1.1. The reaction was then terminated after 30 mins by thorough mixing with chloroform:isoamyl alcohol to deactivate gyrase activity. The treated mixture was then subjected to gel electrophoresis to separate the supercoiled and relaxed plasmid DNA. As supercoiled DNA topoisomers tend to have a more compact conformation, they travel faster and further than the relaxed topoisomers with the more open conformations.

Figure 3.2 S. aureus gyrase DNA supercoiling at a range of KGlu concentrations. *0.5 ng of relaxed pBR322 was supercoiled with 1U S. aureus gyrase in various concentrations (0 – 900 mM) of KGlu (lane 2-8) in conditions described in chapter 2.8.1.1. As relaxed DNA become supercoiled, it becomes more compact and thus travels further than its relaxed topoisomers. Note: as DNA becomes more supercoiled they are less easily separated using gel electrophoresis. Therefore supercoiled DNA appeared as a single band on the gel even if in fact a range of supercoiled topoisomers is present. Figure lables: Rel control (lane 1) – no enzyme is added. Sc control (lane 9) – 1 U of S. aureus added at 500 mM KGlu.*

Figure 3.3 E. coli gyrase DNA supercoiling at a range of KGlu concentrations. *0.5 ng of relaxed pBR322 was supercoiled using 1 U S. aureus gyrase in various concentrations (0 – 900 mM) of KGlu (lane 1-7) in conditions described in chapter 2.8.1.1. The noticeable smearing in lane 6-7 is caused by the high salt concentration in the loaded DNA sample, thereby affecting the migration speed of the DNA sample. Figure labels: –enz (lane 8) - no enzyme was added; Rel pBR322 – relaxed pBR322 plasmid; Sc pBR322 – supercoiled pBR322 plasmid.*

As expected, *Sa* gyrase is unable to supercoil DNA in the absence of KGlu (fig. 3.2, lane 1). In the presence of moderate concentrations of KGlu (150-450 mM) (fig. 3.2, lane 3-5) we were able to observe a clear increase in supercoiling activity with *Sa* gyrase. While little apparent increase in activity was observed between 600-900 mM KGlu (fig. 3.2, lane 6-9), it is difficult to quantify their differences in activity as most DNA substrates in the reactions are already saturated with negative supercoils. In contrast, *Ec* gyrase was able to demonstrate noticeable supercoiling activity in the absence of KGlu (figure 3.3, lane 1), while at 150 mM KGlu full supercoiling activity was observed (figure 3.3, lane 2). Therefore although *Ec* gyrase does not require KGlu to supercoil DNA, inclusion of low concentrations of KGlu dramatically enhanced its activity.

3.3 Quantitative assessment of *Sa* gyrase supercoiling activity versus KGlu

In order to produce a quantitative understanding of *Sa* gyrase supercoiling activity versus KGlu concentration using the gel assay (a semi-quantitative method), time-trial supercoiling experiments with multiple incubation end points was deployed. Supercoiling reactions were setup as described in chapter 2.8.1.1. One-hour incubations with 5 minute time-points were run in the same range of KGlu and KCl concentration (0, 150, 300, 450, 600, 750, 900 mM) as used in previous experiments. The individual Sc reactions were terminated at 5 min intervals and the assay samples were subsequently run on 1% (w/v) agarose gels to separate the supercoiled and relaxed DNA substrates. The intensity of the Sc band for each time point was then quantified using DNA densitometry (Syngene GeneTools). Background signal at 0 time point is used as a reference to reset the baseline for the signals measure at the rest of the time points. The signal reading with the baseline subtracted, the relative intensity of the supercoiled band, was then used as a quantitative measurement of the supercoiling activity. The values generated were then plotted against reaction times and the initial rates of reactions from the plot were then included in a secondary plot against KGlu concentration. As a result, further information about the quantitative differences between the supercoiling activities of *Sa* gyrase in different KGlu concentrations can then be deduced.

As shown in fig. 3.4 & 3.6, a gradual increase in supercoiling activity was observed as KGlu concentration was increased from 150 mM to 600 mM. Supercoiling stimulation then stabilised at ~750-900 mM KGlu, with no apparent increase in activity observed. Again the results confirmed that *Sa* gyrase is inactive in supercoiling in the absence of KGlu and requires high KGlu concentrations (~600 mM) to reach its optimal activity.

In a parallel experiment performed in the presence of KCl, *Sa* gyrase supercoiling activity was limited in almost the entire range of concentrations tested (figure 3.5 & 3.7). Only at 150 mM and 300 mM KCl the enzyme is able to show minimal activity. It is also interesting to note that at 150 mM KCl, small amount of supercoiled DNA was observed at the 5th minute of the incubation; however the quantity of the supercoiled DNA did not increase further as time progressed. This could suggest that *Sa* gyrase

achieve high level of supercoiling and that the supercoiling set point* was significantly reduce by the replacement of Glu⁻ by Cl⁻. As DNA wrapping is known as an important mechanism that determines supercoiling setpoint* of the gyrase [226], Glu⁻/Cl⁻ replacement could have reduced the ability for gyrase to wrap DNA.

***supercoiling set point** – DNA gyrase supercoiling is gradually slowed and eventually stopped by the torsion created in the highly-supercoiled DNA during supercoiling. Supercoiling set point is the highest supercoiling state achievable by gyrase in the specific condition, during which the rate of DNA supercoiling and ATP-independent DNA relaxation are at equilibrium. The higher the supercoiling set point, the more negative supercoils can be introduced into the same DNA substrate. Recent studies [226] found that the supercoiling set point of gyrase can be changed by modification of the DNA wrapping CTD of the GyrA subunit, hinting at a relationship between DNA wrapping process and the limit of supercoil achievable by gyrase.
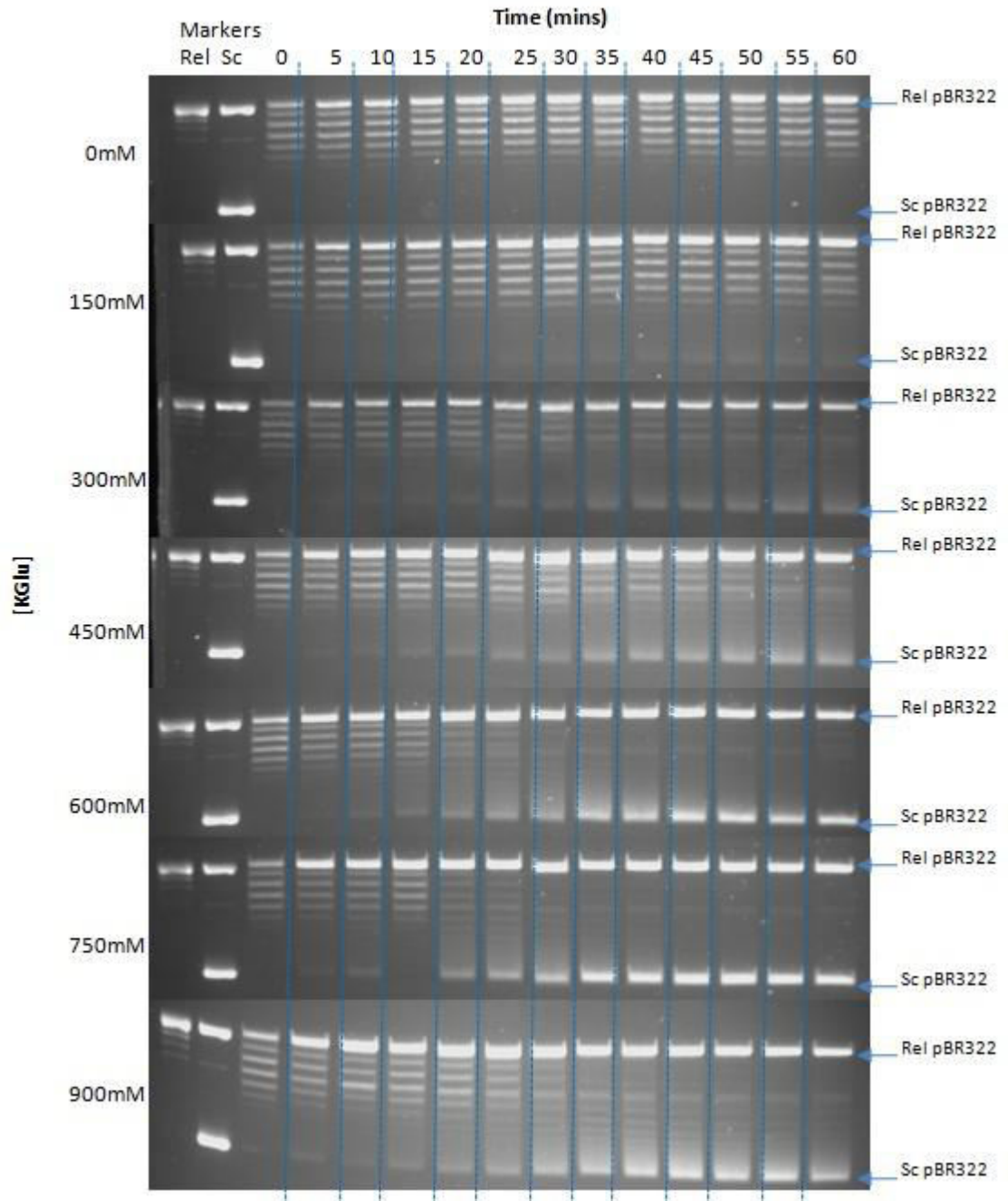
Figure 3.4 Gel image of time-trial of S. aureus DNA gyrase supercoiling assays performed in 0, 150, 300, 450, 600, 750 and 900 mM KGlu. *0.5 ng of DNA is incubated with 1 U of S. aureus DNA gyrase in the conditions described in chapter 2.8.1.1. Reactions prepared and performed simultaneously in a 96 well plate. Reactions are terminated at 5, 10, 15, 20, 25, 30, 35, 40, 45, 50, 55, 60 mins by addition of terminating solution. Note: discrepancy of the results exist in the reaction with 750 mM at 10 mins could be been caused by the lack of mixed of the enzyme and the DNA solutions.*
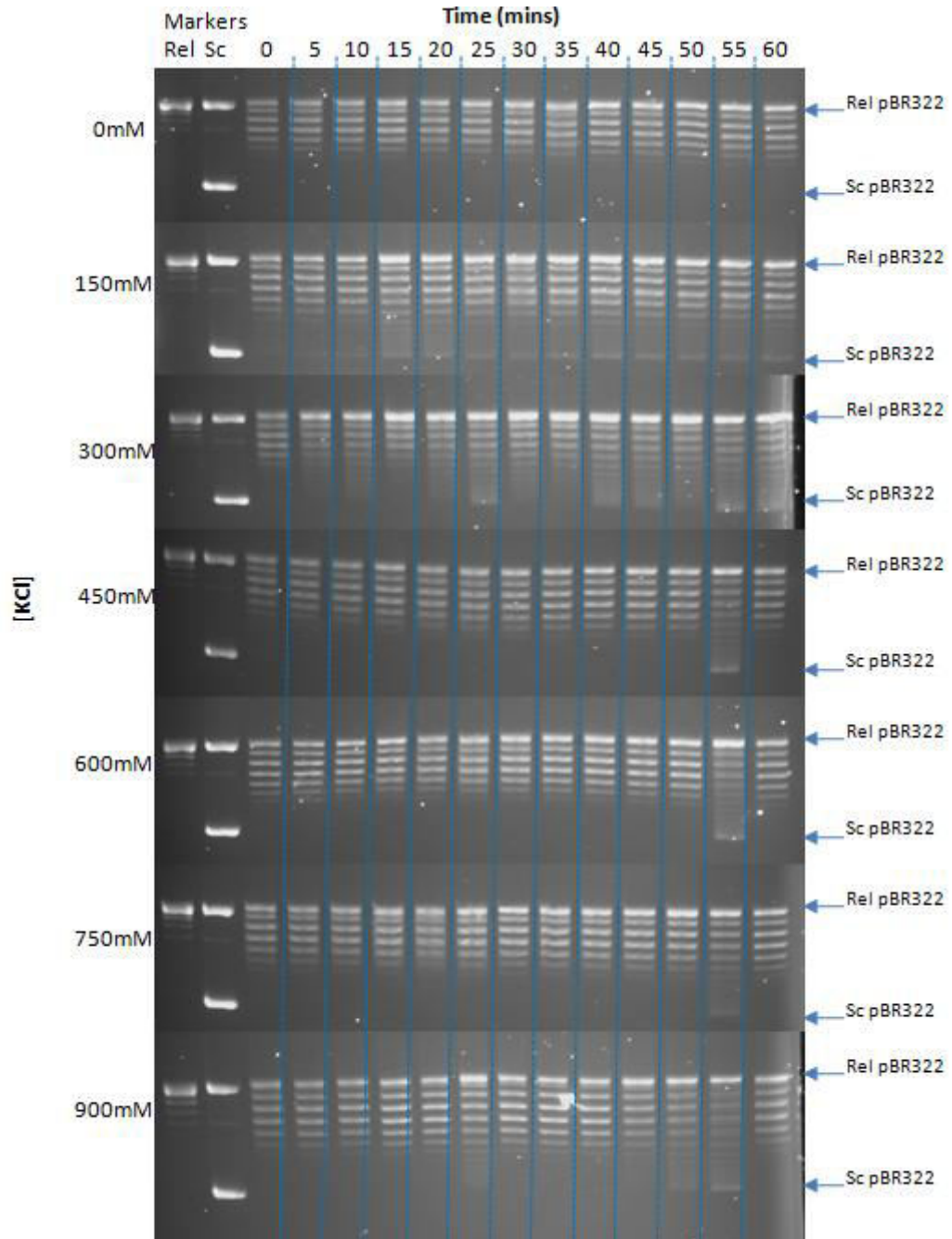
Figure 3.5 Gel image of time-trial of S. aureus DNA gyrase supercoiling assay performed in 0, 150, 300, 450, 600, 750 and 900 mM of KGlu. *0.5 ng of DNA is incubated with 1 U of S. aureus DNA gyrase in the conditions described in chapter 2.8.1.1. Reactions prepared and performed simultaneously in a 96 well plate. Reactions are terminated at 5, 10, 15, 20, 25, 30, 35, 40, 45, 50, 55, 60 mins by addition of terminating solution. Note: Discrepancy in the 55th mins of the experiments with 450 mM, 600 mM, 750 mM and 900 mM KCl could havecaused by mishandling of the multi-channel pipette resulting in the transfer of salt across a single colum/row within the well.*
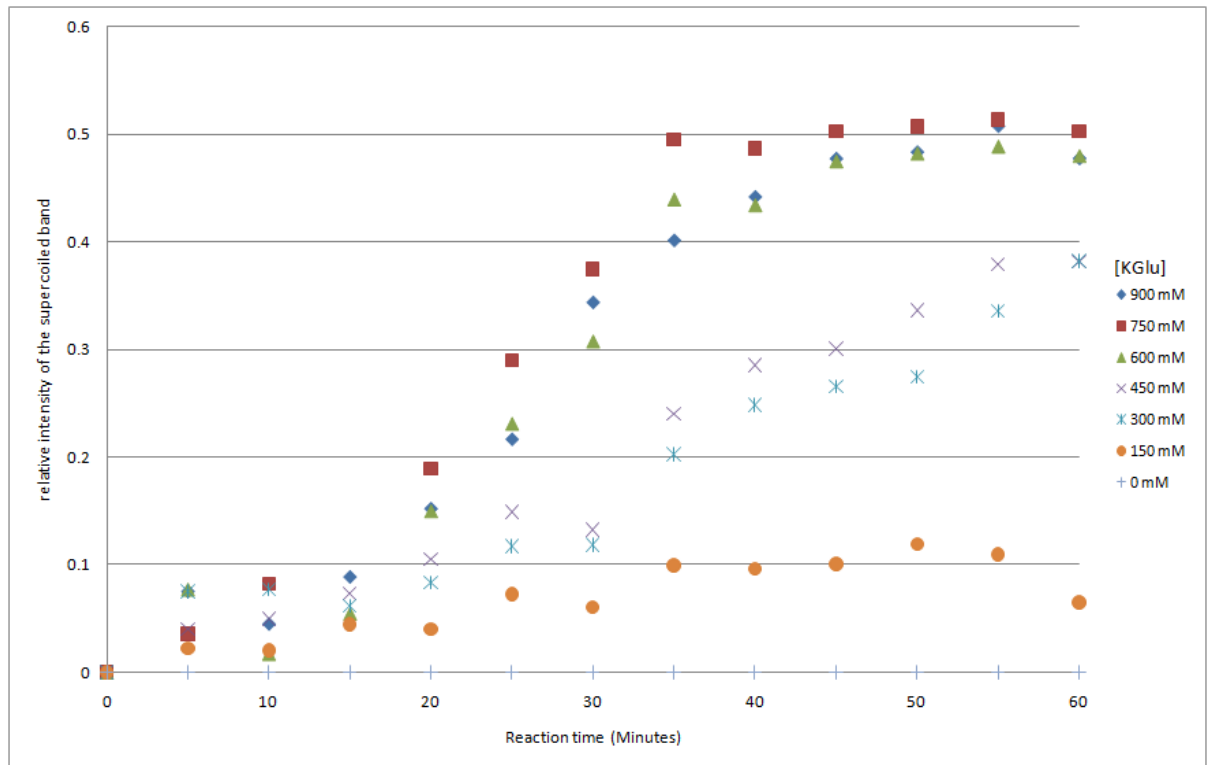
Figure 3.6 Relative quantity of supercoiled DNA substrate between reactions measured by DNA densitometry against the reaction time in various KGlu concentrations. *Supercoiled and relaxed DNA species are separated by gel electrophoresis and visualised by ethidium bromide staining (figure 3.5). The quantities of DNA species within each reaction are quantified by DNA densitometry (describe in chapter 2.8.5). The relative intensity of the supercoiled DNA band was calculated by dividing the intensity of the fully supercoiled DNA band with the intensity of both relaxed and supercoiling DNA bands presence on the same gel column/ in the same supercoiling reaction.*
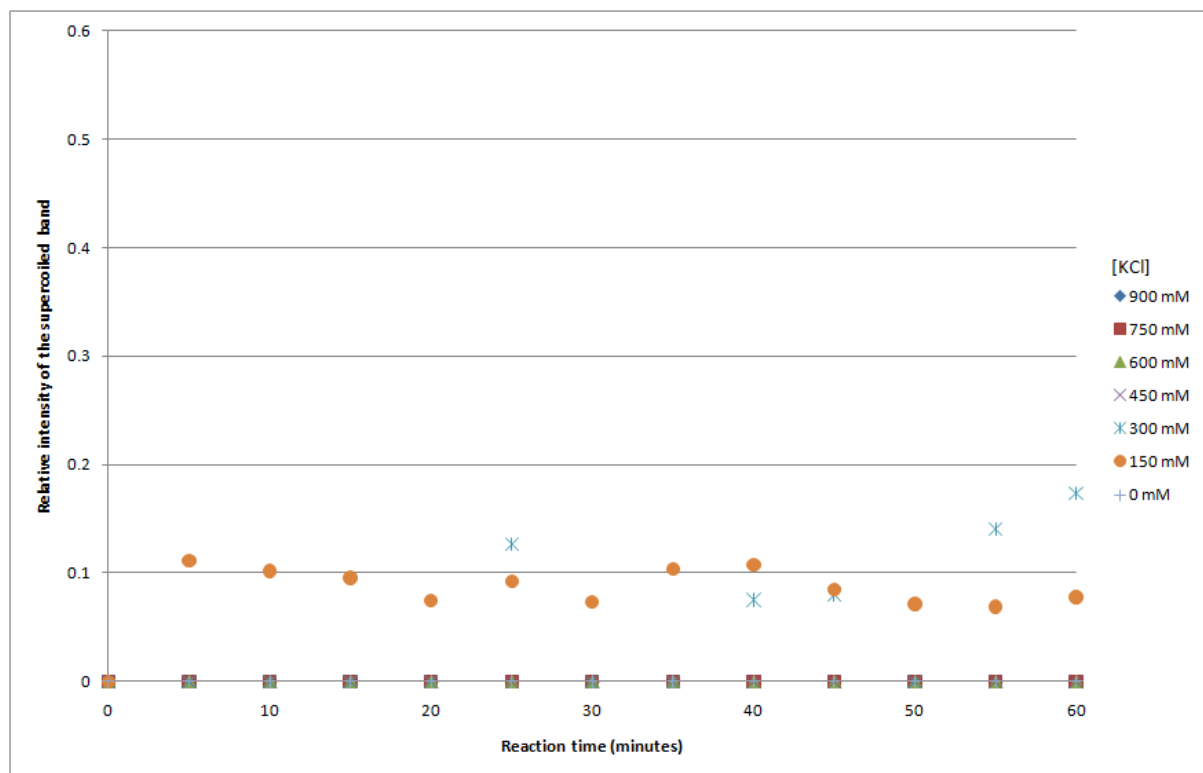
Figure 3.7 Relative quantity of supercoiled DNA substrate between reactions measured by DNA densitometry against the reaction time in various KCl concentrations. *Supercoiled and relaxed DNA species are separated by gel electrophoresis and visualised by ethidium bromide staining (figure 3.5). The quantities of DNA species within each reaction are quantified by DNA densitometry (describe in chapter 2.8.5). The relative intensity of the supercoiled DNA band was calculated by dividing the intensity of the fully supercoiled DNA band with the intensity of both relaxed and supercoiling DNA bands presence on the same gel column/ in the same supercoiling reaction.*

3.4 *Sa* gyrase and *Ec* gyrase folding stability versus KGlu

As experiments have confirmed that *Sa* gyrase activity is dependent on high concentrations of KGlu, it is crucial to confirm that the salt-dependent supercoiling phenomenon is not the results of salt-dependent protein folding. Traditional means of protein folding stability assessments such as circular dichroism and FTIR, however, are inoperable under the concentration of KGlu of interest. To circumvent the

problem, we have decided to use a thermal-shift fluorophore assay to detect protein melting temperature, which involves the use of a environment-sensitive fluorescent dye (SYPRO-orange) that fluoresces strongly in the region of low dielectric constant such as the hydrophobic patches exposed in unfolded proteins (fig. 3.8) . In this experiment, melting temperatures (T_m) of *S. aureus* GyrA and GyrB, and *E. coli* GyrA and GyrB were tested in the presence of 0-900 mM KGlu to examine the influence of KGlu concentration on the folding stabilities of these proteins. The protein samples were subjected to a temperature gradient over time and the fluorescence intensity of the dye was monitored.
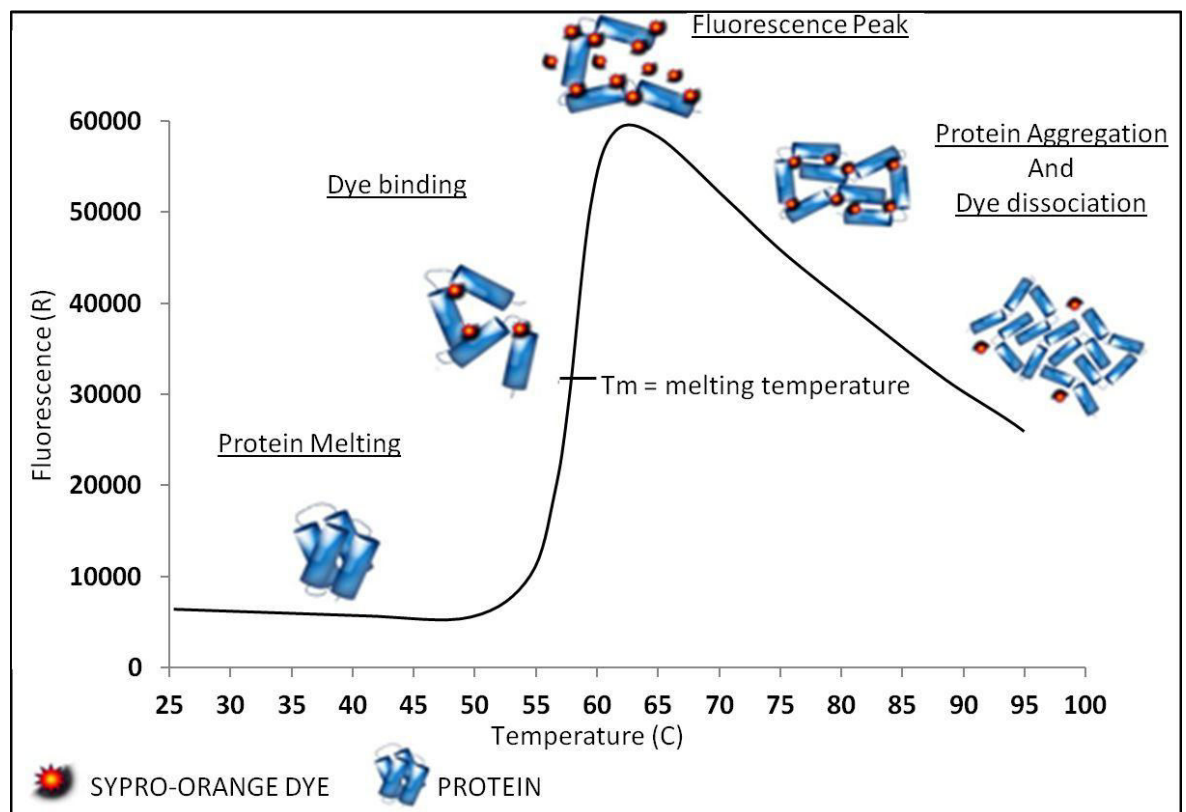
Figure 3.8 Thermal-shift fluorophore assay: general melting profile of protein depicted as the changes in fluorescence signal versus temperature of the reaction. Reproduced from www.bio.anl.gov [227].
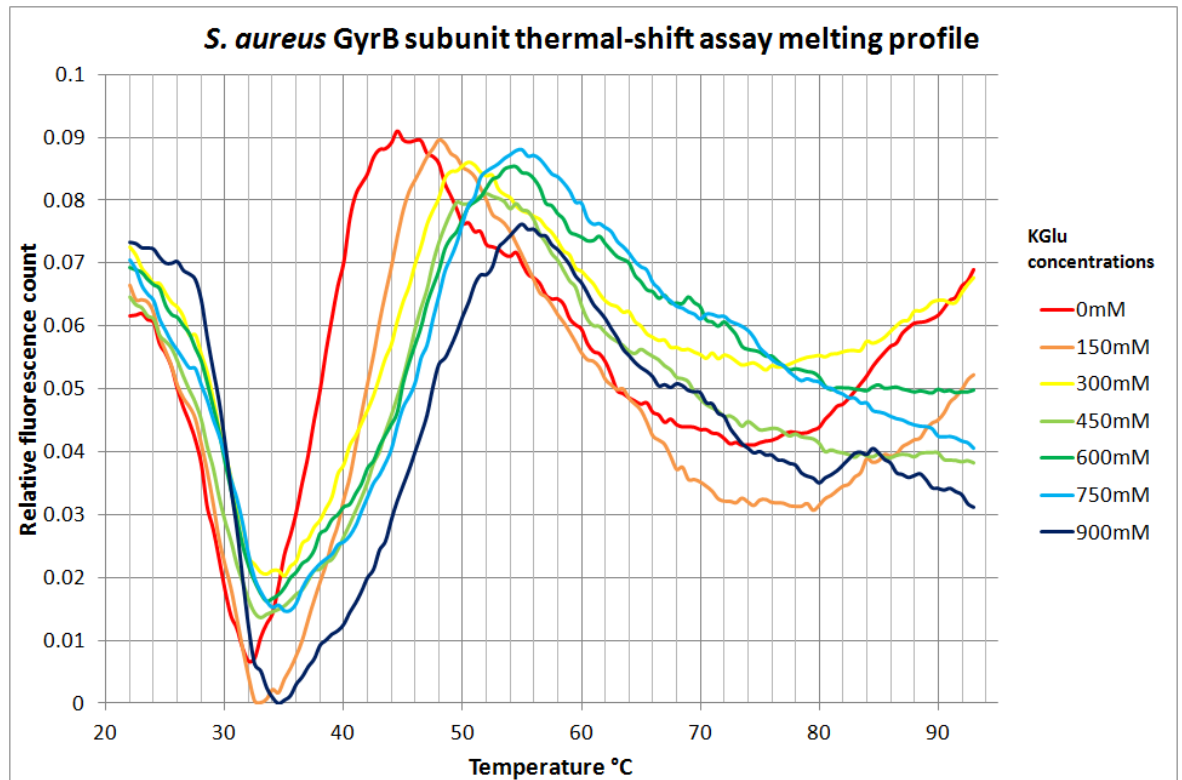
Figure 3.9 Thermal-shift assay melting profile of SaGyrB. *Note that high fluorescence observed between 20-30°C was artefact as a result of high non-specific binding at low temperature.*
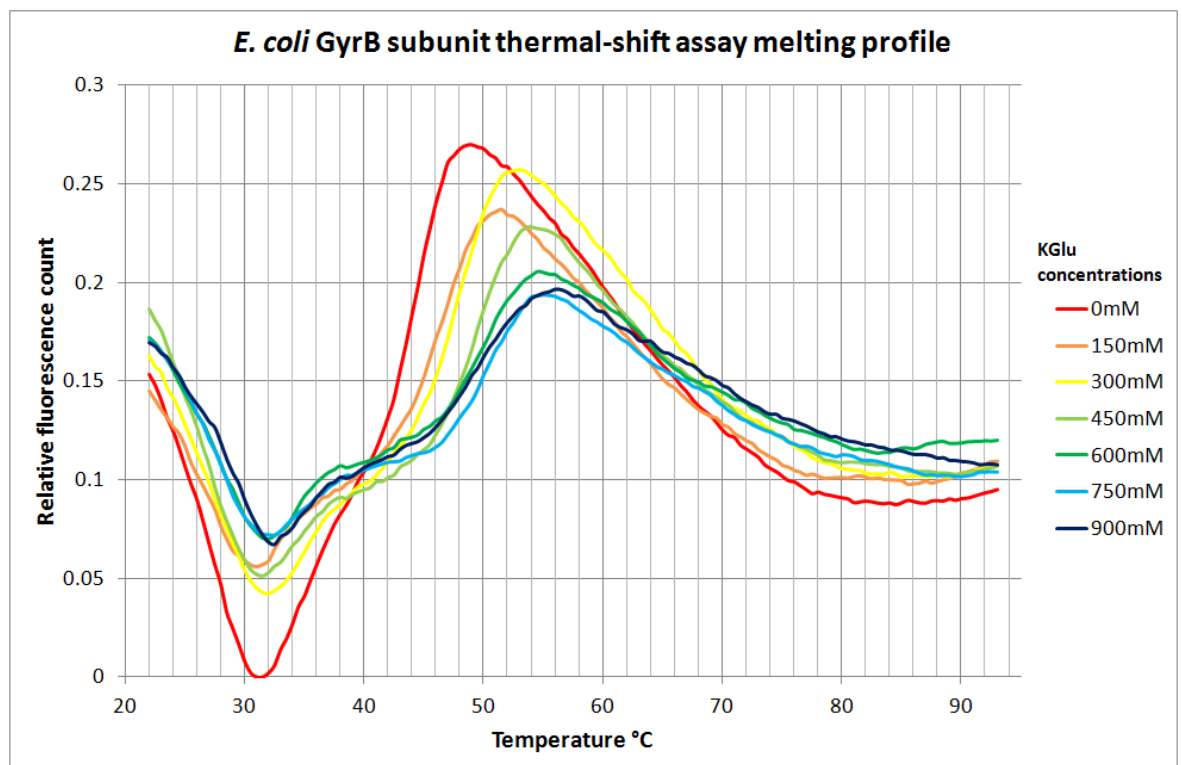
Figure 3.10 Thermal-shift assay melting profile of of EcGyrB.
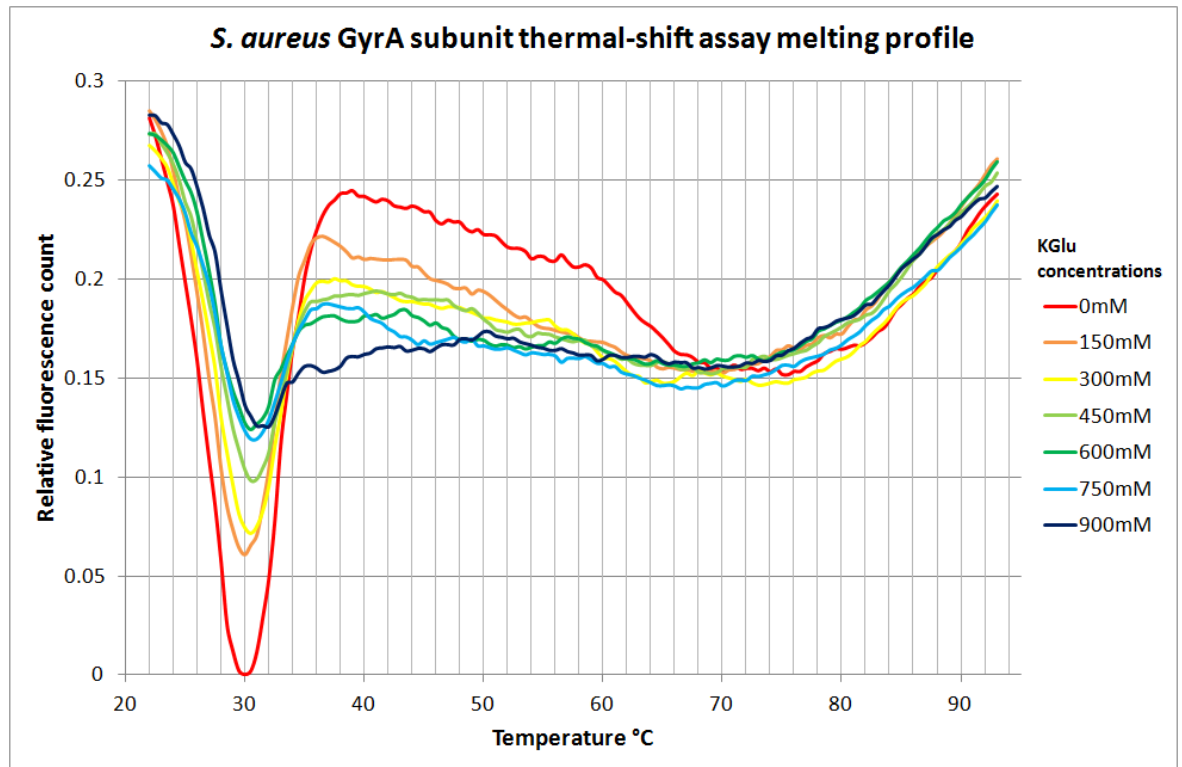
Figure 3.11 Thermal-shift assay melting profile of melting profile of SaGyrA.
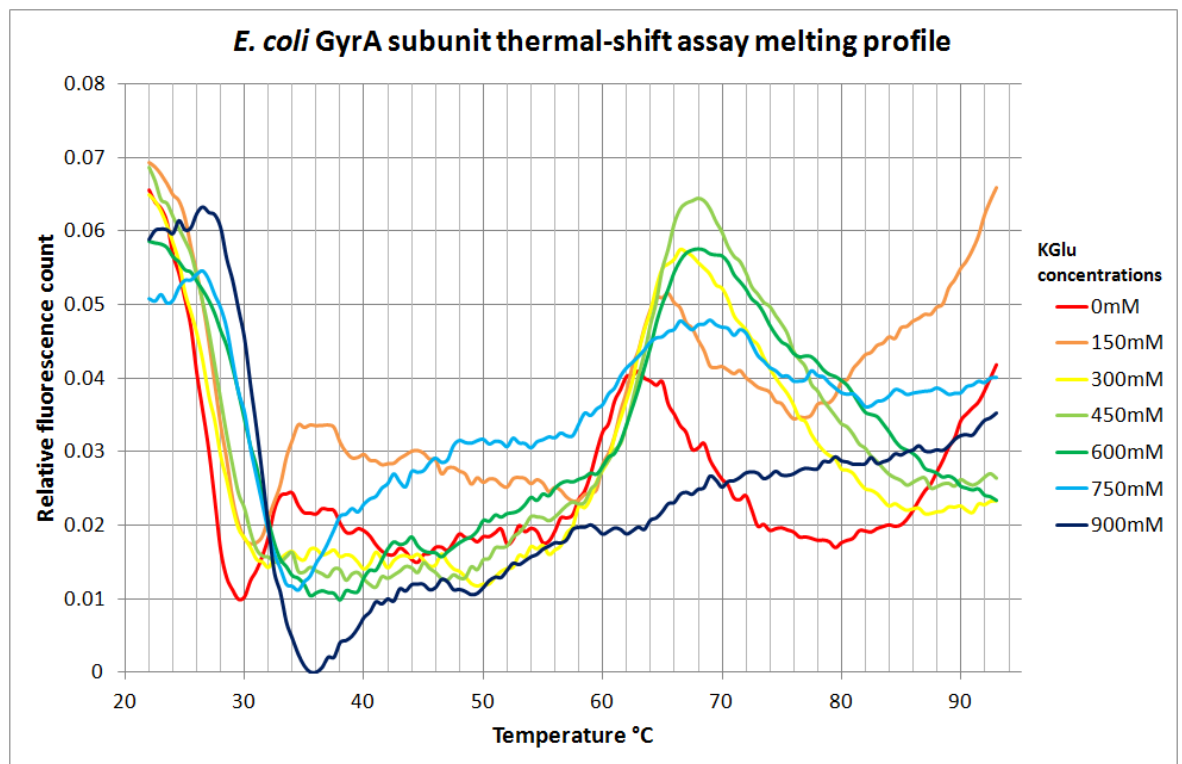
Figure 3.12 Thermal-shift assay melting profile of melting profile of EcGyrA.

In general, the increase of KGlu concentration raised the folding Tm of the proteins assayed (fig. 3.9, 3.10, 3.11, 3.12). No dramatic changes in melting temperature were observed, indicating that the concentration of KGlu does not have great influence on the folding of the proteins tested. The results overall suggested that salt dependency of *Sa* gyrase supercoiling is not related to the folding stability of protein in different KGlu concentration.

It is important to note that the melting temperature of *Sa*GyrA is potentially incorrect, as the results suggested that the protein is melting below the temperature of incubation (37°C) for the supercoiling enzyme assay. This outlying result is possibly caused by the low signal to background ratio, contributed by the lack of hydrophobic patches of *Sa*GyrA for dye binding.

3.5 Relaxation by *S. aureus* gyrase is not dependent on high KGlu concentration

Previously *Sa* gyrase was shown to depend on high concentrations of KGlu to supercoil DNA optimally. Relaxation activity of the gyrase utilises a different T-segment capturing mechanism and does not require the closure of the N-gate (as GyrB ΔNTD alone can support strand passage), ATP hydrolysis and GyrA-CTD-DNA wrapping. Therefore we decided to test relaxation activity of *Sa* gyrase in the presence of 0-900 mM KGlu for a direct comparison with the supercoiling results (fig. 3.13).
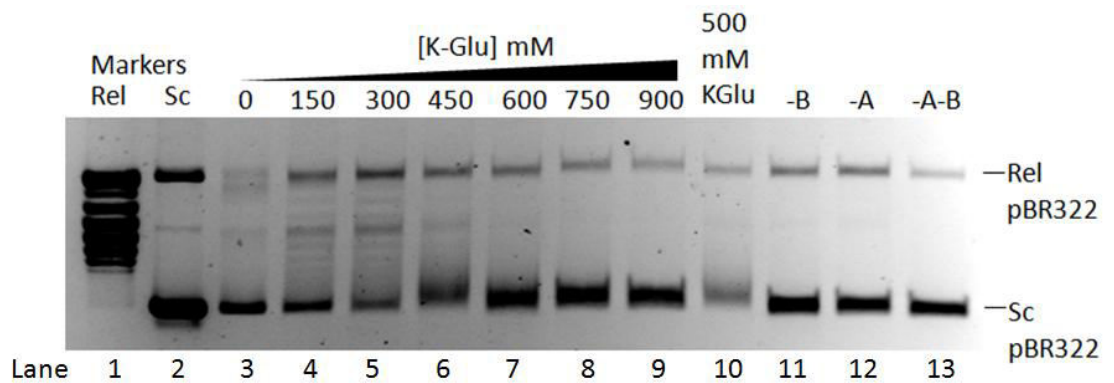
Figure 3.13. Relaxation activity of wt Sa gyrase in different KGlu concentrations showing the optimal relaxation activity between 150-450 mM KGlu.

> *Figure labels:*
>
> *Sc/Rel Markers – Relaxed and supercoiled DNA markers*
>
> *Lane 3-9 - 8 U of Sa Gyrase relaxation reaction with 0.5 ng of supcoiled pBR322 at various KGlu concentrations for 60 mins.*
>
> *Lane 10 – Positive control (0.5 ng Sc pBR322 / 8 U of Sa Gyrase / 500 mM KGlu)*
>
> *Lane 11-13 – Negative control with no Sa GyrB (-B), no Sa GyrA (-A) and no Sa GyrA and GyrB (-A-B).*

As shown in 3.14, *Sa* gyrase was found to relax optimally between 150-450 mM KGlu. Relaxation activity was minimal from >600 mM KGlu onwards. This result confirmed that *Sa* gyrase only required low concentrations of KGlu (150-300 mM) to achieve optimal relaxation while high concentrations of KGlu (>600 mM) inhibit relaxation completely.

3.6 Decatenation of *S. aureus* gyrase is not dependent on high KGlu

In addition, we decided to test KGlu dependency of decatenation in *Sa* gyrase, a strand passage process that involves unlinking catenated DNA circles. As GyrA-CTD is not required for the decatenation reaction, we also decided to use the *Sa*GyrA ΔCTD mutant gyrase to perform the experiment to eliminate the influence of the GyrA-CTD on the reaction.
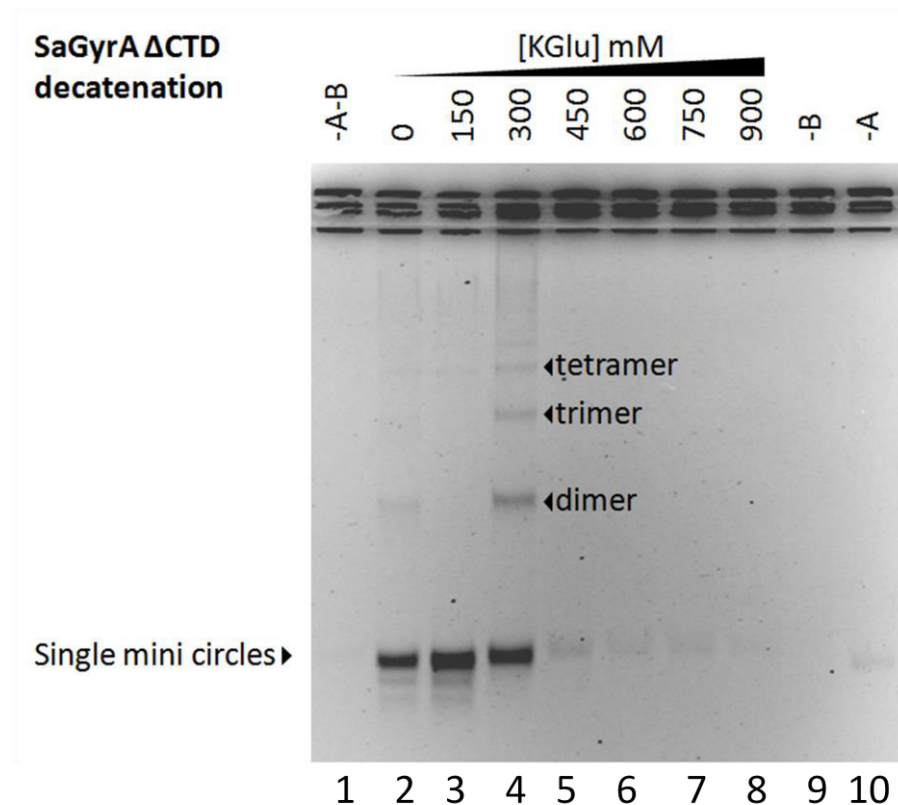
Figure 3.14 Decatenation assay of SaGyrA ΔCTD reconstituted gyrase in various concentrations of KGlu. *Decatenation assays were performed according to chapter 2.8.1.3, where any released DNA minicircles from the kinetoplast DNA (kDNA) are detected by gel-electrophoresis. Control reactions were run in lane 1, 9 and 10 where no enzyme (-A-B), A subunit only (-B) and B subunit only (-A) were included in the reactions respectively. A series of KGlu concentrations were used from lane 2 to lane 8 to assess decatenation activity of SaGyrA ΔCTD gyrase versus [KGlu]. Between 0-300 mM KGlu (lane 2-4) it was able to decatenate kDNA. It is apparent that SaGyrA ΔCTD gyrase decatenates optimally in the 0-150 mM KGlu range. In the 300 mM KGlu reaction, gyrase showing intermediate activity demonstrated by the presence of multimer circular DNA indicating incomplete decatenation.*

87

The detail methods of the decatenation reaction performed is describe in chapter 2.8.1.3. As shown in figure 3.14, *Sa* gyrase displayed decatenation activity and released mini DNA circles from the ketoplast DNA substrate between 0-300 mM KGlu in the presence of ATP (Figure 3.14 lane 2-4). At and above 450 mM negligible activity was observed. This KGlu concentration versus activity profile is fairly similar to the relaxation KGlu optimal profile (150-300 mM). It is not surprising given that the current model suggested that relaxation and decatenation reaction cycle of DNA gyrase both has similar mechanisms that only involves the passage of dsDNA within a DNA juxtaposition and no DNA wrapping . However, one mechanistic feature that decatenation shared with supercoiling yet different from relaxation is the requirement of ATP, as ATP hydrolysis greatly stimulates decatenation and is required for supercoiling but not relaxation. The ability for *Sa* gyrase to display high level of decatenation activity at low KGlu concentration therefore suggested that processes such as ATP binding, hydrolysis, and the subsequent strand passage induced are just as functional at low KGlu as well as at high KGlu.

This provided indirect evidence that ATP hydrolysis, which is crucial for both decatenation and supercoiling activity of gyrase, is not the origin of KGlu dependency.

Together, the lack of KGlu dependency demonstrated in *Sa* gyrase relaxation and decatenation leads to the conclusion that G-segment binding to the NTD of GyrA, which is required for any gyrase-strand passage including relaxation and supercoiling, is present across a wide range of KGlu (0-900 mM). While in most cases high salt concentration prevents DNA-protein binding, this combined results rules out the possibility of KGlu interfering with G-segment DNA binding and contributing to salt dependency.

Moreover, crucial mechanistic processes required for any gyrase-strand passage events (*e.g.,* relaxation, decatenation and supercoiling), such as G-segment DNA binding, DNA cleavage and resealing, DNA gate and C-gate opening, are shown to be functional at across the whole range of KGlu tested (0-900 mM). Therefore the possibility of these processes being the cause of KGlu dependency is excluded. As strand passage, the primary function of *Sa* gyrase is perfectly functional at low KGlu as demonstrated in decatenation assay, it also confirms that *Sa* gyrase is able to adopt

a functional fold in a wide range of KGlu concentration, dismissing the notion that salt dependent supercoiling are the results of salt dependent folding.

3.7 *Sa* gyrase supercoiling stimulation is specific to KGlu

In the preceding experiments it has been established that *Sa* gyrase supercoiling is stimulated by high concentration of KGlu, achieving optimal activity in the concentration range of 600-900 mM. Blanche et al [224] describe that this stimulation is specific to limited types of salt, and that replacing either the cation or anion component of the salt can completely abrogate the stimulation. As an example, both the replacement of K^+ with Na^+ (NaGlu), and Glu^- with Cl^- (KCl) results in the complete loss of supercoiling stimulation. However, as the data and methodology of the experiments were not published, we decided to carry out our own detailed examination on the claims made. Supercoiling activity of *Sa* gyrase was subsequently tested in the presence of 150-900 mM NaGlu and KCl together with KGlu as a positive control.

As shown in Fig 3.16, *Sa* gyrase showed optimal supercoiling activity between 600-900 mM KGlu as expected. When K^+ was replaced with Na^+ (NaGlu), supercoiling activity was almost completely abolished across the whole range of concentration (figure 3.15). At a closer examination, between 300-750 mM NaGlu weak supercoiling activity could be observed. More intriguingly, linear DNA was observed between 150-700 mM, with 450 mM NaGlu generating the most cleaved DNA.

Similarly when Glu^- was replaced with Cl^- (KCl), *Sa* gyrase supercoiling was defective across the whole range of concentration tested. At 150 mM KCl, weak supercoiling activity was observable whilst large amount of cleaved DNA was generated at the same time.

Although *Sa* gyrase requires a high concentration of KGlu to stimulate its DNA supercoiling activity, the fact that neither NaGlu nor KCl was able to stimulate *Sa* gyrase suggested that ionic strength of the solution is not the only factor that underpins the salt dependent stimulation phenomenon. This therefore suggested

that K^+ and Glu^- have the unique properties to provide an environment crucial for the supercoiling reaction mechanism of *Sa* gyrase. This can be elicited in two ways: K^+ and/or Glu^- could influence *Sa* gyrase in a micro sense, which involve specific binding of the ions to a specific site(s) within the *Sa* gyrase ; in a macro sense K^+ and Glu^- could be involved in non-specific binding towards *Sa* gyrase and/or the DNA substrate. Some supercoiling activities were observed when *Sa* gyrase was supplemented with 450-600 mM NaGlu or 150 mM KCl (figure 3.15).
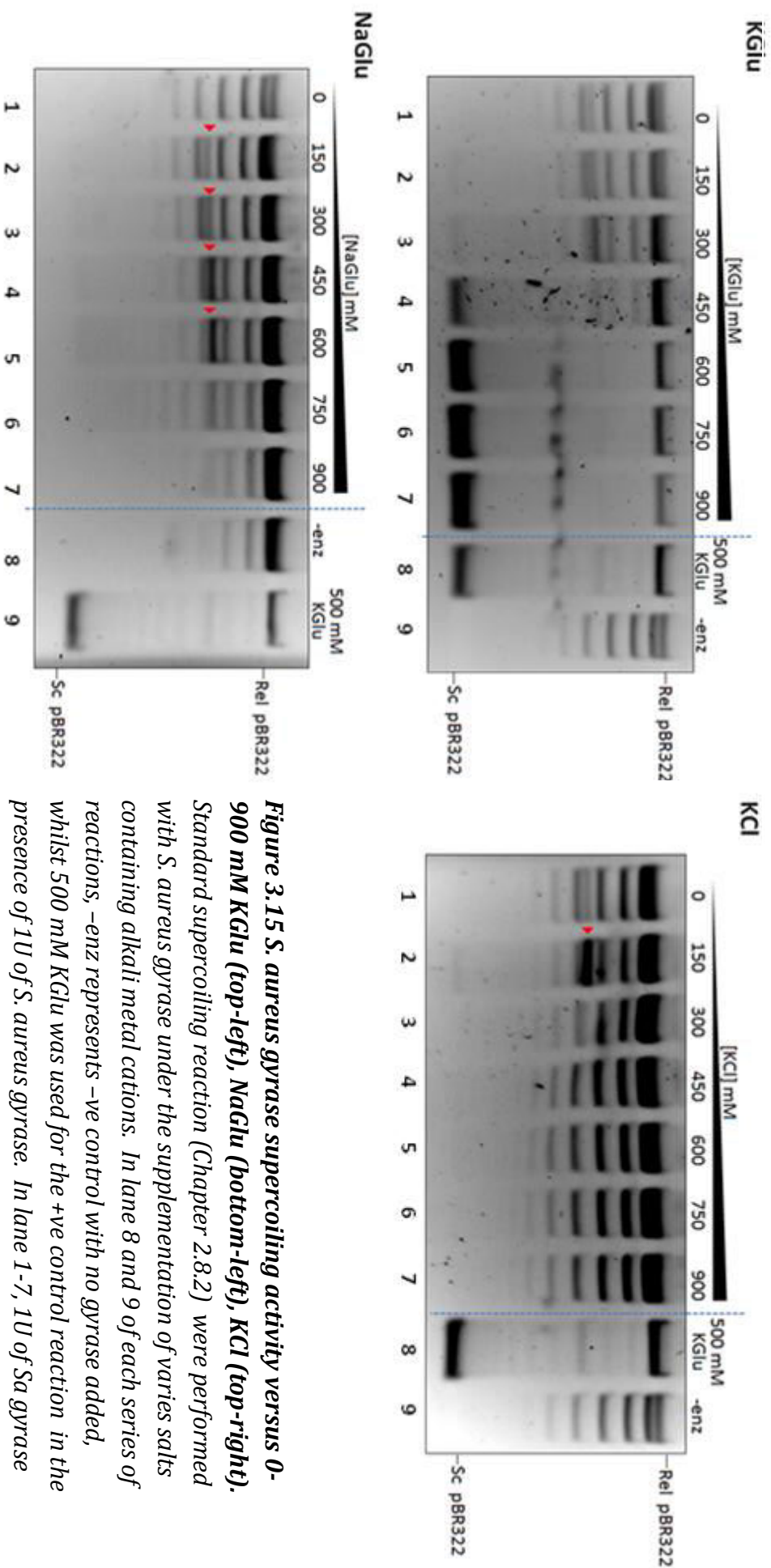
Figure 3.15 S. aureus gyrase supercoiling activity versus 0-900 mM KGlu (top-left), NaGlu (bottom-left), KCl (top-right). *Standard supercoiling reaction (Chapter 2.8.2) were performed with S. aureus gyrase under the supplementation of varies salts containing alkali metal cations. In lane 8 and 9 of each series of reactions, –enz represents –ve control with no gyrase added, whilst 500 mM KGlu was used for the +ve control reaction in the presence of 1U of S. aureus gyrase. In lane 1-7, 1U of Sa gyrase was supplemented with 0-900 mM of KGlu (top-left), NaGlu (bottom-left) and KCl (top-right). As expected Sa gyrase showed a stimulated supercoiling activity in the presence of KGlu between 450 mM and 900 mM. NaGlu and KCl were unable to stimulate supercoiling activity of Sa gyrase. Red arrows indicated the presence of linear DNA produced from dsDNA cleavage.*

3.8 *Ec* **gyrase supercoiling stimulation is not salt-specific**

Following the evidence that *Sa* gyrase supercoiling is dependent on KGlu specifically and that *Ec* gyrase is stimulated by low concentration of KGlu, we investigated if *E. coli* gyrase also displays salt specificity similar to *S. aureus* gyrase. To do that, we subjected *Ec* gyrase to conditions with different concentrations (0-900 mM) of NaGlu and KCl, with KGlu used as a control.

As shown in fig. 3.16, in the presence of >150 mM KGlu, *Ec* gyrase supercoiling is strongly stimulated as expected. Surprisingly, NaGlu (150-300 mM) and KCl (150 mM) were also able to support *Ec* gyrase supercoiling fully. The overall results confirmed that both the dependency of high concentration of KGlu and K+/Glu+ specificity are absent in *E. coli* gyrase and is unique to *S. aureus* gyrase.
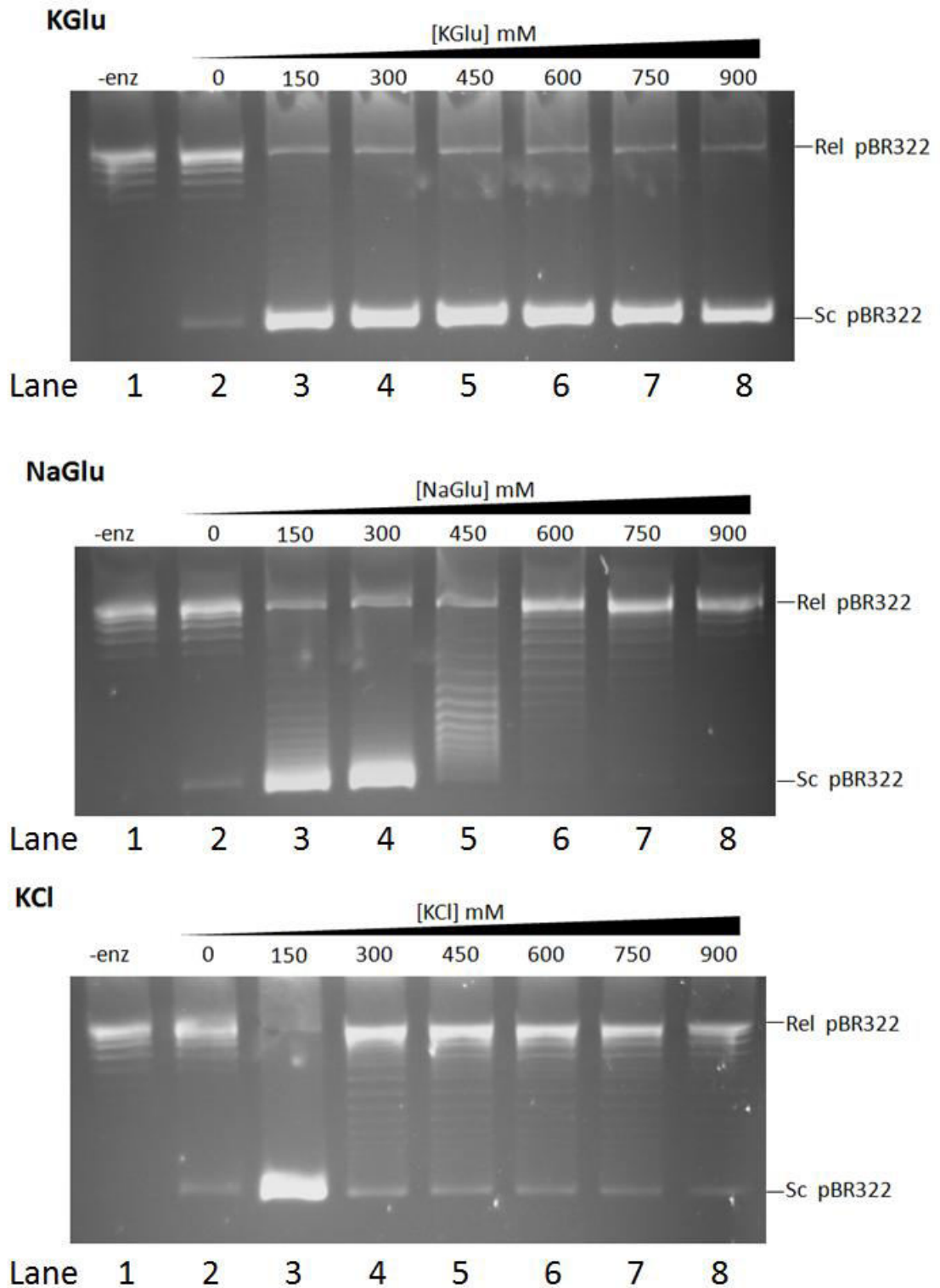
Figure 3.16. E. coli gyrase supercoiling activity versus 0-900 mM KGlu (top), NaGlu (middle), KCl (bottom). *0.5 ng of relaxed pBR322 is reacted with 1 U of E. coli gyrase for 30mins in the conditions describe in chapter 2.8.1.1. Figure labels: –enz: no enzyme control.*

3.9 Origin of salt dependency – mutant studies 1: *Sa* GyrA C-terminal tail deletion (Δ822-887)

The evidence so far suggested that supercoiling but not relaxation is dependent on KGlu, clearly indicating that KGlu plays an important role in the mechanism that sets apart supercoiling from the relaxation reaction cycle. It is understood that the majority of the strand-passage mechanism is identical between the supercoiling and relaxation reactions. The two main features in gyrase distinguish a supercoiling reaction from a relaxation reaction are:

1) The ability of the GyrA-C-terminal domains to wrap DNA.
2) The ability of the GyrB N-terminal domain to utilise energy from hydrolysed ATP to compensate for the energy uphill generated from DNA torsional strain during DNA supercoiling.

Hiasa et al. believed that the CTD of *Sa* GyrA is the origin of salt dependency, as their experimental data suggest a possible salt-dependent difference in the DNA wrapping between *Sa* and *Ec* gyrase [199].

To expand on that hypothesis we undertook a bioinformatic analysis to explore the differences between the *S. aureus* and *E. coli* GyrA C-terminal domains. The protein sequences of *S. aureus* GyrA, GyrB, ParC, ParE were aligned against the sequences of gyrases from 9 other bacteria of diverse phyla (*Brucella melitensis, Escherichia coli, Klebsiella pneumoniae, Helicobacter Pylori, Bacillus subtilis, Streptococcus pneumonia, Clostridium difficile, Corynebacterium diptheriae, Mycobacterium tuberculosis*) using a primary protein sequence alignment program (Invitrogen AlignX).

Based on the alignment data (fig. 3.18), one of the most striking differences between the CTD of *S. aureus* GyrA and *E. coli* GyrA is the addition of 38 amino acids on the C-terminal end of *Sa*GyrA. Amino acid content analysis found that this addition was largely made up of acidic residues (42%). A BLAST analysis found the addition to be present only in *Staphylococcus* organisms. In addition, due to the acidic nature of the addition, protein folding stability prediction server FoldX predicted it to be largely unfolded and hydrated.

94

Figure 3.18 Primary amino acids sequence alignments of GyrA from B. melitensis, E. coli, K. Pneumonia, H. Pylori, B. subtilis, S. pneumonia, C. difficile, C. diptheriae, M. tuberculosis and S. aureus GyrA C-terminus using AlignX®.

Based on this analysis, the highly negatively charged C-terminal peptide possessed by *Sa*GyrA has the potential to interfere with DNA-protein binding and possibly contributes to salt dependency by affecting DNA wrapping of the GyrA-CTD.

Therefore to investigate the effect of the GyrA C-terminal addition on the salt dependency of the *Sa* gyrase, a *Sa*GyrA mutant with the acidic C-terminal tail truncated Δ822-887 (*Sa*GyrA ΔCterm-tail) was produced for a comparison study with the wild-type. The KGlu dependency of *Sa*GyrA ΔCterm-tail reconstituted gyrase was

subsequently investigated.
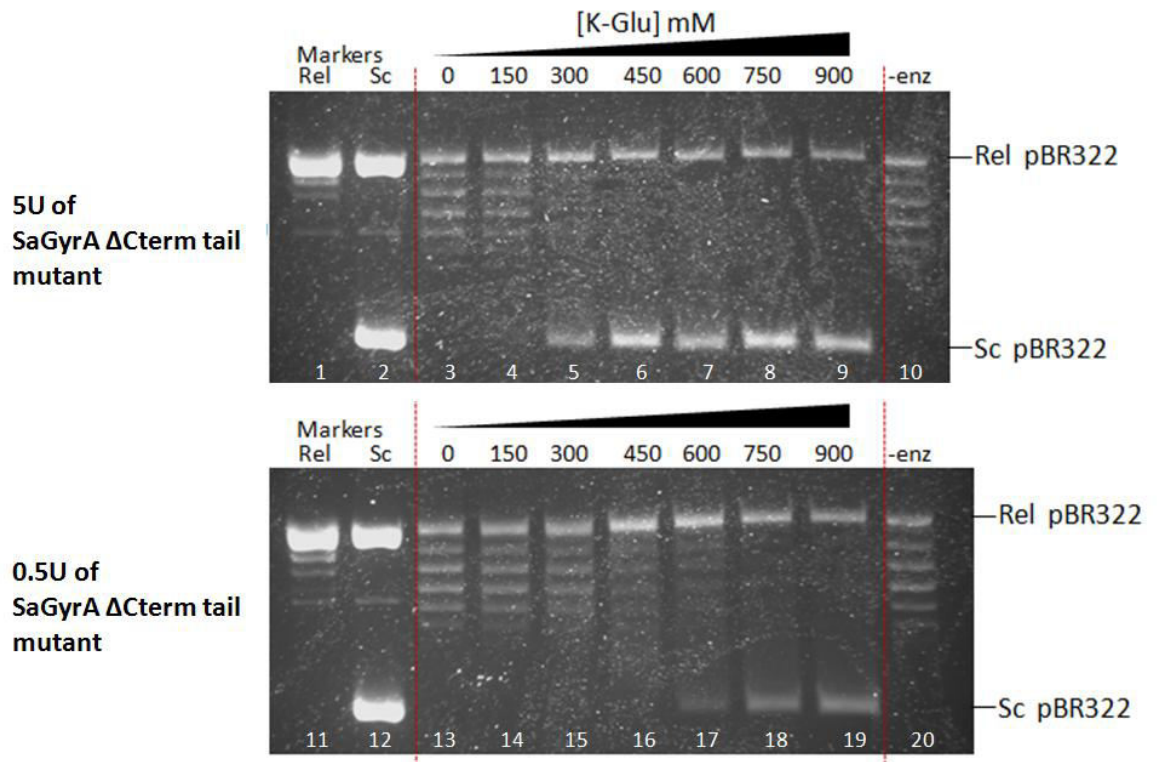
Figure 3.19. Supercoiling activity of SaGyrA ΔCterm-tail reconstituted gyrase (0.5U and 5U) in the presence of 0, 150, 300, 450, 600, 750, 900 mM KGlu . *0.5 ng of relaxed pBR322 was reacted with the reconstituted mutant gyrase for 30mins at 0-900 mM KGlu (5U gyrase: lane 3-9, 0.5 gyrase, lane 13-19). Figure labels: Rel/Sc Markers (Lane 1, 2, 11 & 12): relaxed and supercoiled DNA markers; –enz (lane 10 & 20): no enzyme control.*

As shown in figure 3.19 0.5U and 5 U of *Sa*GyrA ΔCterm-tail reconstituted gyrase was titrated against 0-900 mM KGlu. It is clear that KGlu dependency is still present as the mutant was unable to display supercoiling activity in the absence of KGlu while showing almost full supercoiling activity ~750-900 mM. With intermediate activity between 150-400 mM, the mutant showed the same trend of KGlu stimulation as the wild-type enzyme (fig. 3.20).

Figure 3.20 S. aureus gyrase DNA supercoiling at a range of KGlu concentrations.
0.5 ng of relaxed pBR322 was supercoiled by 1 U S. aureus gyrase in various
concentrations (0 – 900 mM) of KGlu (lane 2-8) in condition described in chapter 2.8.1.1.
As relaxed DNA become supercoiled, it becomes more compact and thus travels further
than its relaxed topoisomers. Note: as DNA becomes more supersoiled they become less
separable using gel electrophoresis. Therefore supercoiled DNA appeared as a single
band on the gel even in fact a range of supercoiled topoisomers is present. Figure labels:
Rel control – no enzyme is added; Sc control – 1 U of S. aureus gyrase added at 500 mM
KGlu.

This result suggests that the acidic C-terminal addition was not responsible for the
KGlu dependency of *Sa* gyrase supercoiling. Assuming that salt dependency is solely
originated from GyrA-CTD as Hiasa et al has suggested [199], the salt dependency would
have to be contributed from the differences in the composition of the core of the
GyrA-CTD.

97

3.10 Origin of salt dependency – mutant studies 2: *Sa*NTD-*Ec*CTD GyrA domain swap mutant (*Sa*ANTD (1-489)- *Ec*ACTD(523-875))

To confirm that salt dependency of *Sa* gyrase supercoiling is indeed solely contributed by the CTD of GyrA, a *Sa*NTD-*Ec*CTD GyrA domain swap protein was made to replace the CTD of *Sa* GyrA completely with its less salt-dependent *E. coli* counterpart (GyrA). The reconstituted mutant gyrase was tested against various KGlu concentrations to verify its KGlu dependency.
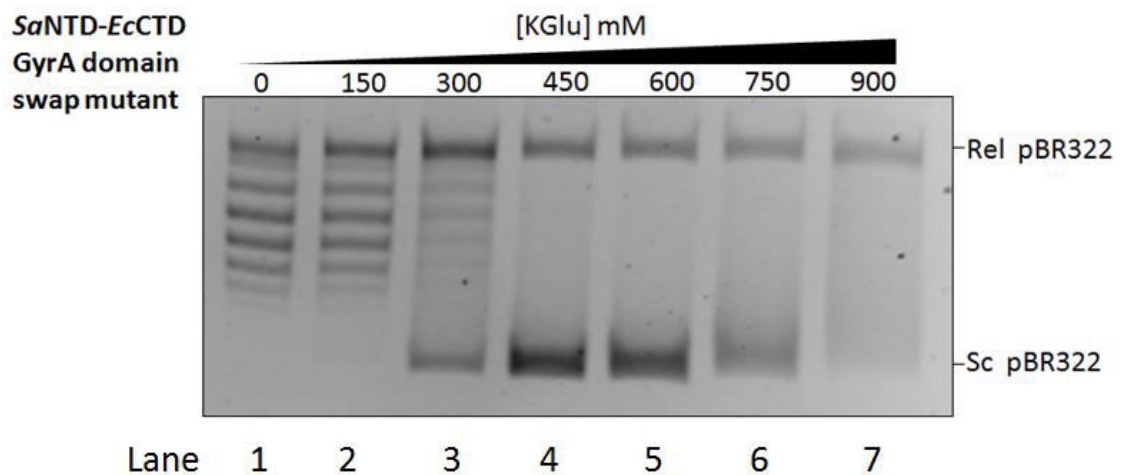
Figure 3.21. Supercoiling activity of SaNTD-EcCTD GyrA + Sa GyrB reconstituted Gyrase versus various KGlu concentrations (0 – 900 mM). *0.5 ng of DNA is supercoiled by 1 U of SaNTD-EcCTD GyrA + Sa GyrB reconstitute gyrase in the conditions described in chapter 2.8.1.1 in addition to the presence of 0, 150, 300, 450, 600, 750, 900 mM for 30 mins at 37°C. In the absence of KGlu the reconstituted mutant gyrase was unable to display supercoiling activity. The mutant gyrase supercoiling activity increases with the increase of KGlu concentration between 150-450 mM. It reaches maximal supercoiling activity between 450 mM and 600 mM, and diminished at 750-900 mM KGlu.*

As shown in fig. 3.21, no activity was observed in the absence of KGlu. Surprisingly the mutant had optimal supercoiling activity at 450-600 mM KGlu and the supercoiling activity of the enzyme at 750-900 mM KGlu concentrations were reduced in comparison to wt *Sa* Gyrase. In comparison with wt *Sa* gyrase (fig. 3.20), the domain swap mutant gyrase operates optimally in ~300 mM less KGlu.

This apparent shift in salt optimal concentration is caused by the swapping of *Sa*GyrA-CTD with *Ec*GyrA-CTD and therefore GyrA-CTD must partially contribute to KGlu dependency in *Sa* gyrase. As a crystal structure of *Sa*GyrA-CTD is not available, we have generated a structural model *via* the Swiss-Model protein structure prediction server based on the existing *E. coli* GyrA-CTD structure (PDB:1ZI0). The model structure predicted no significant structural changes in the no. of blades and integrity of the the six-blade cylinder structure in *Sa* GyrA-CTD in comparison with *Ec* GyrA-CTD. However a comparison of surface electrostatic map between the *Sa* and *Ec* gyrase CTD (fig 3.22) showed that *Sa*GyrA-CTD is much less positively charged than *Ec*GyrA-CTD, and this includes the DNA-wrapping surfaces.
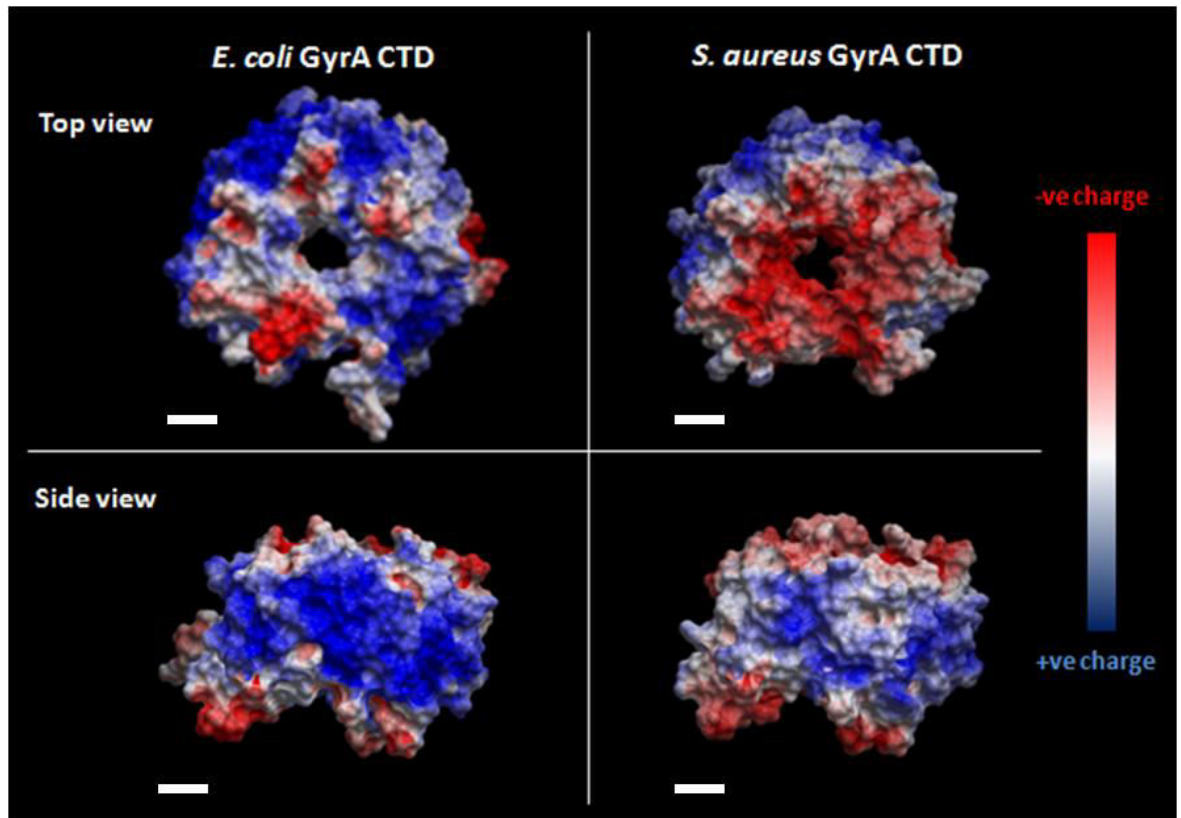
Figure 3.22 Surface electrostatic potentials of C-terminal domain (CTD) of E. coli and S. aureus (swiss model) GyrA subunit generated in Molsoft ICM-Pro. *Both the E. coli and S. aureus GyrA-CTD have cyrindrical appearance, with the its DNA-wrapping outer curved-surface filled with positively charge amino acids. S. aureus GyrA-CTD appeared to have a less electro-negative DNA-wrapping surface than its E. coli counterpart. Scale bars = 10 Å.*

Therefore, one possible explanation of the reduced salt dependency observed in the domain swap mutant is that *Sa* GyrA-CTD has weaker DNA wrapping ability and that KGlu supplementation was needed to support sufficient wrapping to sustain the supercoiling reaction. Although it is difficult to reason how increasing KGlu concentration could benefit DNA wrapping, previous studies[228] suggested how KGlu can stimulate activity of other DNA binding enzymes. It is speculated that while chloride salts encourage dissociation of DNA-protein interaction *via* charge shielding [228], the Glu⁻ ion is much more hydrated due to its kosmotropic nature and does not interfere with DNA-protein interfaces even at high concentration. In fact, high concentration of Glu⁻ ion could strengthen the water network in bulk solvent (increasing surface tension) and thereby encourages DNA-protein interaction by decreasing the entropic cost of DNA-protein association [228].

Alternatively, it is also possible that a structural difference between the *E. coli* and *S. aureus* GyrA-CTD (excluding the acidic tail) can contribute to the salt dependency.

Nevertheless, the domain swap did not completely reverse KGlu dependency to the level observed for *E. coli* gyrase, indicating that while high KGlu dependency of *Sa* gyrase is partially linked to GyrA-CTD composition, the inability to stimulate *Sa* GyrA supercoiling at lower KGlu (0-150 mM) is possibly contributed by other component(s) of *Sa* gyrase.

3.11 ATP hydrolysis does not contribute to KGlu dependency of *Sa* gyrase

Previously, we have been able to establish the partial connection between the CTD of *Sa* GyrA and high KGlu dependency. However it is clear that there is possibly a secondary element that is contributing to the KGlu dependency. Aside from DNA wrapping, ATP hydrolysis is also an essential step for gyrase to introduce negative supercoils to DNA. We therefore decided to investigate and compare *S. aureus* and *E. coli* GyrB ATPase activity in the presence of various concentrations of KGlu, NaGlu and KCl to examine the potential contribution of ATP hydrolysis to KGlu dependency.

100

The experiment utilises the PK/LDH coupled enzyme assay to colorimetrically detect the release of ADP from GyrB. As GyrB hydrolyses ATP and produces ADP + Pi, the ADP release is converted back to ATP by PK (pyruvate kinase), using PEP (phosphoenolpyruvate) as the phosphate donor. PEP is converted into pyruvate, which would be swiftly converted into lactate by LDH (lactate dehydrogenase) using NADH as a reducing agent. NAD^+ would be produced as the end product of the coupled enzyme assay and NADH/NAD conversion is monitored by measuring the decreases of OD at 340 nm. The assays were run for duration of one hour with OD_{340} measured at 1 min intervals. The decrease in OD_{340} was plotted against time to obtain a relative rate of ATP hydrolysis (fig. 3.23), which is then finally compared against the salt concentration used in the experiment.
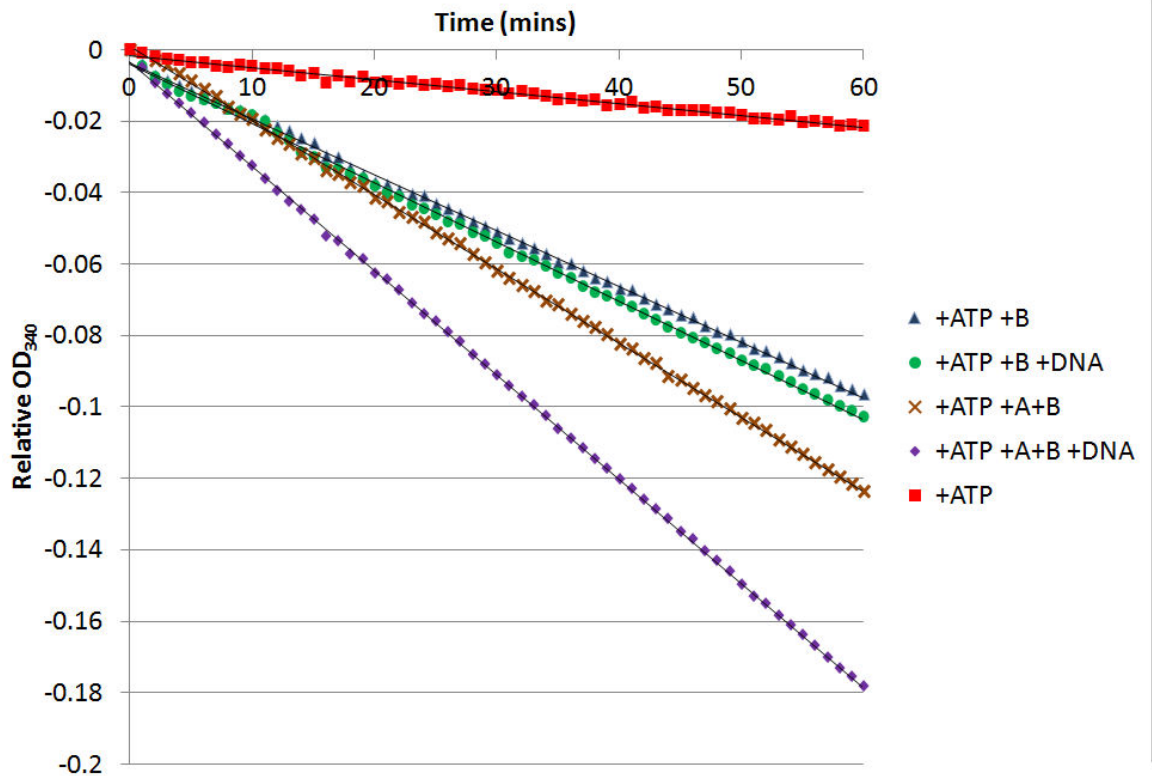
Figure 3.23. Primary absorbance data from a typical PK/LDH coupled ATPase assay. *The ATPase assay is prepared according to chapter 2.8.2. Absorbance reading at 340 nm decreases over time as ATP in the reaction is converted into ADP. Relative OD_{340} of each reaction was calculated by subtracting absorbance data by their OD_{430} reading at 0 min. Figure labels: +ATP: ATP was added; +B: 10 nM of EcGyrB subunit was added; +DNA: 0.5 ng of pBR322 was added; +A: 10 nM of EcGyrA was added. Reaction with ATP and EcGyrB subunit added (+ATP +B) showed the intrinsic ATPase activity of EcGyrB. In the presence of DNA (+ATP +GyrB +DNA), EcGyrB ATPase activity is similar to the +ATP +B reaction showing a slight stimulation. In the presence of GyrA (+ATP+A+B), EcGyrB display is noticeably stimulated in its ATPase activity, possibly as a result of the presence of EcGyrA assisting GyrB dimerisation. In the presence of EcGyrA and DNA (+ATP+A+B+DNA), GyrB displayed the most stimulation in its ATPase activity by triggering the DNA-dependent ATPase activity of Gyrase [84].*

Surprisingly, the stimulation profile of *Sa*GyrB ATP hydrolysis by KGlu (fig. 3.24) was similar to that of *Ec*GyrB (fig. 3.25), both enzymes showed low ATPase activity in the absence of KGlu. While the extent of stimulation varies between different salts, both enzymes hydrolyse ATP optimally beyond 450 mM. This was unexpected, as *Ec* gyrase is able to supercoil optimally in the presence of ~150 mM of KGlu/NaGlu/KCl. In addition, NaGlu and KCl were able to stimulate SaGyrB ATP hydrolysis to a similar extent to KGlu, with optimal activity observed at around ~600-750 mM. This is unexpected as NaGlu and KCl was not able to stimulate *Sa* gyrase supercoiling activity at all.

The results showed that the optimal salt-stimulation of ATPase activity in both *E. coli* and *S. aureus* GyrB does not match with its supercoiling activity versus KGlu profile. This suggested that although ATPase activity is essential to gyrase supercoiling activity, its rate of hydrolysis is only weakly linked to its ability to optimally supercoil DNA. The fact that *Ec* gyrase was able to fully supercoil the DNA substrate based on minimal ATPase activity at 0 mM KGlu also showed that ability for gyrase to supercoil DNA to a high negative supercoil saturation set-point is not dependent on ATP hydrolysis.
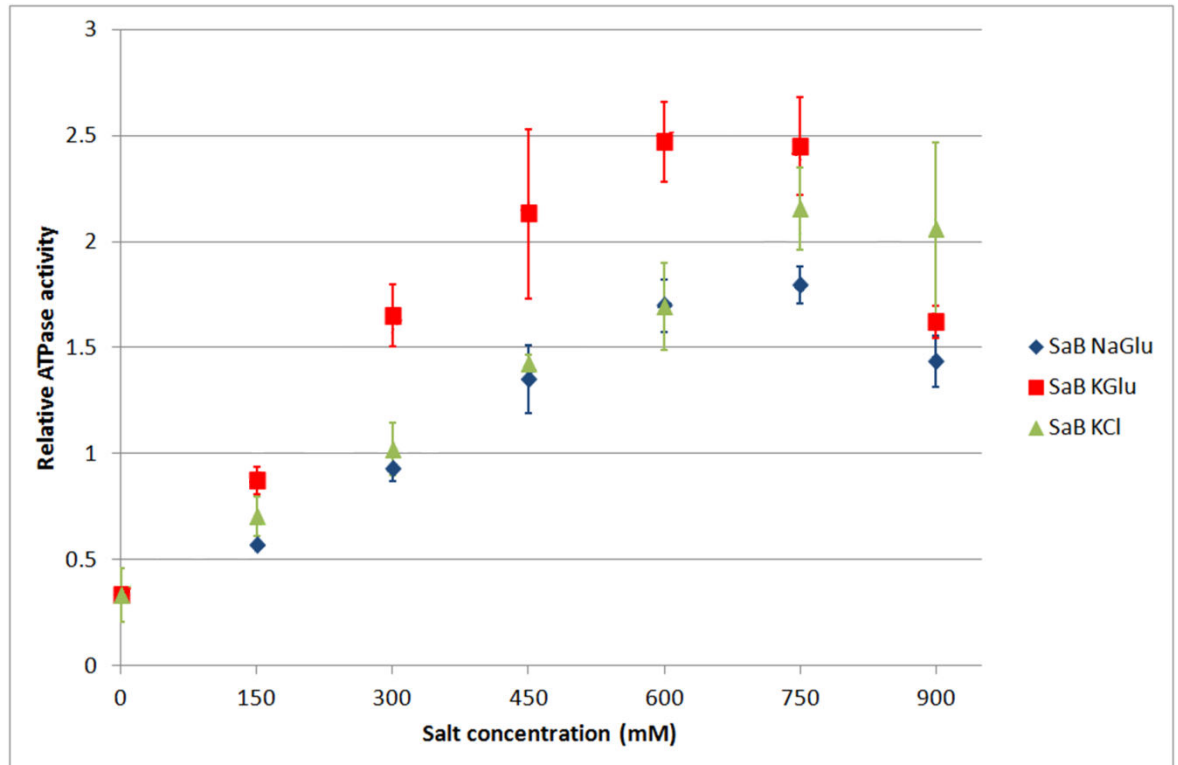
Figure 3.24 S. aureus GyrB DNA-independent ATP hydrolysis rate versus 0-900 mM of KGlu, NaGlu and KCl. *ATP/NADH coupled ATPase assay were preformed according to methods in chapter 2.8.2. using ~64 nM S. aureus GyrB subunit. ATPase activity of S. aureus GyrB were tested in triplicate in 0, 150, 300, 450, 600, 750 and 900 mM concentrations of sodium glutamate (NaGlu), potassium glutamate (KGlu) and potassium chloride (KCl). Linear regression models similar to fig. 3.23 were generated from from each reaction using the OD_{340} absorbance of a minimium of 20 consecutive time points with 1 min intervals. Relative ATPase activity of each reaction was calculated from the gradient of the regression model ($-\Delta OD_{340}.s^{-1}$) of each reactions, as the $-\Delta OD_{340}.s^{-1}$ corresponded to the disappearance of NADH within each reaction, which is proportion to the release of ADP from ATP hydrolysis. Data points on the graph showed the average of the relative ATPase activity from the triplicate reactions, with the error bars showing the standard deviation values calculated from the three sets of data in each concentration.*

This suggests that ATP hydrolysis is not the rate limiting step for the supercoiling cycle. The fact that both enzymes shared similar ATPase activity profile versus KGlu concentration suggested that ATPase activity is not the factor differentiating the two enzymes in terms of KGlu dependency. The comparable ATPase stimulation of the GyrB subunits of *E. coli* and *S. aureus* by KGlu, NaGlu and KCl titration clearly

suggested that ATPase activity does not contribute to salt dependency and specificity observed in *Sa* gyrase.
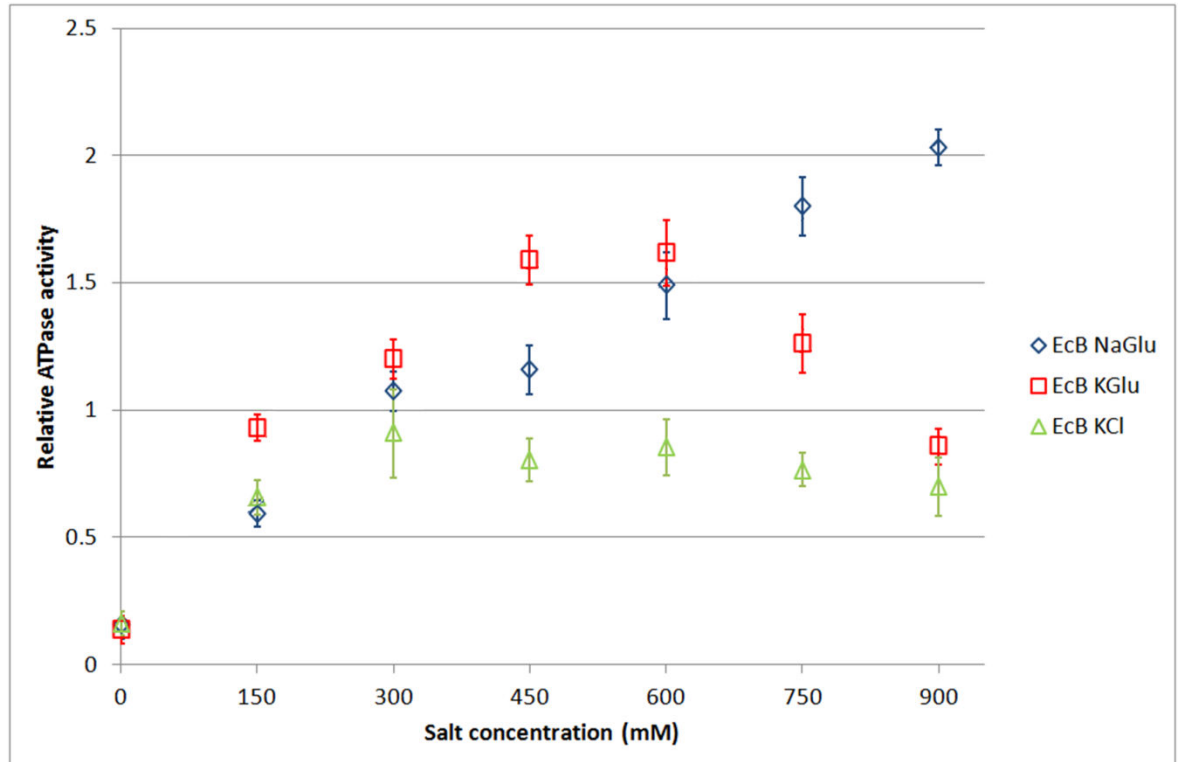
Figure 3.25 E. coli GyrB DNA-independent ATP hydrolysis rate versus 0-900 mM of KGlu, NaGlu and KCl. *ATP/NADH coupled ATPase assay were preformed according to methods in chapter 2.8.2. using ~10 nM concentration of E. coli GyrB subunit. ATPase activity of E. coli GyrB were tested in triplicate in 0, 150, 300, 450, 600, 750 and 900 mM concentrations of sodium glutamate (NaGlu), potassium glutamate (KGlu) and potassium chloride (KCl). Linear regression models similar to fig. 3.23 were generated from from each reaction using the OD_{340} absorbance of a minimium of 20 consecutive time points with 1 min intervals. Relative ATPase activity of each reaction was calculated from the gradient of the regression model ($-\Delta OD_{340}.s^{-1}$) of each reactions, as the $-\Delta OD_{340}.s^{-1}$ corresponded to the disappearance of NADH within each reaction, which is proportion to the release of ADP from ATP hydrolysis. Data points on the graph showed the average of the relative ATPase activity from the triplicate reactions, with the error bars showing thestandard deviation values calculated from the three sets of data in each concentration.*

3.12 Discussion and Conclusion

E. coli gyrase has been the subject of study for the last three decades and continues to be a subject of fascination. Gyrase's multi-fasit mechanism and the dynamism of its supercoiling cycle are intriguing, as it remains unclear how it is able to regulate DNA topology through its coordinated double-strand passage mechanism without causing permanent DNA damage or breakage.

In this chapter, we begin our investigation with the aim to identifiy and explain the effect of salt concentration on the supercoiling activity of *Sa* gyrase. This was carried out originally with the intent to understand the underlying differences in KGlu dependency between *Sa* gyrase and its *E. coli* counterpart. Although previous studies have attempted to identify the cause of this phenomenon [224,229], it was far from conclusive, with no clear explanation offered as to why high concentration of potassium and glutamate specifically was required to support the DNA supercoiling activity of *Sa* gyrase. By understanding this unique feature of *Sa* DNA gyrase, we hoped to unlock more unknown mechanistic details of gyrase.

Through numerous biochemical examinations we were able to gain an improved understanding on the origin of the unusual high KGlu dependency displayed in *Sa* gyrase for its DNA supercoiling activity.

3.12.1 Effect of salt on *Sa* gyrase supercoiling

We began the investigation by studying the relative supercoiling activity of *Sa* gyrase in the presence of various concentrations of KGlu. The *E. coli* gyrase was also tested in identical conditions as a direct comparison. We established that *Sa* gyrase indeed displayed a strong dependency on KGlu for its supercoiling activity as it requires 300 mM to begin to supercoil DNA, whereas *E. coli* gyrase showed some supercoiling activity in salt-less condition. The DNA supercoiling activity of *Sa* gyrase was gradually stimulated as KGlu concentration was increased to upto 750 to 900 mM. This confirms the differential KGlu requirement for *Sa* gyrase but not *E. coli* gyrase, which warranted further investigation.

3.12.2 Specificity of salt stimulation of *S. aureus* gyrase supercoiling

After we confirmed the presence of the KGlu dependent supercoiling stimulation in *Sa* gyrase, we were curious to investigate further on why KGlu in particular was able to support its acitivity. In an attempt to establish the specific salt requirement for the supercoiling activity of *Sa* gyrase, we tested the supercoiling activity of *Sa* gyrase in the presence of various salts with different ion components, such as NaGlu and KCl. We discovered that the supercoiling activity of *Sa* gyrase could not be stimulated by NaGlu as the K^+ component of KGlu is replaced by Na^+. This result implies that the presence of a K^+ ion is crucial to the supercoiling function of *Sa* gyrase and that Na^+ can not support it. Furthermore, Glu^- ion also appears to be essential to the function of *Sa* gyrase as KCl could not support its supercoiling activity.

3.12.3 Effect of salt on *S. aureus* gyrase relaxation and decatenation

Whilst we were able to establish that *Sa* gyrase required K^+ and Glu^- ions specifically to stimulate its supercoiling activity, we were intrigued to find out if relaxation and decatenation of *Sa* gyrase is influenced by salt.

The reaction mechanism responsible for the relaxation of *Sa* gyrase is intrinsically different to that of the supercoiling reaction, as DNA relaxation of gyrase does not require the wrapping of DNA around the CTD of GyrA. Therefore, mechanistically, the enzyme can undergo DNA relaxation in the absence of the CTD of GyrA [230]. This is evidented in a previous study [230] where a mutant E. coli gyrase without CTD of GyrA was able to relax and decatenate DNA but displayed no DNA supercoiling activity. Gyrase DNA decatenation mechanism was proposed to be similar to that of the DNA relaxation [230], where strand-passage was initiated as soon as the DNA juxtaposition in the cross-over between the two dsDNA is recognised by the GyrA and GyrB units.

Interestingly, both relaxation and decatenation activity of *Sa* gyrase did not require high KGlu activity. Decatenation activity of *Sa* gyrase is unaffected by the absence of salt and is able to decatenate at a near optimal level at 0 mM KGlu. On the other hand relaxation activity of *Sa* gyrase required a low concentration of KGlu. It relaxes

optimally at 300 mM KGlu and did not require high concentration of KGlu (>600 mM). This implied that the high KGlu requirement for *Sa* gyrase is confined to its supercoiling activity. The enzyme is able to undergo decatenation in the absence of KGlu also indicates that the strand passage mechanism is fully functional without KGlu. It is important to note that unlike decatenation, relaxation activity of *Sa* gyrase required a low concentration of KGlu. This indicated that subtle differences may lie between the relaxation and decatenation mechanism of gyrase, as they displayed subtle differences in their activity profile against KGlu concentrations.

3.12.4 Folding stability of gyrase as a function of potassium glutamate concentration

As the changes in salt concentration are likely to have an effect to the folding of gyrase, it is necessary to ensure that the KGlu dependency is not the result of salt dependent protein folding. We have tested the thermal stability of A and B unit of both *Sa* and *E. coli* gyrase in the presence of different concentrations of KGlu using the thermal-shift fluorophore assay. Overall the thermal stability of both A and B units of *E. coli* gyrase and the *Sa* GyrB remained stable across the entire range of KGlu concentrations tested (0-900 mM). *Sa* GyrA, however, displayed an surprising melting profile with a Tm of ~37°C. This is not possible as *Sa* gyrase is functional at 37°C, as demonstrated repeatedly by the supercoiling assays (37°C reaction temperature). Alternatively, this could have been a false result or the result of the presence of other contaminants (such as lipids) remained after the purification process. It remained unconclusive as to whether potassium glutamate influences supercoiling activity of the *Sa* gyrase by altering its folding.   However, the fact that *Sa* gyrase is able to complete DNA strand-passage in the absence of KGlu may suggest that it is able to retain its structural intergrity without the presence of KGlu.

3.12.5 The salt dependency of *S. aureus* gyrase is not dependent on the GyrA C-terminal tail.

Hiasa et al. [229] previously proposed that the CTD of GyrA of *Sa* gyrase, responsible for the wrapping of the DNA substrate, is different to that of the *E. coli* gyrase and that this difference contributes to the salt-dependent supercoiling behaviour in *Sa* gyrase. Here, we attempted to identify the key difference between the CTD of SaGyrA and EcGyrA and locate the potential origin of salt dependency. By bioinformatics analysis, we were able to identify a 40 amino acid "tail", consisting of largely negatively charged amino acids, towards the C-terminus of *Sa* GyrA unique to staphylococcus organism. Due to its acidic nature, we initially proposed that it may interfere with the wrapping of DNA.

Subsequently, we have produced a mutant *Sa* gyrase (*SaGyrA ΔCterm-tail*) with a truncated C-terminal tail to investigate the function of the acidic tail. Suprisingly, the C-terminal tail truncation did not produce any notable changes on the supercoiling activity nor the salt-dependency of the enzyme. It is therefore apparent that the origin of KGlu dependency lies in other parts of the *Sa* Gyrase.

3.12.6 The salt dependency of *S. aureus* gyrase is only partially attributed to the CTD region of the GyrA subunit

In order to examine whether the CTD of *Sa* GyrA indeed contributes to the salt-dependent behaviour of *Sa* gyrase, we have produced a domain-swap GyrA mutant which constitutes a NTD from *Sa* GyrA and a CTD from *E. coli* GyrA. The reconstituted domain swap mutant *Sa* gyrase displayed a reduced salt-dependent activity profile when compared with wt *Sa* GyrA. Although we were unable to revert the KGlu dependency of *Sa* gyrase to that of a wt *E. coli* gyrase by the GyrA-CTD domain swap, we were able to deduce that the high KGlu dependent supercoiling activity displayed by *Sa* gyrase is partially attributed to the *Sa*GyrA-CTD. This is a contradicting result to Hiasa et al. [229] as they proposed that salt-dependency is entirely attributed by the CTD of *Sa* gyrase. As the CTD of GyrA is solely responsible for the wrapping of the T-segment DNA, we proposed that the presence of a high concentration of KGlu assisted the wrapping of DNA through an unknown mechanism.

3.12.7 The salt dependency of *S. aureus* gyrase is not dependent on the ATPase reaction

Whilst we were able to confirm that CTD of *Sa* gyrase only partially contributed to its salt-dependent supercoiling characteristics, it was unclear as to what contributed to the remaining salt-dependent supercoiling behaviour of the enzyme. As the hydrolysis of ATP is essential to the supercoiling but not relaxation or decatenation activities of DNA gyrase, we decided to investigate the potential link between salt concentration and the hydrolysis of ATP by gyrase. Intriguigingly, both *Ec* and *Sa* GyrB were able to hydrolyse ATP in the absence of KGlu/KCl/NaClu. Moreover, both ATP hydrolysis of *Ec* and *Sa* gyrase were stimulated as salt concentration was increased. As *Ec* and *Sa* GyrB hydrolyse ATP at a similar rate when exposed to different concentrations of various salts, it is apparent that ATPase hydrolysis does not contribute to high KGlu-dependent and KGlu-specific supercoiling. This was further confirmed as the ATPase activity of *Sa* GyrB was decreased by a third between 750 mM and 900 mM KGlu (figure 3.24), whilst there were no observable differences in the supercoiling activity of *Sa* gyrase between 750 mM and 900 mM KGlu (figure 3.2 & 3.6). Although ATPase activity is crucial to the supercoiling activity of *Sa* gyrase, it only requires a certain rate of ATP hydrolysis to support the rate of supercoiling. Any additional stimulation in ATP hydrolysis beyond a certain threshold does not appear to increase the rate of DNA supercoiling. Thus it can be concluded that ATP hydrolysis is not the rate-limiting step of DNA supercoiling at medium (300 mM) to high (900 mM) salt concentration.

Nevertheless, this is the first time that gyrase ATP hydrolysis was reported to be stimulated by the presence of a monovalent ion-containing salt. In the light of our findings in chapter 5 where two novel monovalent metal ions (M^+) binding sites were identified in close proximity to the ATP binding pocket, it can be argued that the increase of Na^+ and K^+ concentration could potentially stimulate the hydrolysis of ATP by specific binding to the M^+ binding sites. Future investigations could be conducted to further establish if the stimulation of ATP hydrolysis is indeed specific to M^+ containing salts by testing it against other monovalent non-metal ions containing salt, such as ammonium (NH_4) salt.

3.12.7 New lights on the mechanistic understanding of high KGlu-dependent supercoiling in *S. aureus* gyrase

With the new evidence emerged with the current studies, *Sa* gyrase was found to be stimulated by the presence of KGlu in a concentration-dependent manner. Nonetheless, we were unable to deduce the kinetics behind the stimulation without further quantitative evidence. It can be concluded that GyrA CTD of *Sa* gyrase contributed to the KGlu dependent supercoiling. We were, however, unable to revert the KGlu dependency of *Sa* gyrase to that of a wt *Ec* gyrase by domain-swapping the CTD of *Sa*GyrA. Therefore, it can be argued that high-KGlu dependent is not solely contributed by the CTD of GyrA and that a **secondary mechanism** is present, which prevents the progression of the supercoiling reaction cycle of the *S. aureus* gyrase at low KGlu.

Using the experimental evidence gathered in the various investigations carried out, we were able to eliminate the following events as the contributing factor(s) to the salt-dependent supercoiling of *Sa* gyrase:

1. ATPase hydrolysis

2. Protein folding

3. G-segment DNA binding

4. DNA cleavage and resealing

5. DNA gate operation

6. C-gate operation

While we are unable to fully elucidate the origin of KGlu dependency, by examining the processes essential and unique to the supercoiling mechanism of DNA gyrase, we were able to narrow down to two possible causes that could contribute to the secondary origin of KGlu dependency:

1. T-segment DNA capture
2. N-gate operation

The operation of the N-gate has been difficult to study due to its dynamic nature and the lack of structural information for full length GyrB. Recently several SM-FRET studies carried out by Klostermeier et al. [231] were able to give further insight into the intricately co-ordinated processes involved in N-gate operation. Narrowing and closure of the N-gate, T-segment capture and ATP binding are considered to be a series of closely co-ordinated processes that initiate the gyrase strand-passage reaction. In addition, recent studies from the Klostermeier group found that *B. subtilis* gyrase supercoiling activity is dependent on the presence of K^+ [231]. Surprisingly, similar to *Sa* gyrase, Na^+ was unable to stimulate *B. subtilis* gyrase supercoiling. Subsequent SM-FRET further revealed that K^+ is essential to the complete closure of the N-gate. Gubaev et al. [231] speculated that K^+ binding at a monovalent metal cation (M^+) binding site conserved in GHKL ATPase assisted closure of the N-gate. This site was predicted to be an octahedrally-coordinated binding site located around residues Ile94, Val97, A100, G117, S121 and the α-phosphate of the ATP substrate. However, in previous crystal structures, only electron density equivalent to a water molecule was ever observed in the site predicted. Our attempt to co-crystallise *E. coli* GyrB-NTD with sodium and potassium has yielded the discovery of two M^+ binding sites with different ion preferences. This discovery which could potentially explain the missing link in *Sa* gyrase KGlu dependency and *B. subtilis* gyrase K^+ dependency, will be described in chapter 5. Further implications of the discovery of the two M^+ binding sites on KGlu dependency of *Sa* gyrase and K^+ dependency of *B. subtilis* gyrase will be discussed further in chapter 5.

3.12.8 The mistery of KGlu-specific *S. aureus* gyrase supercoiling stimulation

The specific requirement of K^+ and Glu^- to support *Sa* gyrase supercoiling remained unclear. *E. coli* gyrase not only displayed no dependency on high salt, it also showed no salt specificity, as it is able to supercoil in the presence of K^+/Na^+ and Glu^-/Cl^-. Therefore, the strigent requirement of a K^+ and Glu^- ion for DNA supercoiling in *S. aureus* gyrase appears to be unique to the enzyme.

As we established from the model generated for the CTD of *S. aureus* GyrA, it has less positively charged amino acid residue and therefore is likely to display a weaker ability to wrap DNA in comparison to *E. coli* gyrase. Previous studies on the "glutamate effect" on other DNA interacting enzymes suggested that the kosmotropic nature of Glu^- ion could lead to entropy reduction in DNA-protein association [228]. It is therefore possible that the presence of Glu^- could have assisted the weak DNA wrapping ability of *S. aureus* gyrase and enables it to undergo its supercoiling reaction cycle. Replacing Glu^- with Cl^- could therefore upset the entropy reduction effect of Glu^-, which in turn affects the DNA wrapping ability of *S. aureus* gyrase. On the other hand, the increases in concentrations of monovalent ions such as $K+$ in DNA-protein interaction systems are often found to be detrimental. Studies suggested that the K^+ would bind onto the negative charge of the DNA backbone and compete with the DNA-protein surface binding and weakens the DNA-protein interaction.

Additionally, as a secondary origin of KGlu dependency is envisaged, it can be hypothesised that K^+ is directly linked with this secondary factor while Glu^- is associated with the primary-factor, *i.e.,* DNA wrapping. The evidence that K^+ supports supercoiling by ensuring N-gate closure in *B. subtilis* gyrase, and the discovery of the two novel M^+ binding sites on *Ec* GyrB-NTD (Chapter 5) suggests that such an ion binding mechanism can potentially be the secondary origin of *Sa* gyrase supercoiling. The potential K^+/Na^+ preference in the two M^+ binding sites may also provide the K^+-specific stimulation seen in *S. aureus* gyrase and *B. subtilis* gyrase but not *E. coli* gyrase. Further implications of the two GyrB-NTD M^+ binding sites on *Sa* gyrase K^+ dependency and specificity will be discussed in detail in chapter 5.

Chapter 4 - *S. aureus* DNA gyrase as antibacterial target

4.1 Introduction

Ever since the introduction of the fluoroquinolones, the only class of clinically successful gyrase inhibitors, DNA gyrase has been regarded as one of the most effective antibacterial targets. However, as traditional fluoroquinolones were more effective against gram-negative bacteria, DNA gyrase has been relatively neglected as an antibacterial target for the gram-positive pathogens. While the pressure to develop new anti-*S. aureus* treatments are increasing, DNA gyrase could be the "Achilles heel" of MRSA and provides the low-hanging fruits for antibacterial discovery.

4.2 Naphthoquinones

The Naphthoquinones are a class of chemicals widely produced across *Streptomyces* [232-233], plant and fungi [234]. They are found to display a diverse range of bioactivity, including antibacterial [235-237], anti-fungal, antiviral [238], anti-malarial [239], antitrypanosomal and anti-cancer activity [240]. Naphthoquinones in plants often contain the 1,4-Naphthoquinone core (fig 4.1).
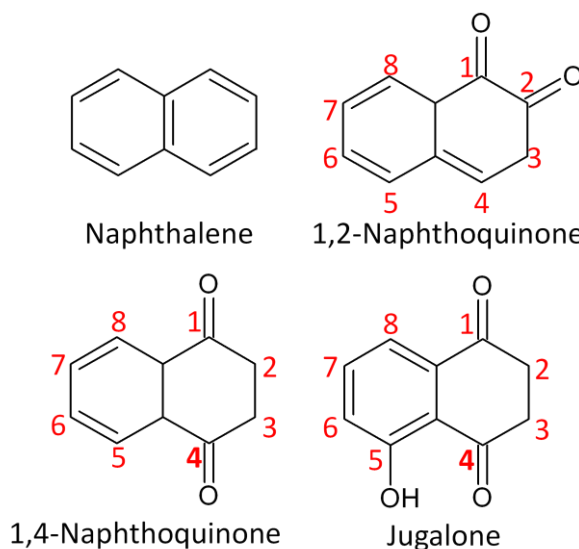
Figure 4.1. Chemical structure of basic naphthoquinones

Naturally occurring naphthoquinones *e.g.,* 7-Methyljuglone (fig. 4.3), diospyrin, Neodiospyrin and Isodiospyrin were first documented in 1972 [241]. They were obtained from the root extract of *Diospyros kaki*, also known as Japanese Persimmon. It was later revealed that these phyto-naphthoquinones are present in other exotic plants used in folk medicines, including *Euclea Natalensis* (fig. 4.2), naturally found in the east coast of South Africa [242], and *Diospyros montana Roxb.* from India [243]. Various structurally analogs of naphthoquinones and bisnaphthoquinones are also found in the extract of *Euclea Natalensis (fig. 4.3, 4.4) [244].*

Figure 4.2 Euclea Natalensis, producer of diospyrin, a widely used medicinal plant distributed in the southern to eastern coast of Africa.
Reproduced from http://www.worldbotanical.com/Euclea-natalensis-pl.jpg [245].

Diospyrin (fig. 4.4) is a natural covalent dimer of 7-methyljuglone (7MJ) (fig.4.5). It has particularly caught the attention of scientists as it was known to possess good antitumour activity [246-247]. Over the years many synthetic analogues of diospyrin have been produced experimentally to study their anticancer [248], antifungal [249] and antibacterial [250] properties. However all of these studies have only produced preliminary experimental results and have not attracted genuine interest to further develop them into drug leads.

Figure 4.3 Structures of naphthoquinones extracted from Euclea Natalensis
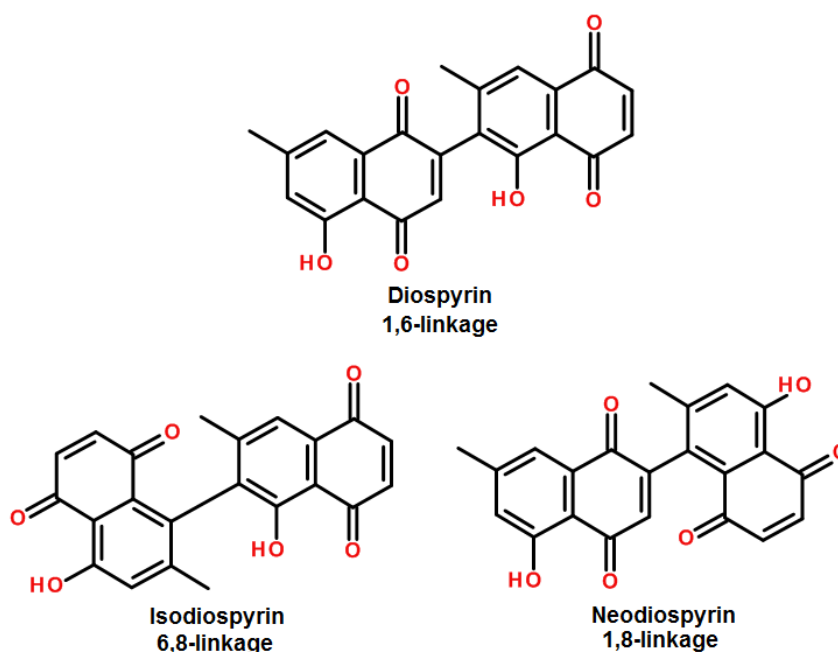
Figure 4.4. Structures of bisnaphthoquinones, covalent dimers of 7-methyljuglone: diospyrin (1,6-linkage), isodidospyrin (6,8-linkage), neodiospyrin (1,8-linkage) extracted from Euclea Natalensis

4.3 Natural naphthoquinones as DNA gyrase inhibitors

Diospyrin and 7-methyljuglone (7MJ) have in the past displayed strong antimicrobial properties, inhibiting topoisomerase I in *Leishmania donovani* [251] and targeting mycothiol disulfide reductase in *M. tuberculosis* [252]. They have been the drugs of interest in Lall's research group [243]. They are phytochemicals that were originally

extracted from *Euclea natalensis* in Lall's research group and were discovered to inhibit growth of *M. tuberculosis* [243].

Intriguingly, S. Karkare discovered that both diospyrin and 7MJ were able to inhibit *M. tuberculosis* DNA gyrase supercoiling at 10 μM [253]. Both diospyrin and 7MJ inhibit relaxation activity of the enzyme with lower potency. *E. coli* gyrase DNA supercoiling is inhibited by diospyrin and 7MJ with similar potency, implying that their binding pocket is likely to involve a conserved region of the enzyme. Some experimental evidence has suggested the binding site of diospyrin to be within the N-terminal domain of the B-subunit, which includes the N-terminal ATPase domain and the transducer domain [253]. Existing inhibitors that binds to the NTD of GyrB [243] include the aminocoumarins, *e.g.,* novobiocin and clorobiocin, which bind to the ATP pocket, directly competing with ATP binding and inhibiting ATP hydrolysis [254-256]. ATP competition experiments from S. Karkare suggested that diospyrin does not compete with ATP binding [253]. In addition diospyrin was able to inhibit the growth of an *E. coli* lab strain at 21 μM [253]. This further demonstrates their potential as an antibacterial lead.

Since both diospyrin and 7MJ has demonstrated their activity against DNA gyrase and showed bioactivity against both gram-negative and mycobacterium, this indicates that these natural naphthoquinones has the capacity to be developed into broad spectrum antibacterials.

4.4 Natural naphthoquinones inhibit *S. aureus* growth in liquid medium

To further explore the antibacterial spectrum of natural naphthoquinones beyond gram-negative bacteria (*E. coli*) and mycobacteria, we decided to test their bioactivity against *S. aureus* as a model bacterium of the gram-positive spectrum.

Due to the lack of commercial availability of these compounds, we decided to deploy micro-titre plates (100 μl per well) for the study to reduce material consumption. Liquid media was chosen over solid media for the ease of preparation, reducing the

possibility degradation of heat-sensitive compounds in hot agar and improved diffusion of the drugs.

A series of concentrations of each naphthoquinone was added to the *S. aureus- ATCC 29213* inoculated-liquid culture and grown overnight. The cultures were incubated in the shaking incubator at 37°C. OD_{600} of the *S. aureus* cultures were measured at the end of the 16 hrs incubation.

As shown in fig. 4.5 all 6 naphthoquinones tested completely inhibited the growth of *S. aureus* at 200 μM. Isodiospyrin and Shinalone moderately inhibited the growth of *S. aureus* in the assay condition with MICs of >64 μM. Neodiospyrin, diospyrin and menadione were more potent, with MIC values between 16-32 μM.

The most obvious and important criteria of the success of an antibiotic is its ability to penetrate the bacteria cell envelop and to subsequently inhibit bacterial growth. Many reagents developed by a target-based approach, which displays strong *in vitro* inhibition could fail to inhibit bacterial growth simply due to their inability to penetrate the bacterial envelope. The ability of these compounds to inhibit the growth *S. aureus* as well as *E. coli* and *M. tuberculosis* means that they can effectively penetrate cell envelopes of various types of bacteria. Assuming that these compounds share the same single specific cellular target, it is possible that the target of inhibition is conserved among these bacteria. All this evidence suggested the potential of naphthoquinones to become wide-spectrum antibiotics.
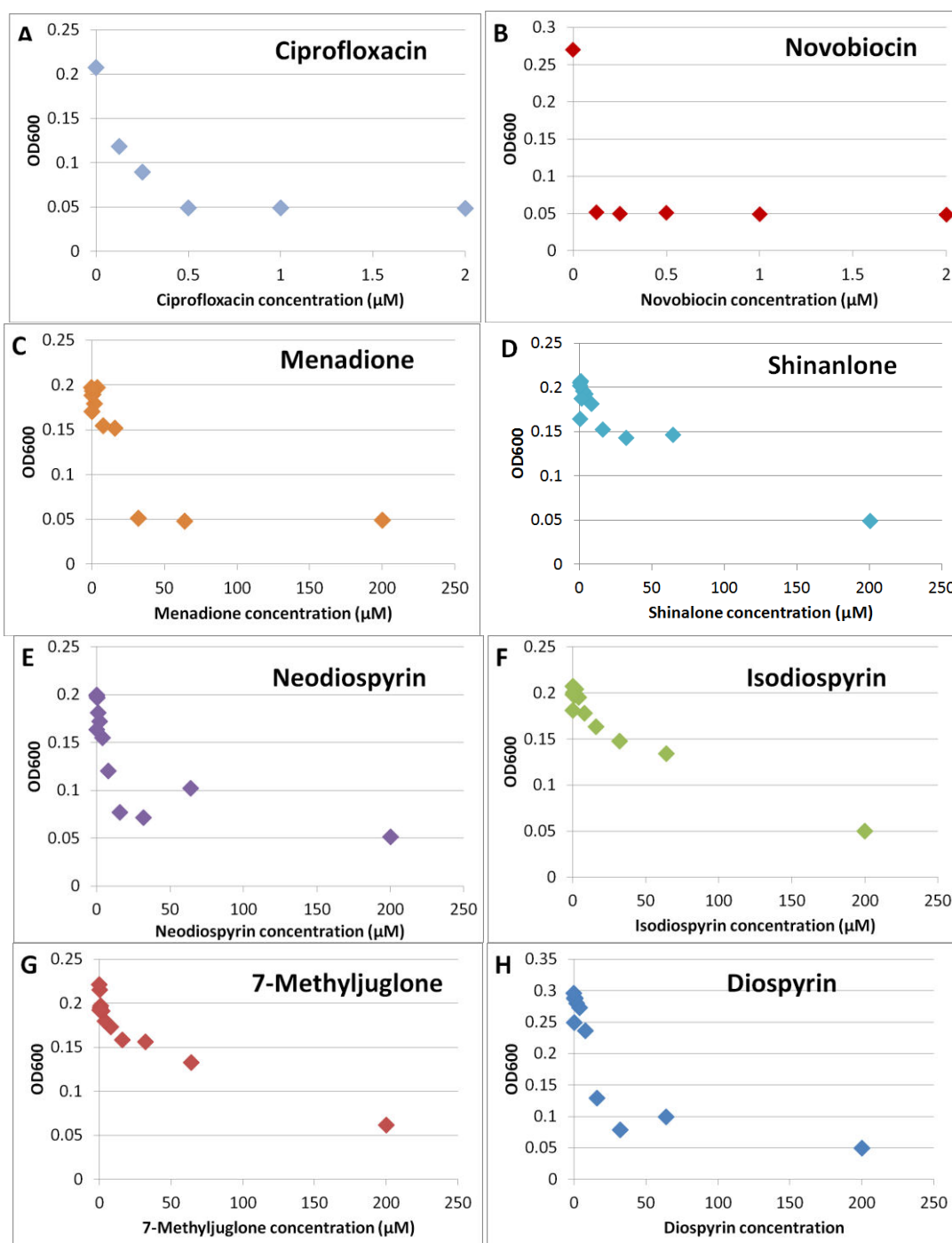
Figure 4.5. Inhibition of S. aureus growth by natural naphthoquinones and existing gyrase inhibitors: A) ciprofloxacin, B) novobiocin, C) menadione, D) shinalone, E) neodiospyrin, F) isodiospyrin, G) 7-methyljuglone, H) diospyrin. *S. aureus ATCC 29213 was inoculated in 100 μl of compounds containing LB media (10% DMSO) and grew for 16 hrs at 37°C with constant shaking. The OD$_{600}$ of the media was then recorded using a SPECTRAmax GEMINI microplate reader at the end of the incubation. As shown in the control ciprofloxacin (A) and novobiocin (B) infused assays, OD$_{600}$ decreases as concentration of the compounds increases, indicating the inhibition of growth.*

4.5 Natural naphthoquinones inhibit *S. aureus* gyrase

Since all the natural naphthoquinones tested on *S. aureus* inhibit its growth to a various degree, and that they share similar chemical structure, there is likely to be a common cellular target. The fact that some of them are inhibitors of *E. coli* and *M. tuberculosis* gyrase has led us to test them in the supercoiling assay of *S. aureus* gyrase. As well as the six natural naphthoquinones, we have decided to include a few other known bacterial topo II inhibitors including simocyclinone D8, Quercetin, Rutin, etc.

As one of the most widely used fluoroquinones, ciprofloxacin has an IC_{50} of ~30 μM, we have decided to assay the compounds at a fixed concentration of 50 μM to identify genuine inhibitors of *S. aureus* gyrase (fig. 4.6). As expected, ciprofloxacin, novobiocin and simocyclinone D8 effectively inhibit *S. aureus* gyrase. All naphthoquinones tested inhibited *S. aureus* gyrase supercoiling to a certain extent, with neodiospyrin and diospyrin being the most potent inhibitors. As menadione was one of the most potent naphthoquinones acting against *S. aureus*, it is surprising to find that it has an IC_{50} exceeding 50 μM. One possible explanation is that mendione inhibits an alternative cellular target and this inhibition is more potent than that of DNA gyrase. However there are no existing studies of mendione inhibition on other bacterial targets.
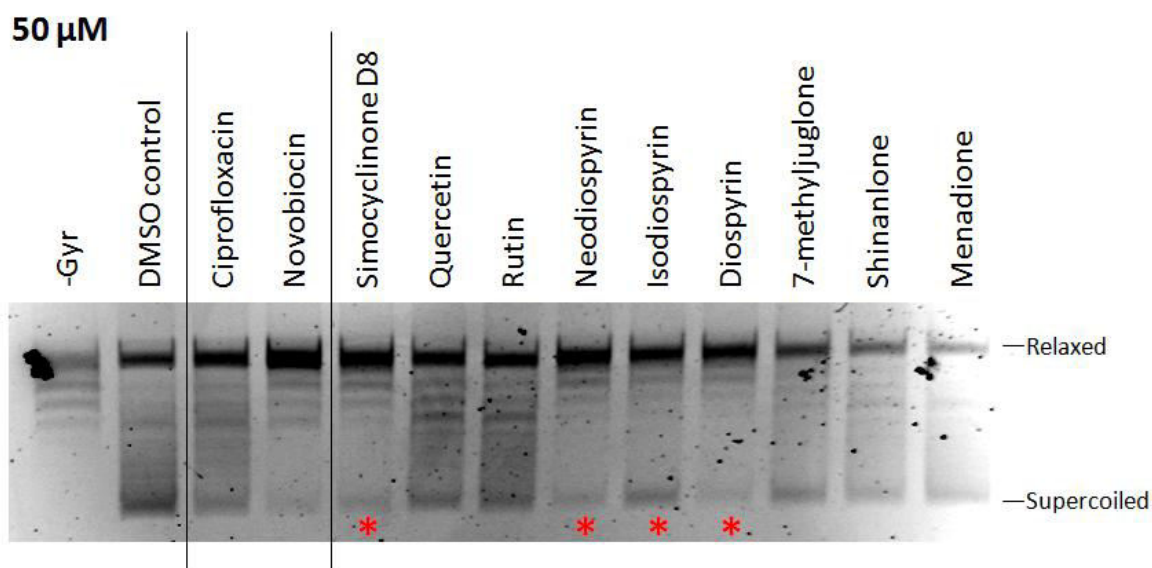
Figure 4.6. S. aureus gyrase supercoiling inhibition at 50 μM by various gyrase inhibitors and naphthoquinones. *0.5 ng of DNA is supercoiled by 1 U of reconstituted gyrase in supercoiling assay conditions (10% DMSO) described in method chapter 2.8.1.1. Lanes with red asterisks highlights supercoiling assay reactions inhibited by the sampled drugs, with a reduced quantity of the supercoiled circular DNA presence. Figure labels: –Gyr – supercoiling assay without gyrase; DMSO control – supercoiling assay with gyrase in 5% (v/v) DMSO.*
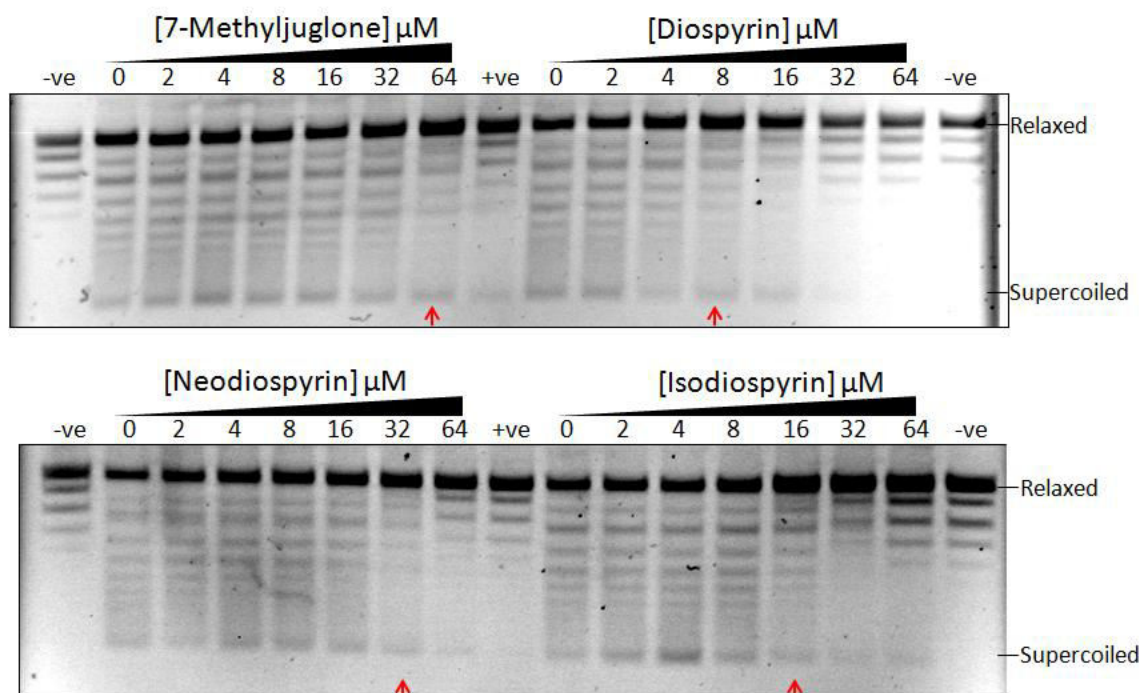
Figure 4.7. S. aureus gyrase DNA supercoiling inhibition by natural naphthoquinones: 7-methyljuglone (top-left), diospyrin (top-right), neodiospyrin (bottom-left) and isodiospyrin (bottom-right). *0.5 ng of DNA is supercoiled by 1 U of reconstituted gyrase in the supercoiling assay conditions (10% DMSO) described in method chapter 2.8.1.1. Lanes with red arrows highlights the intermediate inhibition concentration of the sampled drug, indicating approximate IC$_{50}$ (50% inhibition concentration) of the particular drug against S. aureus gyrase. Figure labels: Relaxed/Supercoiled – relaxed/supercoiled pBR322; –ve: no enzyme control (10% DMSO); +ve: gyrase only control (10% DMSO).*

To further define the inhibitory activity of naphthoquinones, all of the bisnaphthoquinones, together with their chemical progenitor 7-methyljuglone were assayed in detail (fig. 4.7). Diospyrin, which is the most potent inhibitor against *M. tuberculosis* gyrase out of the three bisnaphthoquinones, inhibits *S. aureus* gyrase supercoiling with an IC_{50} of ~8 μM. This figure is comparable to its IC_{50}s against *E. coli* (4 μM) and *M. tuberculosis* gyrases (15 μM) [253]. Both isodiospyrin and neodiospyrin are relatively less active with IC_{50}s values of ~16 μM and ~32 μM, respectively. Surprisingly, while the IC_{50}s of 7MJ and diospyrin for *M. tuberculosis* gyrase were fairly similar, against *S. aureus* gyrase 7MJ (IC_{50}~64 μM) is significantly less potent (8 times) than its dimer analogue diospyrin (IC_{50}~8 μM). These data are summarised in Table 4.1. (page 126)

It is interesting to find that neodiospyrin was superior to both diospyrin and isodiospyrin in the *S. aureus* growth inhibition assay, while neodiospyrin is the least potent of the three in the gyrase assay. Assuming gyrase is the only cellular target of these compounds, it is possible that neodiospyrin possesses structural and/or physicochemical difference that favours cellular accumulation, which in turn makes it more potent than diospyrin. An alternative explanation would be that neodiospyrin has a second cellular target, which gives it an extra dimension of inhibition and thus the extra potency.

4.6 Natural Naphthoquinones inhibit *S. aureus* topo IV

Topo IV is crucial to the survival of most bacteria and is the secondary target of most DNA gyrase inhibitors (including ciprofloxacin and novobiocin) due to its homology with DNA gyase. While most bacterial topo II inhibitors known to date have preferential potency against gyrase over topo IV in gram-negative bacteria [257], some display stronger activity against topo IV than gyrase in *S. aureus* [116,201]. The target preferences have huge implications on the MIC and mutant prevention concentratrion (MPC) of the compound, which directly affects the probabilities of mutant emergence[258].
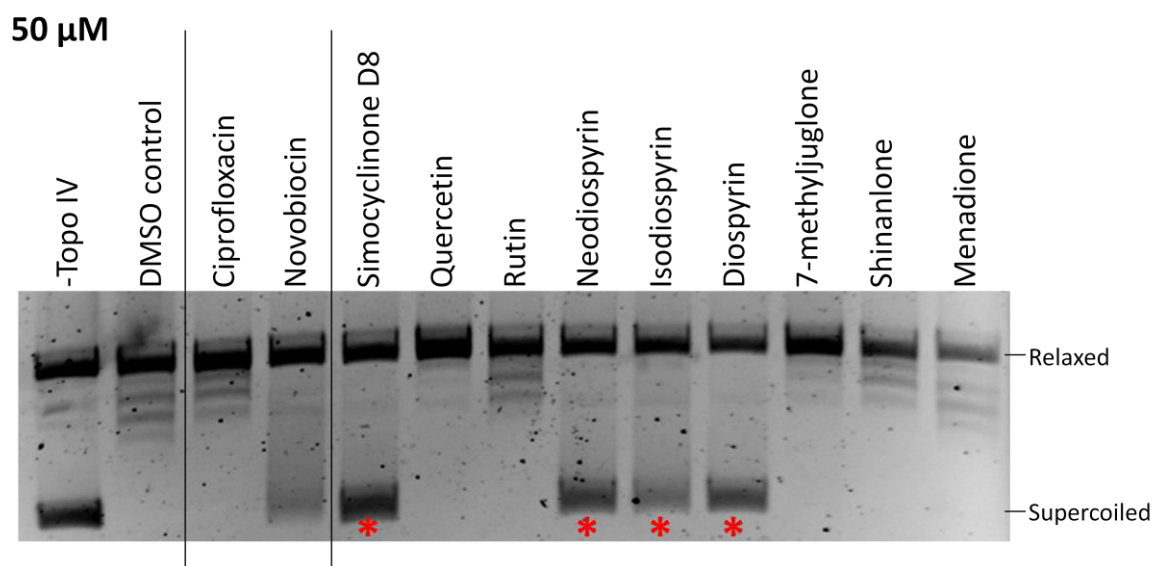
Figure 4.8 S. aureus topo IV DNA relaxation inhibition by natural naphthoquinones by various gyrase inhibitors and naphthoquinones. *0.5 ng of DNA is supercoiled by 1 U of reconstituted gyrase in the supercoiling assay conditions (10% DMSO) described in method chapter 2.8.1.1. Lanes with red asterisks highlights relaxation assay reactions inhibited by the sampled drugs at 50 µM, with an increase quantity of the remaining supercoiled circular DNA. Figure labels: –TopoIV – relaxation assay with topo IV; DMSO control – supercoiling assay with Sa topo IV in 5% (v/v) DMSO.*
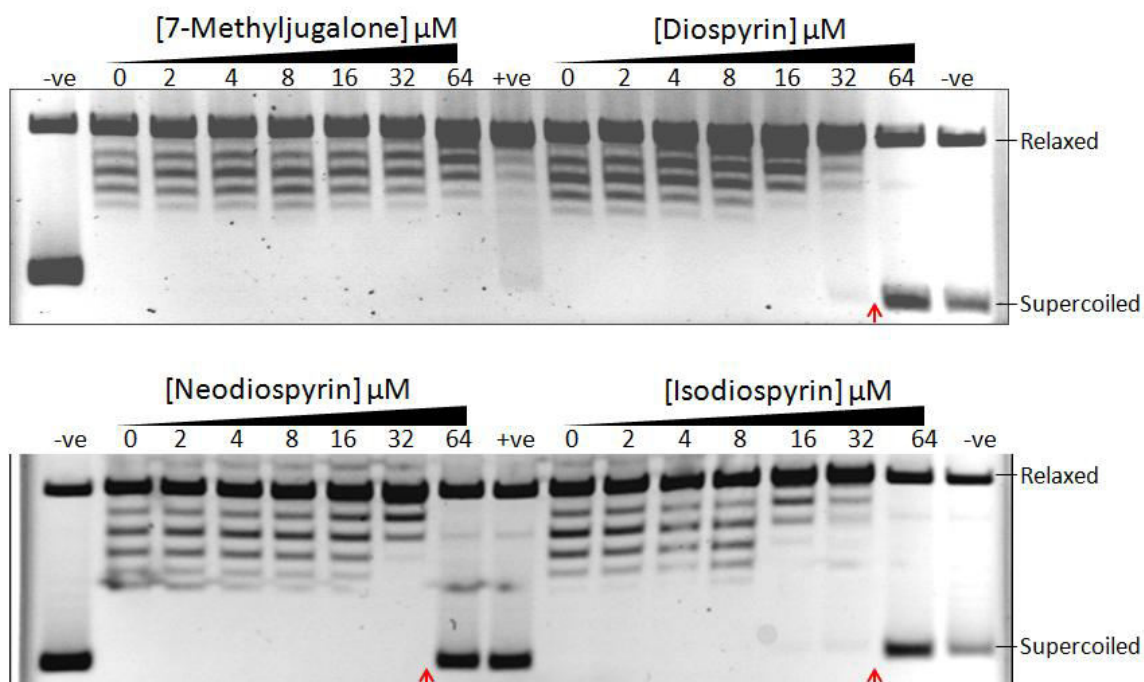
Figure 4.9 Sa topo IV DNA relaxation inhibition by natural naphthoquinones: 7-methyljuglone (top-left), diospyrin (top-right), neodiospyrin (bottom-left) and isodiospyrin (bottom-right). 0.5 ng of DNA is supercoiled by 1 U of reconstitute gyrase in the supercoiling assay conditions (10% DMSO) described in method chapter 2.8.1.1. Lanes with red arrows highlights intermediate inhibition displayed by the stated concentration of the sampled drug corresponding to the lane, indicating approximate IC_{50} (50% inhibition concentration) of the particular drug against S. aureus Topo IV. Figure labels: Relaxed/Supercoiled – relaxed/supercoiled pBR322; –ve: no enzyme control (10% DMSO); +ve: gyrase only control (10% DMSO).

To investigate the target preference of the naphthoquinones, we have tested the four gyrase-inhibiting naphthoquinones against topo IV in a relaxation assay (fig. 4.8 & 4.9). All four naphthoquinones have inferior potency towards topo IV when compared with DNA gyrase. The bisnaphthoquinones (diospyrin, isodiospyrin and neodiospyrin) all have IC_{50}s between 32 to 64 μM. 7MJ has the least activity, with only minor inhibition observed at 64 μM. diospyrin and isodiospyrin are slightly more potent than neodiospyrin and showed observable inhibition from 16 μM and upwards. These data are summarised in Table. 4.1.

4.7 Natural naphthoquinones as inhibitors of bacterial topoisomerase II

In summary, natural naphthoquinones displayed good anti-*S. aureus* activity and inhibit both *S. aureus* gyrase and topo IV, with *S. aureus* gyrase as the preferential target. One of the major concerns with *in vitro* drug screening is that many promising positive hits can in fact be false positives and inhibit the target of interest *via* non-specific inhibition (detergent effect, aggregation etc.). The fact that diospyrin and other naphthoquinone analogs are able to inhibit gyrase from a wide range of organisms and the differential IC_{50} between *S. aureus* gyrase and topo IV provides a strong indication that naphthoquinones do inhibit gyrase and topo IV *via* specific binding.

One of the major problems with the development of an antibacterial agent is that it is difficult to develop an antibacterial that is potent and yet does not show bio-activity towards humans. Human bioactivity is undesired as it induces unwanted side-effects, cytotoxicity and greatly impairs usability of an antibacterial drug. Occasionally, an antibacterial lead has the ability to inhibit a secondary target in humans and thereby displays human bioactivity. For example, novobiocin binds to the ATPase portion of GyrB and was found to inhibit Hsp90[259-260] and other GHKL class ATPases [260]. Such undesirable secondary inhibition is proposed to be the reason for its undesirable side effects [261]. Novobiocin was later abandoned in the clinic.

Naphthoquinone	*Sa* MIC µM	*Sa*Gyr Sc IC_{50} µM	SaTopoIV rel IC_{50} µM
7-methyljuglone	>64	~64	>64
Diospyrin	~32	~8	~32-64
Isodiospyrin	>64	~16	~32-64
Neodiospyrin	~16-32	~32	~32-64
Menadione	~32	>64	N/A
Shinanolone	>64	>64	N/A

Table 4.1 Bioactivities of natural naphthoquinones against S. aureus in vivo (MIC), and Sa Gyrase and Sa Topo IV in vitro (IC_{50}), derived from data in figure 4.5.

Assay	Order of potency
S. aureus in vivo	Neodiospyrin ≥ Diospyrin >>Isodiospyrin ≈ 7-methyljuglone
SaGyr IC$_{50}$	Diospyrin > Isodiospyrin > Neodiospyrin > 7-methyljuglone
SaTopoIV IC$_{50}$	Isodiospyrin > Diospyrin > Neodiospyrin > 7-methyljuglone

Table 4.2 Order of potency for natural naphthoquinones against S. aureus in vivo (MIC), and Sa Gyrase and Sa Topo IV in vitro (IC$_{50}$)

In previous studies, Diospyrin was shown to possess anti-cancer characteristics [262-263]. It is therefore likely that it has a secondary target in human cells and could have undesirable side effects when administered in human. In order to reduce side effects and enhance efficacy of an antibacterial, it is vital to maximise the specificity of the drug to its target. It is therefore important to understand molecular details of the inhibition to obtain positional details of the binding pocket. This would provide valuable insight into future chemical modifications to improve affinity and specificity of the inhibitors. By understanding if the compound binds to an evolutionary conserved portion of the enzyme, it enables the prediction of secondary target binding.

4.8 Diospyrin binds the NTD of GyrB – solution evidence

Previous *in vacuo* evidence from electro-Nano spray MS showed that diospyrin to able to bind to the NTD of E. coli GyrB. This suggested that the binding site of diospyrin is located on the GyrB NTD[253]. However, we have yet to produce solution evidence of diospyrin-GyrB binding to date. Therefore, we designed an experiment involving titration of *Ec*GyrB-NTD into an *S. aureus* DNA gyrase supercoiling assay at an inhibitory concentration of diospyrin. As the NTD of *Ec*GyrB does not have supercoiling activity, any apparent recovery of supercoiling activity with increasing concentration of *Ec*GyrBNTD would be a result of it binding to inhibitors, reducing the bulk inhibitor concentration and thereby relieving inhibition on *S. aureus* gyrase.
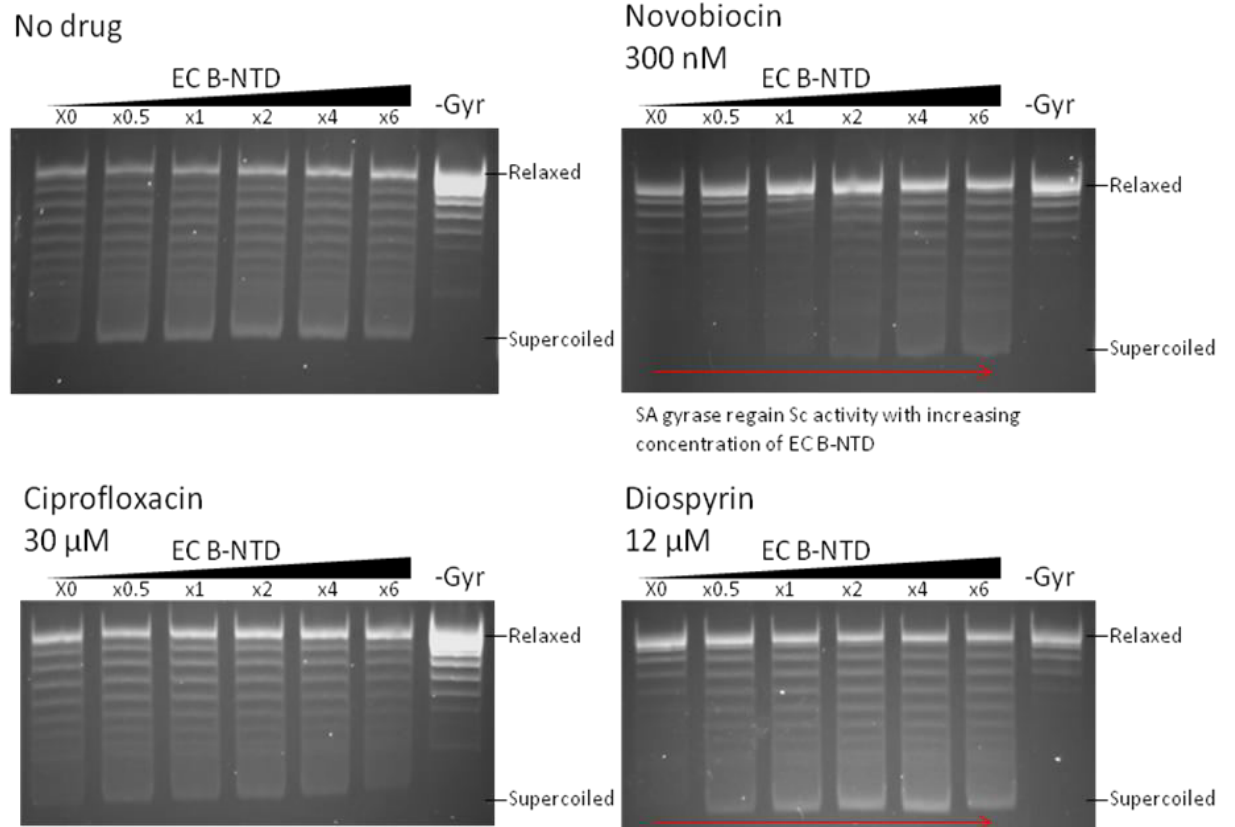
Figure 4.10 Diospyrin-Sa gyrase supercoiling inhibition is relieved by EcB-NTD titration. *The standard DNA supercoiling assay with 0.5 U (~64 nM) of S. aureus gyrase was titrated with a x0, x0.5, x1, x2, x4, x6 molar excess of EcB-NTD in the presence of 30 µM Ciprofloxacin (bottom left), 300 nM Novobiocin (top right) and 12 µM Diospyrin (bottom right) and no drug control (top left). Figure labels: Relaxed/Supercoiled – relaxed/supercoiled pBR322; –Gyr: no enzyme control.*

As shown in fig. 4.10, increasing the *Ec*BNTD concentration does not affect the supercoiling activity of *S. aureus* gyrase (fig. 4.10 top left). A parallel experiment in the presence of 300 nM of novobiocin, which is known to bind to the NTD of GyrB showed that inhibition of *S. aureus* gyrase is gradually reduced by the *Ec*B-NTD titration (fig. 4.10 Top right). Not surprisingly, *Ec*B-NTD titration did not reduce ciprofloxacin inhibition (fig. 4.10 bottom left). Finally, in the presence of diospyrin (fig 4.10 bottom right), *Ec*BNTD titration did reduce inhibition in manner similar to

the novobiocin experiment. Therefore, it is concluded that diospyrin binds to the NTD of GyrB in solution.

4.9 Diospyrin inhibits ciprofloxacin-induced cleavage

Since diospyrin is able to inhibit both the supercoiling and relaxation activities of DNA gyrase, we investigated its ability to inhibit DNA cleavage. Ciprofloxacin is able to induce double-strand DNA cleavage *via* gyrase by inhibiting the DNA religation step within the gyrase strand-passage reaction cycle[264]. By testing ability of diospyrin to inhibit ciprofloxacin-induced DNA cleavage, we hope to gain further understanding on the diospyrin inhibition mechanism.
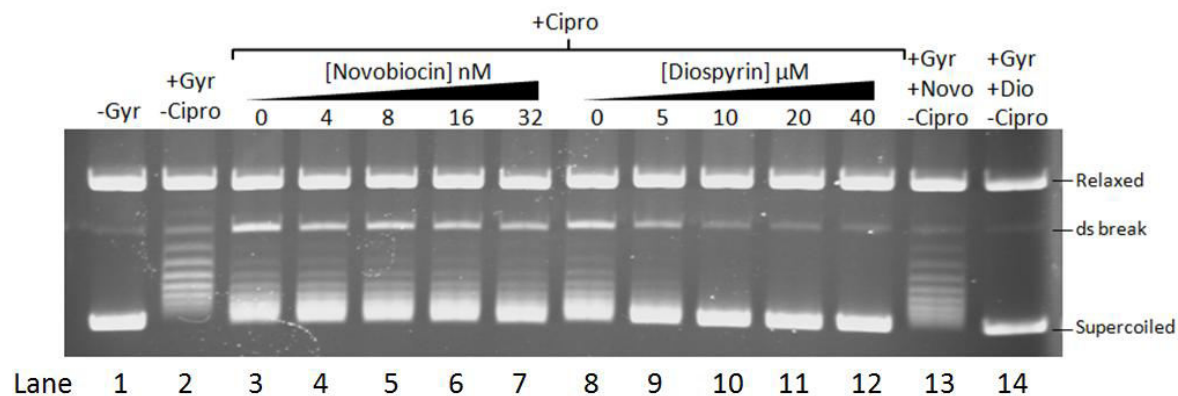
Figure 4.11. Diospyrin but not novobiocin inhibits Ciprofloxacin induced double-strand cleavage by gyrase. *0.3 μg of upercoiled pBR322 plasmid is cleaved by incubating with 10 nM S. aureus induced by the presence of 100 μM ciprofloxacin in a standard supercoiling assay condition (10% DMSO). Lane 3 shows the appearance of an additional band (ds break) demonstrating the cleavage activity, comparing to the no enzyme reaction in lane 1. The increased concentration of diospyrin (lane 8-12) inhibited the ciprofloxacin induced cleavage while the control reaction with Novobiocin (lane 3-7) did not. Figure labels: Relaxed - relaxed pBR322; Supercoiled – supercoiled pBR322; ds break – double-stranded DNA break or linear pBR322; -Gyr – no gyrase added; - Cipro – no ciprofloxacin added; +Novo – 0.1 nM novobiocin added; +Dio – 40 μM diospyrin added.*

As demonstrated in fig. 4.11, increasing concentrations of novobiocin were unable to inhibit ciprofloxacin-induced DNA cleavage. The fact that relaxation does not require the NTD of GyrB [265] and that Cipro alone was able to inhibit relaxation activity of gyrase indicated that N-gate closure was not required for Cipro-induced DNA cleavage. As indicated in fig. 4.11 Cipro-induced DNA cleavage was gradually inhibited when diopsyrin concentration was increased. This suggested that diospyrin was inhibiting the gyrase reaction subsequent to N-gate closure and prior to the initial DNA cleavage reaction step.

4.10 Naphthoquinone partially inhibits the ATPase reaction of *S. aureus* GyrB

Cumulative evidence from mechanistic studies of diospyrin-gyrase inhibition suggested that diospyrin does not compete with ATP binding and binds to the NTD of GyrB. As shown in fig. 4.14 the crystal structure of *E. coli* GyrB-NTD has a compact structure and does not have many apparent pockets available for ligand binding. According to ligand pocket prediction by the Molsoft ICM-Pro software package, a pocket between the ATPase domain and the transducer domain is most likely to be the binding pocket of diospyrin (fig. 4.14).

GyrB possesses intrinsic ATPase activity and is able to hydrolyse ATP in the absence of GyrA and a DNA substrate[266]. This ATP hydrolysing activity is dependent on GyrB dimerisation and it would be affected by disruption in the dimerisation interface . The transducer region is linked to ATPase activity as the absence of transducer domain completely disables ATP hydrolysis[267]. Therefore given the prediction that naphthoquinones bind close to the ATPase portion of GyrB, we would expect its presence to affect ATP hydrolysis. In this experiment, we aimed to investigate this by assessing the rate of ATP hydrolysis in increasing concentrations of diospyrin.
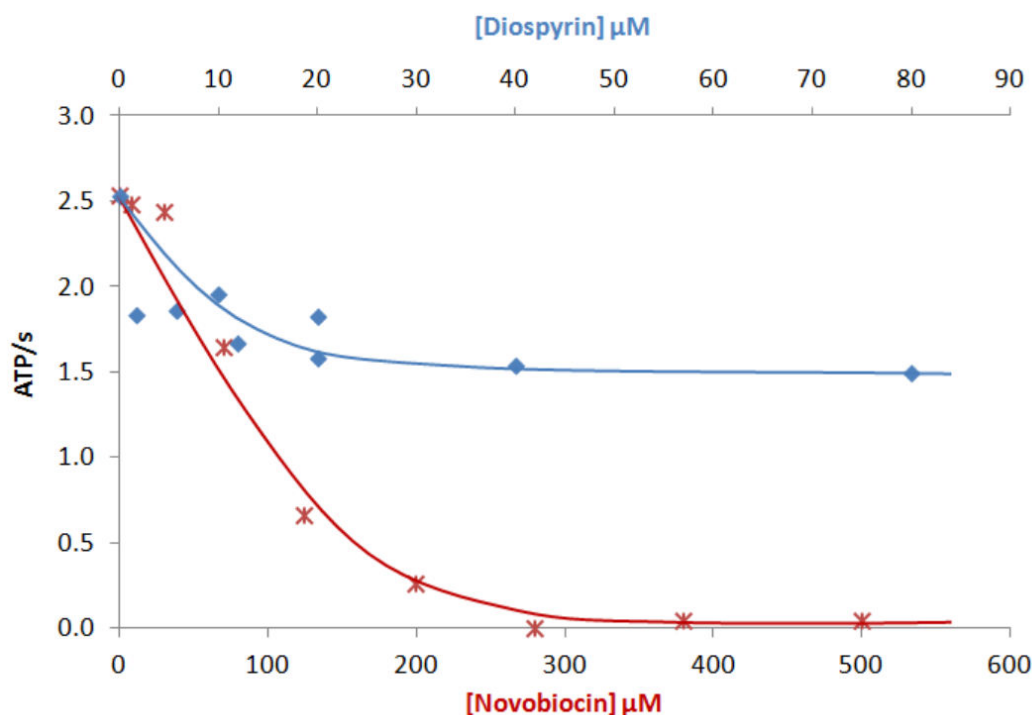
Figure 4.12 ATPase activities of S. aureus GyrB in the presence of Diospyrin and Novobiocin. *The ability for S. aureus GyrB subunit (~64 nM) to hydrolyse ATP in the presence of a series of concentration of Novobiocin and Diospyrin was examined using standard ATP/NADH coupled assay describe in chapter 2.8.2. Using the changes in absorbance at 340 nm, which corresponds to the absorbance peak of NADH, the concentration decrease of NADH and ATP over time interval of 20x 1 minute was calculated using Beer-Lambert law. ATP/s representing the number of ATP hydrolysed by each molecule of GyrB per second is calculated. Novobiocin, a known GyrB ATPase inhibitor was able to completely abolish ATPase activity of GyrB at concentrations of 300 – 500 µM. Diospyrin also displayed inhibition towards GyrB ATPase activity from 2 µM concentration and above but only partially inhibit GyrB at saturating concentrations.*

Fig. 4.12 showed the effect of Diospyrin and novobiocin on the ATPase activity of S. aureus GyrB in ATP/NADH coupled assays. Novobiocin causes near complete-inhibition of the ATPase activity of *S. aureus* GyrB at saturating concentration. This inhibition profile reflects the known fact that novobiocin binds to the ATP binding pocket and competitively inhibits ATPase activity [255]. Diospyrin titration decreased

ATPase activity in the concentration range between 0-20 µM. As the diospyrin concentration was increased further, ATPase inhibition was reduced and stabilised at ~40 µM. This suggested that at ~40 µM all diospyrin binding sites are saturated. Surprisingly diospyrin at saturating concentrations only partially inhibits *S. aureus* GyrB ATPase, with only 1/3 of the intrinsic ATPase activity inhibited, in contrast to the full inhibition seen with novobiocin. This suggests that diospyrin is inhibiting the ATPase of *Sa*GyrB allosterically and does not compete with ATP binding. To confirm the authenticity of these findings, a parallel ATPase experiment was carried out with 7MJ as the inhibitor.

As shown in fig. 4.13 7-methyljuglone titration inhibits ATP hydrolysis of SaGyrB between 0-20 µM, with over 1/3 of the activity inhibited at 20 µM. Similar to diospyrin, 7-methyljuglone ATPase inhibition plateau at ~40 µM and does not further inhibit ATPase activity at 60-80 µM. This result confirms the fact that naphthoquinones do not compete with ATP binding and affects ATPase activity allosterically. The similarities between the inhibition profile of diospyrin and 7MJ suggests that naphthoquinones share the same mode of action and same binding site in gyrase.
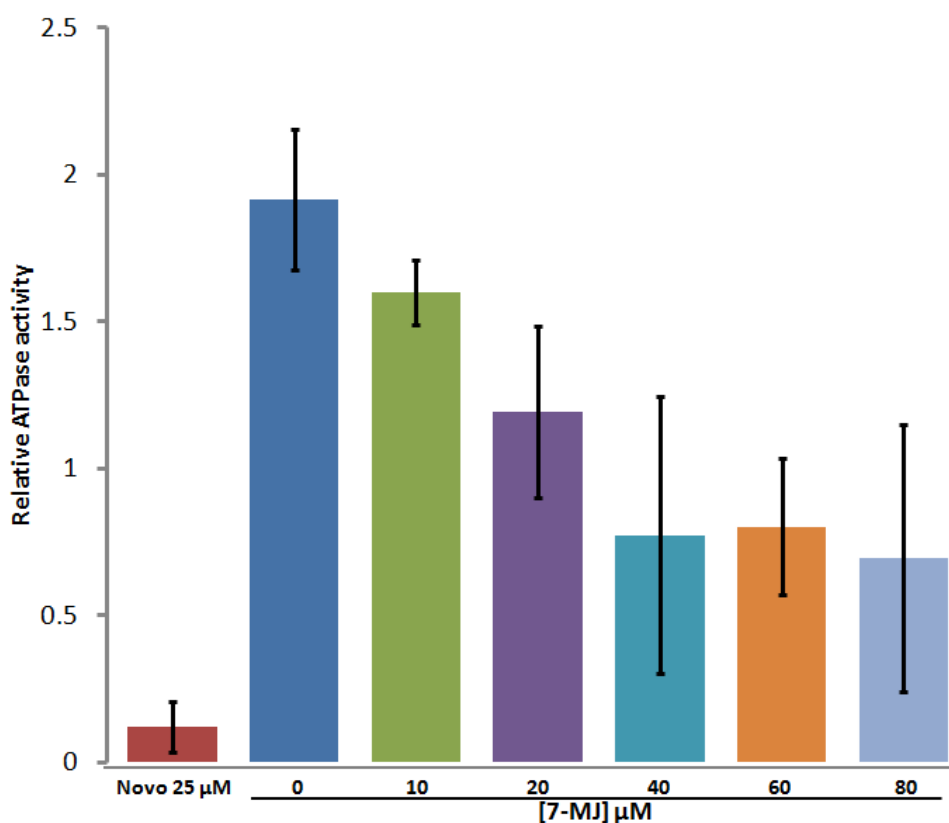
Figure 4.13 7-methyljuglone partially inhibits ATPase activity of SaGyrB

ATP/NADH coupled ATPase assay were preformed according to methods in chapter 2.8.2 using ~64 nM of S. aureus GyrB subunit. ATPase activity of S. aureus GyrB were tested in triplicate in the presence of 0, 10, 20, 40, 60 and 80 mM concentrations of 7-methyljuglone (7-MJ) and 25 µM of Novobiocin. Linear regression models similar to fig. 3.22 were generated from from each reaction using the OD_{340} absorbance of a minimium of 20 consecutive time points with 1 min intervals. Relative ATPase activity of each reaction was calculated from the gradient of the regression model ($-\Delta OD_{340}.s^{-1}$) of each reactions, as the $-\Delta OD_{340}.s^{-1}$ corresponded to the disappearance of NADH within each reaction, which is proportion to the release of ADP from ATP hydrolysis. Data points on the graph showed the average of the relative ATPase activity from the triplicate reactions. The error bars represents the standard deviation values calculated from the three sets of data in each concentration.

4.11 Possible binding pocket for diospyrin
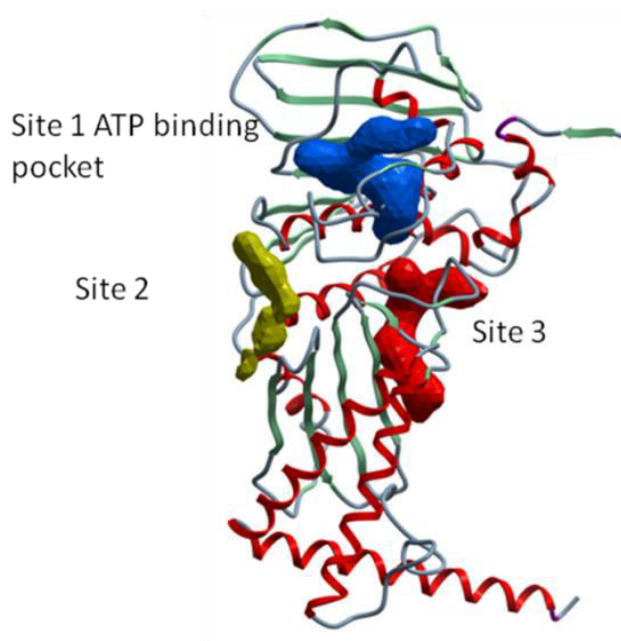
Figure 4.14. Available ligand-binding pockets on E. coli GyrB predicted by Molsoft ICM Pro, ICM pocket finder. *A van der Walls grid map was produce using a carbon atom probe based on algorithm published in An et al.* [268] *designed for the identification of ligand binding sites. Cavities on the grid map produced were then ranked based on their sizes. Three biggest cravities found are visualised in space relative to the protein structure.*

With the availability of the crystal structure of *E. coli* GyrB-NTD fragment (43 kDa), we were able to generate a prediction of available pockets for ligand binding using the Molsoft ICM Pro package. Assuming that the drug-bound protein conformation is the same as the crystal structure, there are three potentially available ligand-binding pockets. Pocket 1 is the ATP-binding pocket, which is also the binding pocket for novobiocin. However as it was established that diospyrin does not compete with ATP binding and that ATP binding completely occupies pocket 1, diospyrin binding to pocket 1 is not anticipated. Both pocket 2 and pocket 3 sit at the boundary between the ATPase domain and the transducer domain. Pocket 2 is about 103 Å^3 in volume and therefore predicted to be too small for diospyrin binding. Therefore pocket 3 is predicted to be the most likely binding site of diospyrin.

4.12 Model of diospyrin inhibition

The binding of diospyrin does not abolish the ATP hydrolysis activity of SaGyrB. However, it appears to bind to the NTD of GyrB, which consists of the ATPase domain and the transducer domain. This suggests that diospyrin may bind to the transducer region of GyrB. However, it is surprising that the NTD of GyrB is not needed for the relaxation activity of gyrase, yet diospyrin was able to influence relaxation activity *via* binding to transducer domain. This could indicate that perhaps diospyrin binding to the transducer domain of the GyrB causes it to adopt a conformation that restricts DNA strand passage. Similarly, diospyrin could inhibit relaxation by simply restricting transducer domain to translate the conformational change needed for DNA cleavage.

Ciprofloxacin is able to induce dsDNA cleavage by preventing religation step of DNA gyrase and is not dependent on the presence of T-segment DNA[264]. The evidence that diospyrin inhibits ciprofloxacin-induced dsDNA cleavage implies that diospyrin inhibits DNA cleavage and possibly prevents steps prior to DNA cleavage.

4.13 Synthetic naphthoquinones

4.13.1 Synthetic naphthoquinones (set I)

While it has been established that natural naphthoquinone such as 7-methyljuglone and diospyrin inhibit DNA gyrase of *S. aureus*, *E. coli* and *M. tuberculosis*, little is known about their structure-activity relationships (SARs). To explore this, we have acquired a range of structurally similar synthetic naphthoquinones from Prof. Vishnu Tandon, Lucknow University, India (Table 4.3). A total of 16 naphthoquinones and related compounds at a concentration of 300 µM were assayed against *S. aureus* gyrase supercoiling to eliminate inactive candidates. Out of the 16 compounds, 7 were shown to display IC_{50}s of <300 µM (fig. 4.14). These were further assayed to establish their detailed IC_{50} values. As shown in fig. 4.15, compounds that had shown inhibition were further assayed at 100 µM. 3 out of the 9 assayed have sub-100 µM IC_{50}s and were later found to have IC_{50}s of ~25 µM (fig. 4.16).

The results of this screen further confirm potential of naphthoquinone as a gyrase inhibitor with 3 candidates that showing equivalent $IC_{50}s$ (25 μM) to ciprofloxacin (~30 μM) prior target specific medicinal chemistry modifications. It is disappointing that none of them demonstrate superior $IC_{50}s$ to diospyrin and that this has not generated significant knowledge on the SAR of naphthoquinones.
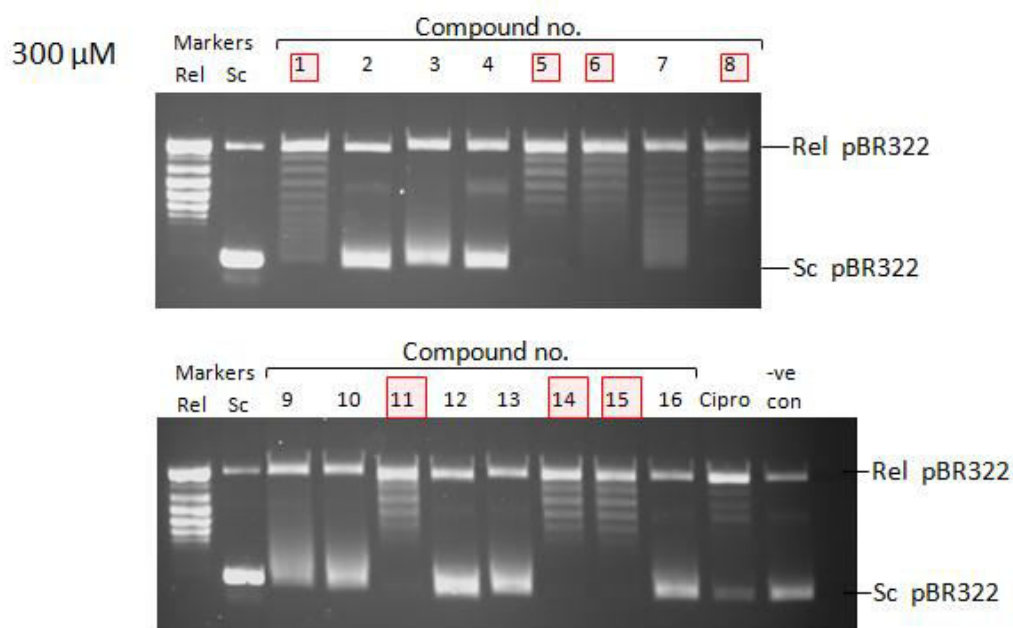
Figure 4.15. Synthetic naphthoquinones (set I) inhibits S. aureus gyrase supercoiling at 300 μM. *0.5 ng of DNA is supercoiled by 1U of reconstitute gyrase in the supercoiling assay conditions (10% DMSO) described in method chapter 2.8.1.1. 16 synthetic analogs of naphthoquinones were tested against S. aureus gyrase. The identity of the naphthoquinones can be identified in table 4.3a and 4.3b. Red boxes highlighted the naphthoquinone samples inhibiting S. aureus gyrase supercoiling at 300 μM. Figure labels: Rel/Sc Markers - relaxed/supercoiled pBR322 markers; Rel/Sc pBR322 – relaxed/supercoiled pBR322; Cipro – gyrase plus 20 μM ciprofloxacin (10%DMSO); –ve con – gyrase only control (10% DMSO).*
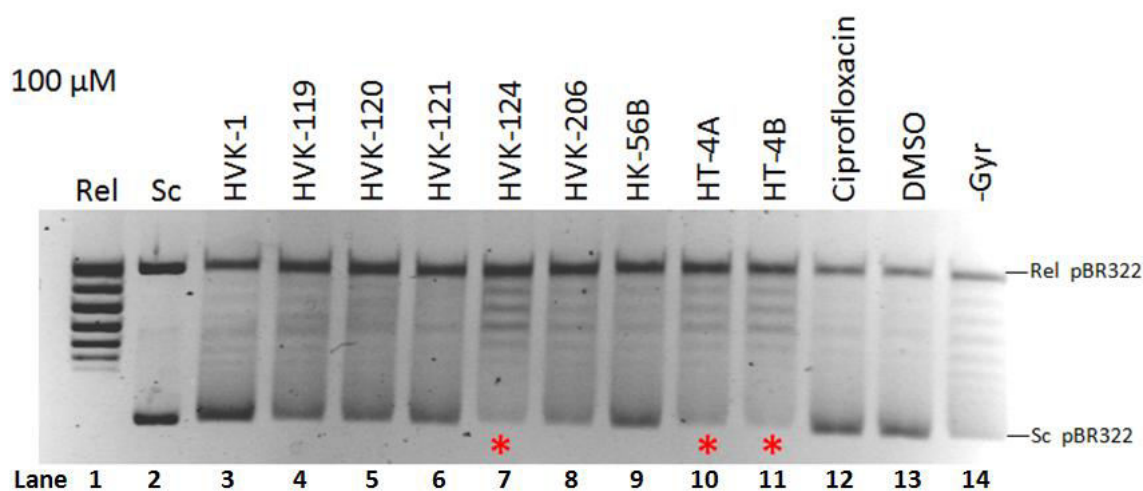
***Figure 4.16 Synthetic naphthoquinones (set I) inhibits S. aureus gyrase
supercoiling at 100 µM.*** *0.5 ng of DNA is supercoiled by 1 U of reconstitute gyrase in
the supercoiling assay conditions (3% DMSO) described in method chapter 2.8.1.1. 9
naphthoquinones with S. aureus gyrase inhibiting activity at 300 µM were tested at 100
µM to eliminate weak or non-specific inhibitors. Naphthoquinones showing inhibition
to S. aureus gyrase at 100 µM were labelled with red asterisk (*). Note: lack of intensity
in lane 14 is the result of a photographic artefact at the edge of a photo after the
contrast of the image was altered to enchance visibility.*

Figure labels: Lane 1-2 - Relaxed (Rel) and supercoiled (Sc) pBR322 markers

Lane 3-11 – S. aureus gyrase supercoiling assay in the presence of various napthoquinones

*Lane 12-14 –Control supercoiling reactions in the presence of 20 µM ciprofloxacin, DMSO only
(DMSO) and without gyrase (-Gyr).*
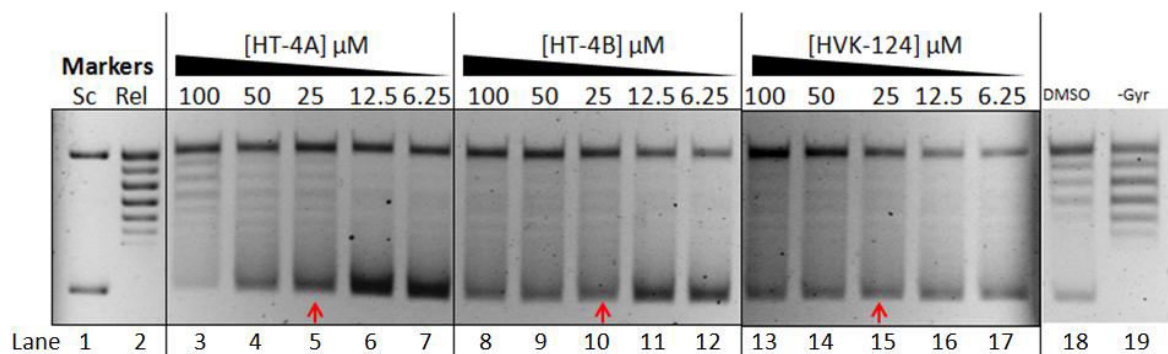
Figure 4.17. Synthetic naphthoquinones: HT-4A, HT-4B, HVK-124 inhibits Sa DNA gyrase. *0.5 ng of DNA is supercoiled by 1 U of reconstitute gyrase in the supercoiling assay conditions (3% DMSO) described in method chapter 2.8.1.1. Three naphthoquinones with S. aureus gyrase inhibiting activity at 100 µM were tested at 6.25, 12.5, 25, 50, 100 µM to identify their individual IC$_{50}$ values. Concentrations of the naphthoquinones showing IC$_{50}$ level of inhibition on S. aureus gyrase were labelled with red arrows.*

Figure labels: (lane 1 & 2) Rel/Sc Markers - relaxed/supercoiled pBR322 markers; control supercoiling reactions (lane 18 &19): DMSO only (DMSO) and without gyrase (-Gyr).

	Name	Chemical structure	*S. aureus* gyrase IC50s (μM)
1	HVK-1		~200-300
2	HVK-3		>300
3	HVK-10		>300
4	HVK-20		>300
5	HVK-119		~150-200
6	HVK-120		~150
7	HVK-206		~200
8	HVK-124		~25
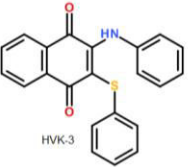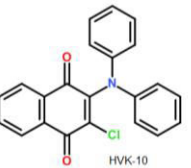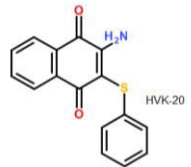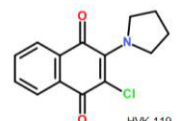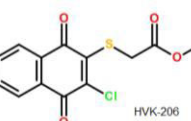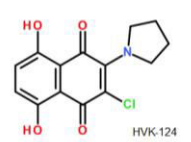
Table 4.3a. IC$_{50}$s of Synthetic naphthoquinones (set I) against S. aureus gyrase

	Name	Chemical structure	*S. aureus* gyrase IC50s (µM)
9	HVK-202		>300
10	HK-54A		>300
11	HK-56B		~50-100
12	HK-56C		>300
13	HK-85		>300
14	HT-4A		~25
15	HT-4B		~25
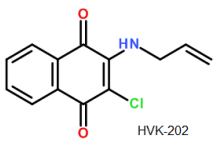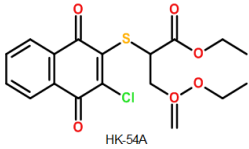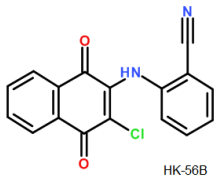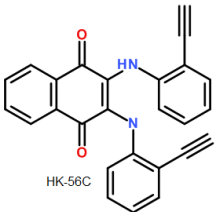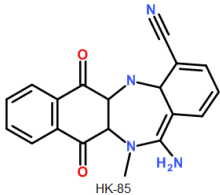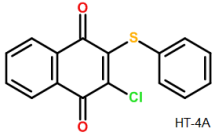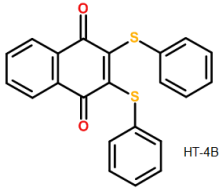
Table 4.3b. IC$_{50}$s of Synthetic naphthoquinones (Tandon) against S. aureus gyrase

4.13 Synthetic naphthoquinones (set II)

In addition, we have acquired an additional set of naphthoquinone related compounds from Dr. David Kinston (Virginia Tech.). This set of compounds consisted of a range of fragmented versions of 7-methyljuglone as well as a few anthraquinones (Table 4.4). As expected, all of the smaller naphthoquinone fragments failed to inhibit *Sa gyrase* at the concentration of 100 μM. Juglone and 5,8-dihydroxyl-1,4-naphthoquinone, both close chemical relatives of diospyrin, were able to inhibit at ~50 μM.
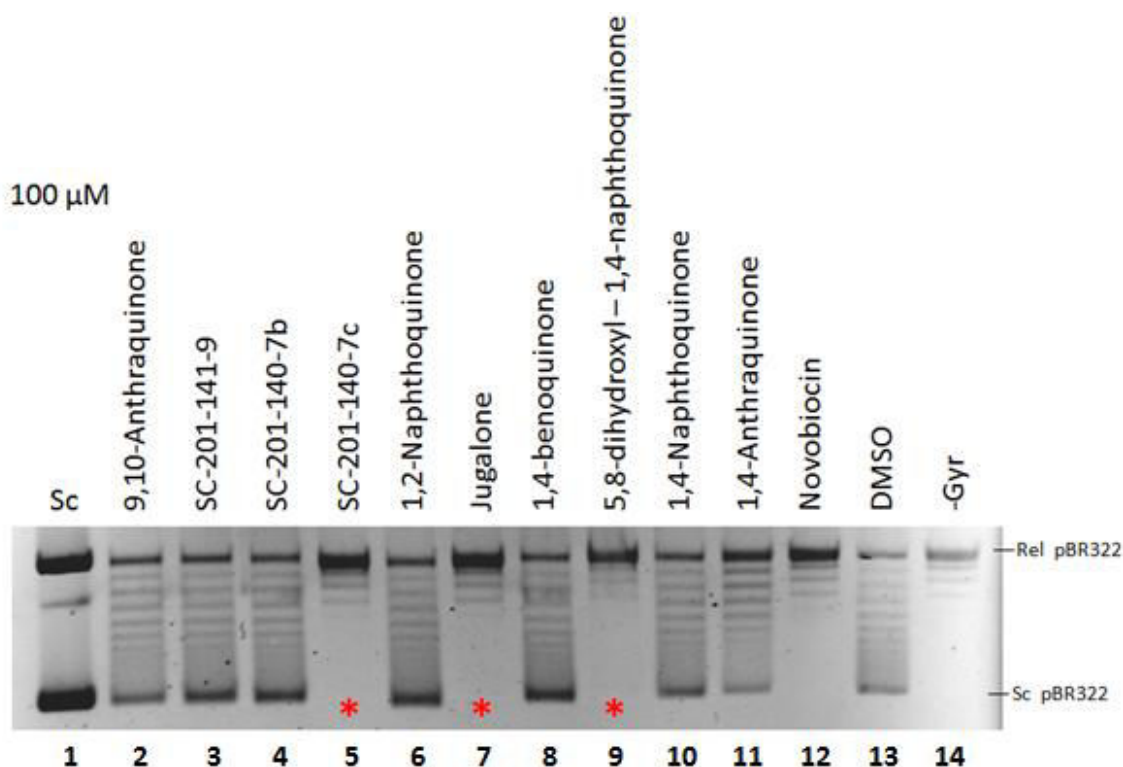
Figure 4.18 Synthetic naphthoquinones (set II) inhibits Sa DNA gyrase at a final concentration of 100 μM, 3% DMSO. Red asterisks at lane 5, 7 and 9 represents gyrase inhibition displayed by the corresponding naphthoquinone compound.

Figure labels: (lane 1) Sc - supercoiled pBR322 markers; control supercoiling reactions (lane 12, 13 & 14): Gyrase added plus 1 μM Novobiocin (Novobiocin), DMSO only (DMSO) and without gyrase (-Gyr).

	Chemical structures of synthetic Naphthoquinones (Vishnu)		
	Name	Chemical structure	*S. aureus* gyrase IC50s (µM)
1	9,10-Anthraquinone		>100
2	SC-201-141-9		>100
3	SC-201-140-7b		>100
4	SC-201-140-7c		?
5	1,2 Naphthoquinone		>100
6	Juglone		~50
7	1,4 benzoquinone		>100
8	5,8-dihydroxy- 1,4 naphthoquinone		~100
9	1,4-Naphthoquinone		>100
10	1,4-Anthraquinone		~100
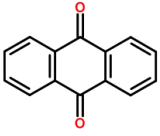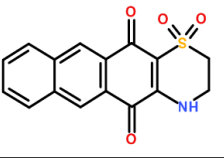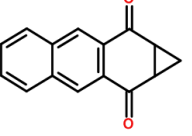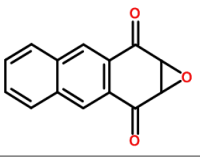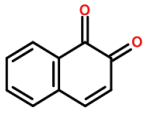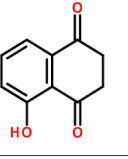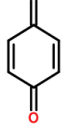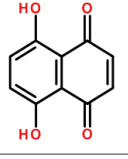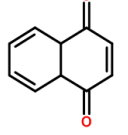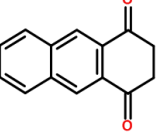
Table 4.4. IC$_{50}$s of synthetic naphthoquinones (set II) against Sa gyrase
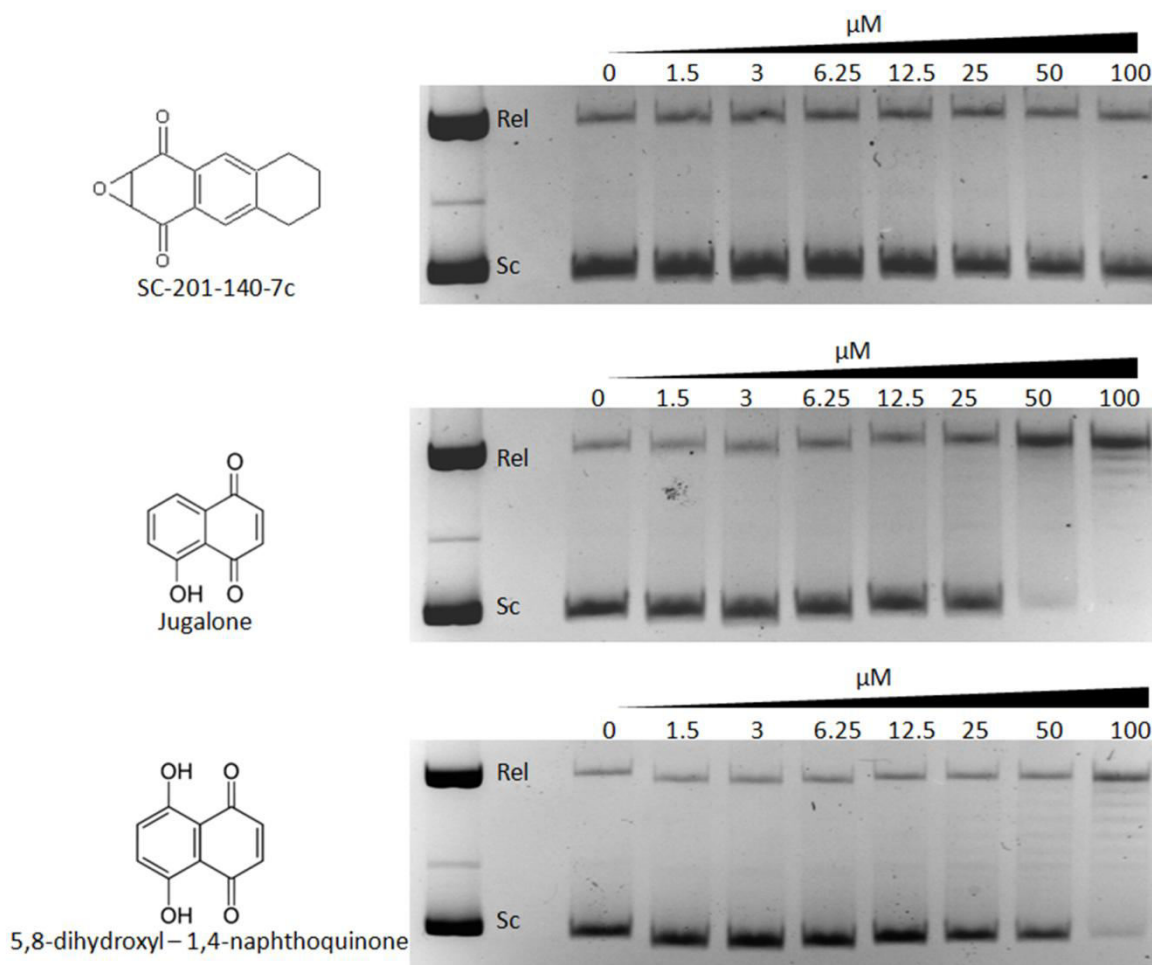
Figure 4.19. Detailed IC$_{50}$ determination of SC-201-140-7c, juglone and 5,8-dihydroxyl-1,4-naphthoquinone against Sa gyrase. 0.5 ng of DNA is supercoiled by 1 U of reconstitute gyrase in the supercoiling assay conditions (10% DMSO) described in method chapter 2.8.1.1. Figure labels: Rel/Sc - relaxed/supercoiled pBR322 markers.

In summary 32 different analogs of naphthoquinones were screened against *S. aureus* gyrase, with 1, 1, 4 and 6 naphthoquinone at found to have a IC$_{50}$ values of below 10 µM, between 10-20 µM IC$_{50}$, between 20-50 µM and between 50-100 µM. While none of the synthetic naphthoquinones screened exceeds the IC$_{50}$s achieved by diospyrin, valuable information was obtained with regard to structural-activity-relationship using pharmacophore modelling (see pharmacophore modelling at chapter 4.14)

4.14 Naphthoquinones Pharmacophore Modelling – LigandScout 3.0

A pharmacophore is the core structure of an inhibitor that makes important contacts with its target. With the number of naphthoquinones screened, there are sufficient IC$_{50}$ data to predict and construct a pharmacophore model by associating the structure of the ligand to its *in vitro* activity. The subsequent model generated could further our understanding on the properties of the naphthoquinone binding site and its structural-activity relationship.

Initially, the most potent inhibitors *in vitro*, diospyrin and isodiospyrin are used as the model training ligands (training-set) to provide initial template for the pharmacophore model. Once the training-set was aligned, other sub-100 μM ligands were then included as a test-set to align with the predicted preliminary pharmacophore. At the end of the alignment analysis several pharmacophore models would be generated and the one with pharmacophore-fits scores that matches closest with the real IC$_{50}$s were chosen as the most accurate model.
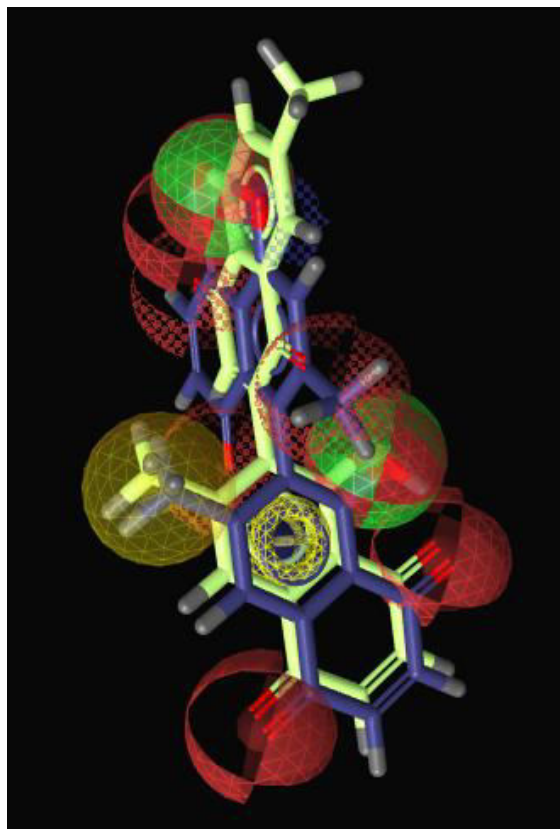
Figure 4.20. 3D Pharmacophore model of Naphthoquinone gyrase inhibitor:

Yellow sticks -> Diospyrin

Blue sticks -> Isodiospyrin

Yellow sphere: Hydrophobic interaction.

Red sphere: Hydrogen bond acceptor.

Red and green: Both hydrogen bond acceptor and donor.

Shadowed sphere: weak pharmacophore fit

144

From the pharmacophore model generated (fig. 4.19 & 4.20), it was predicted that both diospyrin and Isodiospyrin shared the main core of the pharmacophore with their position-6 alkylated naphthoquinone moiety. Most of the ligand interactions occur around the core naphthoquinone, this include the two carbonyl group acting as hydrogen bond donors, aromatic interaction in ring 2, hydrophobic interaction with the 7-methyl-group as well as the additional hydrogen bond with the group five hydroxyl. In addition, carbonyl and hydroxyl groups from the second half of naphthoquinone are predicted contribute to minor hydrogen bonding interactions.

Whilst there is currently no crystal structure of naphthoquinone-bound DNA gyrase available, it is possible that this naphthoquinone pharmacophore model could be used to guide the development of more potent gyrase inhibiting naphthoquinones in the future.
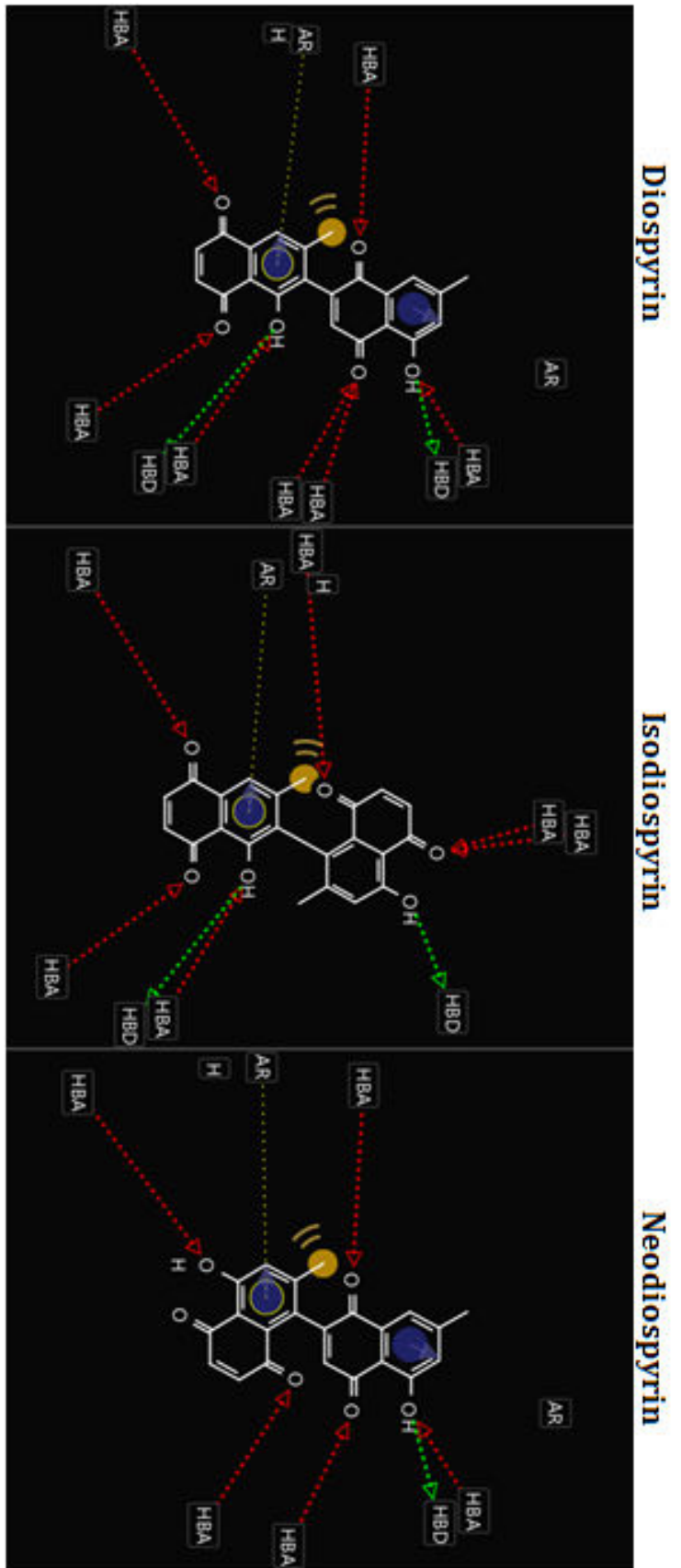
Figure 4.21. 2D Pharmacophore model of Naphthoquinone gyrase inhibitors:

Yellow circle: Hydrophobic interaction.

Red arrow/HBA: Hydrogen bond acceptor.

Green arrow/HBD: Hydrogen bond donor.

Shadowed sphere: weak pharmacophore fit

Blue circle: aromatic interaction

4.15 Discussion

In attempt to address the current needs to develop new classes of antibacterial agents to combat the rises in antibiotics-resistance in *S. aureus*, we explored the targeting of *S. aureus* gyrase as an antibacterial target in this study. In particular, we have focused on examining the potential of natural and synthetic naphthoquinones as a novel class of DNA gyrase inhibitor. Several natural naphthoquinones, including diospyrin, has previously been shown to display *in vivo* activity against *M. tuberculosis* [243]. Naphthoquinone such as diospyrin and 7-methyljuglone were also shown to be inhibitors of *M. tuberculosis* gyrase, with a novel mode of action. As the potential of developing natural naphthoquinones such as diospyrin and 7-methyljugalone as a novel class of gyrase inhibitor hold much promises, their activity against *S. aureus in vivo* as well as *S. aureus* gyrase *in vitro* were chosen as a starting point for the investigation.

4.15.1 Inhibition of *S. aureus* growth in liquid culture

Target-based antibiotics discovery are often hindered by the ability for the reagents to effectively penetrate the cell wall and/or cell membrane of the target bacteria. We therefore decided to begin assessing the potential of naphthoquinones agent against *S. aureus* by monitoring the ability for the compounds to suppress growth or kill the bacteria in liquid culture. All of the six naturally obtained naphthoquinones tested were able to demonstrate dose-dependent growth inhibition against *S. aureus*, of which diospyrin (MIC ~32 µM), neodiospyrin (MIC ~16-32 µM) and menadione (MIC ~32 µM) displayed the strongest responses. Whilst these naphthoquinones do not provide the ideal potency as an immediate candidate for antibiotics, their cell ability to penetrate bacterial are promising given that most drug leads undergo extensive medicinal modifications to improve cell penetration properties before a desireable potency can be reached. Since these natural naphthoquinones represent a good developmental starting point for more potent drugs.

4.15.2 Inhibition of *S. aureus* gyrase and topo IV by natural naphthoquinones

147

Gyrase and Topo IV are proven, efficacious antibacterial targets, owing to their important roles in both bacterial growth and survival. Due to their shared genetic origin, Gyrase and topo IV are also highly structurally similar. Therefore, much of known gyrase inhibitors also inhibit topo IV. The dual-targeting action properties of these reagents provide additional potency as well as prevention against resistant-development. Previous studies Shantanu *et al.* [269] discovered that several natural naphthoquinones, such as diospyrin and 7-methyljuglone were able to inhibit gyrases of *M. tuberculosis* and *E. coli.* Whilst we were able to demonstrate the activity of several natural naphthoquinones *in vivo*, we have decided to investigate the inhibition of these compounds against their potential cellular targets: *S. aureus* gyrase and topo IV. Whilst most gyrase inhibitors displayed fairly comparable activities against topo IV, naphthoquinones showed considerable selectivity against gyrase over topo IV. The dual-targeting feature of naphthoquinones also makes it an attractive agent from the developmental viewpoint. Given the structural similarity of the two enzymes, the dual targeting characteristic of naphthoquinones against gyrase and topo IV also reveal a potentially similar mode of drug binding shared between the two enzymes.

Out of all the naphthoquinones tested, Diospyrin was found to be the most potent naphthoquinone against *S. aureus* gyrase activity, with an IC_{50} value of ~8 μM. This is comparable to the IC_{50} value of ciprofloxacin (~30 μM), one of the most widely used gyrase-inhibiting antibiotics in the clinics. Other natural naphthoquinones which inhibits both gyrase and topo IV includes isodiospyrin (Gyrase IC_{50} ~16 μM), neodiospyrin (Gyrase IC_{50} ~32 μM) and 7-methyljuglone (Gyrase IC_{50} ~64 μM). Isodiospyrin, neodiospyrin and diospyrin all displayed promising activity against gyrase. Diospyrin in particular was able to display sub-10 μM IC_{50} value without medicinal modification. The activity of these naphthoquinone compounds against gyrase, and to a lesser extent against topo IV, suggested promising developmental potential towards more potent naphthoquinone variants.

Bisnaphthoquinones, dimeric analogs of the simple naphthoquinones, are found to be more potent than mono-naphthoquinones *in vitro* and *in vivo*. Interestingly, coumermycin A1, another dimeric gyrase inhibitor was also a more potent inhibitor

than its monomeric analog, novobiocin. Novobiocin binds to the NTD portion of GyrB, whilst its dimer, Coumermycin A1, was found to induce GyrB dimerisation by binding to identical pockets in two individual GyrB monomers[270]. It remain interesting to discover whether both of the monomer naphthoquinone "heads" binds to the same GyrB monomer or if it is able to induce dimerisation by binding to two individual GyrB monomer simultaneuously.

4.15.3 Inhibition of *S. aureus* gyrase by synthetic naphthoquinones

As we discovered that natural naphthoquinones were capable of inhibiting *S. aureus* DNA gyrase and topo IV, we were intrigued to find out if synthetically produced naphthoquinones can reach similar, if not improved potency *in vitro*. Thanks to the generosity of our collaborators, we were able to obtain 25 synthetic naphthoquinone analogs for assays against *S. aureus* gyrase. Although some of the naphthoquinones were found to inhibit gyrase with below 100 μM IC_{50} values, only one candidate (juglone) displayed near 50 μM IC_{50} value against *S. aureus* gyrase. Given the limited chemical diversity in the group of 25 napthquinone analogs tested, it was anticipated that the chances of finding a more potent compound would be slim. If possible, it would be ideal to build a chemical library using the chemical structure of bisnaphthoquinones such as diospyrin as a chemical template in order to increase the chance of developing a compound more potent than natural nathoquinones *e.g.*, diospyrin.

4.15.4 Investigation of the site and mode of action of naphthoquinones against DNA gyrase

In order to further develop naphthoquinones as gyrase inhibitors, it is crucial that its inhibition profile and mechanism are investigated to assess its mode of binding and suitability of modification. However, previous knowledge of naphthoquinones-gyrase inhibition mechanism has been limited. Shantanu *et al.* [269] was able to deduce that diospyrin is likely to bind the NTD portion of GyrB *in vacuo* using electro-Nano spray MS. Unlike other GyrB NTD binding inhibitors such as novobiocin, diospyrin does not appear to compete with ATP binding of GyrB [253]. To further explore the unique

inhibitory mechanism of diospyrin, we studied the GyrB-diospyrin interaction in solution and found that the excess of NTD-GyrB was able reduce diospyrin-induced gyrase inhibition. This confirms the previous evidence that napthoquinone inhibits gyrase by binding to the NTD portion of GyrB subunit. Furthermore, we were able to establish that naphthoquinone *i.e.,* 7-methyljuglone and diospyrin were able to partially inhibit (~1/3) ATPase activity of GyrB at saturating ligand concentrations (80 μM). This inhibition profile is distinct from other known GyrB-NTD targeting gyrase inhibitors *e.g.,* novobiocin, which occupies the ATP pocket and inhibits ATPase activity in a competitive fashion. Furthermore, diospyrin was found to display inhibitory action against Cipro-induced DNA cleavage activity of DNA gyrase. The novel inhibition mechanism displayed by diospyrin showed it to be a truly unique class of inhibitor of DNA gyrase. Through further investigative on the naphthoquinones' precise mode of binding and inhibition, there is hope that this novel inhibitory mechanim can be exploited to design novel anti-gyrase antibacterial agents. In chapter 5, we describe the attempt to examine and define the mode of binding of naphthoquinones against GyrB using protein crystallography.

4.15.4 Pharmcophore modelling of gyrase inhibiting naphthoquinone

Without the structural information of the drug binding site on the target, one of the most used strategies in drug discovery industry is to produce a pharmacophore model. This involves linking the inhibition data of numerous compounds tested and their spatial and chemical characteristic to predict which of these features contributed to improved potency or affinity. This pharmacophore could in turn provide valuable insights to for future ligand designs without the structural knowledge of the target. The range of natural and synthetic naphthoquinones analogues tested against the *S. aureus* gyrase provided a mass of data sufficient for the construction of the pharmacaphore model. The model clearly illustrates positions of potentially important ligand contact, which could be used as a guide in the future for the design of gyrase inhibiting naphthoquinones.

Chapter 5 Protein x-ray crystallography

5.1 Introduction

We have identified two aspects of this current study that have the potential to benefit from structural information from protein crystallography: the binding of diospyrin, and the proposed monovalent metal cation (M^+) binding site of DNA gyrase. Based on extensive evidence from previous experiments (Chapter 4) (*e.g.,* diospyrin affects ATPase hydrolysis and addition of EcB43 to gyrase reduces supercoiling inhibition by diospyrin), there were strong indications that diospyrin reside in the N-terminal domain of GyrB. In addition, there are also suggestions of the putative M^+-ion binding located in GyrB-NTD [231]. Although the putative M^+ ion binding site has not been observed in the previous structures of the EcGyrB-NTD-ADPNP complex [68,271], it is important to note that these data might not have been of sufficient resolution to distinguish a water molecule from a Na^+ ion due to their similarity in electron density. In addition, previous crystallography studies did not include Na^+ and K^+ in the crystallisation conditions thus reducing the chance of observing M^+-binding. We therefore decided to re-examine the possibility of M^+-binding sites by pursuing higher resolution structures of the *E. coli* GyrB-NTD-ADPNP dimer complex in the presence of K^+ and Na^+ ions.

5.2 Production of *Ec*GyrBNTD-ADPNP complex crystals

As there is no existing evidence proving crystallisability of *S. aureus* GyrBNTD, we have decided to utilise established crystallisation condition[218] to produce protein crystals of *E. coli* GyrBNTD-ADPNP complex for ligands soaking and co-crystallisation experiments with diospyrin and 7MJ. *E. coli* GyrB-NTD fragment is expressed and purified according to chapter 2.7.3.5 (figure 5.1). Diffracting protein crystals were successfully produced (fig. 5.2) using the method and conditions described in 2.9.1.2, resulting with a diffraction resolution of ~1.8 - 2.1 Å.
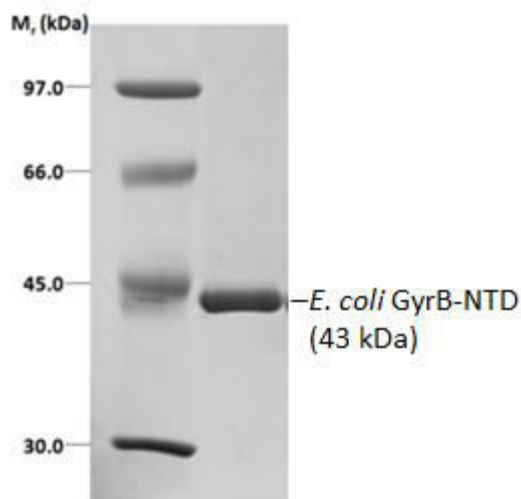
Figure 5.1. SDS PAGE of purified recombinant E. coli GyrB-NTD (43 kDa)
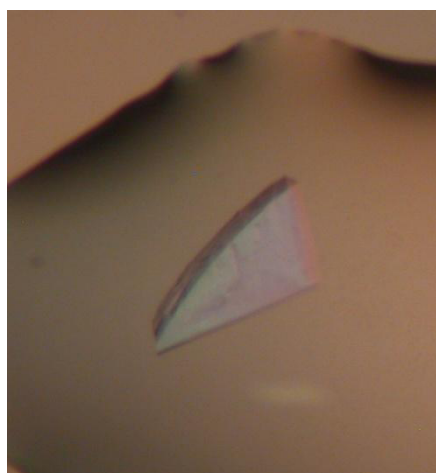
Figure 5.2. Crystals of EcBNTD-ATP obtained in 100 mM Tris.HCl pH 8.0, 15-25% PEG3350, 2 mM MgCl₂ (No salt).

5.3 Crystallisation attempts for 7-methyljuglone (7MJ)- and diospyrin-complexed EcGyrBNTD

As diospyrin and 7MJ were found not to compete with binding of ADPNP, we proposed that its might be possible to generate 7MJ/diospyrin-EcGyrBNTD-ADPNP crystals. As EcGyrBNTD is a proven crystallisable construct, we have chosen this construct for the generation of 7-methyljuglone and diospyrin-bound EcGyrBNTD crystals. To achieve this, we decided to use two strategies: crystal-ligand soaking and co-crystallisation.

5.3.1 Diospyrin and 7-methyljuglone ligand soaking

Although production of the EcGyrBNTD-ADPNP crystal was successful, soaking of the crystals in saturating concentrations of 7MJ and diospyrin for up to 24 hrs failed to produce drug-complexed crystals, as no additional electron density consistent with 7MJ and diospyrin was observed. The solvent content of the crystals was predicted to be ~60% [272]. Therefore, sufficient solvent channels should have been available within the crystal to allow drug diffusion. It is possible that the binding pocket was concealed by tight crystal packing, thereby blocking the access of 7MJ/diospyrin. As diospyrin and 7MJ binding affects ATP hydrolysis, we suspected that 7MJ/diospyrin binding might require conformational changes in the GyrBNTD. Therefore, diospyrin binding might not be permitted with the restricted protein conformation allowed within the rigid crystal packing of EcGyrB-ADPNP crystals.

In order for the ligand soaking approach to succeed, we proposed that generation of new crystal forms with alternative protein conformations that allow diospyrin binding, would be necessary. However, attempts to generate alternative crystal forms for the EcGyrBNTD-ADPNP complex were unsuccessful, since only crystals with morphologies resembling $P222_1$ GyrB-ADPNP crystal were found in the range of crystallisation conditions tested.

From these observations, it can be argued that *Ec*B43 highly favours the formation of protein crystals in the $P222_1$ space group in the presence of ADPNP. As the presence of ADPNP drives the formation of the GyrB dimer, [273] we attempted to explore alternative crystal forms by crystallising EcGyrB-NTD plus or minus diospyrin in the absence of ADPNP using preset commercial crystallisation screens. Disappointingly, we were unable to establish any observable crystals from this approach. This is not entirely surprising, particularly since production of crystals of apo GyrB-NTD has not been reported to date.

5.3.2 Diospyrin and 7-methyljuglone *Ec*GyrBNTD co-crystallisations

Attempts to generate crystals with the EcGyrBNTD-ADPNP-drug complex and the EcB43-drug complex in co-crystallisation trials (table 2.9) were also unsuccessful. As

the solubility of 7MJ and diospyrin in crystallisation conditions were low, we attempted to increase the DMSO concentration of the ligand soak solution to 20-40% (v/v) in order to increase their saturation concentrations. Disappointingly, this strategy generated either crystals with no drug bound, or crystals with crystal packing disrupted by the high DMSO concentration and that did not subsequently diffract. We also generated protein crystals in the presence of 30% (v/v) DMSO in the hope of withstanding soaking of drug at up to 30% (v/v) DMSO. Despite the success in generating protein crystals with 30% (v/v) DMSO, we were unable to generate coloured crystals through soaking. As both 7MJ and diospyrin were strongly orange/brown in colour, this indicated that the attempts directed to generating 7MJ or diospyrin bound crystals were unsuccessful.

Overall, it can be concluded that alternative crystallisation constructs might be required for generating diospyrin co-crystals of diffraction quality.

5.4 Data collection for Na^+/K^+-complex *Ec*GyrBNTD-ADPNP crystals

Crystals for which diffraction data were collected were grown in conditions described in table 2.10. The crystals were also cryoprotected by immersing them in the cryoprotectant described in table 2.10. The diffraction datasets for the H_2O, K^+, Na^+, and K^+ and Na^+ co-crystal of EcB43-ADPNP were collected to 1.95 Å, 1.87 Å, 1.96 Å and 2.04 Å, respectively, (table 5.2) at a synchrotron radiation facility (Diamond Light Source, Oxford, (K^+ and Na^+: I24) (IO4-1, K^+ plus Na^+). In addition, anomalous scattering experiments with the K+ co-crystal of EcB43-ADPNP were collected to 2.92 Å. The data collection strategies used for each crystal are listed in table 5.1. A typical image of the diffraction collected is shown in fig. 5.3

#Salt	Station no.	Wavelength (Å)	No. of images taken	Starting angle (°)	Oscillation (°)	Exposure
No salt	I04-1	0.979	200	79	1.00	1.00 sec
K+	I24	1.033	1500	39	0.15	0.20 sec
Na+	I24	1.033	1500	160	0.15	0.20 sec
K+ *	I24	1.908	2400	0	0.15	0.07 sec
K+ plus Na+	I04	0.979	200	21	1.00	1.00 sec

Table 5.1 X-ray data collection strategies for various GyrB-ADPNP co-crystals

Salt used during co-crystallisation.

*Anomalous data collection.
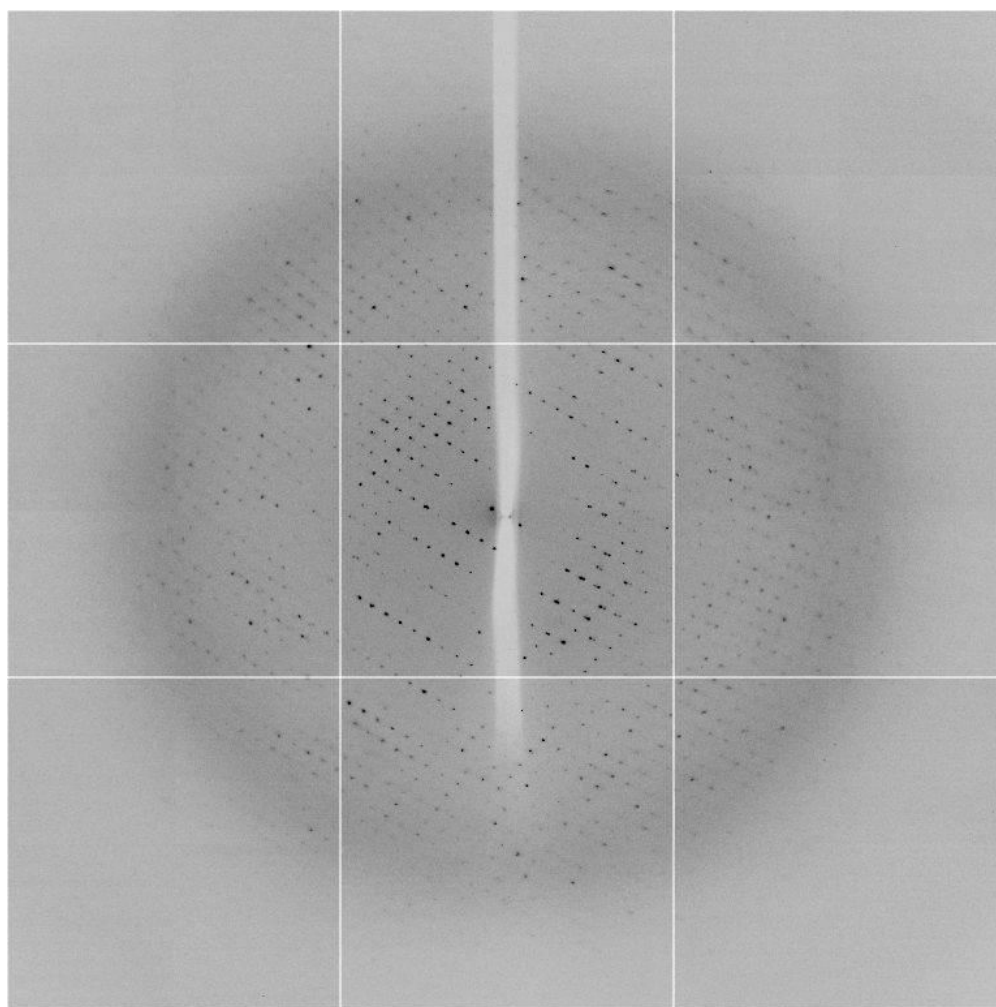
Figure 5.3 Typical image collected from the X-ray diffraction of GyrBNTD-ADPNP crystal grown in the absence of K+/Na+. Images were collected to ~2Å.

5.5 Data processing

The diffraction data collected was processed by MOSFILM [219]and SCALA [220]. Subsequent detailed data analysis was carried out using software packages in the CCP4 suite [274]. Statistics of processing from the data collected are summarised in table 5.2.

	No salt	K$^+$	Na$^+$	K$^+$/Na$^+$	Anomalous K$^+$
Space group	P222$_1$	P222$_1$	P222$_1$	P222$_1$	P222$_1$
Multiplicity	4.1	6.1	8.1	7.8	12.3
Cell parameters (Å)	a = 87.79, b = 141.47, c = 88.29	a = 87.86, b = 141.07, c = 79.55	a = 87.98, b = 140.90, c = 79.450	a = 87.50, b = 140.93, c = 79.86	a = 87.98, b = 140.90, c = 79.450
Resolution range (Å)	54.65-1.95 (2.00-1.95)	28.70-1.87 (6.21-1.87)	27.20-1.96 (8.77-1.96)	74.34-2.04 (6.12-2.04)	43.85-2.92 (13.06-2.92)
Unique reflections	36777 (2671)	35811 (2633)	35811 (2633)	31829 (5102)	1173 (808)
Completeness	99.3% (100%)	99.9% (100%)	99.8% (99.9%)	99.9% (100%)	99.7% (99.7%)
Rmerge	0.102 (0.638)	0.118 (0.688)	0.064 (0.763)	0.122 (0.699)	0.120 (0.883)
<I>/<σI>	14.7 (3.3)	7.2 (2.9)	18.7 (3.7)	10.7 (3.6)	12.6 (4.0)
Wilson B value	41.6	25.69	33.77	27.24	82.76
Solvent content	57.98%	57.46%	57.08%	57.7%	58.18%

Table 5.2. Summary of X-ray data collected for GyrBNTD-ADPNP complexes grown in the presence of various salts. The figures in brackets indicate the values for outer resolution shell.

5.6 Molecular replacement

Coordinates of the previously solved 2.5 Å resolution crystal structure of the GyrBNTD ADPNP dimer complex [271] were used as the search model for molecular replacement after removal of solvent molecules. Molecular replacement was performed using PHASER[221] with the $P222_1$ space group. Preliminary examination of the model with *Coot* [222] suggested two independent molecules with strong resemblance to the EcGyrBNTD dimer to form the asymmetric unit. Solvent content of the crystals was estimated using Matthews Coefficient calculations from the CCP4 package [272]. Calculations from all crystals were shown to contain ∼57-58% of solvent (table 5.2). Low Rmerge values of ∼0.06-0.122 were also obtained from all the data sets collected. This suggested that the overall conformations of the *Ec*B43-ADPNP complex, from all the crystals, are likely to be largely similar to those of the structure of the original template.

5.7 Structure refinement

Further refinement of the model was carried out using the Refmac5 software to perform auto-refinement of the model, typically with ∼5-10 cycles of iteration. The auto-refined model was then manually processed using *Coot* [222] to correct small mis-alignments of local structures, including manual examination and correction of side-chain orientations, peptide flips, etc. This was done using the SIGMAA-weighted $2mF_{obs} - DF_{calc}$ and $mF_{obs} - DF_{calc}$ Fourier electron density map as a reference [222]. Finally, the Phenix software package [223] was used for the modelling of the solvent water molecules.

5.8 *Coot* modeling of M+ binding sites

5.8.1 Unexpected discovery of a monovalent cation (M+) binding site - *Coot* modelling of ADPNP co-ordinating M+ ion binding site (site 1)

From the data collected from the EcB43-ADPNP crystal obtained in the absence of K^+/Na^+, electron density corresponding to a water molecule was observed in a cavity between ADPNP, Ile94, Val97, Ala100, Gly117, and Ser121 (fig. 5.4). A water molecule was subsequently inserted manually into the model using *Coot*.
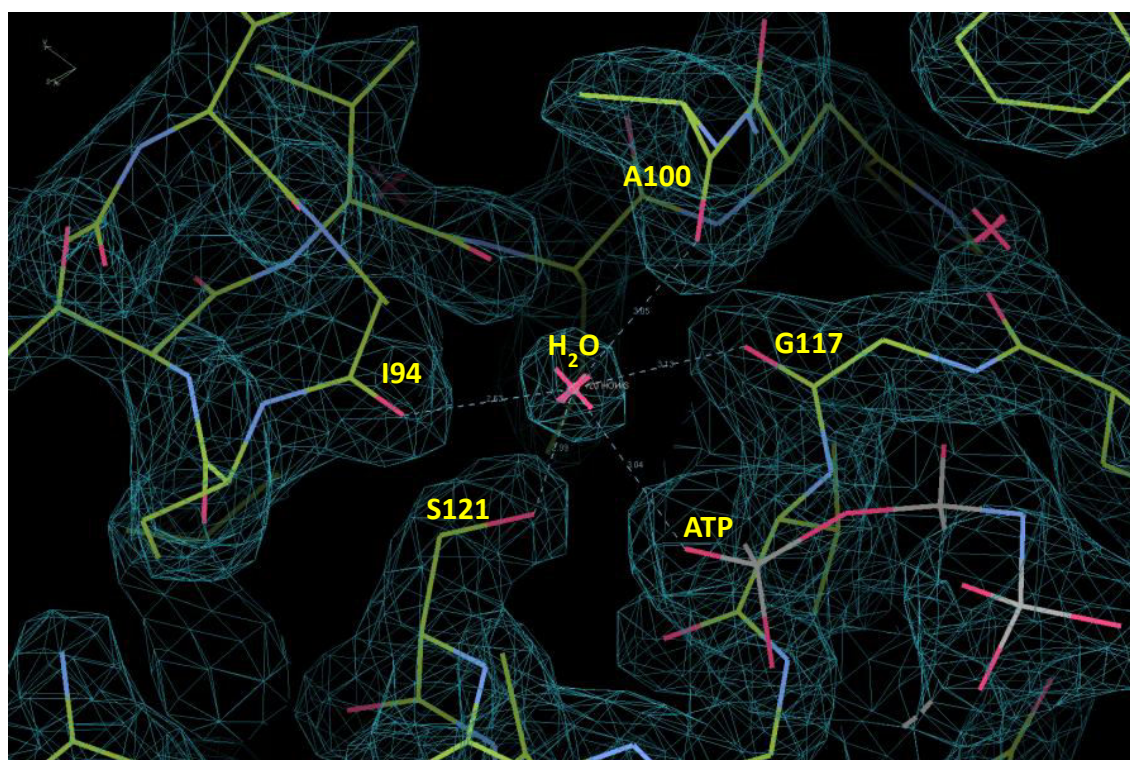
Figure 5.4 Electron density corresponding to the site 1 bound water at the 1.1σ contour level. *The density corresponding to the water is surrounded by six oxygen atoms from Ser121, Ile94, Val97, Ala100, Gly117 and the α-phosphate of the ATP substrate in close proximity.*

Interestingly, we were also able to observe electron density in an identical position in the K+ co-crystal of the EcGyrB-ADPNP complex (fig. 5.5). A manually inserted water molecule was rejected by Refmac5, as the actual density was regarded to be too large to correspond to a single water molecule. Given that K+ was included in the

crystallisation condition, we manually inserted a K⁺ ion by *Coot* into the model; this adjustment was accepted by the auto-refinement process by Refmac5.

In the same coordinates of the Na⁺ co-crystal, we discovered an unusual elongated area of electron density (fig. 5.6). As the only difference in crystallisation conditions in the Na⁺ co-crystal was the inclusion of Na⁺ instead of K⁺, we assumed that the elongated area of electron density to arise from a relatively mobile Na⁺ occupying two slightly different positions.
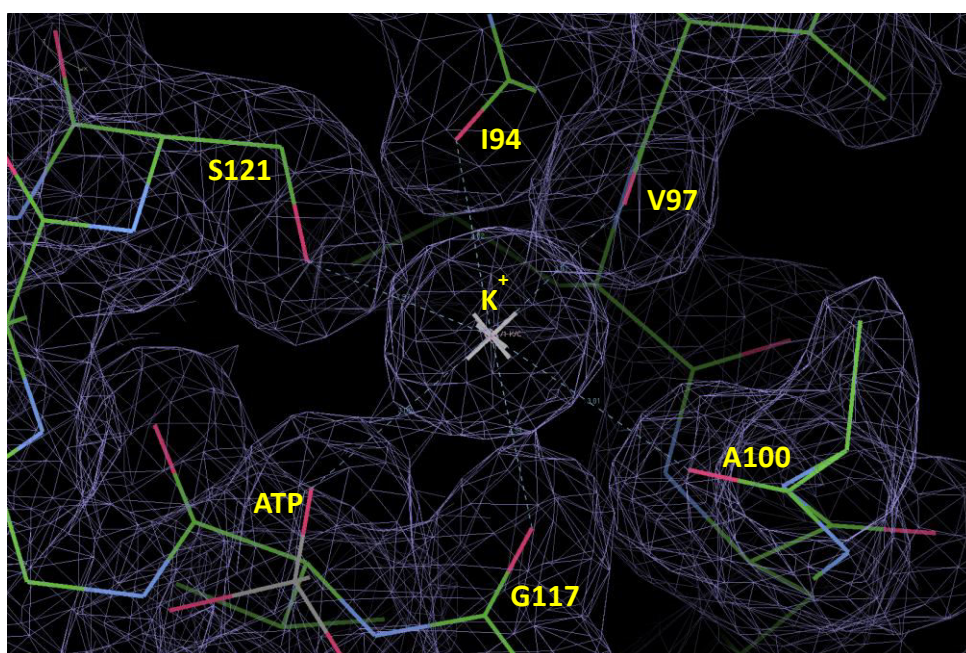
Figure 5.5 Electron density corresponding to the site 1 bound potassium at the 1.1 σ contour level. *The density corresponding to the potassium ion is surrounded by six oxygen atoms from Ser121, Ile94, Val97, Ala100, Gly117 and α-phosphate of the ATP substrate in close proximity.*
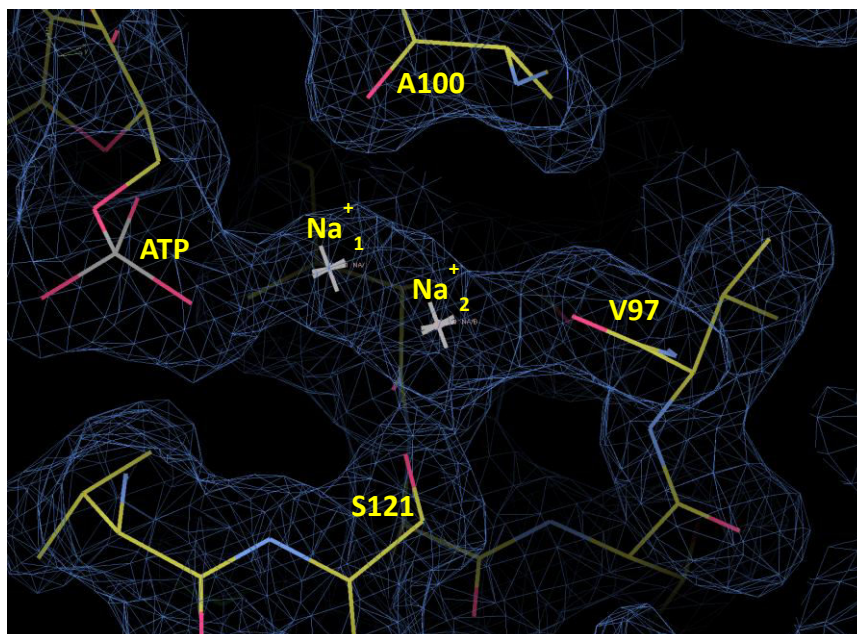
Figure 5.6 Electron density corresponding to the site 1 bound sodium at the 1.1 σ contour level. *The density corresponding to the sodium ion has an elongated appearance, which suggested the sodium ion can occupy two positions at the electron density Na$^+_1$ and Na$^+_2$. The density corresponding to the sodium ion is also surrounded by six oxygen atoms from Ser121, Ile94 (not shown), Val97, Ala100, Gly117 (not shown) and α-phosphate of the ATP substrate in close proximity.*

5.8.2 Discovery of a second M+ binding site - *Coot* modelling of ATP lid co-ordinating M$^+$ ion binding site (site 2)

While a M$^+$ binding was discovered at site 1, we were also able to find a highly coordinated electron density in all co-crystals of EcB43-ADPNP (Na$^+$, K$^+$ and K$^+$ plus Na$^+$) at a second site (fig 5.7). This electron density is coordinated by the backbone carbonyls of Lys103 and Asp105 and four additional areas of electron density resembling water molecules in an octahedral fashion. While manual insertion of a water molecule, a K$^+$ or a Mg^{2+} ion by *Coot* was rejected by Refmac5, insertion of a Na$^+$ ion was accepted. The fact that the density is situated closely (~2.3-2.4) to the

coordinating atoms was also closely matched by the theoretical average Na$^+$-O bond distance (2.5 Å) of an octahedrally coordinated Na$^+$. It is therefore highly possible that this electron density is in fact a highly coordinated Na$^+$ ion, suggesting a second novel M$^+$ binding site in EcGyrB, after the discovery of site 1.
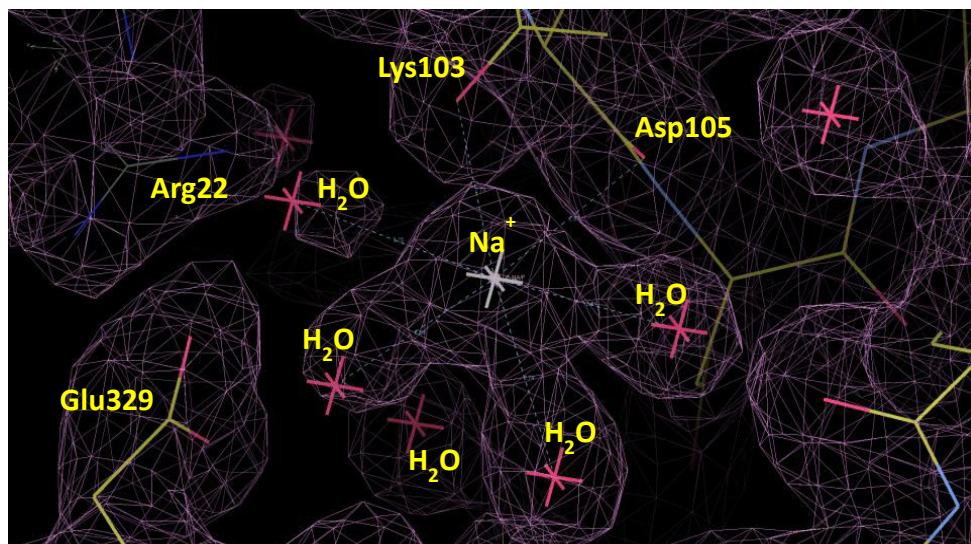
Figure 5.7 Electron density corresponding to the site 2 bound sodium at the 1.1 σ contour level. *The electron density corresponding to the sodium ion was appeared to form a complex with four oxygen atoms from four ordered water molecules, two oxygen atoms from backbone carbonyl of Lys103 and Asp105.*

5.9 Building the disordered loop in NTD GyrB

Prior to initial molecular refinement, it became clear that regions between Asp298-Glu317 of the *Ec*GyrB-NTD consisted of a relatively disordered loop region. As the quality of the electron density of the loop is not sufficient for auto-alignment using automatic refinement (refmac5), we decided to rebuild the loop manually using *Coot*. Initially, the loop region of the model generated by refmac, which aligned poorly with the electron density, was removed. We then manually added amino acids back to the two ends of the deleted region, guided by the poor quality region of the electron density. This was continued, with recurring auto-refinement using refmac5 to refine the new manual additions made until both ends of the deleted ends were met. As a result, a loop with no secondary structure resulted (fig 5.8).

Intriguingly, this flexible loop was discovered to interact with the identical loop of the adjacent symmetric related molecule and formed a key part of the contact. Due to the relatively disordered nature of the loop, a significant gain in entropic energy was envisaged from its stabilisation through crystal contact formation. We therefore proposed that the stabilisation of this disordered loop to be the key energy driver for the crystal lattice formation of the $P222_1$ crystal form.

It possible that this loop contact contributed to the crystal form rigidity observed with EcB43-ADPNP and resulted in $P222_1$ being the only crystal form observed. The fact that this construct strongly favours the formation of this crystal form also prevents the formation of diospyrin-bound crystal forms. Therefore, it is proposed that the deletion of the disordered loop might be necessary to encourage the formation of alternative crystal forms that can accommodate diospyrin binding.
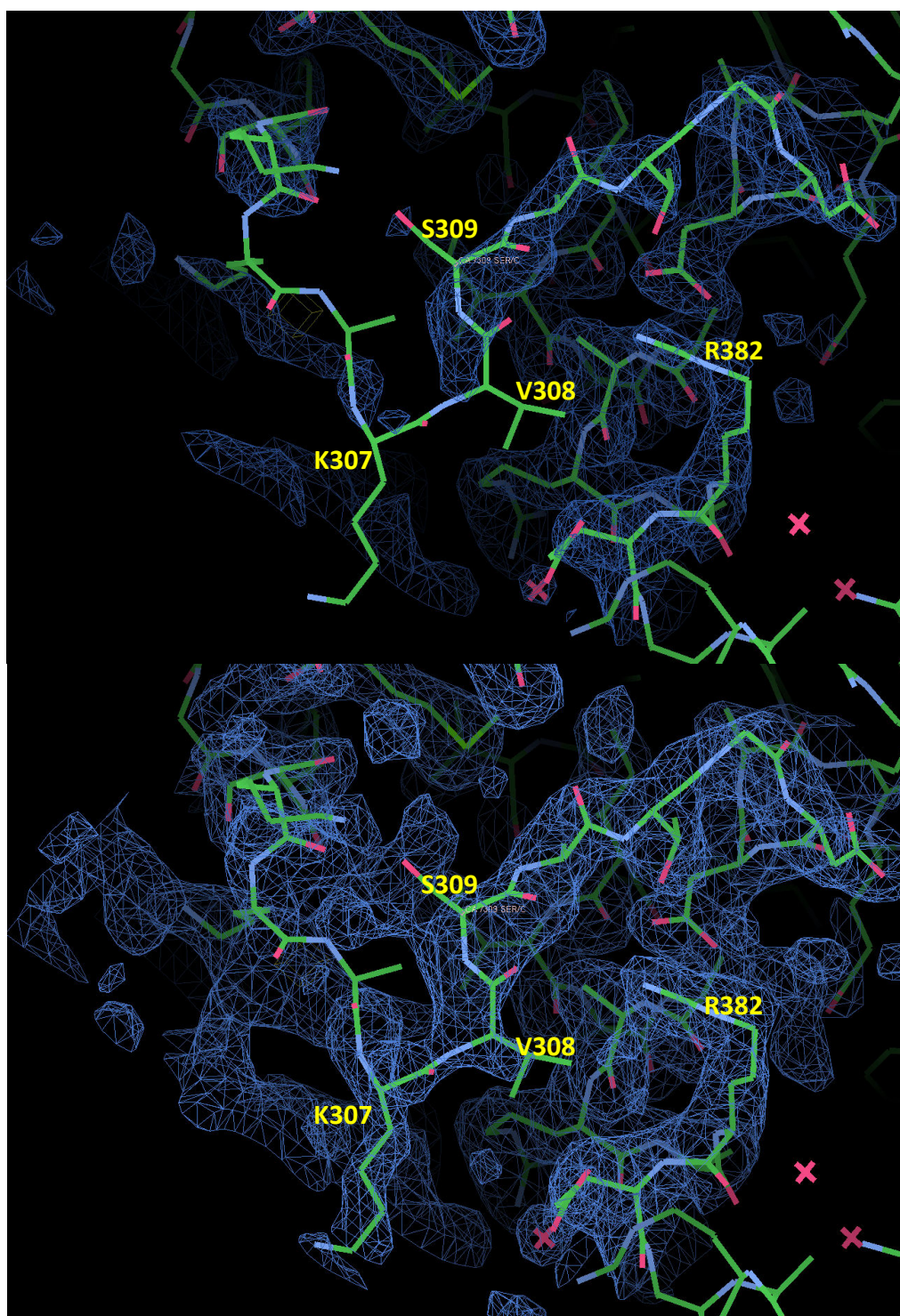
Figure 5.8 Disordered loop in the region between Asp298 - Glu317 of the GyrBNTD-ADPNP structure overlaid with electron density at 1.1 σ (top) and 0.7 σ (bottom). *Note the lack of density around the loop region at 1.1 σ and the reappearance of poor quality electron density at 0.7 σ.*

5.10 Structure validations

Once the model of H_2O, K^+, Na^+ soak crystal structures are fully refined in *Coot*, they were assessed using Ramachandran plots created *via* Molprobity (figs 5.9a & b, & 5.10a & b). It was clear that vast majority of residues fitted well within the plots. Those that were identified as outliers were mainly situated in the disordered loop (chapter 5.9). The outlier are listed as below:

K^+-*Ec*B43-ADPNP co-crystal structure:
- o   178 Asn
- o   303 Ser
- o   308 Val
- o   390 Glu

Na^+-*Ec*B43-ADPNP co-crystal structure:
- o   178 Asn
- o   303 Ser
- o   305 Ala
- o   306 Ala

Note that 178 Asn is listed as an outlier both in the K^+ and the Na^+ structure (figure 5.9a and 5.10a), which is located in the middle of an exposed loop in a beta-sheet. Due to the rotatable nature of the asparagine residue as well as the exposed nature of its location within the structure, the electron density of this residue is not precise as the rest of the structure. This might have led to the poor modelling of the 178 Asn residue and consequently appear as an outliner in the Ramachadran plot. Similarity, the 303 Ser, 308 Val and 390 Glu of the K^+ containing structure and the 303 Ser, 305 Ala and 306 Ala of the Na^+ containing structure are all located within the remodelled disordered loop describe in chapter 5.9. The poor density data of this region of the protein structure has led to the poor modelling and subsequently contributed to the outliers.

Overall, the percentage of outlier is ~1% for both sets of data and it is certained that the modelling process was carried out with sufficient accuracy.
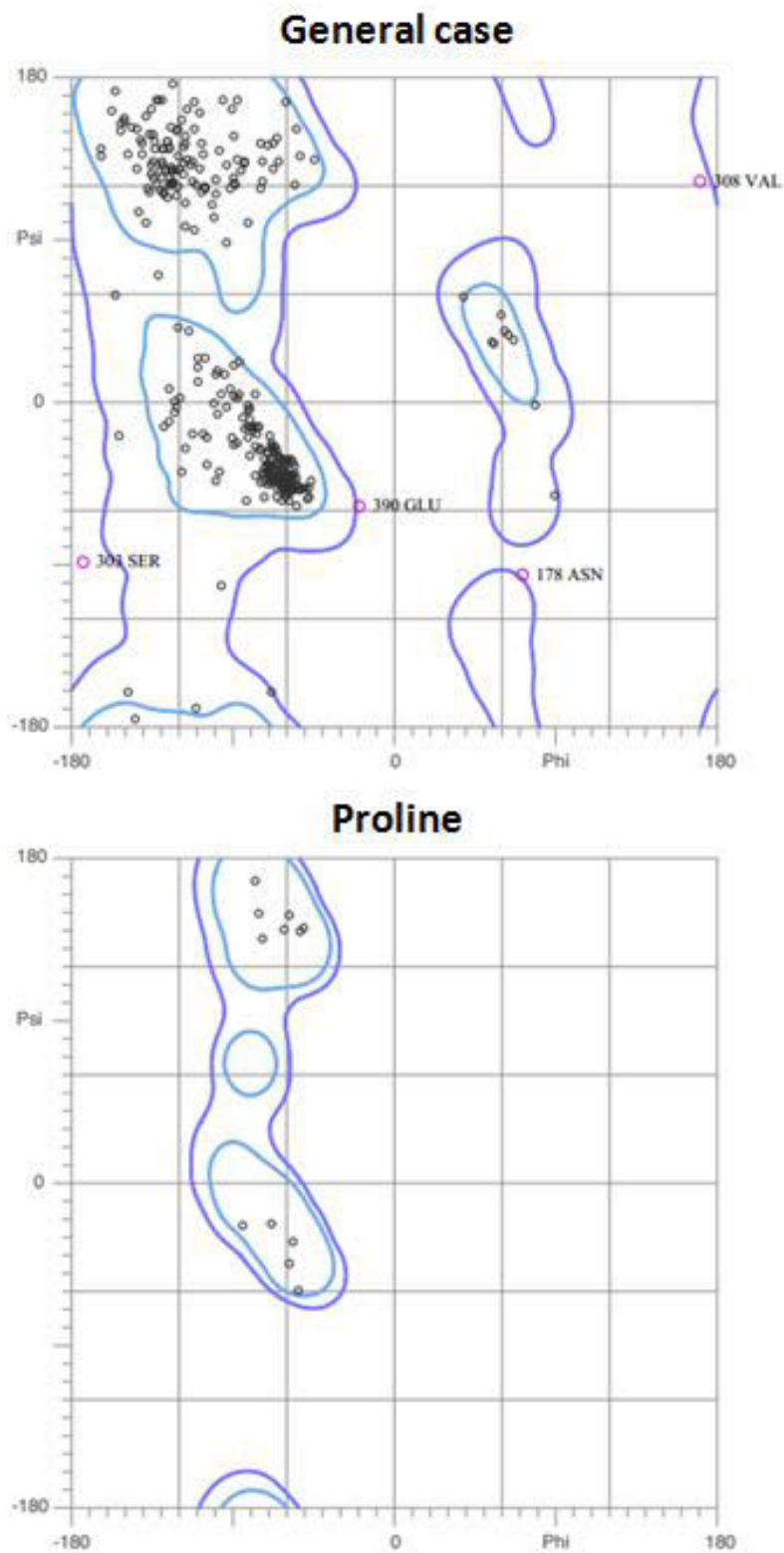
Figure 5.9a. Ramachandran plot (general case (excluding proline, glycine and pre-proline) and proline) generated from the refined K⁺-*Ec*B43-ADPNP co-crystal structure.[275]
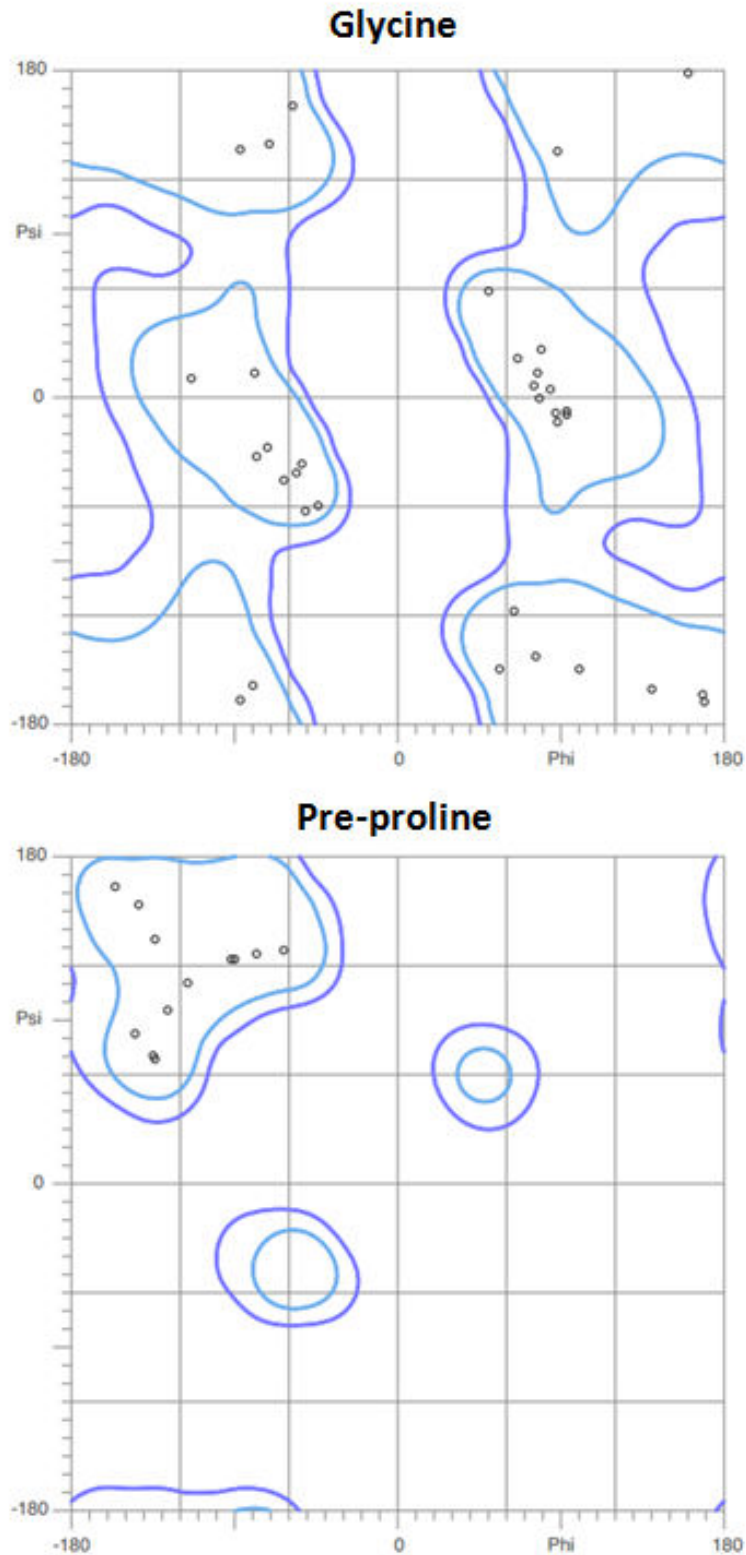
Figure 5.9b. Ramachandran plot (Glycine and pre-proline (the residue before proline)) generated from the refined K+-*Ec*B43-ADPNP co-crystal structure.[275]
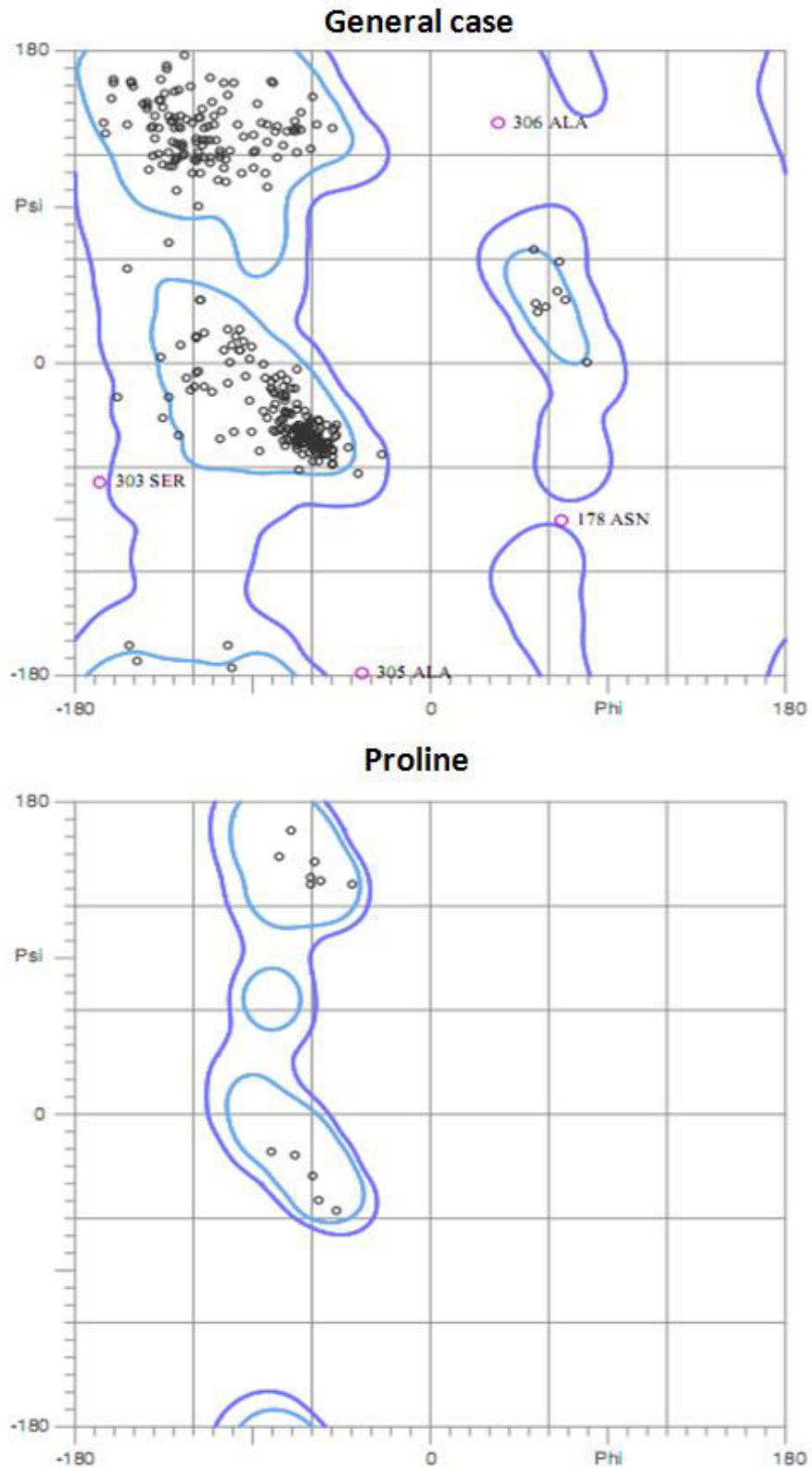
Figure 5.10a. Ramachandran plot (general case (excluding proline, glycine and pre-proline) and proline) generated from the refined Na⁺-*Ec*B43-ADPNP co-crystal structure. [275]
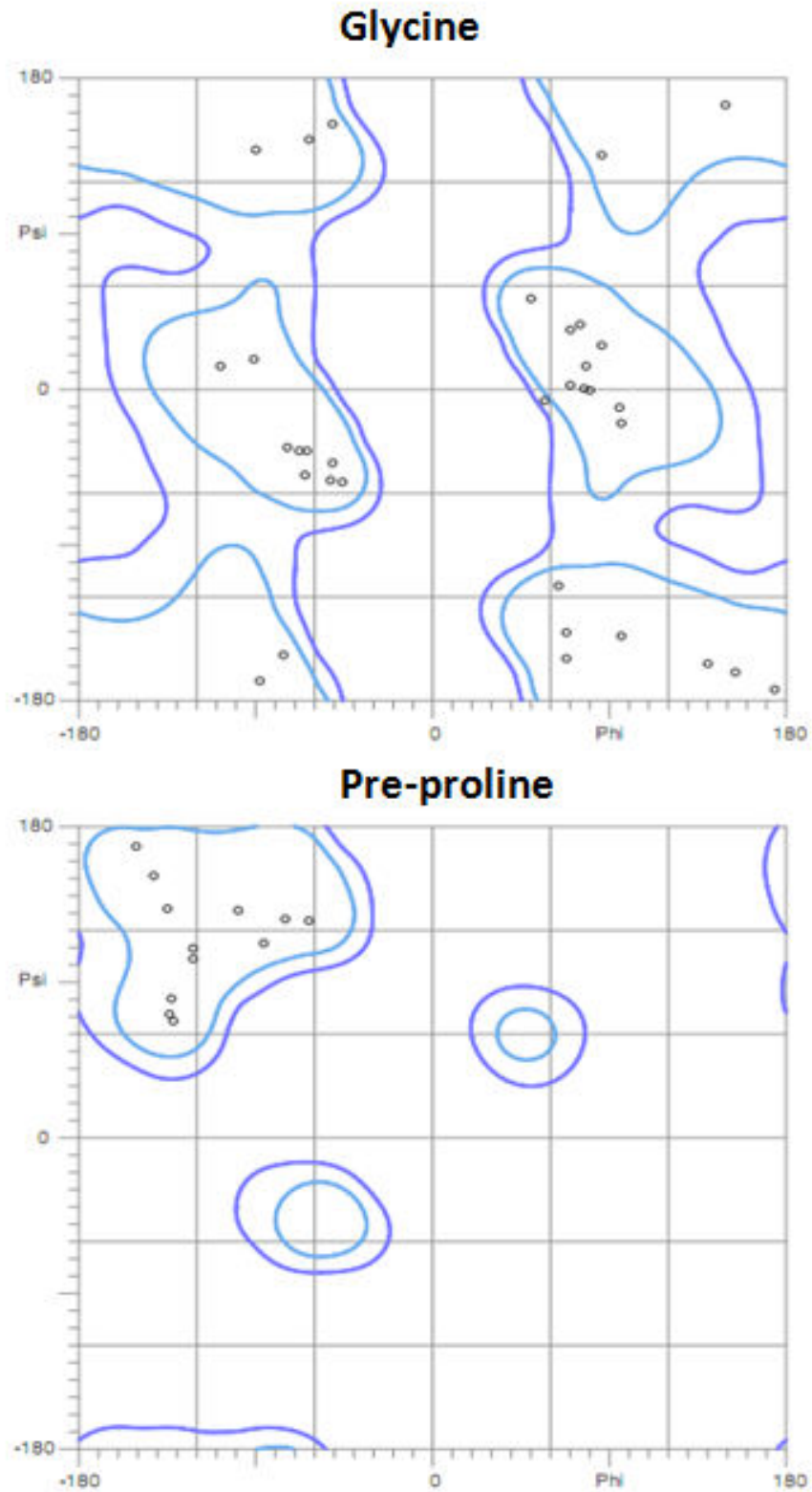
Figure 5.10b. Ramachandran plot (Glycine and pre-proline (the residue before proline)) generated from the refined Na+-*Ec*B43-ADPNP co-crystal structure. [275]

K⁺-*Ec*B43-ADPNP co-crystal structure

Refinement

R_{cryst} (based on 95% of data)	0.2101
R_{free} (based on 5% of data)	0.2436
Ramachandran favoured (%)	96.39%
Ramachandran outliers	4
Rmsd bond distances (Å)	0.026
Rmsd bond angles (°)	2.54
Average temperature factors (Å)	33.9
Contents of model	
Protein residues	392
Magnesium ions	1
Potassium ions	1
Sodium ions	1
ADPNP	1
Waters	172

Table 5.3 Summary of refinement and model parameters for K⁺-EcB43-ADPNP co-crystal structure

Na$^+$-*Ec*B43-ADPNP co-crystal structure

Refinement

R$_{cryst}$ (based on 95% of data)	0.2106
R$_{free}$ (based on 5% of data)	0.2397
Ramachandran favoured (%)	95.36%
Ramachandran outliers	4
Rmsd bond distances (Å)	0.028
Rmsd bond angles (°)	2.489
Average temperature factors (Å)	37.257
Contents of model	
Protein residues	392
Magnesium ions	1
Sodium ions	2
ADPNP	1
Waters	139

Table 5.4 Summary of refinement and model parameters for Na$^+$-EcB43-ADPNP co-crystal structure

5.11 Novel M⁺-binding site in the GyrB N-terminal domain

5.11.1 GyrB-NTD structure: M⁺ ion binding site at the ATP pocket (site 1)

5.11.1.1 K⁺ bound site 1
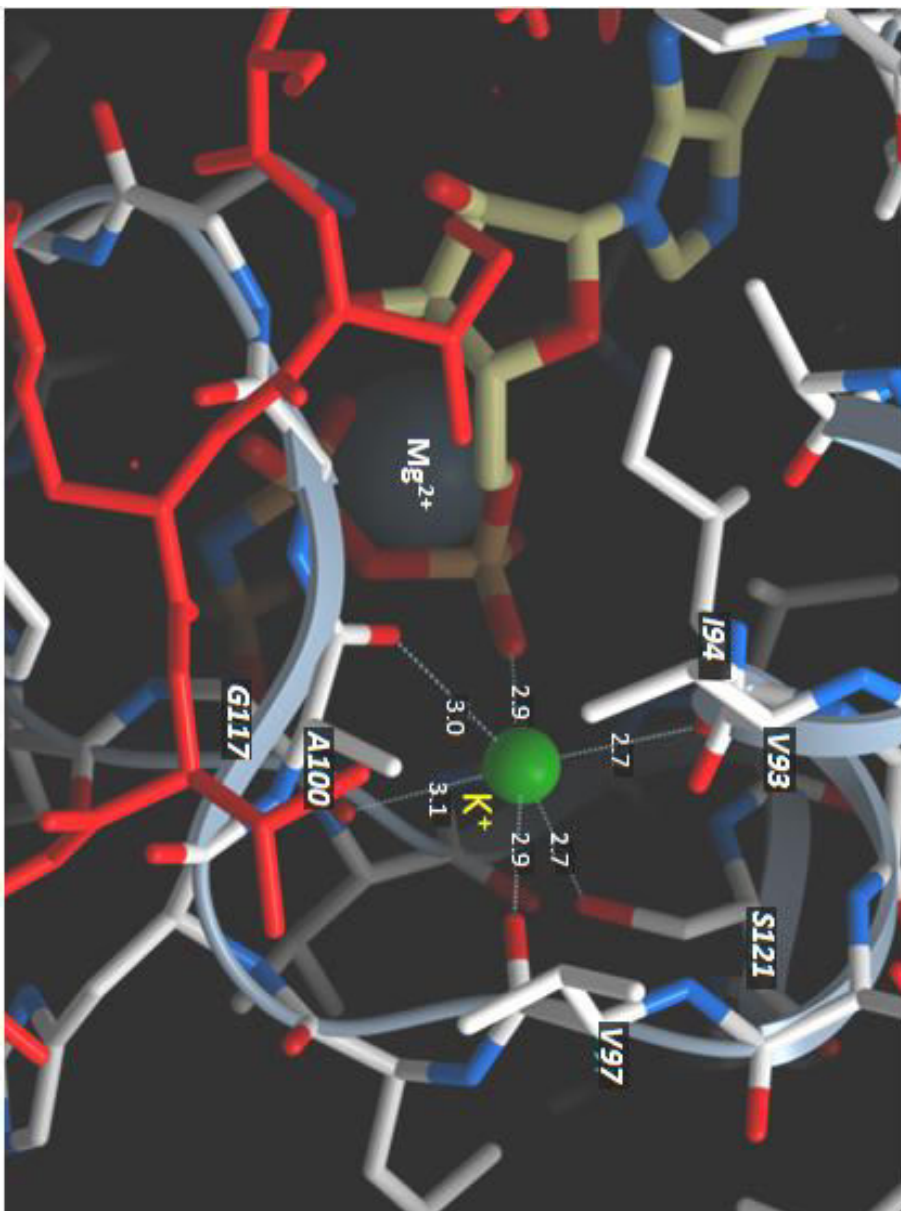
Figure 5.11 Octahedrally-coordinated K⁺ ion in the EcGyrBNTD-ADPNP-Mg²⁺-K⁺-Na⁺ dimer complex.
Distances between the K⁺ ion and its coordinating oxygen atoms are labelled in Å. The α-phosphate of the ADPNP substrate coordinates with the K⁺. The ADPNP chelated Mg²⁺ ion is coloured in grey. The N-terminal strap from adjacent the GyrB monomer makes contact with the ATP-lid, stabilised by the K⁺ ion. Figure was produced in Molsoft ICM-Pro
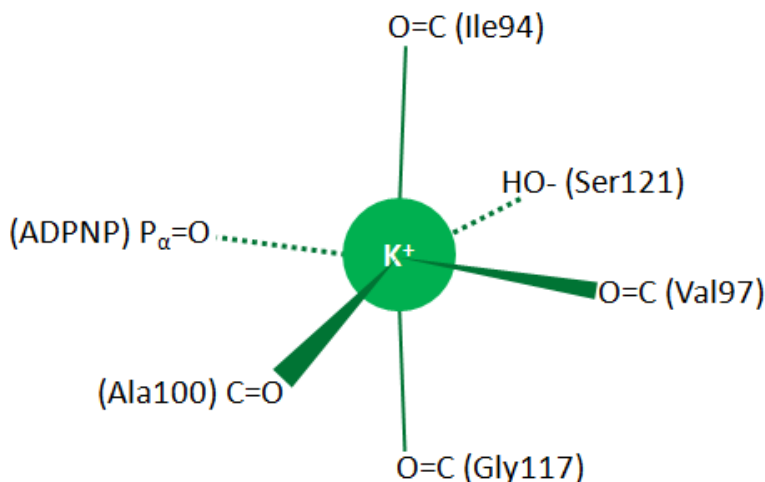
Figure 5.12. Schematic diagram of the site 1 K+ coordination contacts.

From the electron density data, we were able to identify a M+-binding site coordinating the α-phosphate of the ADPNP substrate analogue (site 1). Electron density corresponding to Na+ and K+ ions were present in site 1 in the NaGlu- and KGlu-grown crystal, respectively. Electron density equivalent to a water molecule is found in site 1 when no K+ or Na+ was included in the crystallisation condition. As shown in Figure 5.10, site 1 when bound with K+ is octahedrally coordinated by six oxygen atoms contributed by Ile94 in helix 3, Val97 and Ala100 from the subsequent loop, Gly117 and Ser121 from helix 4 and the oxygen atom from the α-phosphate of the bound ADPNP. The K+ ion is evenly positioned within the octahedral "cage" formed by the six oxygen atoms, with an average M+-O distance of 2.8 Å. This correlates well with previously studied K+-binding proteins, which commonly consist of 4-8 M+ binding ligands with the average M+-O distance of ~2.8 Å [276].

5.11.1.2 Na+ bound site 1

Interestingly, when a Na+ ion occupies site 1 an unusually elongated density is observed (fig. 5.5). It resembles a mobile Na+ freely shifting between two positions towards ADPNP and Val97 of the binding site (figure 5.12). By assuming that the Na+ ion is evenly distributed between the two positions simultaneously, the average M+-O distance of tetrahedrally co-ordinated Na+ in position 1 (closer towards ADPNP) and position 2 (closer towards Val97) are 2.975 Å and 2.55 Å respectively. This would suggest that Na+ is too small to fit into the site 1 M+ binding site and thus appears to have a more mobile mode of binding when compared to K+.
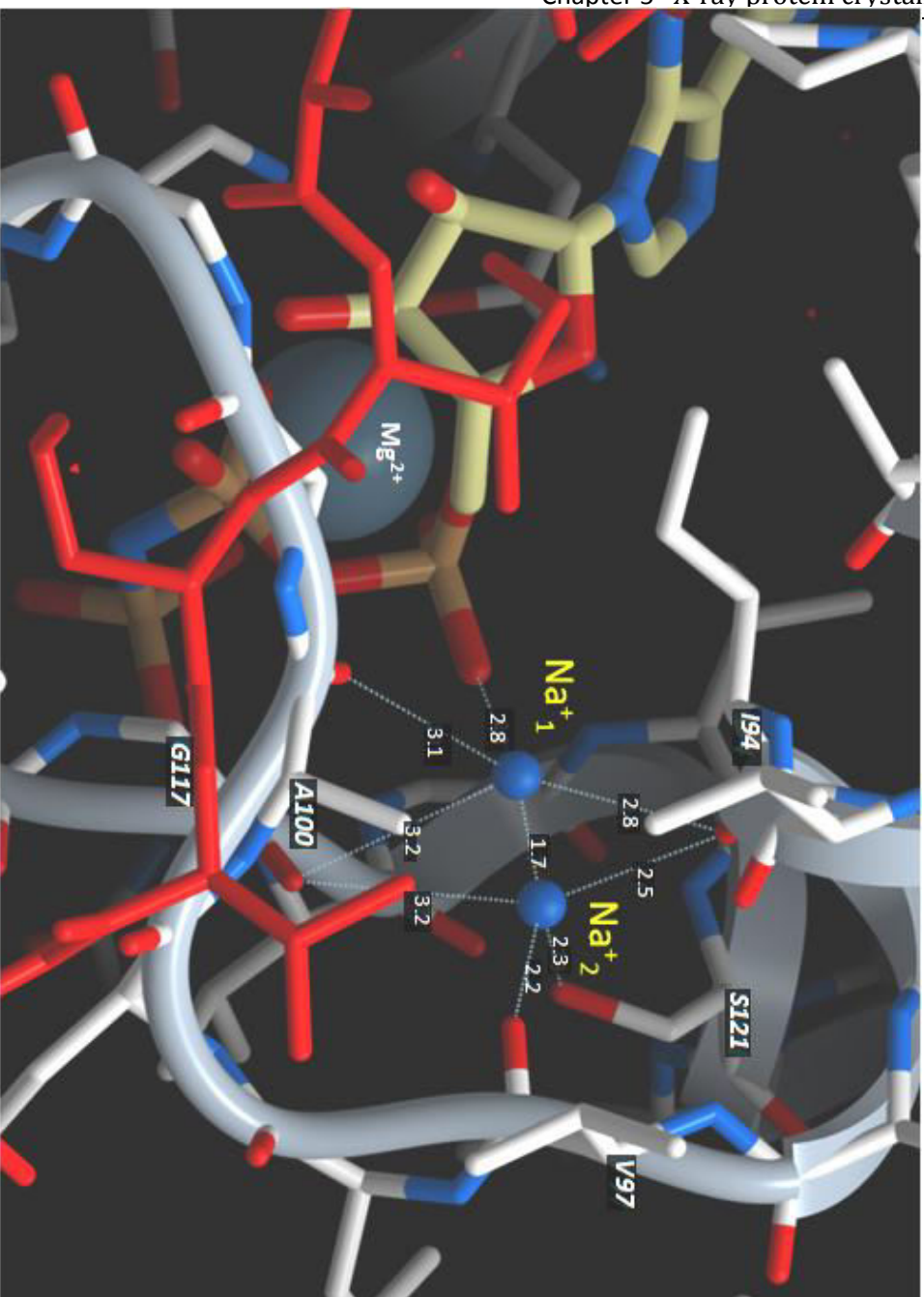
Figure 5.13 . Na+ ion in the site 1 M+ binding site of the EcGyrBNTD-ADPNP-Mg+-K+-Na+ dimer complex. *Notice the two Na+ ions depicted in the diagram are the positions where the Na+ is located with 0.5 occupancy each. Na+ ions are possibly readily shifting between the two depicted positions. Distances of the Na+ ion to the coordinating oxygen atoms are labelled in Å. The α-phosphate from the ADPNP substrate is coordinating the Na+₁ position. The Na+₂ position is too far from the α-phosphate to make any contact beyond van der waals forces. The ATP-chelated Mg²+ ion is coloured in grey. The N-terminal strap from the adjacent GyrB monomer is coloured in red. Figure was produced using Molsoft ICM Pro.*
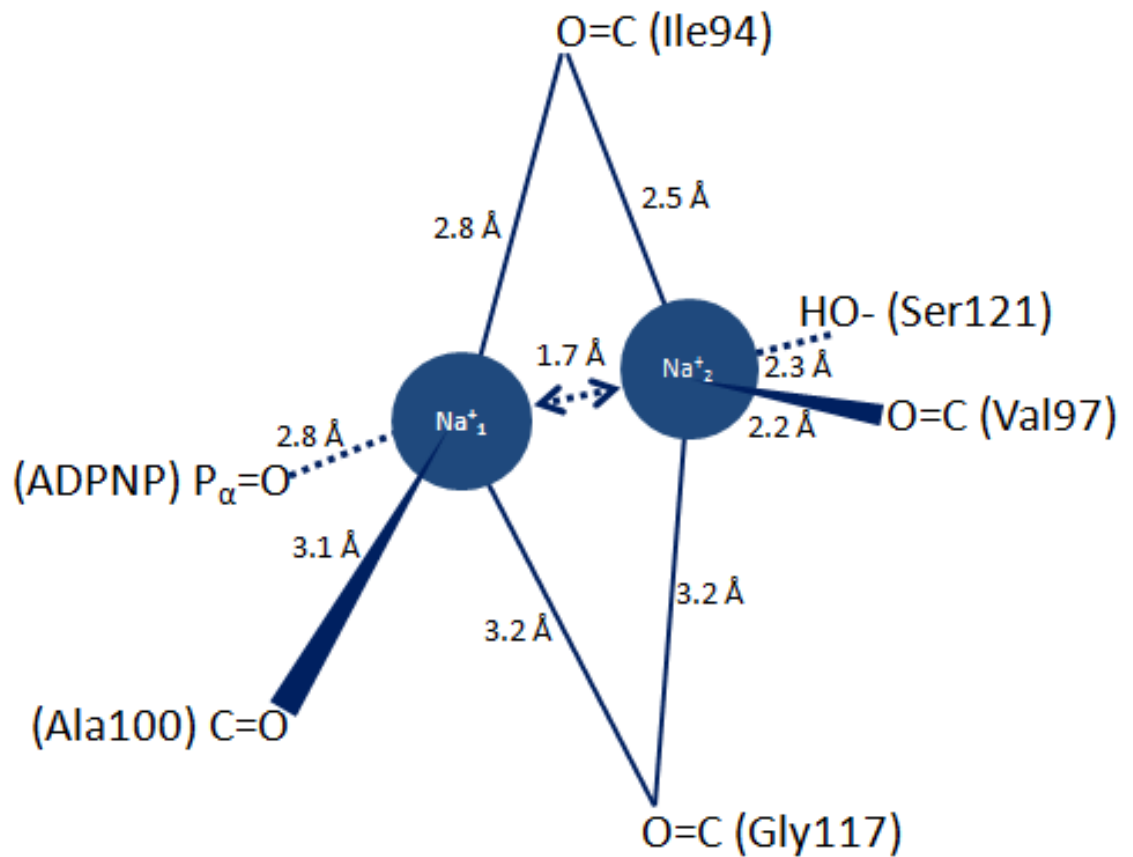
Figure 5.14 Schematic diagram showing details of the site 1 Na^+ coordination contacts and distances between the coordinating O and the Na^+. Na^+_1 and Na^+_2 are the positions occupied by two 0.5 occupancy Na^+.
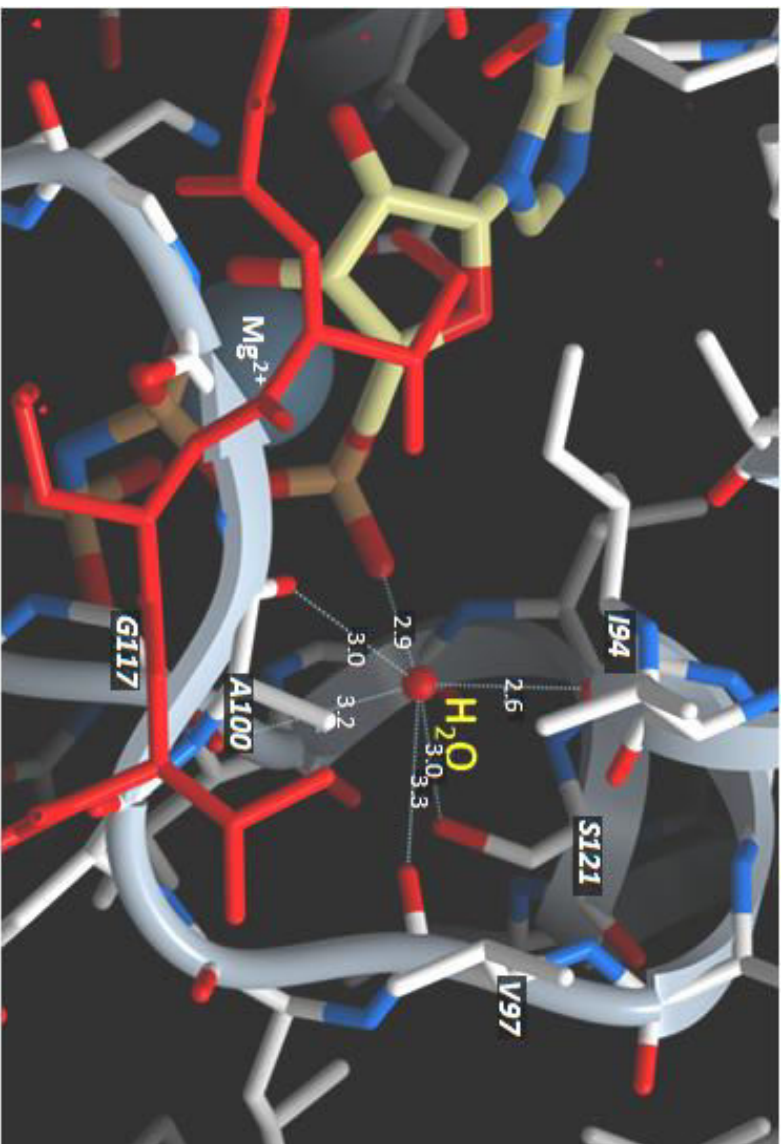
Figure 5.15. Water bound in the site 1 M⁺-binding site of the EcGyrBNTD-ATP-Mg⁺-K⁺-Na⁺ dimer complex. Distances of the water molecule to the coordinating oxygen atoms are labelled in Å. The α-phosphate from the ADPNP substrate is coordinating the water. The ADPNP chelated Mg2+ ion is coloured in grey. The N-terminal strap from the adjacent GyrB monomer is coloured in red. The figure was produced in Molsoft ICM-Pro.

5.11.1.3 K+ binding in site 1 confirmed by anomalous scattering signal

While molecular refinement suggested site 1 to be occupied by K+ in the K+ co-crystal of *Ec*GyrBNTD-ADPNP, we were interested in confirming this finding by detecting the presence of K+ *via* anomalous scattering. The anomalous diffraction data were collected at 1.907 Å wavelength to a resolution of 3.0 Å. The geometry of the anomalous density collected was then lined up with the previously solved *Ec*GyrB-ADPNP-K+ structure (2.04 Å). The coordinates of the K+ were generated using the density from the phased anomalous maps difference map.
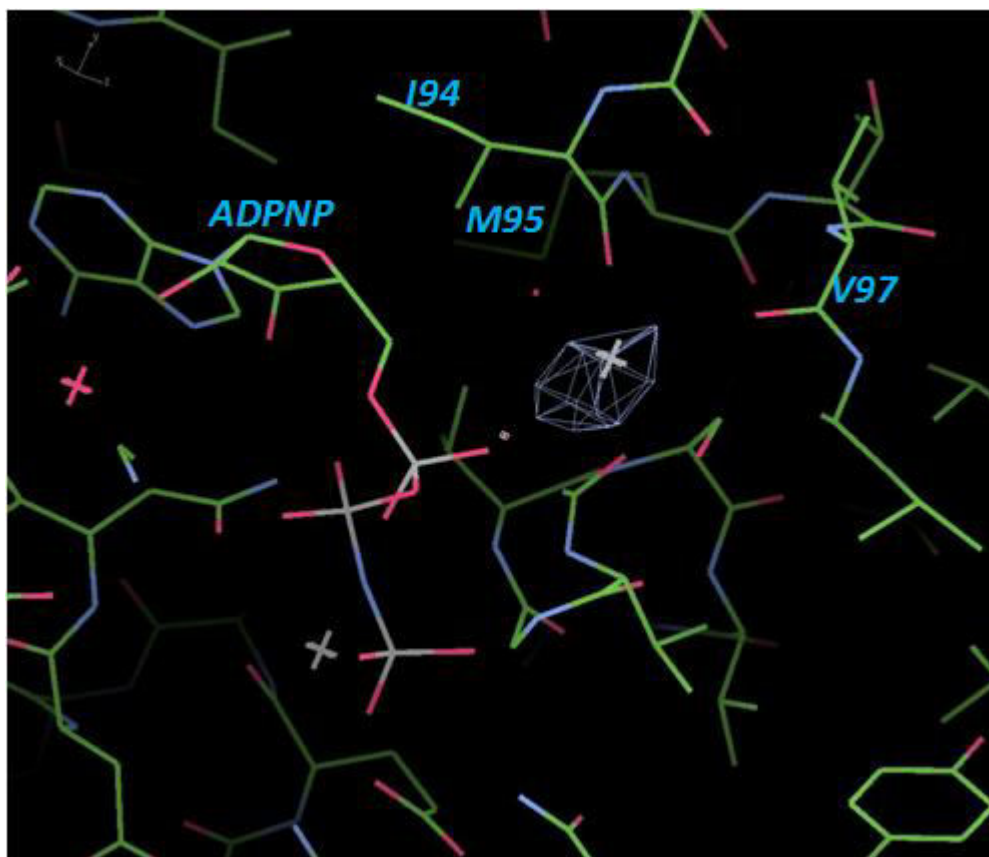
Figure 5.16 Raw anomalous signals observed in site 1 M+ binding site. *The white grid depicts the anomalous signal observed in the K+ co-crystal of EcGyrBNTD-ADPNP at the 5.5 σ contour level. Data were collected at 1.907 Å. The electron density appears to coordinate with the oxgen on the α-phosphate of the ADPNP substrate, carbonyl groups of ile94, Val97, Ala100 and Gly100, and the hydroxyl group of Ser121, which overlays with the position of site 1 K+ in figure 5.11.*

177
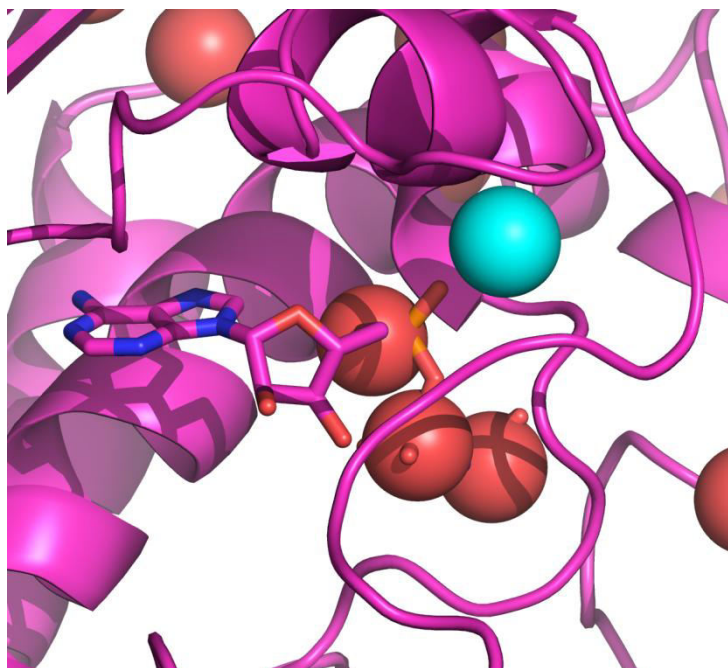
Figure 5.17 Anomalous signals observed in site 1 M⁺ binding site. *Data are collected at 1.907 Å wavelengths. The Cyan sphere depicts the coordinates of the peak of anomalous signals detected in relation to the EcGyrBNTD structure. It appears to overlay with the position of site 1 K⁺ observed in the crystal grown in the presence of K⁺. Minor scattering signals (red spheres) observed are contributed from the phosphorus atoms of the bound ADPNP. Structure of EcGyrBNTD is shown in magenta. Figure was produced in Pymol* [277].

As shown in the figure 5.16 and 5.17, the white grid from figure 5.16 and the cyan sphere from figure 5.17 depict the position of the anomalous density observed. This position completely overlays with the site 1 M⁺ binding site thus confirming that the enlarged electron density observed in site 1 of the K⁺ co-crystal to be a K⁺ ion. Any additional minor anomalous signals observed belonged to the phosphorus atoms from the ADPNP substrate analogue, since phosphorus scatters weakly at the wavelength (1.907 Å) tested. The signals from the three phosphorus ions from the bound ADPNP provided a secondary positional reference and further re-enforced the authenticity of the K⁺ induced anomalous signal at site 1. The presence of anomalous signal, together with the difference in interatomic distances between the K⁺ and Na⁺ GyrB-NTD cocrystal, electron density and the ATPase activity analysis, we conclude that site 1 is occupied by K⁺ instead of Na⁺.

5.11.1.3 K$^+$ binding is preferred in site 1

As K$^+$ and Na$^+$ were both capable of binding to site 1, we decided to explore the preferences between K$^+$ and Na$^+$ binding in site 1 using x-ray crystallography. We re-grew the EcB-NTD-ADPNP complex crystal in the presence of 100 mM NaCl and 100 mM KCl. Diffraction data of the crystal were collected and processed similarly to the K$^+$ containing crystal. The electron density at site 1 M$^+$ recorded in the K$^+$/Na$^+$ co-crystal exhibited a similar relative intensity to that obtained in the K+ co-crystal. Molecular refinement confirmed that the site 1 M$^+$ in the K$^+$/Na$^+$ co-crystal to be K$^+$. This is possibly due to a difference in affinity between the K$^+$ and Na$^+$ ions towards site 1. This demonstrated that site 1 has a preference for K$^+$ binding over Na$^+$. Previous studies on M$^+$ binding proteins showed that selectivity between Na$^+$ and K$^+$ binding are established by geometric constraints of the enzyme and thereby resulting in a change in entropic cost of accommodating M$^+$ ions of difference sizes. We would therefore argue that site 1 of *E. coli* GyrBNTD is geometrically configured to accommodate K$^+$ over Na$^+$. We propose that this constraint is imposed by the "octahedral cage" formed by oxygen atoms from protein backbone carbonyls, a serine residue and α-phosphate of the ATP substrate. Detailed analysis of the geometric difference in the "octahedral cage" between K$^+$/Na$^+$/H$_2$O bound site 1 and the resultant ion selectivity would be discussed in chapter 5.11.1.4.

5.11.1.4 Structural differences between EcB43 with K$^+$/Na/water bound site 1

There is no significant difference in the overall conformation of EcB43 with K$^+$/Na$^+$/water bound at site 1. Nevertheless in a closer examination, we were able to observe slight differences in size of the "octahedral cage" formed by the oxygen atoms that coordinate with the M$^+$ ion (fig. 5.18). As the coordinate errors for the Na$^+$-ECBNTD and K+-ECBNTD structure are 0.17A and 0.1A accordingly, it is unlikely that the observe differences in bond distances are the result of data inaccuracies. When K$^+$ is bound at site 1, the "octahedral cage" is found to be significantly smaller than when Na$^+$ or H$_2$O is bound at site 1 (fig. 5.18 & .19). The reduction in the "cage" size possibly indicates that K$^+$ is able to establish good contacts with the six-coordinates in site 1 and is able to "pull the cage" towards it.

179

In the case of the Na^+-bound site 1, while the theoretical Na^+-O bond distance is expected to be shorter than the K^+-O bond due to its smaller ionic radius, the cage is bigger for the Na^+-bound site 1. This is possibly due to Na^+ not being able to make sufficient contact with the coordinating oxygen atoms within site 1 and as a result was not able to pull the "cage" as well as K^+ does. This notion is supported by the apparent elongated density observed in Na^+-bound site 1 that suggest a relatively mobile Na^+.

The fact that K^+ binding is preferred at site 1 as observed in the anomalous data, together with the evidence above provide strong evidence that Na^+ does not bind to site 1 as well as K^+. While K^+ and Na^+ binding in site 1 is only differentiated by their respective ion sizes and charge density, this suggests that the "octahedral cage" is possibly conformationally restricted and could not form a smaller cage that can comfortably accommodate the Na^+ ion.
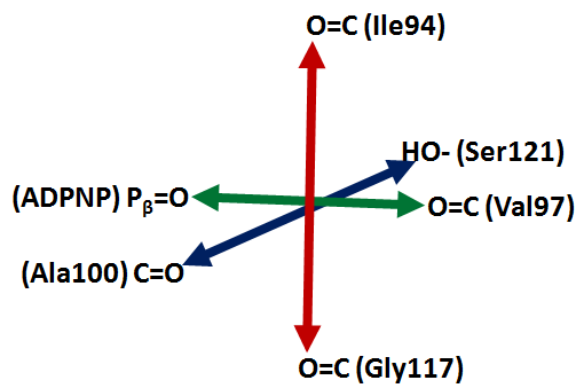
	ADPNP (Pα=O) - Val97 (O=C)	Ile94 (O=C) - Gly117 (O=C)	Ser121 (-OH) - Ala100 (C=O)
K^+	5.8 Å	5.4 Å	5.6 Å
Na^+	6.3 Å	5.6 Å	6.1 Å
H_2O	6.2 Å	5.7 Å	5.8 Å

Figure 5.18 Dimensions of the Octahedral cage of site 1 M+ binding site between the K+/Na+/H₂O bound EcB43-ADPNP structures.
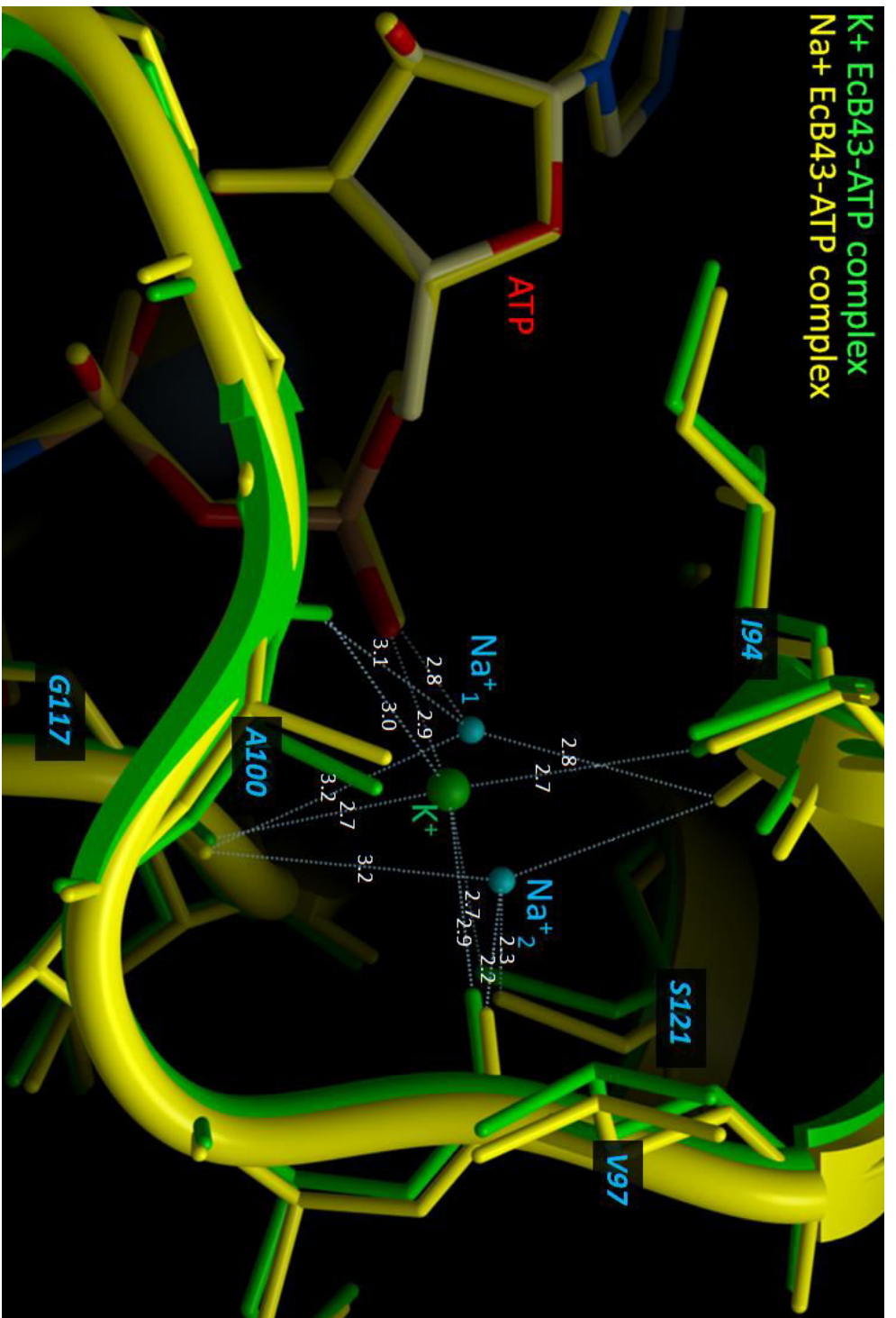
Figure 5.19 Structure overlay of K⁺-EcB43-ATP complex (green) and the Na+-EcB43-ATPcomplex (yellow). *Positions of the two Na⁺ positions and the potassium ion are depicted in cyan and green spheres respectively. Distances between the atoms (dotted lines) are labelled in Å.*

5.11.2. GyrB-NTD structure: site 2 M+ ion binding site

Figure 5.20 Structure of the Na+ bound ATP lid (site 2) in GyrB-NTD-ATP structure. *Position of Na+ is depicted by the cyan sphere. Na+-O interactions and hydrogen-bonds contributed from the water coordinating the Na+ ion were shown in dotted line with distances shown in Å.*
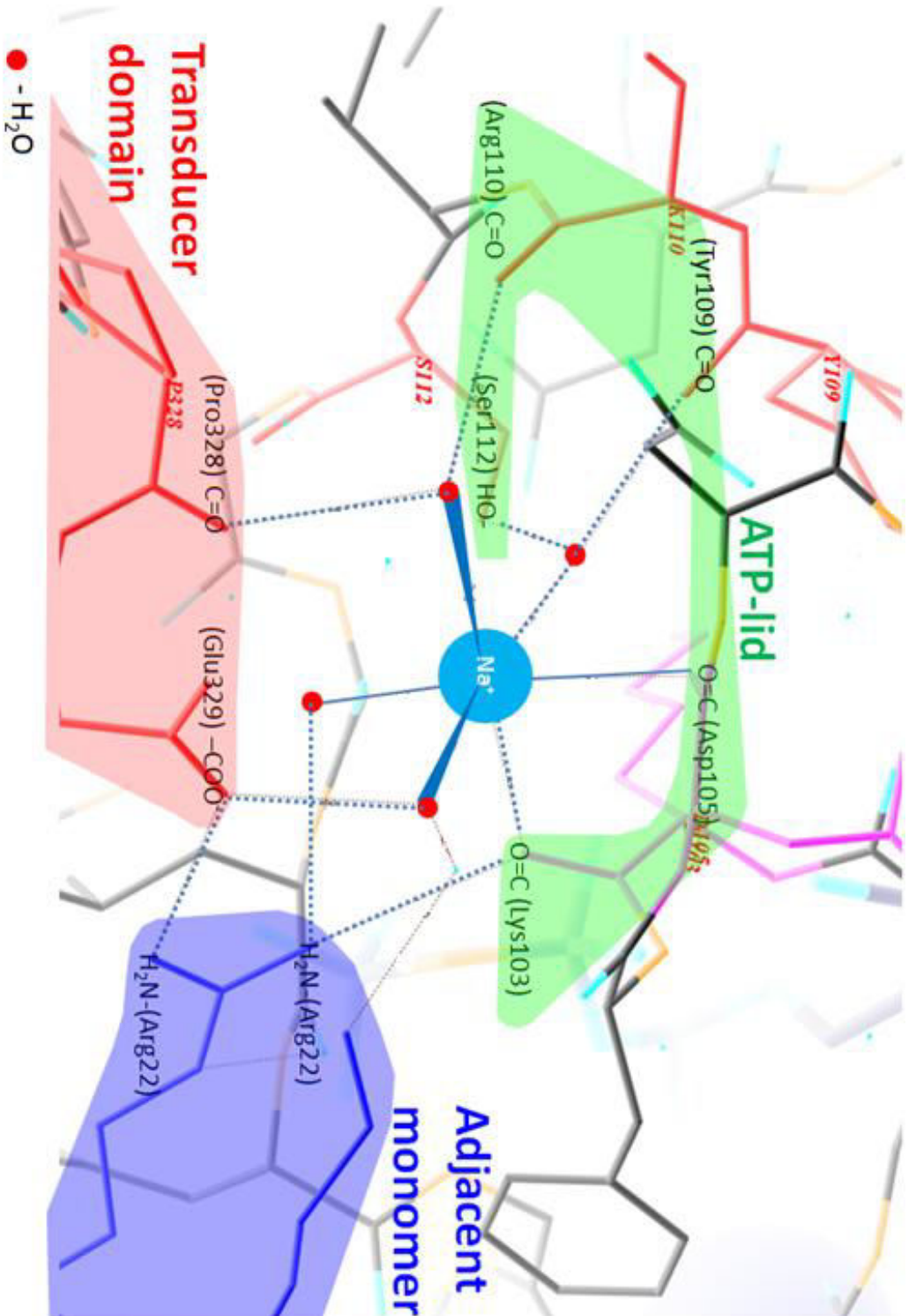
Figure 5.21 Model of the Na⁺ bound ATP lid (site 2) in GyrB-NTD-ADPNP structure. *Na⁺ directly coordinates with the backbone carbonyl oxygen atoms of Arg103 and Glu105. Na⁺ also coordinates with 4 ordered water molecules and forms an extended H-bond network that interacts with residues from the ATP-lid (Tyr109, Arg110, and Ser112), the transducer domain (Pro328, Glu329) and the adjacent monomer (Arg22).*

In all of the EcB43-ADPNP structures where the crystals were grown in the presence of no salt, NaGlu, and KGlu, an electron density corresponding to Na$^+$ was found in the centre of both of the ATP lid of GyrB (fig. 5.20), a flexible loop that forms a major part of the ATP pocket in present in GHKL ATPases. The presence of this novel M$^+$ site (site 2) was not envisaged as, unlike site 1, there was no previous indication of this site in other GHKL ATPases. Although this site has particular amino acid residues that are conserved across the bacteria kingdom (fig. 5.22) (Lys 103 and Asp 105), there are also a range of other conserved amino acids close to the site that are highly conserved. The highly conserved nature around this site might be driven by the needs to accommodate the ATP rather than the need for Na$^+$ ion binding. Similar to site 1, the site 2 M$^+$-binding site is octahedrally coordinated by oxygen atoms.   Two of the oxygen ligands were contributed by the backbone carbonyls of Asp105 and Lys 103 from the ATP lid and interestingly four ordered water molecules were also involved. The coordinating water molecules form an extensive hydrogen bond network with backbone carbonyl and side chain groups of nearby residues, including Tyr109, Arg110 and Ser112 of the ATP lid, Pro328 and Glu329 of the transducer domain, and Arg22 of the adjacent GyrB monomer (figure 5.21 & 5.22). While traditionally water is regarded as a mobile molecule that rapidly exchange in and out of the protein surface [276], it is rather common to find 1-4 water molecules stably bound to M$^+$ and amino acids around the M$^+$ binding sites in M$^+$ activating proteins.

In other M$^+$ activating proteins, the M$^+$-coordinating water molecules would typically form a stable hydrogen bonding network around the amino acid residues around the M$^+$ binding site [278-279], supporting the function of the enzyme by acting as an important structural feature of the protein scaffold. While bulk Na$^+$ exchanges its surface water with the bulk solvent at a high frequency [276], the enclosed environment created by the ATP lid could shield the Na$^+$ from freely exchanging water molecule. This restriction on the movements of the coordinating water molecules subsequently creates the framework that provides the six oxygen atoms crucial for the octadentate binding of the Na$^+$ ion (fig. 5.21).

The hydrogen bond network links together functionally important interfaces between the ATP lid, the transducer domain and the conserved Arg22 from the adjacent GyrB monomer. While the ATP hydrolysis in ATPase domain and the movement in the transducer domain in type IIA topoisomerase have been suggested to be closely linked during strand passage [280], the GyrB-NTD dimer interface determines the integrity of the N-gate, which is crucial to the proposed 2-gate strand passage mechanism [85,281].

This network of interactions created by the presence of Na^+ could potentially stabilise the flexible ATP lid, assist GyrB dimerisation and coordinate movements between the ATPase domain and the transducer domain.
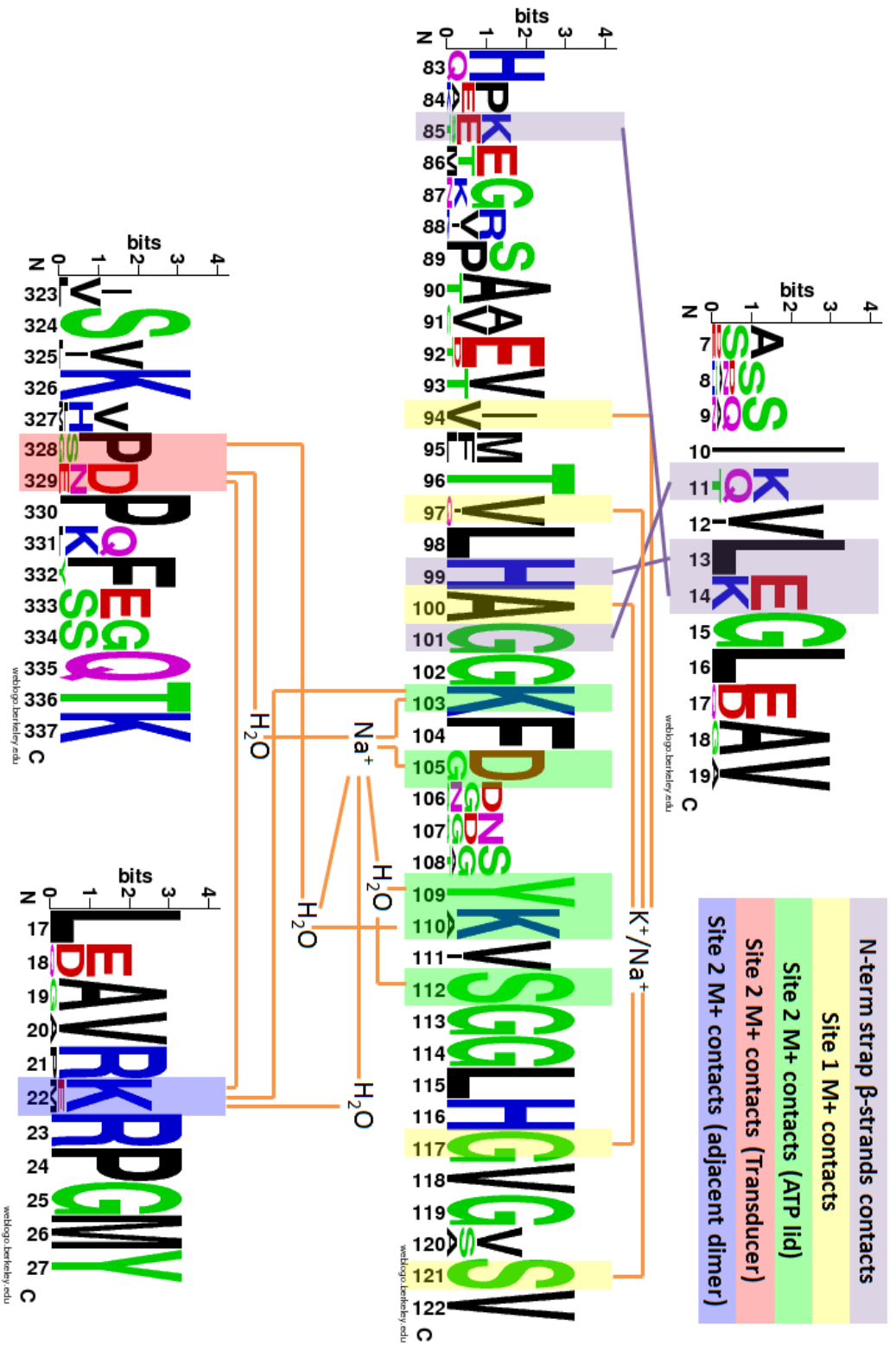
Figure 5.22 Conservation of the residues interacting with site 1 M⁺, site 2 Na⁺ and its coordinating water molecules in 12 pathogenic bacteria (*Brucella melitensis, Escherichia coli, Klebsiella pneumoniae, Helicobacter Pylori, Bacillus subtilis, Streptococcus pneumonia, Clostridium difficile, Corynebacterium diptheriae, Mycobacterium tuberculosis*). *The figure was produced using Weblogo* [220].

As Na$^+$ binding was observed in the absence of Na$^+$ supplement in the crystallisation condition, it is possible that Na$^+$ contamination from the protein stock was sufficient to occupy the site. Interestingly, only a water molecule was observed in site 1 in the same crystallisation condition, which indicates that the affinity of Na$^+$ to site 2 is much stronger than it is to site 1. Additionally, crystals grown in the presence of 100 mM K$^+$ did not displace the Na$^+$ ion bound and therefore suggests that site 2 has a strong if not a complete preference for Na$^+$ binding over K$^+$.

5.12. Discussion

5.12.1 Biochemical function of the M$^+$ sites in GyrB-NTD

While divalent ion binding and function in proteins is well understood [282-284], the roles of monovalent ions on protein structure and function is not as well elucidated. Many proteins are known to require Na$^+$/K$^+$ ion for their activity but there is little understanding on the role that Na$^+$/K$^+$ has on their functions [276]. As the Na$^+$ ion electron density closely resembles a well-ordered water molecule, it is often not easily identified in crystal structures. In the case of *E. coli* GyrB-NTD, stable crystals were obtained readily in the absence of K$^+$ and Na$^+$ in the past[46,60]. Due to the prevalence of a M$^+$ site among GHKL ATPase, there were previous suggestions that the M$^+$ site could exist in GyrB (a GHKL ATPase).

Here two novel M$^+$ binding sites have been identified in the NTD of GyrB, where site 1 can accommodate both K$^+$ and Na$^+$ (with a preference for K$^+$), and site 2 has an explicit preference for Na$^+$. It is suggested that the minimum size of M$^+$ ion that can fit into site 1 is restricted, which leads to Na$^+$ being less well fitted with the smaller ionic radius and shorter M$^+$-O distance. Intriguingly, the differences in ATP hydrolysis rate of *E. coli* GyrB in the presence of K$^+$ is marginally higher than in Na$^+$ from the 150-600 mM range (fig. 3.24), which could be the result of K$^+$ being better fitted to site 1 M$^+$ site. In addition, supplementing *E. coli* gyrase with both Na$^+$ and K$^+$ (described in chapter 3.8, fig. 3.17) also increases their supercoiling activity, with K$^+$ showing significant stimulation over Na$^+$.

The fact that site 2 does not accommodate K^+ yet K^+ was able to stimulate both ATPase and supercoiling activity of *E. coli* gyrase, provides a clear indication that the concentration-dependent stimulation by M^+ is likely to originate from site 1 but not site 2.

5.12.2 Site 1 and 2 M^+ belong to type I and II M^+ activation, respectively

In the review of M^+-activating proteins assembled by Cera et al [276,285], the enzymatic mechanisms of M^+ activation among these proteins were carefully grouped into type I and type II. He described that type I activating M^+ behaves as a co-factor, where the absence of the M^+ completely abolishes enzyme activity[276]. Type II activating M^+ behaves as an allosteric effector and stimulates baseline activity upon binding[276]. From analysis of the structures of M^+ activating enzymes[285], it is found that type I M^+ typically coordinates with the substrate and directly influences its binding. Type II M^+ however does not have direct contact to the substrate and instead would bind to regions where enzyme activity could be influenced indirectly[285]. Structurally, under this system of classification, site 1 and site 2 M^+ binding site of GyrB would belong to type I and type II M^+ respectively.

Furthermore, type I M^+ activation can be further divided into type Ia and Ib (figure 5.23 & 5.24). Type Ia enzymes would require the binding of M^+ for substrate binding, while type Ib enzymes allow substrate binding in the absence of M^+ but cannot catalyse the reaction without the M^+. As a result, despite the absolute M^+ ion requirement of type I enzyme, type Ia activation is not dependent on M^+ concentration. Whereas in a type Ib enzyme, its k_{cat} would increase with the increase in M^+ concentration as the enzyme becomes saturated with M^+.

In the case of GyrB, the M^+ concentration-dependent stimulation profile of ATPase and supercoiling strongly resembles that of a type Ib (fig. 3.24). Indeed, crystallographic evidence also supports the idea that GyrB is capable of binding ADPNP in the absence of a monovalent metal cation (M^+) [46,60], which accords with substrate binding behaviour of type Ib.

Type Ia
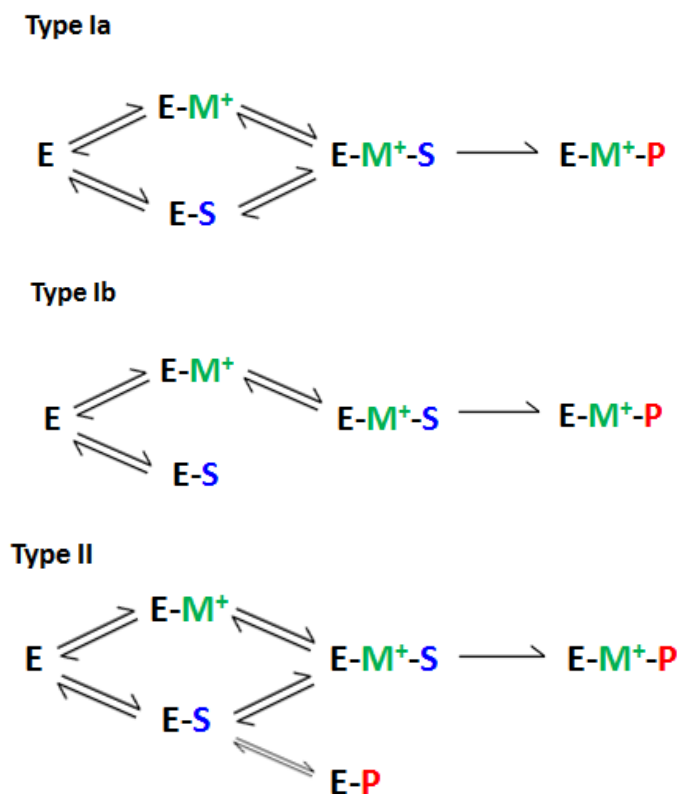
Type Ib

Type II

Figure 5.23 Schematic diagrams showing the kinetics of M^+ activation for type Ia, type Ib and type II. Enzyme (E) freely complexes with the monovalent cation (M^+) and the substrate (S) in all the listed type of M^+ activating enzyme. However, in the case of type Ib, M^+ binding is only possible in the absence of the substrate.
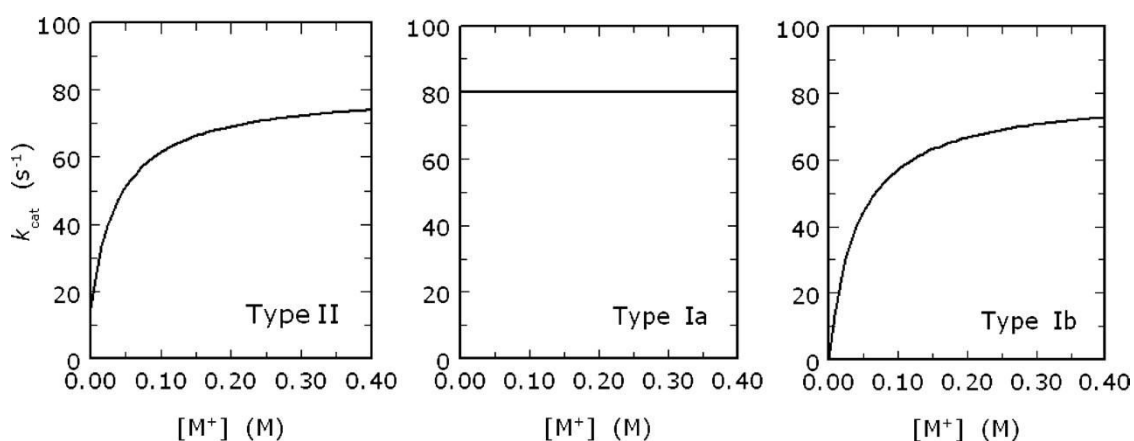
Figure 5.24 Typical profile of k_{cat} versus monovalent alkali metal ion concentration ($[M^+]$) of type Ia, Ib and II M^+ activating enzymes.

Reproduced from Page & Cera 2006 [276]

Although we were able to observe baseline ATPase activity from *E. coli* GyrB in the absence of K$^+$/Na$^+$ supplement (fig. 3.23, fig. 3.24), we proposed that it could be the results of the stimulation from low-level M$^+$ contamination in the enzyme stock. Overall, the evidence further enforces the suggestion that M$^+$ binding in site 1 is crucial to ATPase activity and supercoiling activity of DNA gyrase.

5.12.3 Structural role of site 1 M$^+$ ion in Gyrase – evidence from the conserved M+ ion binding site in GHKL ATPase
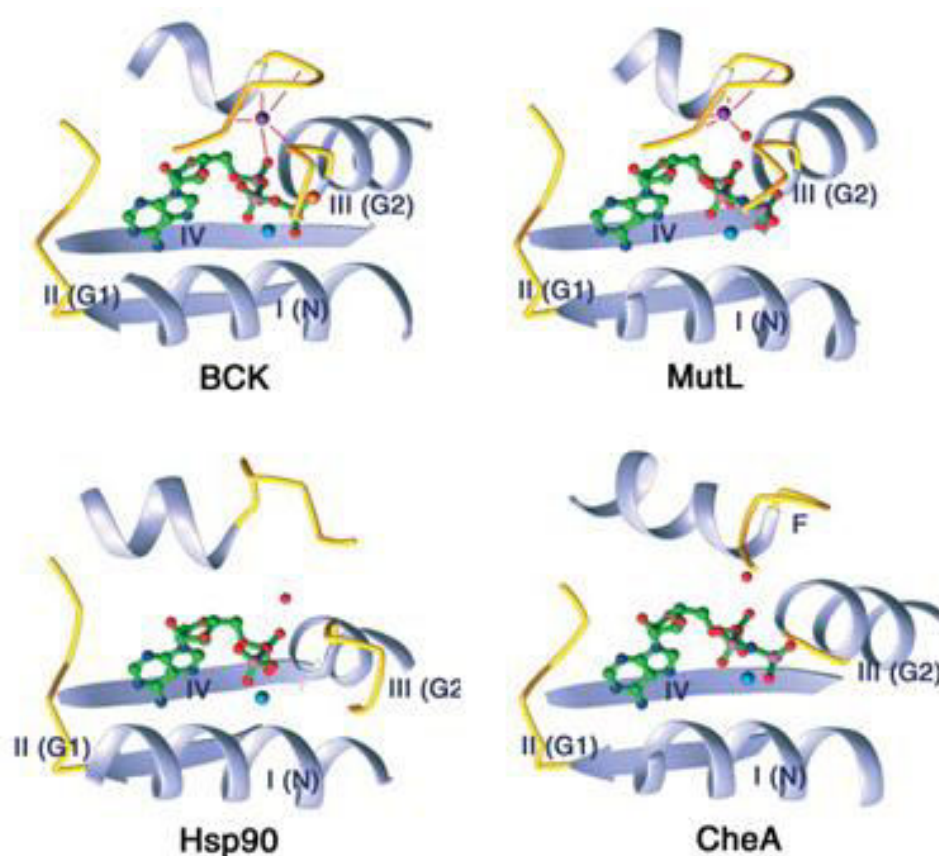
Figure 5.25 Position of monovalent ions (purple and red) in relation to the ADPNP substrate (green) in various GHKL ATPases: *position of Mg^{2+} is indicate as a cyan sphere [61]. Top left – branched-chain α-ketoacid dehydrogenase (BCK); top right – DNA mismatch repair protein MutL; bottom left – heat shock protein 90 (Hsp90); bottom right – CheA histidine kinase (CheA).*

191

The existence of site 1 M[+] was previously predicted [61] as other members of the GHKL ATPase family were found to possess an M[+] binding site in a similar region (fig 5.25). These M[+] sites in other related GHKL ATPase are found to be crucial to their ATP hydrolysis activity [61,286-287]. Moreover, the positioning of the M[+] binding site in site 1 coincides with the predicted position of the putative M[+] site suggested in Gubaev et al [281]. This putative M[+] site was suggested as *B. subtilis* gyrase requires K^{+} but not Na^{+} for its supercoiling activity. Subsequent single molecule experiments showed that the complete closure of the N-gate requires the presence of K^{+} ion. K^{+} binding to this putative site in *B. subtilis* gyrase was suggested to be crucial to establishment of GyrB-NTD dimer contacts[281].

5.12.4 GyrB N-terminal Strap – the link to site 1 M[+] function

On re-examining the Single-Molecule Fluorescence Resonance Energy Transfer (SM-FRET) data from Gubaev et al.[281], narrowing of the N-gate is found to be almost unaffected by the replacement of K^{+} by Na^{+} as the distance between E17C (*B. subtilis* gyrase) residues of the two GyrB monomer is almost identical in the presence of potassium or sodium ions. Yet there is a major difference in the distance between S7C residue residues of the two GyrB monomers, located in the N-terminal strap. Surprisingly, given that *E. coli* gyrase has been the subject of molecular study for the past 30 years, there is little biochemical understanding on the function of the N-terminal strap of GyrB (fig. 5.26).

Structural information on GyrB suggested that the N-terminal strap forms contacts with the ATP lid of the adjacent GyrB monomer, this includes a crucial contact in the form of an antiparallel β-strand, with three backbone H-bonds formed between K11' and G101, L13' and H99 (' indicates amino acids groups from adjacent monomer). This is interesting as A100 (its carbonyl group forms one of the six oxygen atoms that originates site 1 M[+] site), sits in between residues G101 and H99 (fig. 5.27). This close proximity of the M[+] binding site to the dimer-forming interface for the N-strap provides strong indication that the M[+] binding in site 1 results in the difference observed in the N-terminal strap in the presence of K^{+} and Na^{+} in *B. subtilis* gyrase [281].
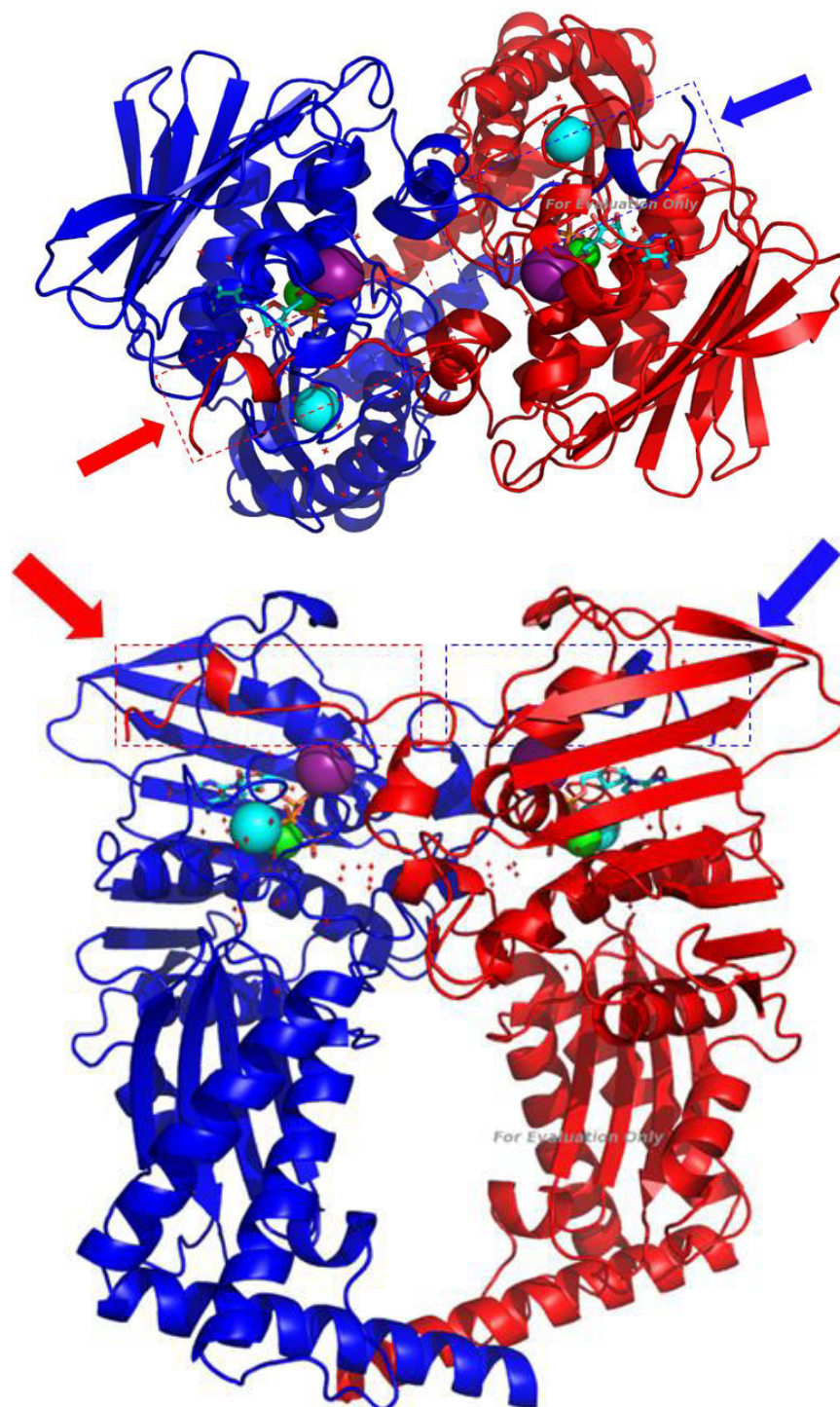
Figure 5.26 (Top) Top view of the EcGyrBNTD-ADPNP-Mg⁺-K⁺-Na⁺ dimer complex, *with opposing monomers in blue and red. Position of ADPNP (cyan stick), K⁺ (purple sphere), Mg⁺ (green sphere), Na⁺ (cyan sphere) in relation to the GyrB dimer are depicted. Positions of the N-terminal straps are indicated by the red arrows and dashed line boxes.* ***(Bottom) Side view of the EcGyrBNTD-ADPNP-Mg⁺-K⁺-Na⁺ dimer complex.*** *Positions of the N-terminal straps are indicated by red/blue arrows and dashed line boxes.*
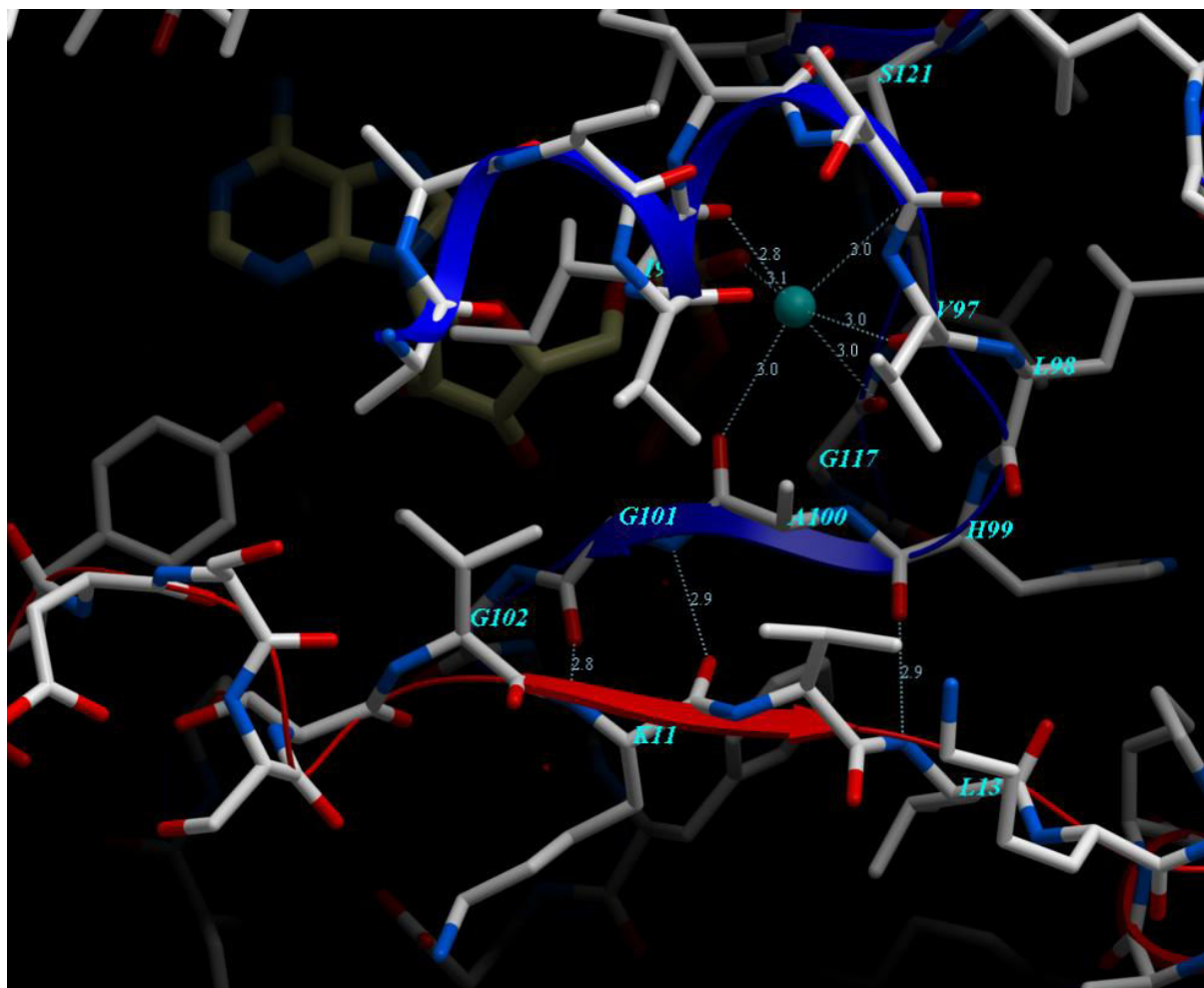
Figure 5.27 Antiparallel β-strand contacts between the N-terminal strap of GyrB (Red), and the ATP lid of the adjacent GyrB monomer (Blue) in an assembled GyrB dimer: Lys11-NH-OC-Gly101, Lys11-CO-HN-Gly101 and L13-NH-OC-His99. The figure also illustrates the proximity of the strap contacts to site 1 M+ bound.

Although it is clear that K+ and Na+ are likely to influence the inter-dimer contact in the N-terminal strap, we currently do not understand how the binding of M+ would contribute to this effect. As depicted in the structure (fig. 5.27), the region between Leu98 and Gly102 would lack secondary structure in the absence of the adjacent monomer. The binding of M+ ion on site 1 could act as an anchor and support correct positioning of the loop region between Leu98 to Gly 102 in relation to the rest of the protein, enforcing a conformation that allows crucial β sheet contacts to be made with the N-terminal strap of adjacent GyrB monomer.

5.12.5 M[+] specificity of site 1 - implication on K^{+} specificity in *S. aureus* and *B. subtilis* gyrase

When the crystals were grown in presence of equimolar of K^{+} and Na^{+}, K^{+} was found to occupy site 1. In addition, the electron density resembles the K^{+} density observed in the K^{+}-only crystal and is bigger than the Na^{+} in site 1 of the EcGyrBNTD-ADPNP crystals grown in NaCl only. This ultimately suggested that K^{+} is the preferred ion in site 1 and it is quite possibly the result of a large K_d difference between K^{+} and Na^{+} binding in site 1.

As Na^{+} is able to replace the function of K^{+} in *E. coli* gyrase by supporting ATP hydrolysis and supercoiling, it is apparent that the Na^{+}-binding is stable enough to maintain the function of the site 1 M[+] site in *E. coli* GyrB despite the ill fit. No major conformational difference was observed between the GyrBNTD-ADPNP complex with water, K^{+} and Na^{+} bound in site 1, despite the obvious activity difference between the presence and the absence of K^{+}/Na^{+}. This is not surprising, as previous structures, *i.e.,* MutL (GHKL ATPase) in complex with Na^{+}, K^{+} and Rb^{+} in the equivalent site, showed little structural difference despite the difference in the enzyme stimulation between the ions [61]. This overall indicates that K^{+}/Na^{+} does not influence GyrB conformation but perhaps functions as a structural stabiliser which ensures the integrity of the N-gate during supercoiling.

In the case of *S. aureus* and *B. subtilis* gyrase, they both exclusively require K^{+} for their supercoiling activity [224,231]. Sodium ion (Na^{+}) supplementation could not stimulate the supercoiling activity of *S. aureus* and *B. subtilis* gyrase in the absence of K^{+} [224]. If M[+] binding in site 1 is indeed the origin of this ion preference, deriving from the observation that Na^{+} is less tightly fitted in site 1 and that site 1 M[+] binding might be size dependent, we hypothesised that M[+] binding site 1 of *S. aureus* and *B. subtilis* gyrase might not support Na^{+} binding and therefore only K^{+} can support its activity.

5.12.6 Number of site 1 M+ ions required for gyrase supercoiling and ATPase activity

Mutagenesis studies [288] suggested that hydrolysis of ATP in only one of the GyrB monomers was sufficient to support a single round of DNA strand passage in gyrase. However, as the mutant enzyme studied was able to bind to ATP [288], it can be argued that the binding of a second ATP is potentially important to gyrase supercoiling and ATPase activity. The discoveries of the novel site 1 M+ binding site located in the ATP pocket therefore raised the question of whether M+ binding on one or both of monomer(s) of the GyrB dimer is required for gyrase activity.

On closer examination, we found that stimulation of DNA-independent ATPase of *S. aureus* gyrase by low concentration of Na+ and K+ (0-700 mM) (fig. 3.23) show characteristics of sigmoidal kinetics. In addition, both *S. aureus* gyrase supercoiling also showed weak evidence of sigmoidal stimulation by K+ (fig. 3.8). This sigmodial concentration-dependent stimulation by K+ and Na+ could be signs of a cooperative binding event from K+. However it would certainly require evidence from more detail kinetic studies in order to support the claim and prove the existence of the sigmodial relationship between K+ concentration and enzyme activity.

5.12.7 Possible function of site 2 M+ – the key to ion specificity in *S. aureus* and *B. subtilis* gyrase

It is interesting to note that Gross et al [289] discovered a mutant gyrase with a point mutation at Lys103 has intact ATPase, yet defective supercoiling activity. This phenotype is consistent with both *S. aureus* and *B. subtilis* gyrase in the presence of Na+ only. Interestingly, Lys103 is one of the two residues coordinating the site 2 M+ ion in the EcB43 structure. If the defective supercoiling activity observed in Na+-supplemented *S. aureus* and *B. subtilis* gyrase is indeed contributed by site 2 M+, it is possible that the K+ specificity is the result of site 2 preferences in K+ binding in *S. aureus* and *B. subtilis* gyrase.

Currently there is no clear evidence that could suggest the distinction in function between the two M$^+$ binding sites and which of these sites leads to the K$^+$ dependency and specificity of *S. aureus* and *B. subtilis*. The transitional mechanism of gyrase between closing of the N-gate and the opening of the DNA gate during the strand passage event is one of the least understood steps within the dynamic reaction cycle of gyrase supercoiling. Further understanding of the functions these two M$^+$ have on supercoiling could gives us important insight of this transitional mechanism.

5.12.8 Biological implication of M$^+$-binding sites and K$^+$-dependent supercoiling activity stimulation

The latest evidence of a structural mechanism of M$^+$ binding on supercoiling activity of DNA gyrase enables further suggestion that the intracellular concentration of K$^+$/Na$^+$ could affect the DNA supercoiling activity of gyrase *in vivo*. It is known that intracellular concentrations of K$^+$ and Na$^+$ varies in *S. aureus* to counteract osmotic stress asserted by the extracellular environment [290]. Such variation in K$^+$ and Na$^+$ is known to affect global DNA topology of the bacterial chromosome, as DNA stacking and supercoiling is sensitive to the ionic environment [291-292]. It would therefore be expected that a cellular mechanism has been evolved to swiftly adjust the supercoiling state of the bacterial chromosome in response to the osmotic changes.

There is a previous proposal of intracellular ATP/ADP concentration ratio being the primary control of intracellular gyrase activity and that DNA topology would be attuned by this mechanism to react to metabolic activity of the bacteria and availability of nutrient. In *E. coli*, a salt shock induced by 0.5 M NaCl increases both negative supercoiling as well as intracellular [ATP]/[ADP] ratio [293]. It is not known if the increase in negative supercoiling is the result of the changes in [ATP]/[ADP] ratio or *vice versa*. There is a secondary mechanism which regulates DNA topology by adjusting expression level of gyrase *via* the Leu500 promoter that is up-regulated when the chromosome becomes positively supercoiled [294]. Both of these mechanisms could be slow to respond to rapid environmental changes *e.g.,* osmotic changes, which could exert instant changes on DNA topology intracellularly[295].

Based upon the finding that gyrase supercoiling is sensitive to the concentration of the M^+, possibly *via* the novel M^+ binding sites discovered, we propose a third possible mechanism, in which DNA gyrase activity and DNA topology are directly regulated by changes in K^+/Na^+ intracellular concentration as a result of external osmotic changes. As DNA topology could temporarily collapse when halotolerant bacterial are subjected to sharp changes in osmotic stress [296-297], DNA interacting proteins *e.g.,* DNA and RNA polymerase could stall under the intense DNA torsion [297-298]. Under these circumstances, this newly proposed mechanism could provide a kick start to these processes by restoring DNA topology swiftly, by the increases in gyrase supercoiling activity as a result of M^+-dependent stimulation. In the case of *S. typhimurium and E. coli*, the subsequent changes in DNA topology could trigger up-regulation of the proU locus, which produce components of the glycine betaine transport system to counteract the osmotic stress [296]. It is envisaged that this mechanism would be particularly important in bacteria capable of adapting to a wide range of osmotic environment *e.g.,* the halotolerant *S. aureus.*

Chapter 6 General Discussion

6.1 Advances in understanding the *S. aureus* DNA gyrase mechanism

S. aureus DNA gyrase has been known for its unique dependency on relatively high concentrations of KGlu for its ability to negatively supercoil DNA [199,224]. This interesting phenomenon has led us to believe that there are unknown mechanisms and features of the enzyme that is responsible for the difference in KGlu dependency between *S. aureus* gyrase and other gyrases studied in the past. Here, we have utilised an array of mutagenesis and biochemical assays to probe and elucidate the origin of the KGlu dependency of *S. aureus* DNA supercoiling activity in detail.

Deriving from the results of the mutagenesis study on the domain swap *Sa*NTD-*Ec*CTD GyrA mutant, we successfully demonstrated that the CTD of *Sa* GyrA have partially contributed to the KGlu dependency. Primary sequence analysis and 3D protein model predictions did not reveal possible structural differences in the *Sa*GyrA-CTD. However, analysis of surface electrostatic charges of the protein model of *S. aureus* gyrase indicated a reduction in positive charges on the DNA contact surface when compared with *E. coli* gyrase. We proposed that this change on the DNA wrapping surface reduces the ability for *S. aureus* gyrase to wrap DNA, thereby leading to its characteristic salt dependency.

Although we noticed an extended C-terminal acidic tail located in GyrA, deletion mutant did not show any reduction in salt dependency and therefore proving that the C-terminal tail did not contribute to the KGlu dependency at all.

Since ATPase activity is vital to supercoiling ability of gyrase, we also investigated the effects of KGlu, NaGlu and KCl on ATPase of *Sa* gyrase. We found the ATPases of both *Sa* and *Ec* GyrB to be significantly stimulated by KGlu/NaGlu/KCl at lower ranges of concentration ($\sim$150-200 mM), thereby showing a K^+/Na^+ dependent stimulation of ATP hydrolysis in both *Sa* and *Ec* GyrB. This would also explain the less than optimal supercoiling activities in *E. coli* gyrase with no salt. Despite the KGlu-specific nature of supercoiling stimulation, replacement of Glu^- with Cl^- as a counter ion to K^+ did not

have significant affect on ATP hydrolysis of *Sa* and *Ec* gyrase. We proposed that the differential behaviour in the DNA wrapping by GyrA-CTD in *S. aureus* gyrase is responsible for the KGlu-dependent stimulation at high salt concentration (600-900 mM), whilst ATPase also contributes to the salt-dependent supercoiling at lower concentrations (150-450 mM).

Through structural data of GyrB obtained from X-ray protein crystallography. We have discovered two novel M^+ ion binding sites in the NTD of GyrB. One of the M^+ sites directly coordinates the non-hydrolysable ADPNP substrate and the ATP binding site, while the second M^+ site is found under the ATP lid, in the structurally crucial interface between the ATPase domain, the transducer domain and the adjacent GyrB monomer. As the second M^+ binding site in *E. coli* gyrase explicitly accommodates Na^+, we proposed that M^+ binding site 1 is responsible for the K^+/Na^+ ability to stimulate ATPase activity in a concentration dependent manner. Intriguingly, both K^+ and Na^+ are able to stimulate ATPase activity of *B. subtilis* gyrase, while K^+ but not Na^+ is specifically required for the closure of its N-gate [281]. We therefore anticipated that one/both of these M^+ site(s) has/have two mechanistically different roles; both of them are vital to the function of DNA gyrase:

1. Activation of ATPase activity;
2. Maintaining the integrity of the N-gate (possibly *via* the GyrB "N-terminal strap")

Whilst it has been more than 30 years since the discovery of DNA gyrase, it is exciting that we are still able to unearth novel mechanisms that underpin its dynamic reaction cycles. This is another addition to the mechanistic complexity of DNA gyrase, which employs numerous strategies to ensure good coordination between the intermediate steps within the reaction cycles.

6.2 Novel chemical scaffolds, novel inhibition mechanisms and potentially novel drug leads from naphthoquinone gyrase-inhibitors

Herein, we have established that natural naphthoquinones are both inhibitors of *S. aureus* bacterial growth *in vivo* and inhibitors of *S. aureus* gyrase and topo IV *in vitro.*

We found that one of the natural naphthoquinones tested, diospyrin, displayed a novel mode of inhibition of gyrase by binding to an unidentified region within the NTD of GyrB. Diospyrin, unlike other known GyrB inhibitors, inhibits the activity of gyrase without competing with the binding of ATP. Furthermore, it also inhibits the DNA cleavage activity of DNA gyrase. The overall characteristics of diospyrin-gyrase inhibition concluded that it is an inhibitor that inhibits gyrase in a novel mechanism.

We believe that naphthoquinone could become a useful chemical scaffold for the design of novel gyrase inhibitors owing to the simplicity of their chemistry and potential ease to synthesise. Overall, we believe that diospyrin exhibits the potential to be an ideal drug lead, and naphthoquinone as a potential gyrase-inhibiting antibacterial agent merits further investigation.

6.3 Future work

6.3.1 M$^+$ ion binding kinetics, its role in enzyme coordination and potential for drug design

Following the discovery of the two novel M$^+$ binding sites in EcGyrBNTD, it would be of interest to investigate the binding kinetics of these two M$^+$ binding sites individually using calorimetric methods (*e.g.,* ITC). It is also believed that the binding of one or both of the M$^+$ can have a crucial influence on the ATP binding kinetics of the GyrB subunit. The generation of mutant gyrase bearing modifications surrounding the two M$^+$ sites to alter its M$^+$ binding affinity, could be useful in dissecting the individual roles of the two M$^+$ ions on gyrase function. However, as most of the direct contact between GyrB and the two M$^+$ ions involves backbone carbonyls, it is envisaged that binding affinity of these M$^+$ ions would be difficult to alter by simply mutating the amino acids in contact with the ion. Nonetheless, it might be possible to

disrupt the network of connections by producing mutations around the M^+ binding sites to create subtle differences in the distances between the six coordinating-oxygen atoms and the M^+ ion.

In light of the current evidence of the novel M^+ binding sites and previous discovery on the effect of K^+ on the dimerisation of the N-terminal strap of *B. subtilis*[231], a crucial link between one or two of the M^+ binding sites and complete N-gate closure is envisaged. Experiments in a similar format to the single-molecule FRET (smFRET) studies conducted by Gubaev *et al.*[231] could potentially be used to examine the function of these M^+ binding sites using mutant gyrase with altered M^+ binding properties. It would also be intriguiging to study the effect of M^+ on the strength of N-gate assembly. This can be investigated using DNA-attached magnetic tweezers to study the amount of force required to break open the N-terminal gate in the presence and absence of K^+ or Na^+ ions.

6.3.2 The possible role of M^+ in gyrase activity regulation *in vivo*

The role of M^+ on DNA gyrase *in vivo* can be examined, by exploring the hypothesis of the gyrase-dependent mechanism that adjusts DNA topology of the cell in response to osmotic pressure and intracellular K^+/Na^+ concentration. This could involve replacing *wt* gyrase with a mutant gyrase that shows reduced or increased affinity to K^+/Na^+ *in vivo*. As the potency of the gyrase-targeting antibiotics is closely linked to the activity of gyrase, it would be important to understand the relationship between the osmolarity of the bacteria's external environment and the enzymatic activity of gyrase.

6.3.3 Identification of the diospyrin-binding pocket

As we are confident of the potential of naphthoquinones as gyrase-inhibiting antibiotics, it would be vital to identify the binding pocket of diospyrin in order to understand molecular details of the contacts between the enzyme and the drug. Our failed attempts to co-crystallise diospyrin with the GyrBNTD construct suggests that alternative constructs may be required for the production of diospyrin-GyrB co-crystals. Flexible regions within the GyrBNTD construct can be deleted in order to improve the ability for the construct to be crystallised. Alternatively, alanine

scanning of the surface residues in the NTD of GyrB could possibly reveal the binding location of diospyrin, should diospyrin-GyrBNTD protein crystals prove to be unattainable.

Diospyrin is the only known inhibitor that is able to inhibit DNA cleavage of gyrase. We believe that a more comprehensive understanding of the mechanism, involving diopsyrin inhibition, could further enhance our knowledge on the molecular events crucial to the initiation of the DNA cleavage process.

6.3.4 Development of naphthoquinones as novel antibacterial agents

With the lack of attention on developing new classes of Gyrase-inhibiting antibacterial, gyrase is a proven antibacterial target that has been under-exploited. A new class of Gyrase inhibitors could be the "low hanging fruit" that pharmaceutical companies have been searching for. The discovery of diospyrin as a novel gyrase inhibitor and its *in vivo* activity as an anti-*S. aureus* agent in this study showed a promising starting point of a novel anti-bacterial. In order to further develop naphthoquinones, aside from the further information needed for its mode of binding, it is crucial to explore new naphthoquinone entities from a medicinal chemistry view point. This study has showed limited yet crucial pharmocophore information, which provides guidance for the medicinal development for a more effective naphthoquinones. In the future, it would be crucial to confirm and extend the current pharmcophore model to develop nathphquinones with improved affinity.

During the development process of a new reagent, whilst it is important to improve its affinity towards its cellular target, the success of an antibacterial agent will also depend heavily on its ability to penetrate bacterial and human cells, as well as its toxicity profile. In order to achieve this, further studies have to be conducted to assess the properties of naphthoquinones through *in vitro* cellular assays. This will need to be carried out in conjunction with medicinal modifications to improve naphthoquinones cell permeability (logP) profile as well as improving toxicity by reducing the occurance of secondary targets interactions in human cells.

Recently, various two "headed" reagents with two separate pocket-binding moieties with excellent gyrase inhibition properties has been found [168]. This ignites the potential of designing new reagents with improved potency, capable of binding multiple pockets on the surfaces of DNA gyrase. Previously we speculated that binaphthoquinones, such as diospyrin and Neodiospyrin, may bind to multiple binding pockets simultaneously. It may be possible to further improve the potency of naphthoquinones by altering the "heads" or the "linker" region via medicinal chemistry.

6.3.5 Further understanding the gyrase supercoiling mechanism

The complexity of DNA gyrase reaction steps and the interplay between the gyrase and the DNA substrate has captured the curiosity of scholars in the past 3 decades. Due to the complex nature of gyrase, scientists are still yet to fully understand the mechanism of this DNA machinery. Although great advances have been made to understand the static structure of gyrase and its subdomains, the dynamic movements of these subdomains in relation to each other, during the reaction cycle, are poorly understood. Recent efforts from the Klostermeier group [299-301] and other single molecule studies [88,302-303], have shed light on the dynamics of some of these processes. All of these studies have been carried out in native DNA gyrase, therefore potential studies using gyrase mutants with altered properties using these single molecule techniques may provide further clues to its dynamic properties.

6.4 Concluding remarks

Antibacterial resistance is a long battle that would endure with the continuous use of antibiotics for bacterial infection treatments. It is clear that there is no single "magic bullet" for the combat the resilience of these bacteria, supported by the most successful biological process, evolution. Antibiotics are urgeably one of the most important types of drug and is the pilar of the western health care system, not only providing a safety net to the range of bacterial infections encountered but also to ensure the safety and recovery of all open wounded surgery operations. Currently, pharmaceutical companies are opting to invest on therapeutic areas with greater financial return, such as cancer, pain and inflammation and mental illnesses, rather

than bacterial infection [231]. Therefore improvement in the progress of antibiotics discovery can only be instigated with a radical change in the currently dysfunctional financial model of antibiotics funding, perhaps with governmental backing. Moreover the daunting technical prospect to sustain the continual fight against the worsening antibacterial resistance would certainly require a concerted effort of scientists, medics, drug developers and the government.

Whilst novel anti-bacterial therapy such as phage therapy, antibody-based therapy, quorum sensing and other preventive therapy such as vaccination offer glimpses of hope towards improving prospects of antibacterial treatment, much of these approaches are in their infancy and each of them presents their own unique challenges. It will be a long time until they are ready to replace the convenience, immediacy and efficacy of current antibacterial treatments. Although it would only be a matter of time these new technologies will become viable treatment options, antibacterial-resistance development will not cease and patients suffering daily from reoccurring bacterial infections will be desperate for the new treatments. Given the urgency of tackling the global problem of antibiotics resistance, we truly believe that old and reliable antibacterial targets, such as DNA gyrase would provide the perfect target for the next generation of "golden bullets".

Chapter 7 References

1   Fleming, A. Vol. 10   226 (Blackwell Publishing, 1929).

2   McKee, C. M. & Houck, C. L. Induced Resistance to Penicillin of Cultures of
        Staphylococci, Pneumococci and Streptococci. Exp Biol Med **53**, 33-34 (1943).

3   Eriksen, K. R. Studies on induced resistance to penicillin in a pneumococcus type I.
        Acta pathologica et microbiologica Scandinavica **22**, 398-405 (1945).

4   Payne, D. J., Gwynn, M. N., Holmes, D. J. & Pompliano, D. L. Drugs for bad bugs:
        confronting the challenges of antibacterial discovery. *Nat Rev Drug Discov* **6**, 29-40,
        doi:nrd2201 [pii]

10.1038/nrd2201 (2007).

5   Levy, S. B. & Marshall, B. Antibacterial resistance worldwide: causes, challenges and
        responses. *Nat Med* **10**, S122-129, doi:nm1145 [pii]

10.1038/nm1145 (2004).

6   America, I. D. S. o. *Bad Bugs, No Drugs*, <http://www.idsociety.org/pa/IDSA_

Paper4_final_web.pdf> (

7   Chan, M. *Antimicrobial resistance in the European Union and the world*,
        <http://www.who.int/dg/speeches/2012/amr_20120314/en/> (2012).

8   Lowy, F. D. Antimicrobial resistance: the example of *Staphylococcus aureus. The
        Journal of clinical investigation* **111**, 1265-1273 (2003).

9   Noskin, G. A. *et al.* The burden of *Staphylococcus aureus* infections on hospitals in the
        United States - An analysis of the 2000 and 2001 nationwide inpatient sample
        database. *Arch Intern Med* **165**, 1756-1761 (2005).

10   Kim, T., Oh, P. I. & Simor, A. E. The economic impact of methicillin-resistant
        Staphylococcus aureus in Canadian hospitals. *Infect Cont Hosp Ep* **22**, 99-104 (2001).

11   Schito, G. C. The importance of the development of antibiotic resistance in
        Staphylococcus aureus. Clin Microbiol Infec **12**, 3-8 (2006).

12   Stapleton, P. D., Gettert, J. & Taylor, P. W. Epicatechin gallate, a component of green
        tea, reduces halotolerance in *Staphylococcus aureus. International journal of food
        microbiology* **111**, 276-279 (2006).

13   Moss, B., Squire, J. R. & et al. Nose and skin carriage of *Staphylococcus aureus* in
        patients receiving penicillin. *Lancet* **1**, 320-325 (1948).

14   Casewell, M. W. The nose: an underestimated source of *Staphylococcus aureus* causing
        wound infection. *The Journal of hospital infection* **40 Suppl B**, S3-11 (1998).

15   Haley, C. E., Marling-Cason, M., Smith, J. W., Luby, J. P. & Mackowiak, P. A. Bactericidal activity of antiseptics against methicillin-resistant *Staphylococcus aureus*. *Journal of clinical microbiology* **21**, 991-992 (1985).

16   Agency, N. P. S. *NHS Cleanyourhands Campaign*, <http://www.npsa.nhs.uk/cleanyourhands/about-us/> (2011).

17   Office for National Statistics, U. *Deaths Involving MRSA: England and Wales, 2008 to 2011*, <http://www.ons.gov.uk/ons/rel/subnational-health2/deaths-involving-mrsa/2008-to-2011/stb---mrsa.html#tab-Key-findings> (2011).

18   Kallen, A. J. *et al.* Health care-associated invasive MRSA infections, 2005-2008. *Jama* **304**, 641-648.

19   David, M. Z., Medvedev, S., Hohmann, S. F., Ewigman, B. & Daum, R. S. Increasing burden of methicillin-resistant *Staphylococcus aureus* hospitalizations at US academic medical centers, 2003-2008. *Infect Control Hosp Epidemiol* **33**, 782-789 (2012).

20   Poirel, L., Lagrutta, E., Taylor, P., Pham, J. & Nordmann, P. Emergence of metallo-beta-lactamase NDM-1-producing multidrug-resistant *Escherichia coli* in Australia. *Antimicrobial agents and chemotherapy* **54**, 4914-4916 (2010).

21   Johnson, J. R., Johnston, B., Clabots, C., Kuskowski, M. A. & Castanheira, M. *Escherichia coli* sequence type ST131 as the major cause of serious multidrug-resistant E. coli infections in the United States. *Clin Infect Dis* **51**, 286-294 (2010).

22   Gandhi, N. R. *et al.* Multidrug-resistant and extensively drug-resistant tuberculosis: a threat to global control of tuberculosis. *Lancet* **375**, 1830-1843 (2010).

23   Lister, P. D., Wolter, D. J. & Hanson, N. D. Antibacterial-resistant Pseudomonas aeruginosa: clinical impact and complex regulation of chromosomally encoded resistance mechanisms. *Clinical microbiology reviews* **22**, 582-610 (2009).

24   Huang, H., Weintraub, A., Fang, H. & Nord, C. E. Antimicrobial resistance in Clostridium difficile. *International journal of antimicrobial agents* **34**, 516-522 (2009).

25   Smith, T. Antibiotics from soil bacteria. *Nature structural biology* **7**, 189-190 (2000).

26   Walsh, C. Where will new antibiotics come from? *Nature Revs. Microbiol.* **1**, 65-70 (2003).

27   Wheeler, R. *Supercoiled structure of circular DNA molecules with low writhe*, <http://commons.wikimedia.org/wiki/File:Circular_DNA_Supercoiling.png> (2007).

28   De Wyngaert, M. & Hinkle, D. C. Involvement of DNA gyrase in replication and transcription of bacteriophage T7 DNA. *Journal of virology* **29**, 529-535 (1979).

29   Cook, D. N., Ma, D., Pon, N. G. & Hearst, J. E. Dynamics of DNA supercoiling by transcription in Escherichia coli. *Proceedings of the National Academy of Sciences of the United States of America* **89**, 10603-10607 (1992).

30   Schoeffler, A. J. & Berger, J. M. DNA topoisomerases: harnessing and constraining energy to govern chromosome topology. *Quarterly reviews of biophysics* **41**, 41-101 (2008).

31   Grompone, G., Ehrlich, S. D. & Michel, B. Replication restart in gyrB *Escherichia coli* mutants. *Molecular microbiology* **48**, 845-854 (2003).

32   Schvartzman, J. B. & Stasiak, A. A topological view of the replicon. *EMBO reports* **5**, 256-261 (2004).

33   Zechiedrich, E. L., Khodursky, A. B. & Cozzarelli, N. R. Topoisomerase IV, not gyrase, decatenates products of site-specific recombination in Escherichia coli. *Genes & development* **11**, 2580-2592 (1997).

34   Corbett, K. D. & Berger, J. M. Structure, molecular mechanisms, and evolutionary relationships in DNA topoisomerases. *Annual review of biophysics and biomolecular structure* **33**, 95-118 (2004).

35   Gellert, M. DNA topoisomerases. *Annual review of biochemistry* **50**, 879-910 (1981).

36   Wang, J. C. DNA Topoisomerases - Why So Many. *J Biol Chem* **266**, 6659-6662 (1991).

37   Zechiedrich, E. L. & Cozzarelli, N. R. Roles of topoisomerase IV and DNA gyrase in DNA unlinking during replication in *Escherichia coli*. *Genes & development* **9**, 2859-2869 (1995).

38   Schoeffler, A. J. & Berger, J. M. DNA topoisomerases: harnessing and constraining energy to govern chromosome topology. *Q. Rev. Biophys.* **41**, 41-101, doi:S003358350800468X [pii]

10.1017/S003358350800468X (2008).

39   Nakasu, S. & Kikuchi, A. Reverse gyrase; ATP-dependent type I topoisomerase from Sulfolobus. *The EMBO journal* **4**, 2705-2710 (1985).

40   Stivers, J. T., Harris, T. K. & Mildvan, A. S. Vaccinia DNA topoisomerase I: evidence supporting a free rotation mechanism for DNA supercoil relaxation. *Biochemistry* **36**, 5212-5222 (1997).

41   Roca, J., Berger, J. M., Harrison, S. C. & Wang, J. C. DNA transport by a type II topoisomerase: direct evidence for a two-gate mechanism. *Proceedings of the National Academy of Sciences of the United States of America* **93**, 4057-4062 (1996).

42   Roca, J. & Wang, J. C. DNA transport by a type II DNA topoisomerase: evidence in favor of a two-gate mechanism. *Cell* **77**, 609-616 (1994).

43   Holdgate, G. A. *et al.* The entropic penalty of ordered water accounts for weaker binding of the antibiotic novobiocin to a resistant mutant of DNA gyrase: a thermodynamic and crystallographic study. *Biochemistry* **36**, 9663-9673 (1997).

44   Morais Cabral, J. H. *et al.* Crystal structure of the breakage-reunion domain of DNA gyrase. *Nature* **388**, 903-906 (1997).

45   Corbett, K. D., Shultzaberger, R. K. & Berger, J. M. The C-terminal domain of DNA gyrase A adopts a DNA-bending beta-pinwheel fold. *Proceedings of the National Academy of Sciences of the United States of America* **101**, 7293-7298 (2004).

46   Brino, L. *et al.* Dimerization of *Escherichia coli* DNA-gyrase B provides a structural mechanism for activating the ATPase catalytic center. *The Journal of Biological Chemistry* **275**, 9468-9475 (2000).

47   Bellon, S. *et al.* Crystal structures of *Escherichia coli* topoisomerase IV ParE subunit (24 and 43 kilodaltons): a single residue dictates differences in novobiocin potency against topoisomerase IV and DNA gyrase. *Antimicrobial agents and chemotherapy* **48**, 1856-1864 (2004).

48   Corbett, K. D., Schoeffler, A. J., Thomsen, N. D. & Berger, J. M. The structural basis for substrate specificity in DNA topoisomerase IV. *Journal of molecular biology* **351**, 545-561 (2005).

49   Classen, S., Olland, S. & Berger, J. M. Structure of the topoisomerase II ATPase region and its mechanism of inhibition by the chemotherapeutic agent ICRF-187. *Proceedings of the National Academy of Sciences of the United States of America* **100**, 10629-10634 (2003).

50   Fass, D., Bogden, C. E. & Berger, J. M. Quaternary changes in topoisomerase II may direct orthogonal movement of two DNA strands. *Nat Struct Biol* **6**, 322-326 (1999).

51   Dong, K. C. & Berger, J. M. Structural basis for gate-DNA recognition and bending by type IIA topoisomerases. *Nature* **450**, 1201-1205 (2007).

52   Bates, A. D. & Maxwell, A. Energy coupling in type II topoisomerases: why do they hydrolyze ATP? *Biochemistry* **46**, 7929-7941 (2007).

53   Cozzarelli, N. R. DNA gyrase and the supercoiling of DNA. *Science (New York, N.Y* **207**, 953-960 (1980).

54   Marians, K. J. DNA gyrase-catalyzed decatenation of multiply linked DNA dimers. *The Journal of Biological Chemistry* **262**, 10362-10368 (1987).

55   Reece, R. J. & Maxwell, A. DNA gyrase: structure and function. *Critical reviews in biochemistry and molecular biology* **26**, 335-375 (1991).

56   Liu, L. F. & Wang, J. C. DNA-DNA Gyrase Complex - Wrapping of DNA Duplex Outside Enzyme. *Cell* **15**, 979-984 (1978).

57   Ruthenburg, A. J., Graybosch, D. M., Huetsch, J. C. & Verdine, G. L. A superhelical spiral in the *Escherichia coli* DNA gyrase A C-terminal domain imparts unidirectional supercoiling bias. *The Journal of Biological Chemistry* **280**, 26177-26184 (2005).

58   Dutta, R. & Inouye, M. GHKL, an emergent ATPase/kinase superfamily. *Trends in biochemical sciences* **25**, 24-28 (2000).

59   Costenaro, L., Grossmann, J. G., Ebel, C. & Maxwell, A. Modular structure of the full-length DNA gyrase B subunit revealed by small-angle X-ray scattering. *Structure* **15**, 329-339 (2007).

60   Wigley, D. B., Davies, G. J., Dodson, E. J., Maxwell, A. & Dodson, G. Crystal structure of an N-terminal fragment of the DNA gyrase B protein. *Nature* **351**, 624-629 (1991).

61   Hu, X., Machius, M. & Yang, W. Monovalent cation dependence and preference of GHKL ATPases and kinases. *FEBS letters* **544**, 268-273 (2003).

62   Tingey, A. P. & Maxwell, A. Probing the role of the ATP-operated clamp in the strand-passage reaction of DNA gyrase. *Nucleic acids research* **24**, 4868-4873 (1996).

63   Aravind, L., Leipe, D. D. & Koonin, E. V. Toprim--a conserved catalytic domain in type IA and II topoisomerases, DnaG-type primases, OLD family nucleases and RecR proteins. *Nucleic acids research* **26**, 4205-4213 (1998).

64   Podobnik, M., McInerney, P., O'Donnell, M. & Kuriyan, J. A TOPRIM domain in the crystal structure of the catalytic core of *Escherichia coli* primase confirms a structural link to DNA topoisomerases. *Journal of molecular biology* **300**, 353-362 (2000).

65   Sissi, C. *et al.* DNA gyrase requires DNA for effective two-site coordination of divalent metal ions: Further insight into the mechanism of enzyme action. *Biochemistry* **47**, 8538-8545 (2008).

66   Noble, C. G. & Maxwell, A. The role of GyrB in the DNA cleavage-religation reaction of DNA gyrase: a proposed two metal-ion mechanism. *Journal of molecular biology* **318**, 361-371 (2002).

67   Sissi, C. & Palumbo, M. Effects of magnesium and related divalent metal ions in topoisomerase structure and function. *Nucleic acids research* **37**, 702-711 (2009).

68   Brino, L. *et al.* Dimerization of *Escherichia coli* DNA-gyrase B provides a structural mechanism for activating the ATPase catalytic center. *The Journal of Biological Chemistry* **275**, 9468-9475. (2000).

69   Laponogov, I. *et al.* Structural insight into the quinolone-DNA cleavage complex of type IIA topoisomerases. *Nat. Struct. Mol. Biol.* **16**, 667-669 (2009).

70   Schmidt, B. H., Burgin, A. B., Deweese, J. E., Osheroff, N. & Berger, J. M. A novel and
        unified two-metal mechanism for DNA cleavage by type II and IA topoisomerases.
        Nature **465**, 641-644, doi:nature08974 [pii]

10.1038/nature08974 (2010).

71   Smiley, R. D., Collins, T. R., Hammes, G. G. & Hsieh, T. S. Single-molecule measurements
        of the opening and closing of the DNA gate by eukaryotic topoisomerase II.
        Proceedings of the National Academy of Sciences of the United States of America **104**,
        4840-4845 (2007).

72   Morrison, A., Higgins, N. P. & Cozzarelli, N. R. Interaction between DNA Gyrase and Its
        Cleavage Site on DNA. *J Biol Chem* **255**, 2211-2219 (1980).

73   Kampranis, S. C. & Maxwell, A. Conversion of DNA gyrase into a conventional type II
        topoisomerase. *Proceedings of the National Academy of Sciences of the United States of
        America* **93**, 14416-14421 (1996).

74   Kramlinger, V. M. & Hiasa, H. The "GyrA-box" is required for the ability of DNA gyrase
        to wrap DNA and catalyze the supercoiling reaction. *The Journal of Biological
        Chemistry* **281**, 3738-3742 (2006).

75   Sugino, A., Higgins, N. P. & Cozzarelli, N. R. DNA gyrase subunit stoichiometry and the
        covalent attachment of subunit A to DNA during DNA cleavage. *Nucleic acids research*
        8, 3865-3874 (1980).

76   Horowitz, D. S. & Wang, J. C. Mapping the active site tyrosine of *Escherichia coli* DNA
        gyrase. *The Journal of Biological Chemistry* **262**, 5339-5344 (1987).

77   Costenaro, L., Grossmann, J. G., Ebel, C. & Maxwell, A. Small-angle X-ray scattering
        reveals the solution structure of the full-length DNA gyrase a subunit. *Structure* **13**,
        287-296 (2005).

78   Roca, J. & Wang, J. C. DNA transport by a type II DNA topoisomerase: evidence in favor
        of a two-gate mechanism. *Cell* **77**, 609-616 (1994).

79   Roca, J. & Wang, J. C. DNA Transport by a Type-Ii DNA Topoisomerase - Evidence in
        Favor of a 2-Gate Mechanism. *Cell* **77**, 609-616 (1994).

80   Roca, J., Berger, J. M., Harrison, S. C. & Wang, J. C. DNA transport by a type II
        topoisomerase: Direct evidence for a two-gate mechanism. *P Natl Acad Sci USA* **93**,
        4057-4062 (1996).

81   Fu, G. *et al.* Crystal structure of DNA gyrase B' domain sheds lights on the mechanism
        for T-segment navigation. *Nucleic Acids Res* **37**, 5908-5916, doi:gkp586 [pii]

10.1093/nar/gkp586 (2009).

82   Reece, R. J. & Maxwell, A. The C-terminal domain of the *Escherichia coli* DNA gyrase A subunit is a DNA-binding protein. *Nucleic acids research* **19**, 1399-1405 (1991).

83   Brino, L. *et al.* Dimerization of *Escherichia coli* DNA-gyrase B provides a structural mechanism for activating the ATPase catalytic center. *J Biol Chem* **275**, 9468-9475 (2000).

84   Maxwell, A. & Gellert, M. The DNA dependence of the ATPase activity of DNA gyrase. *J. Biol. Chem.* **259**, 14472-14480 (1984).

85   Gubaev, A. & Klostermeier, D. DNA-induced narrowing of the gyrase N-gate coordinates T-segment capture and strand passage. *Proceedings of the National Academy of Sciences of the United States of America* **108**, 14085-14090.

86   Corbett, K. D. & Berger, J. M. Structural dissection of ATP turnover in the prototypical GHL ATPase TopoVI. *Structure* **13**, 873-882 (2005).

87   Reece, R. J. & Maxwell, A. Tryptic fragments of the *Escherichia coli* DNA gyrase A protein. *The Journal of Biological Chemistry* **264**, 19648-19653 (1989).

88   Gore, J. *et al.* Mechanochemical analysis of DNA gyrase using rotor bead tracking. *Nature* **439**, 100-104 (2006).

89   Khodursky, A. B. *et al.* Analysis of topoisomerase function in bacterial replication fork movement: Use of DNA microarrays. *P Natl Acad Sci USA* **97**, 9419-9424 (2000).

90   Champion, K. & Higgins, N. P. Growth rate toxicity phenotypes and homeostatic supercoil control differentiate *Escherichia coli* from Salmonella enterica serovar Typhimurium. *J Bacteriol* **189**, 5839-5849 (2007).

91   Jeon, J. H. & Sung, W. How topological constraints facilitate growth and stability of bubbles in DNA. *Biophys J* **95**, 3600-3605 (2008).

92   Goldstein, E. & Drlica, K. Regulation of bacterial DNA supercoiling: plasmid linking numbers vary with growth temperature. *Proceedings of the National Academy of Sciences of the United States of America* **81**, 4046-4050 (1984).

93   Hsieh, L. S., Rouviere-Yaniv, J. & Drlica, K. Bacterial DNA supercoiling and [ATP]/[ADP] ratio: changes associated with salt shock. *Journal of bacteriology* **173**, 3914-3917 (1991).

94   Westerhoff, H. V., O'Dea, M. H., Maxwell, A. & Gellert, M. DNA supercoiling by DNA gyrase. A static head analysis. *Cell biophysics* **12**, 157-181 (1988).

95   Yamamoto, N. & Droffner, M. L. Mechanisms determining aerobic or anaerobic growth in the facultative anaerobe Salmonella typhimurium. *Proceedings of the National Academy of Sciences of the United States of America* **82**, 2077-2081 (1985).

96   Malik, M., Hussain, S. & Drlica, K. Effect of anaerobic growth on quinolone lethality with Escherichia coli. *Antimicrobial agents and chemotherapy* **51**, 28-34 (2007).

97   Hsieh, T. J., Farh, L., Huang, W. M. & Chan, N. L. Structure of the topoisomerase IV C-terminal domain: a broken beta-propeller implies a role as geometry facilitator in catalysis. *The Journal of Biological Chemistry* **279**, 55587-55593 (2004).

98   Kramlinger, V. M. & Hiasa, H. The "GyrA-box" is required for the ability of DNA gyrase to wrap DNA and catalyze the supercoiling reaction. *Journal of Biological Chemistry* **281**, 3738-3742 (2006).

99   Corbett, K. D., Schoeffler, A. J., Thomsen, N. D. & Berger, J. M. The structural basis for substrate specificity in DNA topoisomerase IV. *J. Mol. Biol.* **351**, 545-561 (2005).

100   Rybenkov, V. V., Ullsperger, C., Vologodskii, A. V. & Cozzarelli, N. R. Simplification of DNA topology below equilibrium values by type II topoisomerases. *Science (New York, N.Y* **277**, 690-693 (1997).

101   Kato, J. *et al.* New topoisomerase essential for chromosome segregation in E. coli. *Cell* **63**, 393-404 (1990).

102   Khodursky, A. B. *et al.* Analysis of topoisomerase function in bacterial replication fork movement: use of DNA microarrays. *Proceedings of the National Academy of Sciences of the United States of America* **97**, 9419-9424 (2000).

103   Cole, S. T. *et al.* Deciphering the biology of Mycobacterium tuberculosis from the complete genome sequence. *Nature* **393**, 537-544 (1998).

104   Manjunatha, U. H. *et al.* Functional characterisation of mycobacterial DNA gyrase: an efficient decatenase. *Nucleic acids research* **30**, 2144-2153 (2002).

105   Lesher, G. Y., Froelich, E. J., Gruett, M. D., Bailey, J. H. & Brundage, R. P. 1,8-Naphthyridine Derivatives. a New Class of Chemotherapeutic Agents. *Journal of medicinal and pharmaceutical chemistry* **91**, 1063-1065 (1962).

106   King, D. E., Malone, R. & Lilley, S. H. New classification and update on the quinolone antibiotics. *Am Fam Physician* **61**, 2741-2748 (2000).

107   Chen, C. R., Malik, M., Snyder, M. & Drlica, K. DNA gyrase and topoisomerase IV on the bacterial chromosome: Quinolone-induced DNA cleavage. *J Mol Biol* **258**, 627-637 (1996).

108   Hiasa, H., Yousef, D. O. & Marians, K. J. DNA strand cleavage is required for replication fork arrest by a frozen topoisomerase-quinolone-DNA ternary complex. *J Biol Chem* **271**, 26424-26429 (1996).

109   Hiasa, H. & Shea, M. E. DNA gyrase-mediated wrapping of the DNA strand is required for the replication fork arrest by the DNA gyrase-quinolone-DNA ternary complex. *J Biol Chem* **275**, 34780-34786 (2000).

110   Filutowicz, M. & Jonczyk, P. The gyrB gene product functions in both initiation and chain polymerization of *Escherichia coli* chromosome replication: suppression of the initiation deficiency in gyrB-ts mutants by a class of rpoB mutations. *Mol Gen Genet* **191**, 282-287 (1983).

111   Dwyer, D. J., Kohanski, M. A., Hayete, B. & Collins, J. J. Gyrase inhibitors induce an oxidative damage cellular death pathway in Escherichia coli. *Molecular systems biology* **3**, 91 (2007).

112   Pfeiffer, E. S. & Hiasa, H. Determination of the primary target of a quinolone drug and the effect of quinolone resistance-conferring mutations by measuring quinolone sensitivity based on its mode of action. *Antimicrobial agents and chemotherapy* **51**, 3410-3412 (2007).

113   Deguchi, T. *et al.* Alterations in the GyrA subunit of DNA gyrase and the ParC subunit of topoisomerase IV in quinolone-resistant clinical isolates of Klebsiella pneumoniae. *Antimicrobial agents and chemotherapy* **41**, 699-701 (1997).

114   Fujimura, S., Kato, S., Iinuma, K. & Watanabe, A. In vitro activity of fluoroquinolone and the gyrA gene mutation in Helicobacter pylori strains isolated from children. *Journal of medical microbiology* **53**, 1019-1022 (2004).

115   Yonezawa, M., Takahata, M., Matsubara, N., Watanabe, Y. & Narita, H. DNA gyrase gyrA mutations in quinolone-resistant clinical isolates of Pseudomonas aeruginosa. *Antimicrobial agents and chemotherapy* **39**, 1970-1972 (1995).

116   Takei, M., Fukuda, H., Kishii, R. & Hosaka, M. Target preference of 15 quinolones against *Staphylococcus aureus*, based on antibacterial activities and target inhibition. *Antimicrobial agents and chemotherapy* **45**, 3544-3547 (2001).

117   Pan, X. S. & Fisher, L. M. Targeting of DNA gyrase in Streptococcus pneumoniae by sparfloxacin: selective targeting of gyrase or topoisomerase IV by quinolones. *Antimicrobial agents and chemotherapy* **41**, 471-474 (1997).

118   Khodursky, A. B., Zechiedrich, E. L. & Cozzarelli, N. R. Topoisomerase-Iv Is a Target of Quinolones in Escherichia-Coli. *P Natl Acad Sci USA* **92**, 11801-11805 (1995).

119   Strahilevitz, J. & Hooper, D. C. Dual targeting of topoisomerase IV and gyrase to reduce mutant selection: direct testing of the paradigm by using WCK-1734, a new fluoroquinolone, and ciprofloxacin. *Antimicrobial agents and chemotherapy* **49**, 1949-1956 (2005).

120   Siegmund, K. *et al.* Molecular details of quinolone-DNA interactions: solution
       structure of an unusually stable DNA duplex with covalently linked nalidixic acid
       residues and non-covalent complexes derived from it. *Nucleic acids research* **33**,
       4838-4848 (2005).

121   Kawai, Y., Matsubayashi, K. & Hakusui, H. Interaction of quinolones with metal cations
       in aqueous solution. *Chem Pharm Bull* **44**, 1425-1430 (1996).

122   Turel, I. The interactions of metal ions with quinolone antibacterial agents. *Coordin
       Chem Rev* **232**, 27-47 (2002).

123   Gootz, T. D. & Brighty, K. E. Fluoroquinolone antibacterials: SAR, mechanism of action,
       resistance, and clinical aspects. *Med Res Rev* **16**, 433-486 (1996).

124   Mitsuyama, J. Structures of existing and new quinolones and relationship to
       bactericidal activity against Streptococcus pneumoniae. *J Antimicrob Chemoth* **44**,
       201-207 (1999).

125   Domagala, J. M. Structure-Activity and Structure-Side-Effect Relationships for the
       Quinolone Antibacterials. *J Antimicrob Chemoth* **33**, 685-706 (1994).

126   Gould, K. A., Pan, X. S., Kerns, R. J. & Fisher, L. M. Ciprofloxacin dimers target gyrase in
       Streptococcus pneumoniae. *Antimicrob Agents Ch* **48**, 2108-2115 (2004).

127   Gootz, T. D., McGuirk, P. R., Moynihan, M. S. & Haskell, S. L. Placement of alkyl
       substituents on the C-7 piperazine ring of fluoroquinolones: dramatic differential
       effects on mammalian topoisomerase II and DNA gyrase. *Antimicrobial agents and
       chemotherapy* **38**, 130-133 (1994).

128   Elsea, S. H., Mcguirk, P. R., Gootz, T. D., Moynihan, M. & Osheroff, N. Drug Features That
       Contribute to the Activity of Quinolones against Mammalian Topoisomerase-Ii and
       Cultured-Cells - Correlation between Enhancement of Enzyme-Mediated DNA
       Cleavage in-Vitro and Cytotoxic Potential. *Antimicrob Agents Ch* **37**, 2179-2186
       (1993).

129   Morrissey, I. *et al.* Mechanism of differential activities of ofloxacin enantiomers.
       Antimicrob Agents Ch **40**, 1775-1784 (1996).

130   Elsea, S. H., Westergaard, M., Burden, D. A., Lomenick, J. P. & Osheroff, N. Quinolones
       share a common interaction domain on topoisomerase II with other DNA cleavage-
       enhancing antineoplastic drugs. *Biochemistry-Us* **36**, 2919-2924 (1997).

131   Fabian, I. *et al.* Moxifloxacin enhances antiproliferative and apoptotic effects of
       etoposide but inhibits its proinflammatory effects in THP-1 and Jurkat cells. *Brit J
       Cancer* **95**, 1038-1046 (2006).

132   Hooper, D. C. Mechanisms of fluoroquinolone resistance. *Drug Resist Update* **2**, 38-55 (1999).

133   Neyfakh, A. A., Borsch, C. M. & Kaatz, G. W. Fluoroquinolone Resistance Protein Nora of Staphylococcus-Aureus Is a Multidrug Efflux Transporter. *Antimicrob Agents Ch* **37**, 128-129 (1993).

134   Kaatz, G. W. & Seo, S. M. Mechanisms of fluoroquinolone resistance in genetically related strains of *Staphylococcus aureus*. *Antimicrob Agents Ch* **41**, 2733-2737 (1997).

135   Robicsek, A., Jacoby, G. A. & Hooper, D. C. The worldwide emergence of plasmid-mediated quinolone resistance. *The Lancet infectious diseases* **6**, 629-640 (2006).

136   Hegde, S. S. *et al.* A fluoroquinolone resistance protein from Mycobacterium tuberculosis that mimics DNA. *Science (New York, N.Y* **308**, 1480-1483 (2005).

137   Merens, A. *et al.* The pentapeptide repeat proteins MfpAMt and QnrB4 exhibit opposite effects on DNA gyrase catalytic reactions and on the ternary gyrase-DNA-quinolone complex. *Journal of bacteriology* **191**, 1587-1594 (2009).

138   Cambau, E., Bordon, F., Collatz, E. & Gutmann, L. Novel gyrA point mutation in a strain of *Escherichia coli* resistant to fluoroquinolones but not to nalidixic acid. *Antimicrobial agents and chemotherapy* **37**, 1247-1252 (1993).

139   Yoshida, H., Bogaki, M., Nakamura, M. & Nakamura, S. Quinolone resistance-determining region in the DNA gyrase gyrA gene of Escherichia coli. *Antimicrobial agents and chemotherapy* **34**, 1271-1272 (1990).

140   Kanematsu, E. *et al.* Alterations in the GyrA subunit of DNA gyrase and the ParC subunit of DNA topoisomerase IV associated with quinolone resistance in Enterococcus faecalis. *Antimicrobial agents and chemotherapy* **42**, 433-435 (1998).

141   Willmott, C. J. R. & Maxwell, A. A Single Point Mutation in the DNA Gyrase-a Protein Greatly Reduces Binding of Fluoroquinolones to the Gyrase-DNA Complex. *Antimicrob Agents Ch* **37**, 126-127 (1993).

142   Wohlkonig, A. *et al.* Structural basis of quinolone inhibition of type IIA topoisomerases and target-mediated resistance. *Nat Struct Mol Biol* **17**, 1152-1153, doi:nsmb.1892 [pii]
10.1038/nsmb.1892 (2010).

143   Yoshida, H., Bogaki, M., Nakamura, M., Yamanaka, L. M. & Nakamura, S. Quinolone resistance-determining region in the DNA gyrase gyrB gene of Escherichia coli. *Antimicrobial agents and chemotherapy* **35**, 1647-1650 (1991).

144   Heddle, J. & Maxwell, A. Quinolone-binding pocket of DNA gyrase: Role of GyrB. *Antimicrob Agents Ch* **46**, 1805-1815 (2002).

145   Friedman, S. M., Lu, T. & Drlica, K. Mutation in the DNA gyrase A gene of *Escherichia coli* that expands the quinolone resistance-determining region. *Antimicrob Agents Ch* **45**, 2378-2380 (2001).

146   Shen, L. L. & Pernet, A. G. Mechanism of inhibition of DNA gyrase by analogues of nalidixic acid: the target of the drugs is DNA. *Proceedings of the National Academy of Sciences of the United States of America* **82**, 307-311 (1985).

147   Noble, C. G., Barnard, F. M. & Maxwell, A. Quinolone-DNA interaction: Sequence-dependent binding to single-stranded DNA reflects the interaction within the gyrase-DNA complex. *Antimicrob Agents Ch* **47**, 854-862 (2003).

148   Shen, L. L., Baranowski, J. & Pernet, A. G. Mechanism of inhibition of DNA gyrase by quinolone antibacterials: specificity and cooperativity of drug binding to DNA. *Biochemistry* **28**, 3879-3885 (1989).

149   Richter, S. N. *et al.* Hot-spot consensus of fluoroquinolone-mediated DNA cleavage by Gram-negative and Gram-positive type II DNA topoisomerases. *Nucleic acids research* **35**, 6075-6085 (2007).

150   Critchlow, S. E. & Maxwell, A. DNA cleavage is not required for the binding of quinolone drugs to the DNA Gyrase - DNA complex. *Biochemistry-Us* **35**, 7387-7393 (1996).

151   Shen, L. L. *et al.* Mechanism of inhibition of DNA gyrase by quinolone antibacterials: a cooperative drug--DNA binding model. *Biochemistry* **28**, 3886-3894 (1989).

152   Palu, G., Valisena, S., Ciarrocchi, G., Gatto, B. & Palumbo, M. Quinolone Binding to DNA Is Mediated by Magnesium-Ions. *P Natl Acad Sci USA* **89**, 9671-9675 (1992).

153   Turel, I., Leban, I., Zupancic, M., Bukovec, P. & Gruber, K. An adduct of magnesium sulfate with a member of the quinolone family (ciprofloxacin). *Acta Crystallogr C* **52**, 2443-2445 (1996).

154   Drevensek, P. *et al.* X-ray crystallographic, NMR and antimicrobial activity studies of magnesium complexes of fluoroquinolones - racemic ofloxacin and its S-form, levofloxacin. *J Inorg Biochem* **100**, 1755-1763 (2006).

155   Laponogov, I. *et al.* Breakage-reunion domain of Streptococcus pneumoniae topoisomerase IV: crystal structure of a gram-positive quinolone target. *PLoS ONE* **2**, e301 (2007).

156   David, N. A. & Burgner, P. R. Clinical effectiveness and safety of novobiocin. *Antibiotic medicine & clinical therapy* **2**, 219-229 (1956).

157   Bryan, L. E. *Bacterial resistance and susceptibility to chemotherapeutic agents.* (1982).

158   Steffensky, M., Muhlenweg, A., Wang, Z. X., Li, S. M. & Heide, L. Identification of the novobiocin biosynthetic gene cluster of Streptomyces spheroides NCIB 11891. *Antimicrobial agents and chemotherapy* **44**, 1214-1222 (2000).

159   Flatman, R. H., Eustaquio, A., Li, S. M., Heide, L. & Maxwell, A. Structure-activity relationships of aminocoumarin-type gyrase and topoisomerase IV inhibitors obtained by combinatorial biosynthesis. *Antimicrobial agents and chemotherapy* **50**, 1136-1142 (2006).

160   Kampranis, S. C., Howells, A. J. & Maxwell, A. The interaction of DNA gyrase with the bacterial toxin CcdB: evidence for the existence of two gyrase-CcdB complexes. *Journal of molecular biology* **293**, 733-744 (1999).

161   Yorgey, P. *et al.* Posttranslational modifications in microcin B17 define an additional class of DNA gyrase inhibitor. *Proceedings of the National Academy of Sciences of the United States of America* **91**, 4519-4523 (1994).

162   Hegde, S. S. *et al.* A fluoroquinolone resistance protein from Mycobacterium tuberculosis that mimics DNA. *Science (New York, N.Y* **308**, 1480-1483 (2005).

163   Manjunatha, U. H., Maxwell, A. & Nagaraja, V. A monoclonal antibody that inhibits mycobacterial DNA gyrase by a novel mechanism. *Nucleic acids research* **33**, 3085-3094 (2005).

164   Dao-Thi, M. H. *et al.* Molecular basis of gyrase poisoning by the addiction toxin CcdB. *Journal of molecular biology* **348**, 1091-1102 (2005).

165   Vizan, J. L., Hernandez-Chico, C., del Castillo, I. & Moreno, F. The peptide antibiotic microcin B17 induces double-strand cleavage of DNA mediated by E. coli DNA gyrase. *The EMBO journal* **10**, 467-476 (1991).

166   Holzenkampfer, M. & Zeeck, A. Biosynthesis of simocyclinone D8 in an 18O2-rich atmosphere. *The Journal of antibiotics* **55**, 341-342 (2002).

167   Flatman, R. H., Howells, A. J., Heide, L., Fiedler, H. P. & Maxwell, A. Simocyclinone D8, an inhibitor of DNA gyrase with a novel mode of action. *Antimicrobial agents and chemotherapy* **49**, 1093-1100 (2005).

168   Edwards, M. J. *et al.* A crystal structure of the bifunctional antibiotic, simocyclinone D8, bound to DNA gyrase. *Science* **326**, 1415-1418 (2009).

169   Nakada, N. *et al.* Biological characterization of cyclothialidine, a new DNA gyrase inhibitor. *Antimicrobial agents and chemotherapy* **37**, 2656-2661 (1993).

170   Rudolph, J. *et al.* seco-Cyclothialidines: new concise synthesis, inhibitory activity toward bacterial and human DNA topoisomerases, and antibacterial properties. *Journal of medicinal chemistry* **44**, 619-626 (2001).

171   Nishino, C. *et al.* Antibacterial Activity of Flavonoids against Staphylococcus-Epidermidis, a Skin Bacterium. *Agr Biol Chem Tokyo* **51**, 139-143 (1987).

172   Xu, H. X. & Lee, S. F. Activity of plant flavonoids against antibiotic-resistant bacteria. *Phytother Res* **15**, 39-43 (2001).

173   Suzgec, S., Mericli, A. H., Houghton, P. J. & Cubukcu, B. Flavonoids of Helichrysum compactum and their antioxidant and antibacterial activity. *Fitoterapia* **76**, 269-272 (2005).

174   Alcaraz, L. E., Blanco, S. E., Puig, O. N., Tomas, F. & Ferretti, F. H. Antibacterial activity of flavonoids against methicillin-resistant *Staphylococcus aureus* strains. *J Theor Biol* **205**, 231-240 (2000).

175   Tsuchiya, H. *et al.* Comparative study on the antibacterial activity of phytochemical flavanones against methicillin-resistant *Staphylococcus aureus. Journal of ethnopharmacology* **50**, 27-34 (1996).

176   Sohn, H. Y., Son, K. H., Kwon, C. S., Kwon, G. S. & Kang, S. S. Antimicrobial and cytotoxic activity of 18 prenylated flavonoids isolated from medicinal plants: Morus alba L., Morus mongolica Schneider, Broussnetia papyrifera (L.) Vent, Sophora flavescens Ait and Echinosophora koreensis Nakai. *Phytomedicine* **11**, 666-672 (2004).

177   Otsuka, N. *et al.* Anti-methicillin resistant *Staphylococcus aureus* (MRSA) compounds isolated from Laurus nobilis. *Biol Pharm Bull* **31**, 1794-1797 (2008).

178   Arima, H., Ashida, H. & Danno, G. Rutin-enhanced antibacterial activities of flavonoids against Bacillus cereus and Salmonella enteritidis. *Biosci Biotech Bioch* **66**, 1009-1014 (2002).

179   Cushnie, T. P. T., Hamilton, V. E. S., Chapman, D. G., Taylor, P. W. & Lamb, A. J. Aggregation of *Staphylococcus aureus* following treatment with the antibacterial flavonol galangin. *J Appl Microbiol* **103**, 1562-1567 (2007).

180   Cushme, T. P. T. & Lamb, A. Assessment of the antibacterial activity of galangin against 4-quinolone resistant strains of *Staphylococcus aureus. Phytomedicine* **13**, 187-191 (2006).

181   Bernard, F. X. *et al.* Glycosylated flavones as selective inhibitors of topoisomerase IV. *Antimicrob Agents Ch* **41**, 992-998 (1997).

182   Plaper, A. *et al.* Characterization of quercetin binding site on DNA gyrase. *Biochemical and biophysical research communications* **306**, 530-536 (2003).

183   Gradisar, H., Pristovsek, P., Plaper, A. & Jerala, R. Green tea catechins inhibit bacterial DNA gyrase by interaction with its ATP binding site. *Journal of medicinal chemistry* **50**, 264-271 (2007).

184   Fujii, N., Yamashita, Y., Arima, Y., Nagashima, M. & Nakano, H. Induction of
        Topoisomerase-Ii-Mediated DNA Cleavage by the Plant Naphthoquinones Plumbagin
        and Shikonin. *Antimicrob Agents Ch* **36**, 2589-2594 (1992).

185   Ferriola, P. C., Cody, V. & Middleton, E. Protein-Kinase C Inhibition by Plant Flavonoids
        - Kinetic Mechanisms and Structure-Activity-Relationships. *Biochem Pharmacol* **38**,
        1617-1624 (1989).

186   deAzevedo, W. F. *et al.* Structural basis for specificity and potency of a flavonoid
        inhibitor of human CDK2, a cell cycle kinase. *P Natl Acad Sci USA* **93**, 2735-2740
        (1996).

187   Kaatz, G. W., Seo, S. M. & Ruble, C. A. Efflux-mediated fluoroquinolone resistance in
        Staphylococcus aureus. *Antimicrobial agents and chemotherapy* **37**, 1086-1094 (1993).

188   Lyon, B. R. & Skurray, R. Antimicrobial resistance of *Staphylococcus aureus*: genetic
        basis. *Microbiological reviews* **51**, 88-134 (1987).

189   Kalmeijer, M. D., van Nieuwland-Bollen, E., Bogaers-Hofman, D., de Baere, G. A. J. &
        Kluytmans, J. A. J. W. Nasal carriage of *Staphylococcus aureus* is a major risk factor for
        surgical-site infections in orthopedic surgery. *Infect Cont Hosp Ep* **21**, 319-323 (2000).

190   Noble, W. C. *Staphylococcus aureus* on Hair. *J Clin Pathol* **19**, 570-& (1966).

191   Sesso, R. *et al.* Staphylococcus-Aureus Skin Carriage and Development of Peritonitis in
        Patients on Continuous Ambulatory Peritoneal-Dialysis. *Clin Nephrol* **31**, 264-268
        (1989).

192   Scott, W. J. Water Relations of Staphylococcus-Aureus at 30-Degrees-C. *Aust J Biol Sci*
        6, 549-564 (1953).

193   Vilhelmsson, O., Hafsteinsson, H. & Kristjansson, J. K. Extremely halotolerant bacteria
        characteristic of fully cured and dried cod. *International journal of food microbiology*
        36, 163-170 (1997).

194   Salmond, G. P. C. & Whittenbury, R. Biology of Microorganisms, 4th Edition - Brock,Td,
        Smith,Dw, Madigan,Mt. *Nature* **314**, 49-49 (1985).

195   M. T. Madigan, J. M. M., J. Parker. *Brock Biology of Microorganisms*. (2003).

196   Graham, J. E. & Wilkinson, B. J. *Staphylococcus aureus* osmoregulation: roles for
        choline, glycine betaine, proline, and taurine. *Journal of bacteriology* **174**, 2711-2716
        (1992).

197   Bruins, M. J., Juffer, P., Wolfhagen, M. J. & Ruijs, G. J. Salt tolerance of methicillin-
        resistant and methicillin-susceptible *Staphylococcus aureus*. *Journal of clinical
        microbiology* **45**, 682-683 (2007).

198   Todar, K. in *Todar's Online Textbook of Bacteriology*
       (http://textbookofbacteriology.net/, 2008).

199   Hiasa, H., Shea, M. E., Richardson, C. M. & Gwynn, M. N. *Staphylococcus aureus* gyrase-
       quinolone-DNA ternary complexes fail to arrest replication fork progression in vitro.
       Effects of salt on the DNA binding mode and the catalytic activity of S. aureus gyrase.
       The Journal of Biological Chemistry **278**, 8861-8868 (2003).

200   Blanche, F. *et al.* Differential behaviors of *Staphylococcus aureus* and *Escherichia coli*
       type II DNA topoisomerases. *Antimicrobial agents and chemotherapy* **40**, 2714-2720
       (1996).

201   Pan, X. S. & Fisher, L. M. Streptococcus pneumoniae DNA gyrase and topoisomerase IV:
       overexpression, purification, and differential inhibition by fluoroquinolones.
       Antimicrobial agents and chemotherapy **43**, 1129-1136 (1999).

202   Anderson, V. E., Zaniewski, R. P., Kaczmarek, F. S., Gootz, T. D. & Osheroff, N.
       Quinolones inhibit DNA religation mediated by *Staphylococcus aureus* topoisomerase
       IV. Changes in drug mechanism across evolutionary boundaries. *The Journal of*
       Biological Chemistry **274**, 35927-35932 (1999).

203   Fournier, B., Zhao, X. L., Lu, T., Drlica, K. & Hooper, D. C. Selective targeting of
       topoisomerase IV and DNA gyrase in *Staphylococcus aureus*: Different patterns of
       quinolone-induced inhibition of DNA synthesis. *Antimicrob Agents Ch* **44**, 2160-2165
       (2000).

204   Hiasa, H. & Shea, M. E. DNA gyrase-mediated wrapping of the DNA strand is required
       for the replication fork arrest by the DNA gyrase-quinolone-DNA ternary complex.
       The Journal of Biological Chemistry **275**, 34780-34786 (2000).

205   Fournier, B. & Klier, A. Protein A gene expression is regulated by DNA supercoiling
       which is modified by the ArlS-ArlR two-component system of *Staphylococcus aureus*.
       Microbiol-Sgm **150**, 3807-3819 (2004).

206   Bjorklind, A. & Arvidson, S. Influence of Amino-Acids on Synthesis of an Extracellular
       Proteinase from Staphylococcus-Aureus. *J Gen Microbiol* **107**, 367-375 (1978).

207   Miller, K. J., Zelt, S. C. & Bae, J. H. Glycine Betaine and Proline Are the Principal
       Compatible Solutes of Staphylococcus-Aureus. *Curr Microbiol* **23**, 131-137 (1991).

208   Graham, J. E. & Wilkinson, B. J. Staphylococcus-Aureus Osmoregulation - Roles for
       Choline, Glycine Betaine, Proline, and Taurine. *J Bacteriol* **174**, 2711-2716 (1992).

209   Koujima, I., Hayashi, H., Tomochika, K., Okabe, A. & Kanemasa, Y. Adaptational change
       in proline and water content of *Staphylococcus aureus* after alteration of

environmental salt concentration. *Applied and environmental microbiology* **35**, 467-470 (1978).

210   Pourkomailian, B. & Booth, I. R. Glycine betaine transport by *Staphylococcus aureus*: evidence for two transport systems and for their possible roles in osmoregulation. *Journal of general microbiology* **138**, 2515-2518 (1992).

211   Bae, J. H., Anderson, S. H. & Miller, K. J. Identification of a high-affinity glycine betaine transport system in *Staphylococcus aureus*. *Applied and environmental microbiology* **59**, 2734-2736 (1993).

212   Pourkomailian, B. & Booth, I. R. Glycine betaine transport by *Staphylococcus aureus*: evidence for feedback regulation of the activity of the two transport systems. *Microbiology (Reading, England)* **140 (Pt 11)**, 3131-3138 (1994).

213   Bae, J. H. & Miller, K. J. Identification of two proline transport systems in *Staphylococcus aureus* and their possible roles in osmoregulation. *Applied and environmental microbiology* **58**, 471-475 (1992).

214   Townsend, D. E. & Wilkinson, B. J. Proline transport in *Staphylococcus aureus*: a high-affinity system and a low-affinity system involved in osmoregulation. *J Bacteriol* **174**, 2702-2710 (1992).

215   Lillford, P. J. & Holt, C. B. In vitro uses of biological cryoprotectants. *Philosophical transactions of the Royal Society of London* **357**, 945-951 (2002).

216   Verdrengh, M., Collins, L. V., Bergin, P. & Tarkowski, A. Phytoestrogen genistein as an anti-staphylococcal agent. *Microbes and infection / Institut Pasteur* **6**, 86-92 (2004).

217   Bradford, M. M. A rapid and sensitive method for the quantitation of microgram quantities of protein utilizing the principle of protein-dye binding. *Anal. Biochem.* **72**, 248-254 (1976).

218   Jackson, A. P., Maxwell, A. & Wigley, D. B. Preliminary crystallographic analysis of the ATP-hydrolysing domain of the *Escherichia coli* DNA gyrase B protein. *J. Mol. Biol.* **217**, 15-17 (1991).

219   Leslie, A. G. The integration of macromolecular diffraction data. *Acta Cryst.* **D62**, 48-57 (2006).

220   Evans, P. Scaling and assessment of data quality. *Acta Cryst.* **D62**, 72-82 (2006).

221   McCoy, A. J. *et al.* Phaser crystallographic software. *J. Appl. Crystallogr.* **40**, 658-674, doi:10.1107/S0021889807021206 (2007).

222   Emsley, P. & Cowtan, K. Coot: model-building tools for molecular graphics. *Acta crystallographica* **60**, 2126-2132 (2004).

223   Adams, P. D. *et al.* PHENIX: a comprehensive Python-based system for macromolecular structure solution. *Acta crystallographica* **66**, 213-221.

224   Blanche, F. *et al.* Differential behaviors of *Staphylococcus aureus* and *Escherichia coli* type II DNA topoisomerases. *Antimicrob. Agents Chemotherap.* **40**, 2714-2720 (1996).

225   Komaratat, P. & Kates, M. The lipid composition of a halotolerant species of Staphylococcus epidermidis. *Biochimica et biophysica acta* **398**, 464-484 (1975).

226   Tretter, E. M. & Berger, J. M. Mechanisms for defining supercoiling set point of DNA gyrase orthologs: I. A nonconserved acidic C-terminal tail modulates *Escherichia coli* gyrase activity. *The Journal of Biological Chemistry* **287**, 18636-18644.

227   *Argonne National Laboratory*, <http://www.bio.anl.gov/molecular_and_systems_biology/Sensor/sensor2.html> (

228   Deredge, D. J., Baker, J. T., Datta, K. & Licata, V. J. The glutamate effect on DNA binding by pol I DNA polymerases: osmotic stress and the effective reversal of salt linkage. *Journal of molecular biology* **401**, 223-238.

229   Hiasa, H. & Shea, M. E. DNA gyrase-mediated wrapping of the DNA strand is required for the replication fork arrest by the DNA gyrase-quinolone-DNA ternary complex. *J. Biol. Chem.* **275**, 34780-34786 (2000).

230   Kampranis, S. C. & Maxwell, A. Conversion of DNA gyrase into a conventional type II topoisomerase. *Proc. Natl. Acad. Sci. USA* **93**, 14416-14421 (1996).

231   Gubaev, A. & Klostermeier, D. Potassium Ions Are Required for Nucleotide-induced Closure of Gyrase N-gate. *The Journal of Biological Chemistry* **287**, 10916-10921 (2012).

232   Fiedler, H. P., Kulik, A., Schuz, T. C., Volkmann, C. & Zeeck, A. Biosynthetic capacities of actinomycetes. 2. Juglomycin Z, a new naphthoquinone antibiotic from Streptomyces tendae. *J Antibiot (Tokyo)* **47**, 1116-1122 (1994).

233   Johnson, L. E. & Dietz, A. Kalafungin, a new antibiotic produced by Streptomyces tanashiensis strain Kala. *Appl Microbiol* **16**, 1815-1821 (1968).

234   Medentsev, A. G. & Akimenko, V. K. Naphthoquinone metabolites of the fungi. *Phytochemistry* **47**, 935-959 (1998).

235   Ambrogi, V. *et al.* Studies on the antibacterial and antifungal properties of 1, 4-naphthoquinones. *British journal of pharmacology* **40**, 871-880 (1970).

236   Tandon, V. K., Maurya, H. K., Mishra, N. N. & Shukla, P. K. Design, synthesis and biological evaluation of novel nitrogen and sulfur containing hetero-1,4-naphthoquinones as potent antifungal and antibacterial agents. *European journal of medicinal chemistry* **44**, 3130-3137 (2009).

237   Tandon, V. K., Yadav, D. B., Singh, R. V., Chaturvedi, A. K. & Shukla, P. K. Synthesis and biological evaluation of novel (L)-alpha-amino acid methyl ester, heteroalkyl, and aryl substituted 1,4-naphthoquinone derivatives as antifungal and antibacterial agents. *Bioorganic & medicinal chemistry letters* **15**, 5324-5328 (2005).

238   Tandon, V. K., Singh, R. V. & Yadav, D. B. Synthesis and evaluation of novel 1,4-naphthoquinone derivatives as antiviral, antifungal and anticancer agents. *Bioorganic & medicinal chemistry letters* **14**, 2901-2904 (2004).

239   Ehrhardt, K. *et al.* The antimalarial activities of methylene blue and the 1,4-naphthoquinone 3-[4-(trifluoromethyl)benzyl]-menadione are not due to inhibition of the mitochondrial electron transport chain. *Antimicrobial agents and chemotherapy* **57**, 2114-2120 (2013).

240   Kongkathip, N. *et al.* Potent antitumor activity of synthetic 1,2-Naphthoquinones and 1,4-Naphthoquinones. *Bioorganic & medicinal chemistry* **11**, 3179-3191 (2003).

241   Michiko , M., Masanori, K., Kunitoshi, Y. & Shinsaku, N. Naphthoquinone Derivatives from the Ebenaceae. IV. Naphthoquinone Derivatives from Diospyros kaki THUNB. and D. kaki THUNB. var. sylvestris MAKINO. *Chemical & pharmaceutical bulletin* **20**, 2029-2035 (1972).

242   Lall, N. & Meyer, J. J. Antibacterial activity of water and acetone extracts of the roots of Euclea natalensis. *J Ethnopharmacol* **72**, 313-316 (2000).

243   Lall, N., Das Sarma, M., Hazra, B. & Meyer, J. J. Antimycobacterial activity of diospyrin derivatives and a structural analogue of diospyrin against Mycobacterium tuberculosis in vitro. *J Antimicrob Chemother* **51**, 435-438 (2003).

244   Weigenand, O., Hussein, A. A., Lall, N. & Meyer, J. J. Antibacterial activity of naphthoquinones and triterpenoids from Euclea natalensis root bark. *Journal of natural products* **67**, 1936-1938 (2004).

245   *Euclea natalensis, Guarri - TopTropicals*, <http://www.worldbotanical.com/Euclea-natalensis-pl.jpg> (

246   Sagar, S., Kaur, M., Minneman, K. P. & Bajic, V. B. Anti-cancer activities of diospyrin, its derivatives and analogues. *European journal of medicinal chemistry* **45**, 3519-3530.

247   Kumar, B. *et al.* Diospyrin derivative, an anticancer quinonoid, regulates apoptosis at endoplasmic reticulum as well as mitochondria by modulating cytosolic calcium in human breast carcinoma cells. *Biochemical and biophysical research communications* **417**, 903-909.

248   Hazra, B., Sur, P., Roy, D. K., Sur, B. & Banerjee, A. Biological activity of diospyrin towards Ehrlich ascites carcinoma in Swiss A mice. *Planta medica* **50**, 295-297 (1984).

249   Rodriguez, S., Wolfender, J. L., Hakizamungu, E. & Hostettmann, K. An antifungal naphthoquinone, xanthones and secoiridoids from Swertia calycina. *Planta medica* **61**, 362-364 (1995).

250   Adeniyi, B. A., Fong, H. H., Pezzuto, J. M., Luyengi, L. & Odelola, H. A. Antibacterial activity of diospyrin, isodiospyrin and bisisodiospyrin from the root of Diospyros piscatoria (Gurke) (Ebenaceae). *Phytother Res* **14**, 112-117 (2000).

251   Ray, S., Hazra, B., Mittra, B., Das, A. & Majumder, H. K. Diospyrin, a bisnaphthoquinone: a novel inhibitor of type I DNA topoisomerase of Leishmania donovani. *Mol Pharmacol* **54**, 994-999 (1998).

252   Mahapatra, A. *et al.* Activity of 7-methyljuglone derivatives against Mycobacterium tuberculosis and as subversive substrates for mycothiol disulfide reductase. *Bioorganic & medicinal chemistry* **15**, 7638-7646, doi:S0968-0896(07)00773-0 [pii] 10.1016/j.bmc.2007.08.064 (2007).

253   Karkare, S. *Development of Mycobacterium tuberculosis DNA gyrase as a target for antibacterial chemotherapy* PhD thesis, University of East Anglia, (2010).

254   Hooper, D. C., Wolfson, J. S., McHugh, G. L., Winters, M. B. & Swartz, M. N. Effects of novobiocin, coumermycin A1, clocobiocin, and their analogs on *Escherichia coli* DNA gyrase and bacterial growth. *Antimicrob. Agents Chemother.* **22**, 662-671 (1982).

255   Sugino, A., Higgins, N. P., Brown, P. O., Peebles, C. L. & Cozzarelli, N. R. Energy coupling in DNA gyrase and the mechanism of action of novobiocin. *Proc. Natl. Acad. Sci. USA* **75**, 4838-4842 (1978).

256   Lamour, V., Hoermann, L., Jeltsch, J. M., Oudet, P. & Moras, D. An open conformation of the Thermus thermophilus gyrase B ATP-binding domain. *J. Biol. Chem.* **277**, 18947-18953 (2002).

257   Drlica, K. & Zhao, X. DNA gyrase, topoisomerase IV, and the 4-quinolones. *Microbiol. Mol. Biol. Revs.* **61**, 377-392 (1997).

258   Smith, H. J., Walters, M., Hisanaga, T., Zhanel, G. G. & Hoban, D. J. Mutant prevention concentrations for single-step fluoroquinolone-resistant mutants of wild-type, efflux-positive, or ParC or GyrA mutation-containing Streptococcus pneumoniae isolates. *Antimicrobial agents and chemotherapy* **48**, 3954-3958 (2004).

259   Ban, C. & Yang, W. Crystal structure and ATPase activity of MutL: implications for DNA repair and mutagenesis. *Cell* **95**, 541-552 (1998).

260   Marcu, M. G., Chadli, A., Bouhouche, I., Catelli, M. & Neckers, L. M. The heat shock protein 90 antagonist novobiocin interacts with a previously unrecognized ATP-

binding domain in the carboxyl terminus of the chaperone. *J. Biol. Chem.* **275**, 37181-37186. (2000).

261   Marcu, M. G., Schulte, T. W. & Neckers, L. Novobiocin and related coumarins and depletion of heat shock protein 90-dependent signaling proteins. *J. Natl. Cancer Inst.* **92**, 242-248. (2000).

262   Sagar, S., Kaur, M., Minneman, K. P. & Bajic, V. B. Anti-cancer activities of diospyrin, its derivatives and analogues. *European journal of medicinal chemistry* **45**, 3519-3530 (2010).

263   Kumar, B. *et al.* Diospyrin derivative, an anticancer quinonoid, regulates apoptosis at endoplasmic reticulum as well as mitochondria by modulating cytosolic calcium in human breast carcinoma cells. *Biochemical and biophysical research communications* **417**, 903-909 (2011).

264   Snyder, M. & Drlica, K. DNA gyrase on the bacterial chromosome: DNA cleavage induced by oxolinic acid. *J. Mol. Biol.* **131**, 287-302 (1979).

265   Wu, J. *et al.* The dimer state of GyrB is an active form: implications for the initial complex assembly and processive strand passage. *Nucleic Acids Res* **39**, 8488-8502, doi:gkr553 [pii]

10.1093/nar/gkr553 (2011).

266   Mizuuchi, K., O'Dea, M. H. & Gellert, M. DNA gyrase: subunit structure and ATPase activity of the purified enzyme. *Proc. Natl. Acad. Sci. USA* **75**, 5960-5963 (1978).

267   Gilbert, E. J. & Maxwell, A. The 24 kDa N-terminal sub-domain of the DNA gyrase B protein binds coumarin drugs. *Molec. Microbiol.* **12**, 365-373 (1994).

268   An, J., Totrov, M. & Abagyan, R. Pocketome via comprehensive identification and classification of ligand binding envelopes. *Mol Cell Proteomics* **4**, 752-761, doi:M400159-MCP200 [pii]

10.1074/mcp.M400159-MCP200 (2005).

269   Karkare, S. *et al.* The naphthoquinone diospyrin is an inhibitor of DNA gyrase with a novel mechanism of action. *The Journal of Biological Chemistry* **288**, 5149-5156, doi:M112.419069 [pii]

10.1074/jbc.M112.419069 (2013).

270   Ali, J. A., Jackson, A. P., Howells, A. J. & Maxwell, A. The 43-kDa N-terminal fragment of the gyrase B protein hydrolyses ATP and binds coumarin drugs. *Biochemistry* **32**, 2717-2724 (1993).

271   Wigley, D. B., Davies, G. J., Dodson, E. J., Maxwell, A. & Dodson, G. Crystal structure of an N-terminal fragment of the DNA gyrase B protein. *Nature* **351**, 624-629 (1991).

272 Matthews, B. W. Solvent content of protein crystals. *J. Mol. Biol.* **33**, 491-497 (1968).

273 Ali, J. A., Orphanides, G. & Maxwell, A. Nucleotide binding to the 43-kilodalton N-terminal fragment of the DNA gyrase B protein. *Biochemistry* **34**, 9801-9808 (1995).

274 Collaborative Computational Project, N. The CCP4 suite: programs for protein crystallography. *Acta Cryst.* **D50**, 760-763 (1994).

275 Davis, I. W. *et al.* MolProbity: all-atom contacts and structure validation for proteins and nucleic acids. *Nucleic Acids Res.* **35**, W375-383 (2007).

276 Page, M. J. & Di Cera, E. Role of Na+ and K+ in enzyme function. *Physiological reviews* **86**, 1049-1092 (2006).

277 DeLano, W. L. *The PyMOL User's Manual.* (DeLano Scientific, 2002).

278 Pineda, A. O. *et al.* Molecular dissection of Na+ binding to thrombin. *The Journal of Biological Chemistry* **279**, 31842-31853 (2004).

279 Wilbanks, S. M. & McKay, D. B. How potassium affects the activity of the molecular chaperone Hsc70. II. Potassium binds specifically in the ATPase active site. *The Journal of Biological Chemistry* **270**, 2251-2257 (1995).

280 Wei, H., Ruthenburg, A. J., Bechis, S. K. & Verdine, G. L. Nucleotide-dependent domain movement in the ATPase domain of a human type IIA DNA topoisomerase. *The Journal of Biological Chemistry* **280**, 37041-37047 (2005).

281 Gubaev, A. & Klostermeier, D. Potassium ions are required for nucleotide-induced closure of gyrase N-gate. *The Journal of Biological Chemistry* **287**, 10916-10921 (2011).

282 Finney, L. A. & O'Halloran, T. V. Transition metal speciation in the cell: insights from the chemistry of metal ion receptors. *Science (New York, N.Y* **300**, 931-936 (2003).

283 Rizzuto, R. & Pozzan, T. Microdomains of intracellular Ca2+: molecular determinants and functional consequences. *Physiological reviews* **86**, 369-408 (2006).

284 Armstrong, R. N. Mechanistic diversity in a metalloenzyme superfamily. *Biochemistry* **39**, 13625-13632 (2000).

285 Di Cera, E. A structural perspective on enzymes activated by monovalent cations. *The Journal of Biological Chemistry* **281**, 1305-1308 (2006).

286 Machius, M., Chuang, J. L., Wynn, R. M., Tomchick, D. R. & Chuang, D. T. Structure of rat BCKD kinase: nucleotide-induced domain communication in a mitochondrial protein kinase. *Proceedings of the National Academy of Sciences of the United States of America* **98**, 11218-11223 (2001).

287   Surette, M. G. *et al.* Dimerization is required for the activity of the protein histidine kinase CheA that mediates signal transduction in bacterial chemotaxis. *The Journal of Biological Chemistry* **271**, 939-945 (1996).

288   Kampranis, S. C. & Maxwell, A. Hydrolysis of one ATP is sufficient to promote supercoiling by DNA gyrase. *J. Biol. Chem.* **273**, 26305-26309 (1998).

289   Gross, C. H. *et al.* Active-Site Residues of *Escherichia coli* DNA Gyrase Required in Coupling ATP Hydrolysis to DNA Supercoiling and Amino Acid Substitutions Leading to Novobiocin Resistance. *Antimicrobial agents and chemotherapy* **47**, 1037-1046 (2003).

290   Christian, J. H. & Waltho, J. A. The Composition of *Staphylococcus aureus* in Relation to the Water Activity of the Growth Medium. *Journal of general microbiology* **35**, 205-213 (1964).

291   Yakovchuk, P., Protozanova, E. & Frank-Kamenetskii, M. D. Base-stacking and base-pairing contributions into thermal stability of the DNA double helix. *Nucleic acids research* **34**, 564-574 (2006).

292   Smith, S. B., Cui, Y. & Bustamante, C. Overstretching B-DNA: the elastic response of individual double-stranded and single-stranded DNA molecules. *Science (New York, N.Y* **271**, 795-799 (1996).

293   Hsieh, L.-S., Rouviere-Yaniv, J. & Drlica, K. Bacterial DNA supercoiling and the [ATP]/[ADP] ratio: changes associated with salt shock. *J. Bacteriol.* **173**, 3914-3917 (1991).

294   Spirito, F. & Bossi, L. Long-distance effect of downstream transcription on activity of the supercoiling-sensitive leu-500 promoter in a topA mutant of Salmonella typhimurium. *Journal of bacteriology* **178**, 7129-7137 (1996).

295   Dorman, C. J. & Ni Bhriain, N. DNA topology and bacterial virulence gene regulation. *Trends in microbiology* **1**, 92-99 (1993).

296   Higgins, C. F. *et al.* A physiological role for DNA supercoiling in the osmotic regulation of gene expression in S. typhimurium and E. coli. *Cell* **52**, 569-584 (1988).

297   Roca, J. Transcriptional inhibition by DNA torsional stress. *Transcription* **2**, 82-85 (2011).

298   Postow, L. *et al.* Positive torsional strain causes the formation of a four-way junction at replication forks. *The Journal of Biological Chemistry* **276**, 2790-2796 (2001).

299   Lanz, M. A. & Klostermeier, D. Guiding strand passage: DNA-induced movement of the gyrase C-terminal domains defines an early step in the supercoiling cycle. *Nucleic Acids Res* **39**, 9681-9694, doi:gkr680 [pii]

10.1093/nar/gkr680 (2011).

300   Gubaev, A., Hilbert, M. & Klostermeier, D. The DNA-gate of *Bacillus subtilis* gyrase is predominantly in the closed conformation during the DNA supercoiling reaction. *Proceedings of the National Academy of Sciences of the United States of America* **106**, 13278-13283, doi:0902493106 [pii]

10.1073/pnas.0902493106 (2009).

301   Klostermeier, D. Single-molecule FRET reveals nucleotide-driven conformational changes in molecular machines and their link to RNA unwinding and DNA supercoiling. *Biochem Soc Trans* **39**, 611-616, doi:BST0390611 [pii]

10.1042/BST0390611 (2011).

302   Nollmann, M. *et al.* Multiple modes of *Escherichia coli* DNA gyrase activity revealed by force and torque. *Nat Struct Mol Biol* **14**, 264-271 (2007).

303   Basu, A., Schoeffler, A. J., Berger, J. M. & Bryant, Z. ATP binding controls distinct structural transitions of *Escherichia coli* DNA gyrase in complex with DNA. *Nat Struct Mol Biol* **19**, 538-546, doi:nsmb.2278 [pii]

10.1038/nsmb.2278 (2012).